Inverse problems for deep bed filtration in porous media

A.C. Alvarez

February 28, 2005

Instituto Nacional de Matemática Pura e Aplicada

Inverse problems for deep bed filtration in porous media

Author: Amaury Alvarez Cruz

Adviser: Dan Marchesin

Rio de Janeiro, Brasil
February, 2005

Para minha avó Lorenza e
para minha mãe Cila

AGRADECIMENTOS

Agradeço aos professores, colegas e aos trabalhadores do IMPA, que fazem do IMPA um centro de excelência de pesquisa.

Gostaria de agradecer ao meu orientador Dan Marchesin pelas lições, colaboração e ajuda durante os quatro anos de doutorado. Eu agradeço a Marcus Sarkis pelas lições de Análise Numérica e suas aulas de Salsa Cubana. Agradeço a André Nachbin pelas lições de Dinâmica de Fluidos e gostaria de agradecer a Bárbara Melo pelas aulas de Inglês. Também ao Jorge Zubelli por suas aulas sobre problemas inversos e ao Rafael Iorio por as aulas de Teoria Espectral.

Agradeço a meu amigo e mestre cubano Baldomero Valiño Alonso por suas lições e ajuda.

Agradeço a Pavel Bedrikovetsky que originou o problema tratado nesta tese; sou grato por inúmeras discussões esclarecedoras.

Agradeço ao Water Managment Group in Applied Earth Sciences of Delft University of Technology: Prof. Peter K. Currie, Dr. Win M.G.T van den Broek and Firas A. H. Al-Abduwani por ter fornecido dados experimentais utilizados neste trabalho.

Agradeço a Beata Gundelach por sua ajuda, por "apoiar-me" durante tanto tempo e por corrigir o Inglês de minha tese. Agradeço também a Mônica Souza por me trasmitir otimismo.

Gostaria de agradecer a Miosotis e Meissa por serem a razão e felicidade da minha vida.

Um especial agradecimento a família Quiroga: Hector, Lya, Ricardo e Valeria por sua ajuda e seu carinho. Um especial agradecimento a Milena por tudo. Quero agradecer aos meus amigos brasileiros Sonia, Nely, Nair, Christian, Gustavo, Monique, Fatima, Andrea, Edinho, Miguel, Nubia, Luzia, Rosita, Alfredo, Miguel(Chileno), Ely, meus amigos cubanos Leonel, Mayra, Ramon, Leonel Ivan, aos meus irmãos Osvaldo, Rey e a minha Tia Clary pela solidariedade. Também agradeço a meu amigo mexicano Pablo pela leitura cuidadosa da tese.

Agradeço em Cuba a Ramon, Yoima, Ania, Rodolfo, Paco, Kenia, Trista, Jose Luis, Mirtha, Ofelita, Hermes, Jesus, Maria del Carmen e Yamila por a ajuda a minha familia.

Agradeço a Mayra por facilitar uma comunicação permanente com minha Mãe.

Agradeço ao Instituto de Oceanologia de Cuba, UMALCA, CNPq e FAPERJ pelo apoio financeiro deste trabalho através das bolsas 141298/2001-04 e E-26/150.408/2004.

Finalmente, gostaria de agradecer ao povo brasileiro que me recebeu calorosamente no Rio de Janeiro e me fez sentir em minha querida Cuba.

Index

1 Introduction **7**

2 Physical Model. Flow of water with particles in porous media **11**

2.1 Preliminaries . . . 11

2.1.1 Boundary and initial conditions . . . 12

2.1.2 Pressure drop integral equation . . . 13

2.1.3 Dimensionless equations . . . 13

2.2 Solution for flow of water with suspended particles . . . 14

2.3 Semianalytical solution for flow suspensions . . . 17

2.4 Asymptotic behavior of the deep bed filtration model . . . 19

2.5 Analytical examples . . . 21

2.5.1 Constant filtration . . . 21

2.5.2 Linear filtration with decreasing slope . . . 22

2.5.3 Linear filtration with increasing slope . . . 24

2.5.4 Behavior of concentration and deposition in time and space . . . 25

2.6 Non-constant inlet concentration . . . 25

2.7 Bounds of the solution . . . 27

2.8 Global solution for the direct problem . . . 28

3 Functional equation for the filtration function **32**

3.1 Recovery method . . . 32

3.1.1 Derivation of the functional equation . . . 33

3.1.2 Solution of the functional equation . . . 35

3.2 Stabilization of the inverse problem for the filtration function . . . 41

3.2.1 Statement of the problem . . . 41

3.2.2 Well-posedness of $\mathcal{A}_1$ and $\mathcal{A}_4$ . . . 42

3.2.3 Well-posedness of $\mathcal{A}_2$ . . . 43

3.2.4 Well-posedness of $\mathcal{A}_3$ . . . 47

3.2.5 Well-posedness of the inverse problem . . . 47

4 The inverse problem for the porous rock damage function **49**

4.1 The integral equation . . . 49

4.2 Conditions for existence, uniqueness and stability . . . 52

4.2.1 Ill-posedness of the inverse problem . . . 52

4.2.2 Regularization method . . . 54

4.2.3 Choice of regularization parameter value . . . 54
4.2.4 Solution in Sobolev spaces . . . 57
4.3 Collocation method for the integral equation . . . 59
4.3.1 Formulation . . . 59
4.3.2 Numerical algorithm . . . 59
4.4 Regularization by parametrization . . . 66
4.5 Applications of the algorithm . . . 68
4.5.1 Synthetic data . . . 68
4.5.2 Numerical results and discussion . . . 68
4.5.3 Condition number . . . 71
4.5.4 The Picard condition . . . 72
4.6 Convergence results . . . 75
4.6.1 Preliminaries . . . 75
4.6.2 Auxiliary lemmas . . . 76
4.6.3 Convergence of the regularized solution . . . 78

5 Recovery of the permeability reduction and filtration functions from concentration and pressure histories 79
5.1 Preliminaries . . . 79
5.2 Least square solution . . . 80
5.3 Parametrization . . . 81
5.4 Filtration function from effluent concentration . . . 82
5.4.1 Well-posedness of the inverse problem . . . 82
5.4.2 Implementation . . . 83
5.5 Permeability reduction and filtration functions from pressure distribution history 86
5.5.1 Well-posedness of the inverse problem . . . 87
5.5.2 Implementation . . . 89
5.6 The recovery method . . . 91

6 Filtration function from particle deposition 96
6.1 Recovery methods . . . 96
6.1.1 Method I. Direct formulation . . . 96
6.1.2 Method II. Integral equation . . . 97
6.1.3 Method III. Functional equation . . . 98
6.1.4 Method IV. Optimization method . . . 98

7 Sensitivity analysis 100
7.1 Sensitivity coefficients . . . 101
7.2 Interrelationship between parameters . . . 101
7.3 Sensitivity of the optimal solution . . . 102
7.4 Sensitivity analysis for effluent concentration . . . 102
7.5 Sensitivity analysis for the pressure drops . . . 103

8 Validation of the model from experimental measurements **106**
8.1 Experimental methodology . . . 106
8.2 Results and discussion . . . 107
8.2.1 First study . . . 108
8.2.2 Second study . . . 108
8.2.3 Results . . . 109

9 Conclusion **114**

A Basic results **124**
A.1 Functional analysis . . . 124
A.2 Hilbert scales . . . 125
A.3 Inverse problem . . . 126
A.3.1 Generalized inverse . . . 128
A.3.2 Singular value decomposition . . . 129
A.4 Tikhonov regularization . . . 130
A.4.1 Solvability of the regularized equation . . . 132
A.4.2 Discrete ill-posed problem and its regularization . . . 133
A.4.3 Numerical implementation of Tikhonov regularization . . . 135
A.4.4 Regularization for nonlinear operators . . . 136
A.4.5 Parameter identification problem . . . 138
A.5 Convergence analysis . . . 139

B The Singular Value Decomposition (SVD) **141**
B.1 SVD on matrices . . . 141
B.2 Generalized Singular Value Decomposition (GSVD) . . . 142

C Experimental data **143**

D Optimization **145**
D.1 Gauss-Newton-Levenberg-Marquardt method . . . 145
D.2 Spectral projected gradient method . . . 146
D.3 Interior trust region method . . . 148
D.4 Implementation . . . 148
D.5 Regularization method and simple iterative procedure . . . 149
D.5.1 Scaling method . . . 149
D.5.2 Optimization method . . . 149
D.5.3 Iterative procedure . . . 150

E Topics on differentiation **151**

Chapter 1

Introduction

Most of the oil in the world is produced by injecting water in some wells and recovering oil in other wells. However, severe fall of injectivity occurs from the practice in offshore fields of injecting sea water containing organic and mineral inclusions. The injection of a poor quality water in a well curtails its injectivity because the particles suspended in the fluid are trapped while passing through the porous rock. Thus, in this work we study the deep filtration during injection of water containing solid particles, which is essential to predict the loss of injectivity in wells.

Mathematical models for filtration processes contain functions describing properties of the fluid or the porous medium where the flow occurs. Recovery methods for determining these functions indirectly from laboratory measurements of quantities such as the pressure or flow rate of the fluids in flow experiments have been developed by several authors. Such methods lead to mathematical inverse problems in parameter estimation theory, which are very ill-conditioned linear and nonlinear optimization problems. Regularization methods are useful to solve these problems because they provide approximate solutions in a stable way.

Many laboratory studies were carried out to understand the filtration process, ([35], [11], [1] and [60]). Our work is based on the model for *deep bed filtration*, developed in [10] based on [60], which consists of equations expressing the particle mass conservation, the particle retention kinetics and Darcy's law ([10], [60] and [80]). This quasilinear system of equations has two empirical coefficients, the permeability reduction function $k(\sigma)$, which expresses the formation damage in the porous rock and the filtration function $\lambda(\sigma)$, which represents the kinetics of particle retention. The *direct problem* consists in solving this system of equations in time.

In one dimensional flow laboratory experiments it is possible to measure accurately the following quantities, in increasing order of difficulty:

(i) the pressure drop time series $\Delta p(T)$;

(ii) the pressure time series $p_l(T)$ at some points $X = X_l$, $l = 1, \dots n$, along the rock;

(iii) the effluent concentration time series $c_e(T)$;

(iv) the average particle deposition $\sigma(X,T)$ between points X_{l-1} and X_l, $l = 2, \dots n$ at the end time of the experiment;

(v) the particle deposition $\sigma(X,T)$ at many points (X_l,T_j), $l=1,\dots n$, $j=1,\dots,m$.

Naturally, such experimental measurements are used in the inverse problem of determining the permeability reduction $k(\sigma)$ and the filtration function $\lambda(\sigma)$.

The recovery of the permeability reduction and filtration functions leads to several different types of ill-posed inverse problems, which are the object of our work. The solution techniques used here lead to large matrices upon discretization which have huge condition numbers and must be treated with care.

Methods for the determination of a constant filtration function $\lambda(\sigma)=\lambda_0$ from the effluent concentration history $c_e(T)$ were presented in [93] and [112]. A recovery method for the general case under the assumption that the injected concentration of particles is constant was presented in [10] and [12], based on a functional equation. The first derivation of this functional equation, based on the invariance of c/σ along the characteristics lines was found in [10] and [12]. However, stabilization conditions of the inverse method as well as experimental validation of the model were not considered. In this work, we obtain stabilization conditions for the recovery method and we relax the assumption made in [10] of constant injected particle concentration. Moreover, we present another recovery method to obtain the filtration function $\lambda(\sigma)$ based on an optimization method.

The invariance of c/σ along the characteristics lines was found first by Herzig et al. ([60]), based on a simplified model of the filtration process. However, the same relationship was derived for a more general model by Bedrikovetsky et al. ([10]) under analogous assumptions. Because its relevance for the recovery method and the validation of the model, we reproduce an analogous derivation in this work.

Methods for the determination of the permeability reduction function $k(\sigma)$ from the pressure drop history $\Delta p(T)$ were presented in [93], [112] and [11] for constant coefficient and one parameter family of solutions. In this work, we obtain a more general method using the Tikhonov regularization method. Moreover, we present the regularization by parametrization method which is analogous to developed in [2] for two parameters function.

In [10] two problems were solved: the direct problem of calculating the deposition $\sigma(X,T)$ and concentration of particles $c(X,T)$ for a given filtration function $\lambda(\sigma)$, as well as the inverse problem of determining the filtration function $\lambda(\sigma)$ from the effluent concentration history $c_e(T)$, by assuming that the injected concentration of particles is constant.

We solve the following inverse problems in this work. First, the porous rock damage function $k(\sigma)$ is recovered from the pressure drop history $\Delta p(T)$ in one dimensional deep bed filtration flow. This problem was formulated by Bedrikovetsky et al. in [11] and [13]. In this case, we assume that the filtration function $\lambda(\sigma)$ has been calculated first, either by the method presented in Chapter 5, based on optimization, or by the method developed in Chapter 3, based on a functional equation. Second, the filtration function $\lambda(\sigma)$ and the permeability reduction function $k(\sigma)$ are recovered from the effluent concentration $c_e(T)$ and the pressure histories $p_l(T)$ at different points in the core. Third, a recovery method for obtaining the filtration function $\lambda(\sigma)$ from the particle deposition $\sigma(X_l,T_j)$ is proposed.

We start by establishing the well-posedness of the direct time evolution problem. Then the inverse problems are stated as operator equations. Hence the analysis consists in guaranteeing the existence, uniqueness and stability of the solution of these equations. Thus, we are led to the study of regularity of linear and nonlinear ill-posed problems. Several assumptions about the solution based on specific information on the physical processes must be made in order to ensure the well-posedness of the operator equation solutions in Tikhonov's sense. Finally, a practical numerical recovery procedure is described for each inverse problem.

Our work is organized as follows. In Chapter 2 we present the physical model, the well-posedness of the direct problem, the asymptotic analysis of its solution and discuss certain illustrative analytical solutions.

In Chapter 3, we present the recovery method for the filtration function $\lambda(\sigma)$ from the injected and effluent concentration history by means of a functional equation. We study the existence, uniqueness and stability of the solution of this inverse method, issues that are fundamental for developing a numerical procedure to determine the filtration function $\lambda(\sigma)$ based on the functional equation.

In Chapter 4, we study the inverse problem of determining the permeability reduction function $k(\sigma)$ from a given pressure drop history $\Delta p(T)$, assuming that the filtration function $\lambda(\sigma)$ has already been found. We derive an integral equation of Volterra type for the rock formation damage function $k(\sigma)$ and we discuss conditions for well-posedness of the operator equation. An analogous integral equation was derived in [8]. We describe a numerical implementation to calculate the permeability reduction function $k(\sigma)$ within an appropriate subset of feasible solutions.

The classical Tikhonov or Tikhonov-Phillips regularization is used to reduce the ill-posed Volterra equation of first kind to a well posed problem ([105], [32] and [94]). Optimization and LU factorization methods are useful in finding the solution of the linear system of equations obtained by discretizing the continuous equation. Finally, the convergence of the regularized solution is obtained assuming that the feasible solution is uniformly bounded with respect to a Sobolev norm of higher order; this is the smoothness property. To do so, we use a sufficient condition for the iterates of the integral operator equation to converge to an approximate solution with almost minimal norm.

The convergence result is obtained using Hilbert scales, which provide useful bounds to measure the errors of Tikhonov regularization. Moreover, they are a perfect tool for characterizing both the degree of ill-posedness and the smoothness of the solution ([59], [91], [102], [78], [79] [89]).

In Chapter 5, an optimization method for calculating both the porous rock damage $k(\sigma)$ and the filtration function $\lambda(\sigma)$ from the effluent concentration and the pressure drop histories is presented. Moreover, an optimization method for obtaining the filtration function from the effluent particle concentration history is also described. The well-posedness of each inverse problem is studied as well.

In both cases, the recovery procedure consists in minimizing a nonlinear functional using the projection gradient method with box constraints developed and implemented by Martinez et al. ([82], [69], [36], [37] and [38]). The functional is obtained from the least square formulation taking into account the difference between the experimental data and the corresponding quantities predicted by the model, see e.g. [104]. The evaluation of this functional requires the implementation of an accurate and stable numerical method for the direct problem. The box constraints are determined from properties of the solution such as positivity and monotonicity. We establish the well-posedness of the recovery methods for the filtration function

$\lambda(\sigma)$ from the effluent concentration history as well as the well-posedness of the recovery of the permeability reduction function $k(\sigma)$ from the pressure drop history. Finally, a method to recover both functions at the same time is developed.

In Chapter 5, we study certain nonlinear ill-posed operator equations. There exists no general theory for nonlinear ill-posed problem, as opposed to the linear situation (see Chapter 4). However, for the nonlinear the operators studied here, there exist some results of convergence and stability, because these operators have the nice properties of compactness and weak closedness on appropriate domains.

In Chapter 6, methods for recovering the filtration function $\lambda(\sigma)$ from the particle deposition distribution history $\sigma(X, T)$ are proposed. There are several recovery procedures: the first one uses the direct formulation of the deep bed filtration model equations. The differentiation in time of particle deposition causes the main numerical difficulty in this case. In the second procedure the filtration function $\lambda(\sigma)$ is calculated as the solution of a Volterra integral equation of the first kind through characteristic lines. We will see that the method presented in Chapter 4 is useful for this equation as well. In the third procedure the filtration function $\lambda(\sigma)$ is obtained by means a functional equational, which is similar to the one used in Chapter 3. In the fourth procedure, an optimization method recovers the filtration function $\lambda(\sigma)$, with the methodology described in Chapter 5.

In all inverse problems, before recovering the empirical function parameters, we need to know conditions under which these parameters are identifiable, whether the observation data are sufficient for determining the inverse solution and how sensitive the inverse solution is to observation errors. In this way we determine the best experimental design for identifying the filtration and permeability reduction functions. These issues are treated in Chapter 7.

Finally, in Chapter 8, a comparison of the deep bed filtration model with laboratory measurements is done, using the methods developed here and the experimental data from [1].

Chapter 2

Physical Model. Flow of water with particles in porous media

In this chapter we present the physical model for the flow of water with suspended particles suffering retention in porous media. This model was developed in [10] based on [60]. Representative analytical solutions are obtained together with the analysis of their behavior in space and time. Moreover, an introduction to the sensitivity analysis of the solution with respect to parameters is presented.

2.1 Preliminaries

When water containing suspended particles flows in a porous medium, gradually the suspended particles are retained, reducing the permeability of the medium. This phenomenon, called *deep bed filtration*, is modelled as follows: assuming that water is incompressible and that the density of the solid particles in dispersed and entrapped states are both equal to the water's density, the conservation of mass is equivalent to the conservation of total volume, $\partial U/\partial x = 0$, i.e. the flow U depends only on t, and its value is determined by boundary data, either pressure drop along the core or injection rate. Neglecting diffusive effects, the mass conservation equation for the particles can be written as

$$\frac{\partial}{\partial t}\left(\phi c\text{'} + \sigma\text{'}\right) + U\frac{\partial c\text{'}}{\partial x} = 0. \tag{2.1}$$

Here the concentrations of dispersed and deposited particles are $c\text{'}(x,t)$ and $\sigma\text{'}(x,t)$. The quantity c' has values between 0 and 1, while the quantity σ' has values between 0 and ϕ. Here ϕ is a dimensionless quantity between 0 and 1, called the *rock porosity*: it is the fraction of the rock volume available to the fluid.

The model requires a law for particle deposition rate

$$\frac{\partial \sigma\text{'}}{\partial t} = \lambda\text{'}(\sigma\text{'})Uc\text{'}. \tag{2.2}$$

The right hand side of Eq. (2.2) means that the retention probability is proportional to flow velocity and to the available concentration of suspended particles. This probabilistic proportionality law remains valid if $\sigma' \ll \phi$ holds. Eq. (2.2) expresses the kinetics of particle retention. The dependence of the retention rate on σ' is expressed by $\lambda'(\sigma')$, which is called the *filtration function*. A sketch of the porous rock is presented in Fig. 2.1.

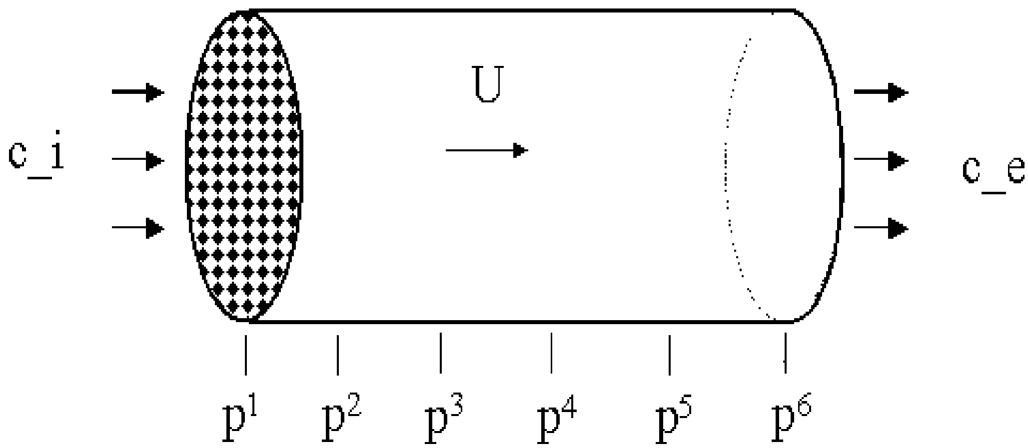

Figure 2.1: Porous rock. c_i: injected particle concentration, c_e: effluent particle concentration, p^l: pressure, $l = 1, \ldots, 6$.

It should be noted that the filtration function encompasses different parameters, such as the average particle size to average pore size ratio, among others. A serious limitation of the filtration theory is that it posits that these other parameters can either be neglected or assumed to be dependent only on the particle deposition σ. Several authors (e.g. [74] and [84]) have shown that, in some cases, it is necessary to differentiate between distinct types of deposition (e.g., injected particles depositing on matrix rock vs. injected particles depositing on previously deposited injected particles).

We assume that permeability reduction is due to particle retention, and that it is a decreasing function of retained concentration. So, Darcy's law relating the flow U and the pressure p becomes

$$U = -\frac{k_0\, k'(\sigma')}{\mu} \frac{\partial p'}{\partial x}. \tag{2.3}$$

Here k_0 is the absolute rock permeability and $k'(\sigma')$ is the permeability reduction due to the retained particles σ'; when expressed as a function of σ' it is called the *formation damage function*. It is normalized so that $k'(0) = 1$, i.e. it is one for clean porous rock. In general, the phase viscosity μ is a constant for small particle concentrations. For homogeneous rock k_0 is constant. Otherwise, it depends on x.

2.1.1 Boundary and initial conditions

We assume that the injected solid particle concentration $c'_i(t)$ is known, i.e.,

$$x = 0 : \quad c'(0,t) = c'_i(t) > 0. \tag{2.4}$$

Then along the line $x = 0$ we obtain from Eq. (2.2)

$$\frac{d\sigma'}{dt} = \lambda(\sigma')Uc'_i(t) \quad \sigma'(0) = 0. \tag{2.5}$$

Integrating Eq. (2.5) provides $\sigma'(0,t)$, which is always positive and increasing. We assume that at time zero the rock was initially clean, i.e.,

$$\sigma'(x,0) = 0 \quad \text{and} \quad c'(x,0) = 0. \tag{2.6}$$

2.1.2 Pressure drop integral equation

We take a partition of the interval $[0, L]$ as $0 = x_1 < \ldots < x_l < x_{l+1} < \ldots \leq L$, and we take into account the spatial heterogeneity of the rock medium in the absence of particles. To do so, we take the absolute permeability depending on x. More precisely, we assume that it is constant in each core segment, i.e., $k_0(x) = k_0^l$ for $x_l \leq x \leq x_{l+1}$ and $l = 1, \ldots, m_p$.

For one-dimensional linear flow in a rock core with length L, we replace k_0 by $k_0(x)$ in Eq. (2.3), and multiply it by $1/k'(\sigma'(x,t))U$; integrating the resulting equation from x_l a x_{l+1}, we obtain the following relationship between deposited particle distribution and pressure drop histories

$$-\int_{x_l}^{x_{l+1}} \frac{dx}{k'(\sigma'(x,t))} = \frac{k_0^l}{\mu U}\Delta p'^l(t)\,, \tag{2.7}$$

where $\Delta p'^l = p'(x_{l+1},t) - p'(x_l,t)$ is the pressure drop in each interval $x_l \leq x \leq x_{l+1}$.

2.1.3 Dimensionless equations

Let us assume for simplicity that U is constant in time; then we can introduce dimensionless length, dimensionless time, scaled concentration c, scaled retention σ, scaled filtration function λ, scaled damage function and dimensionless pressure:

$$X = \frac{1}{L}x\,, \quad T = \frac{U}{\phi L}t\,, \quad c = c'\,, \quad \sigma = \frac{1}{\phi}\sigma'\,, \quad \lambda(\sigma) = L\lambda'(\sigma')\,, \quad k(\sigma) = k'(\sigma'), \quad p = \frac{k_0}{\mu U L}p',$$
$$\text{for} \quad 0 \leq \sigma \leq 1 \quad \text{and} \quad 0 \leq X \leq 1. \tag{2.8}$$

This scaling is compatible with the time normalization which is usual in petroleum engineering, where dimensionless time is measured in porous volumes injected (P.V.I.). Using the change of variables (2.8) in (2.1), (2.2) and (2.7) we obtain a coupled system of equations in one spatial dimension.

$$\frac{\partial}{\partial T}(c + \sigma) + \frac{\partial c}{\partial X} = 0, \tag{2.9}$$

$$\frac{\partial \sigma}{\partial T} = \lambda(\sigma)c, \tag{2.10}$$

$$-\int_{X_l}^{X_{l+1}} \frac{dX}{k(\sigma)} = \Delta p^l, \quad \text{with} \quad l = 1, \ldots, m_p. \tag{2.11}$$

The system (2.9)-(2.11) describes the evolution of the pressure drops Δp^l, the concentration of dispersed particle distribution c and the concentration of retained particle distribution

σ. Notice that this system depends on the filtration function and on the formation damage function; these quantities must be given to determine the solution of the direct problem, i.e., to obtain the evolution in time of σ, c and Δp^l for all X, T from the given initial and boundary values.

2.2 Solution for flow of water with suspended particles

In this section, we present the solutions of the system (2.9)-(2.10) obtained in [10] by the method of characteristics. These formulae are used to obtain a fast numerical method. Also, we will use it in the study of several inverse problems.

Since the inverse problem is reduced to estimating certain parameters, the analytical solution is very useful in the calibration of the recovery algorithm. Moreover, scaling, monotonocity and boundedness of the analytical solution with respect to the parameters are studied here.

Notice that (2.11) can be solved after (2.9) and (2.10) are solved. Thus, the direct and inverse problem for (2.9) and (2.10) can be solved without considering the pressure drops Δp^l. The same paper [10] contains a numerical procedure to obtain the filtration function based on effluent particle concentration measurements $c(1,T)$ in coreflood tests. Once the filtration function in the model is known we predict the deposition distribution in one–dimensional flow.

Solution for the deposition distribution

The system of two equations (2.9)-(2.10), with the dimensionless form of (2.4) and (2.6), is a boundary-value initial-value problem which determines two unknowns $c(X,T)$ and $\sigma(X,T)$. The initial conditions (2.6) for this system reflect particle absence in the reservoir before injection

$$T = 0: \quad c(X,0) = 0, \quad \sigma(X,0) = 0. \tag{2.12}$$

Using the method of characteristics and an appropriate separation of variables it is possible to reduce the system (2.9)-(2.10) to a single ordinary differential equation for σ. We assume that the filtration function $\lambda(\sigma)$ either is C^1 with $\lambda(\sigma) > 0$ for $0 \leq \sigma \leq 1$ or it is C^1 except for certain σ_1 in $(0,1)$ with $\lambda(\sigma) > 0$ for $\sigma \in [0,\sigma_1)$ and $\lambda(\sigma) = 0$ for $\sigma \in [\sigma_1, 1]$. We can define the first integral Ψ of $1/\lambda$, i.e., we can define Ψ on $[0,\sigma_1)$ so that $\Psi(0) = 0$ as follows

$$\Psi(\sigma) = \int_0^{\sigma} \frac{d\eta}{\lambda(\eta)} . \tag{2.13}$$

Now, differentiating (2.13) and using (2.10) we obtain

$$\frac{\partial \Psi(\sigma)}{\partial T} = c, \quad \text{for} \quad \sigma \text{ in } [0,\sigma_1). \tag{2.14}$$

Let us consider a solution of (2.9)-(2.10), (2.12) and (2.21); we can expect that it is C^1 except at $X = T$, because there is a mismatch between the initial and boundary data for c

at $(0,0)$. We will focus our attention on the trapezoid $\{(X,T) : 0 \le X \le 1,\ T \ge X \ge 0\}$, see Fig. 2.2, and make the assumption

$$\sigma(X,T) = 0 \quad \text{for} \quad T = X, \text{ on the lower side of the trapezoid.} \tag{2.15}$$

So, the derivative of (2.14)

$$\frac{\partial c}{\partial T} = \frac{\partial^2 \Psi(\sigma)}{\partial T^2}, \tag{2.16}$$

is well defined for $X \neq T$. Substituting expression (2.14) for $c(X,T)$ and (2.16) in (2.1) and interchanging the order of differentiation in X and T we have

$$\frac{\partial^2 \Psi(\sigma)}{\partial T^2} + \frac{\partial^2 \Psi(\sigma)}{\partial T \partial X} = -\frac{\partial \sigma}{\partial T} \quad \text{or} \quad -\frac{\partial}{\partial T}\left(\frac{d\Psi(\sigma)}{dX}\right) = -\frac{\partial \sigma}{\partial T}, \tag{2.17}$$

which is well-defined because Ψ is a C^2 function for $X \neq T$. In $(2.17b)$ $\frac{d}{dX}$ is the differentiation along characteristic lines $X - T = constant$, i.e. $\frac{d}{dX} = \frac{\partial}{\partial X} + \frac{\partial}{\partial T}$, see Fig. 2.2.

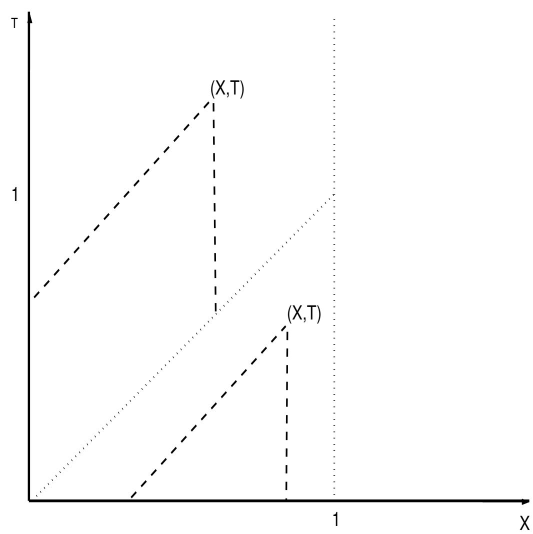

Figure 2.2: Characteristic lines; triangle(lower) and trapezoid(upper).

Now, we consider (2.17) in the infinite trapezoid $\{(X,T) : 0 \le X \le 1,\ T \ge X \ge 0\}$. Integrating $(2.17b)$ in T from the front $T = X$ to a fixed (X,T) we obtain

$$\frac{d\Psi(\sigma)}{dX} - \left.\frac{d\Psi(\sigma)}{dX}\right|_{T=X} = \sigma - \sigma|_{T=X}, \tag{2.18}$$

Using in (2.18) that $\sigma|_{T=X} = 0$ and $\left.\frac{d\Psi(\sigma)}{dX}\right|_{T=X} = 0$ we obtain

$$\frac{\partial \Psi(\sigma)}{\partial T} + \frac{\partial \Psi(\sigma)}{\partial X} = -\sigma. \tag{2.19}$$

or

$$\frac{1}{\sigma}\frac{\partial \Psi(\sigma)}{\partial T} + \frac{1}{\sigma}\frac{\partial \Psi(\sigma)}{\partial X} = -1. \tag{2.20}$$

Remark 2.1 *From Eq.*(2.19) *it follows that, as long as* σ *is positive,* $\Psi(\sigma)$ *is strictly monotone decreasing along characteristics with slope 1. Since* Ψ *is strictly monotone,* σ *is also strictly decreasing along these characteristics.*

We assume that the injected solid particle concentration is a given by

$$X = 0: \qquad c(0,T) = c_i(T) > 0. \tag{2.21}$$

Also, it is assumed that the experimental injected concentration $c_i(t)$ is a C^1 function for $T > 0$. Then along the line $X = 0$ we obtain from (2.10)

$$\frac{d\sigma(0,T)}{dT} = \lambda(\sigma(0,T))c_i(T)\,, \quad \sigma(0,0) = 0. \tag{2.22}$$

Equation (2.22) provides $\sigma(0,T)$, which is always positive and increasing. Other important relationships obtained in [10] use the auxiliary primitive

$$\chi(\sigma) = \int^{\sigma} \frac{d\eta}{\eta\lambda(\eta)}\,\cdot \tag{2.23}$$

The integral $\chi(\sigma)$ is well defined as follows

$$\chi(\sigma) = \int_0^{\sigma} \frac{d\eta}{\eta}\left(\frac{1}{\lambda(\eta)} - \frac{1}{\lambda_0}\right) + \frac{1}{\lambda_0}\int_1^{\sigma}\frac{d\eta}{\eta}, \tag{2.24}$$

where $\lambda_0 = \lambda(0)$; notice that the first integrand remains bounded near 0, so that the first integral tends to zero as $\sigma \to 0$. Integrating (2.20) from 0 to σ and using the definition of $\chi(\sigma)$ in Eq. (2.24), we obtain that along the characteristic lines $X = T + const$ the following equation holds

$$\frac{d}{dT}\,\chi(\sigma) = -1, \tag{2.25}$$

For $T > X$, integrating Eq. (2.25) in T from $T - X$ to T, we obtain

$$\chi(\sigma(X,T)) = \chi(\sigma(0,T-X)) - X. \tag{2.26}$$

Inverting the left hand side of Eq. (2.26), σ is found for any (X,T) in terms of $\sigma(0,T)$, i.e.

$$\sigma(X,T) = \chi^{-1}(\chi(\sigma(0,T-X)) - X), \tag{2.27}$$

where χ^{-1} denotes the inverse of χ. The method for evaluating $\sigma(X,T)$ using (2.27) requires the availability of χ^{-1} and χ.

The function χ^{-1} can be calculated numerically; however it can be calculated analytically in certain cases. For example, taking a linear filtration function, e.g., $\lambda(\sigma) = \lambda_0 - a\sigma$ for $\sigma \in [0, \lambda_0/a)$ and $\lambda(\sigma) = 0$ for $\sigma \in [\lambda_0/a, 1]$, we have the following results. Integrating (2.22), we obtain the solution

$$\sigma(0,T) = \frac{\lambda_0}{a}(1 - e^{-a\int_0^T c_i(\tau)d\tau}). \tag{2.28}$$

On the other hand, from Eq. (2.24) we obtain for $0 \leq \sigma \leq \min(1, \lambda_0/a)$

$$\chi(\sigma) = \frac{1}{\lambda_0} \log\left(\frac{\sigma}{1 - a\sigma/\lambda_0}\right); \tag{2.29}$$

and the inverse function χ^{-1} is

$$\sigma(\chi) = (e^{-\lambda_0 \chi} + a/\lambda_0)^{-1}. \tag{2.30}$$

Now, notice that substituting Eq. (2.24) into Eq. (2.25) we obtain in general

$$\int_{\sigma(X,T)}^{\sigma(0,T-X)} \frac{d\eta}{\eta\lambda(\eta)} = X. \tag{2.31}$$

In this way the filtration function satisfies the integral equation (2.31) along the characteristic lines $T - X = constant$. This equation will be used to obtain $\lambda(\sigma)$ from retained particle concentration $\sigma(X,T)$. In the next section we show examples of analytical solutions of the system (2.9) and (2.10) using the method developed in this section.

2.3 Semianalytical solution for flow suspensions

In this Section we introduce a semianalytical method of solution to be used when λ depends on position. This method will be used in the parameter estimation method described in Sections 5.4.1 and 5.5.

From (2.13) and (2.19) we obtain

$$\frac{\partial \sigma}{\partial T} + \frac{\partial \sigma}{\partial X} = -\lambda(\sigma)\sigma. \tag{2.32}$$

For $T \leq X$, $\sigma(X,T) = 0$. For $T > X$, we integrate Eq. (2.32) in T on a characteristic line from $(X - \tau, T - \tau)$ to (X,T) obtaining the following ordinary differential equation

$$\frac{d\sigma}{dX} = -\lambda(\sigma)\sigma. \tag{2.33}$$

with initial data $\sigma(X - \tau, T - \tau)$ given at $X - \tau$. Thus we obtain σ at X.

This integral was calculated analytically in the previous section; here we propose to integrate it numerically, obtaining $\sigma(X,T)$.

Numerical Method Let us assume that we found the solution at time n and that we have σ stored at (X^j, T^n), $j = 1, 2, 3, \cdots$. To compute the solution at time $n+1$, we first compute $\sigma(0, T^{n+1})$ from $\sigma(0, T^n)$ using an ODE solver on Eq. (2.22).

For other points (X^{j+1}, T^{n+1}) with $j < n$, we solve the ODE (2.33) with known initial data (X^j, T^n), and obtain $\sigma(X^{j+1}, T^{n+1})$. Finally, if $j \geq n$, $\sigma(X^{j+1}, T^{n+1}) = 0$. On the other hand, $c(X^j, T^n) = 0$ for $j \geq n$, and the values of $c(X^j, T^n)$ for $j < n$ are obtained using (2.37).

In the inverse problem solution for obtaining the filtration function, we need to solve Eqs. (2.22) and (2.32) several times as part of an optimization procedure. Thus, it is necessary to solve Eqs. (2.22) and (2.32) with high speed and accuracy.

Remark 2.2 *Substituting c from* (2.10) *in* (2.9), *we obtain*

$$\frac{\partial c}{\partial T}+\frac{\partial c}{\partial X}=-\lambda(\sigma)c, \tag{2.34}$$

or

$$\frac{dc}{dX}=-\lambda(\sigma)c. \tag{2.35}$$

Thus, from (2.33) *and* (2.35) *we see that σ and c satisfies a system of ordinary differential equations along characteristic lines. Since $c(0,t)=c_i(t)$ is usually known and $\sigma(0,t)$ follows from* (2.22), *the system* (2.35)-(2.33) *can be solved along characteristic lines.*

To increase the calculation speed, we can solve the system using the following strategy, which uses Remark 2.2. At the beginning, we choose a small time separation between characteristic lines where the solution is calculated, but for long times, we choose larger time separations. To obtain the value of the solution between two characteristic lines, we can use an interpolation method in time (for fixed X); this procedure is cheaper than solving the partial differential equation with a fine grid.

Solution for the concentration distribution

From Eqs. (2.33) and (2.35), we obtain along characteristics

$$\frac{d\sigma}{dc}=\frac{\sigma}{c}. \tag{2.36}$$

Integrating Eq. (2.36) along characteristics of slope 1, we obtain

$$\frac{\sigma(X,T)}{c(X,T)}=\frac{\sigma(0,T-X)}{c(0,T-X)}. \tag{2.37}$$

Now we present how to obtain the concentration $c(X,T)$ from the deposition particle concentration. Since for $T<X$, $\sigma(X,T)=0$, from (2.10) it follows that $c(X,T)=0$. In order to obtain $c(X,T)$ for $T>X$ we use Eq. (2.37), which furnishes an expression for $c(X,T)$ once $\sigma(X,T)$, $\sigma(0,T-X)$ and $c(0,T-X)$ are known.

Remark 2.3 *Equation* (2.37) *means that c/σ is constant along characteristic lines with slope 1.*

Remark 2.4 *In the case when the effluent particle concentration $c(0,T)=c_e(t)$ is known, the solution of the ODE's* (2.33), (2.35) *and* (2.22) *can be obtained by solving the ODE's* (2.33) *and* (2.35) *with*

$$\frac{d\sigma(1,T)}{dT}=\lambda(\sigma(1,T))c_e(T)\,, \quad \sigma(1,0)=0. \tag{2.38}$$

2.4 Asymptotic behavior of the deep bed filtration model

For solving the inverse problem we need other results in order to increase the calculation speed. We shall see that the computational efficiency of the algorithm for the direct problem can be increased by taking into account that the model has two time scales. In this section we assume for simplicity that the injected concentration is constant, i.e., $c_i(T) = c_{io}$.

Let us denote $\hat{c} = c/c_{io}$. Now we calculate how $\partial\hat{c}/\partial T$ depends on the filtration function for $T > X$.

From Eq. (2.37) we obtain

$$\frac{\partial\hat{c}(X,T)}{\partial T} = \left(\frac{\partial\sigma(X,T)}{\partial T}\sigma(0,T-X) - \sigma(X,T)\frac{\partial\sigma(0,T-X)}{\partial T}\right)/\sigma(0,T-X)^2 \tag{2.39}$$

Because (see Eq. (2.10))

$$\frac{\partial\sigma(X,T)}{\partial T} = \lambda(\sigma(X,T))c(X,T), \quad \text{so} \quad \frac{\partial\sigma(0,T-X)}{\partial T} = \lambda(\sigma(0,T-X))c_{io} \tag{2.40}$$

we can rewrite (2.39) as

$$\frac{\partial\hat{c}(X,T)}{\partial T} = \Big(\lambda(\sigma(X,T))c(X,T)\sigma(0,T-X) - \lambda(\sigma(0,T-X))c_{io}\sigma(X,T)\Big)/\sigma(0,T-X)^2. \tag{2.41}$$

Using again Eq. (2.37) we obtain

$$\frac{\partial\hat{c}(X,T)}{\partial T} = \Big(\lambda(\sigma(X,T))c(X,T) - \lambda(\sigma(0,T-X))c(X,T)\Big)/\sigma(0,T-X) \tag{2.42}$$

or

$$\frac{\partial\hat{c}(X,T)}{\partial T} = c_{io}\hat{c}(X,T)\frac{\lambda(\sigma(X,T)) - \lambda(\sigma(0,T-X))}{\sigma(0,T-X)} \tag{2.43}$$

Notice that if $\lambda(\sigma(X,T)) - \lambda(\sigma(0,T-X)) << \sigma(0,T-X))$ then $\frac{\partial\hat{c}(X,T)}{\partial T}$ is very small. This can happen in several situations, for example if $\lambda(\sigma(X,T))$ is monotone decreasing to zero.

Remark 2.5 *In particular if the filtration function is constant then* $\frac{\partial\hat{c}(X,T)}{\partial T} = 0$ *and* $\frac{\partial c(X,T)}{\partial T} = 0$ *for* $T > 1$*, i.e.* c *does not depend on* T*, if the injected concentration is constant.*

Remark 2.6 *Assuming that the particle deposition is decreasing in* X *we have* $\sigma(X,T) < \sigma(0,T-X)$ *for* $T > X$*. Then from* (2.43) *we obtain* $\frac{\partial c(X,T)}{\partial T} > 0$ *if the filtration function is decreasing, and* $\frac{\partial c(X,T)}{\partial T} < 0$ *if the filtration function is increasing.*

More generally the following lemma is valid.

Lemma 2.7 *If*

$$\frac{\lambda(\sigma(X,T)) - \lambda(\sigma(0,T-X))}{\sigma(0,T-X)} < \epsilon, \tag{2.44}$$

then

$$\frac{\partial\hat{c}(X,T)}{\partial T} < c_{io}\epsilon. \tag{2.45}$$

Proof: From (2.43) we obtain

$$\frac{\partial \hat{c}(X,T)}{\partial T} < c_{io}\hat{c}\epsilon. \tag{2.46}$$

Equation (2.37) can be rewritten as

$$\hat{c} = \frac{\sigma(X,T)}{\sigma(0,T-X)}. \tag{2.47}$$

Now, using Remark 2.1 and (2.47) we obtain that $\hat{c} < 1$. Thus we obtain that (2.45) holds $\square$.

Remark 2.8 *Since in practical situations c_{io} is of order 10^{-6}, we obtain that if $c_{io} << \epsilon$, e.g. $\epsilon = 1$ then $\frac{\partial \hat{c}(X,T)}{\partial T}$ is not greater than 10^{-6} and as a consequence $\frac{\partial c(X,T)}{\partial T}$ is of order 10^{-12}.*

In the case treated in Remarks 2.5 and 2.8 the term $\frac{\partial c(X,T)}{\partial T}$ can be neglected. So, the system of equation (2.9) and (2.10) can be rewritten as in [60], i.e.,

$$\frac{\partial \sigma}{\partial T} + \frac{\partial c}{\partial X} = 0, \tag{2.48}$$

$$\frac{\partial \sigma}{\partial T} = \lambda(\sigma)c. \tag{2.49}$$

We now prove that the system of equations (2.48) and (2.49) has two time scales and one space scale. Numerical methods for simulating deep bed filtration should to take into account the two time scales.

Scales in linear deep bed filtration problems

By inspecting Eq. (2.9), we see that characteristic speed associated to the suspended concentration is 1. In unscaled variables, this is U/ϕ, see Eq. (2.1). This sets a dimensionless time scale $T = 1$.

In actual solutions of the problem, one observes that there is an initial period until $T = 1$ when the injected particle concentration profile gets established. During this time period, the deposited concentration changes from zero to a value of the same magnitude as the injected suspended concentration, which is very small. These facts are clearly seen in the exact solution (2.60), (2.59).

However, after this initial period, the suspended concentration profile changes very little (in fact, it does not change at all in the case of the exact solution (2.60)), while the deposited concentration values change very slowly as compared to a typical value of deposition, which is ϕ or perhaps 0.1ϕ.

Reflecting this observation, Herzig and Leclerc [60] propose another set of equations, which should hold later in the evolution of the system (2.48)-(2.49). Notice that there is an imbalance in these equations: c is 10^5 times smaller than σ. To fix this imbalance, we can divide both equations by a typical value c_{i0} of the injected suspended concentration, and define

$$\hat{c} = \frac{c}{c_{i0}}, \quad \tau = c_{i0}T, \tag{2.50}$$

and the equations (2.48)-(2.49) become

$$\frac{\partial \hat{c}}{\partial X} = -\frac{\partial \sigma}{\partial \tau}, \tag{2.51}$$

$$\frac{\partial \sigma}{\partial \tau} = \lambda(\sigma)\hat{c}. \tag{2.52}$$

We see that another time scale appears, the time scale for deposited concentration change, from the equation (2.52). It corresponds to $\tau \cong 1$, or

$$T \cong \frac{1}{c_{i0}\lambda}. \tag{2.53}$$

This new time scale appears very clearly in the exact solution (2.60).

Summarizing, there is one spatial scale in this problem and two time scales. The first time scale is fast, and it controls the evolution until about one pore volume is injected. The second one is slow, and it controls the evolution at later times.

Remark 2.9 *Numerical methods for simulating deep bed filtration should take into account this change of time scale.*

2.5 Analytical examples

In this Section we present a summary of the solution of the direct problem in coreflood tests given by Eqs. (2.9), (2.10). It was obtained in [10] by means of the method of characteristics for constant and linear filtration functions with a given input particle concentration. Moreover, we present the sensitivity analysis of the formulas with respect to certain parameters. These formulas are used to validate the procedure proposed in this work for calculating the permeability reduction $k(\sigma)$. In this example we assume that the inlet concentration of particles $c(0,T) = c_{io}$ is constant.

2.5.1 Constant filtration

For constant filtration function $\lambda(\sigma) = \lambda_0$ and knowing the initial condition $c(X,0) = \sigma(X,0) = 0$ and the boundary condition $c(0,T) = c_i(T) = c_{i0}$, the particle deposition and concentration the particles are given by

$$\sigma(X,T) = c_{i0}\lambda_0(T-X)e^{-\lambda_0 X} \quad \text{for} \quad T > X \quad \text{and} \quad \sigma(X,T) = 0 \quad \text{for} \quad T < X. \tag{2.54}$$

and

$$c(X,T) = c_{i0}\, e^{-\lambda_0 X}, \;\; T \geq X \quad \text{and} \quad c(X,T) = 0 \quad \text{for} \quad T < X. \tag{2.55}$$

To summarize, we observe that after $T > 1$ the suspended concentration does not depend on time and that it is exponentially decreasing in X; the decay rate is λ_0. Moreover, the retained concentration increases linearly with time, which is unphysical for very large time.

2.5.2 Linear filtration with decreasing slope

For linear filtration function in the vanishing case (with $a \geq \lambda_0$) (see [13]), i.e.,

$$\lambda(\sigma) = \lambda_0 - a\sigma, \quad \text{for} \quad 0 \leq \sigma < \lambda_0/a \tag{2.56}$$

and

$$\lambda(\sigma) = 0 \quad \text{for} \quad \lambda_0/a \leq \sigma \leq 1, \tag{2.57}$$

or $\lambda(\sigma) = \max\{\lambda_0 - a\sigma, 0\}$, we obtain

$$\sigma(X,T) = 0 \quad \text{for} \quad T < X, \tag{2.58}$$

and using Eqs. (2.27), (2.28), (2.29) and (2.30) we obtain for $T > X$

$$\sigma(X,T) = \frac{\lambda_0}{a}\left[1 + \frac{e^{-c_{i0}aT}\, e^{(\lambda_0 + c_{i0}a)X}}{1 - e^{-c_{i0}a(T-X)}}\right]^{-1}, \tag{2.59}$$

So, from Eq. (2.37) the concentration of dispersed particles is

$$c(X,T) = \frac{c_{i0}a\sigma(X,T)}{\lambda_0(1 - e^{-c_{i0}a(T-X)})} \quad \text{for} \quad T > X, \text{ and } \; c(X,T) = 0 \quad \text{for} \quad X > T. \tag{2.60}$$

Setting $X = 1$ in Eq. (2.37), we obtain a relationship involving c and σ at the inlet and outlet

$$\frac{\sigma(1,T)}{\sigma(0,T-1)} = \frac{c(1,T)}{c_{i0}}. \tag{2.61}$$

Using Eq. (2.60) with $X = 1$, we obtain for $T > 1$

$$c(1,T) = \frac{c_{i0}}{(1 + e^{-c_{i0}a(T-1)}(e^{\lambda_0} - 1))}. \tag{2.62}$$

We can interpret the formulas above as follows. There is a jump in the concentration across the front $T = X$. We can see from Eq. (2.28) that the retained concentration along the inlet boundary $X = 0$ increases to a limiting value λ_0/a, which is more realistic than in the constant filtration function case (2.54) and (2.55). Moreover, from Eq. (2.59) it can be verified that for $T > X$ the retained concentration decreases in space X and increases in time T. The suspended concentration has the same behavior as the retained concentration with respect to space and time (see Figs. 2.3, 2.4 for examples).

The effluent concentration $c(1,T)$ given in (2.62) is very useful to calibrate the model, because its history can be measured in laboratory experiments, so we study this function in more detail in this section. We determine the sensitivity of $c(1,T)$ with respect to the parameters λ_0 and a. This study is used in the inverse problem for determining the appropriate parameter range for each data set.

For large time T in Eq. (2.62), i.e., $T >> 1$, we obtain

$$c(1,T) \approx c_{i0}\frac{1}{1 + (e^{\lambda_0} - 1)e^{-c_{io}aT}}. \tag{2.63}$$

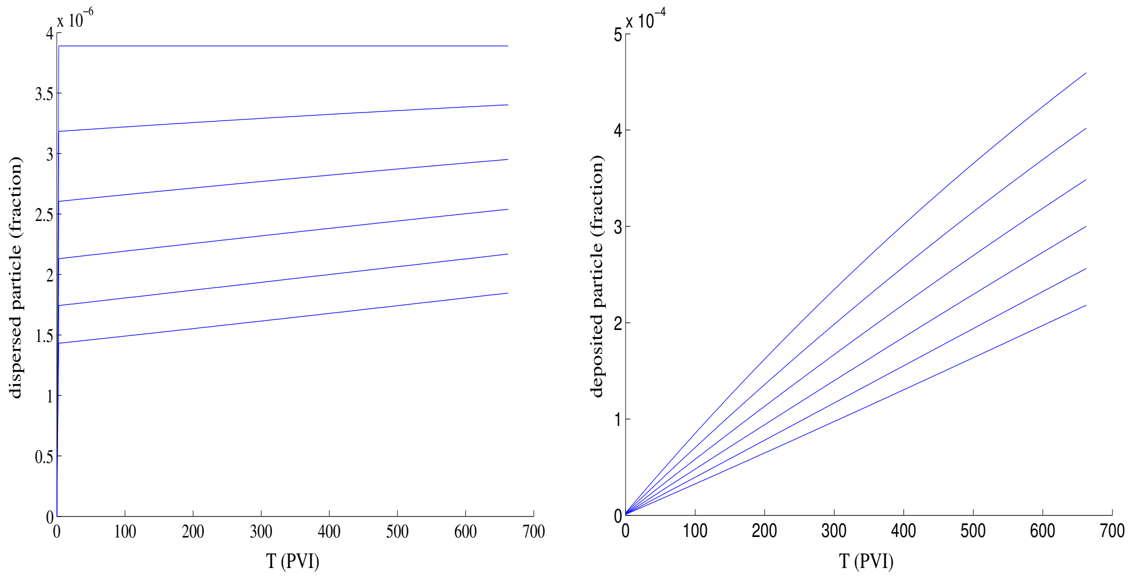

a) Particle concentration $c(X^*, T)$ b) Particle deposition $\sigma(X^*, T)$

Figure 2.3: Histories in T at $X^* = 0, 0.2, 0.4, 0.6, 0.8, 1$ and $\lambda(\sigma) = \max\{1 - 171\sigma, 0\}$.

In particular, for time T and parameter a such that $c_{io}aT$ is small, Eq. (2.63) can be approximated using Taylor's formula by

$$c(1, T) = c_{i0}e^{-\lambda_0} + c_{i0}\frac{e^{\lambda_0} - 1}{e^{2\lambda_0}}c_{i0}aT + O(c_{i0}aT)^2. \tag{2.64}$$

Thus it follows from Eq. (2.64) that for small values of $c_{i0}aT$ the values of $c(1, T) \approx c_{i0}e^{-\lambda_0}$ suffer no significant change for small variations of the parameter a. Thus $c(1, T)$ is insensitive to the parameter a in the above case, i.e., $c(1, T)$ exhibits low sensitivity relative to the time T as well as to a if $c_{i0}a$ is very small and the time T is large. Moreover, since $c(1, T) < c_{io}$ (see Chapter 2), if we make the approximation that the filtration function is constant, i.e., $\lambda(\sigma) = \lambda_0$ and assuming that $c(1, T)$ and c_{io} have the same order of magnitude (more precisely, $1 < \frac{c_{io}}{c(1,T)} < 10$), then the parameter λ_0 is smaller than 2. This fact is important to determine ranges of interest in certain optimization procedures.

In parameter recovery it will be necessary to know the behavior of $c(1, T)$ with respect to time T relative to certain parameters. For this study, we need

$$\frac{\partial c(1, T)}{\partial T} = \frac{c_{io}(c_{io}a)e^{c_{io}a(1-T)}(e^{\lambda_0} - 1)}{(e^{-c_{io}a(T-1)}(e^{\lambda_0} - 1) + 1)^2}. \tag{2.65}$$

Remark 2.10 *Notice that* $\frac{\partial c(1,T)}{\partial T} > 0$ *in* (2.65) *for* $\lambda_0 > 0$. *This fact is an a priori information that must be taken into account for recovering the filtration function from the effluent concentration.*

Now we present another case, where the filtration function is linear with an increasing slope. We will see that this case can be used as a model for the situation when the effluent concentration decreases in time.

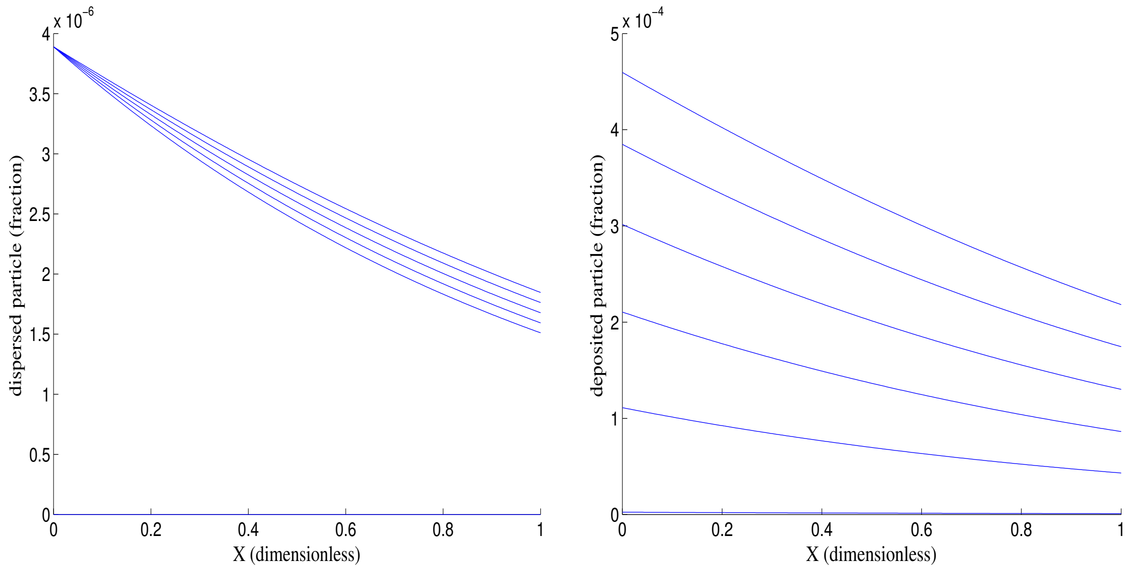

a) Particle concentration $c(X,T^*)$ b) Particle deposition $\sigma(X,T^*)$

Figure 2.4: Profiles in X at $T^* = 0, 133, 266, 399, 532, 662$ and $\lambda(\sigma) = \max\{1 - 171\sigma, 0\}$.

2.5.3 Linear filtration with increasing slope

For increasing linear filtration function λ, with $b > 0$

$$\begin{cases} \lambda(\sigma) = \lambda_0 + b\sigma > 0 \quad \text{for} \quad 0 \le \sigma \le 1 \\ \lambda(\sigma) = 0 \quad \text{for} \quad \sigma = 1. \end{cases} \tag{2.66}$$

From Eq. (2.22), at $X = 0$, $\dfrac{d\sigma}{dT} = c_{i0}\lambda_0$ for $\sigma = 0$ in both vanishing and nonvanishing cases, so we obtain from Eq. (2.8) the same formula for both cases

$$\begin{cases} \sigma(0,T) = \frac{\lambda_0}{b}\left(e^{c_{i0}bT} - 1\right) \quad \text{for} \quad T \le (c_{i0}b)^{-1}\log(1 + b/\lambda_0)\,, \\ \sigma(0,T) = \phi \quad \text{for} \quad T \ge (c_{i0}b)^{-1}\log(1 + b/\lambda_0)\,. \end{cases} \tag{2.67}$$

From Eq. (2.24), we obtain for $0 \le \sigma < \phi$

$$\chi(\sigma) = \frac{1}{\lambda_0}\,\log\left(\frac{\sigma}{1 + b\sigma/\lambda_0}\right). \tag{2.68}$$

The inverse function χ^{-1} is

$$\sigma(\chi) = (e^{-\lambda_0\chi} - b/\lambda_0)^{-1}. \tag{2.69}$$

From Eqs. (2.26), (2.67) and (2.68),

$$\chi(\sigma(X,T)) = \frac{1}{\lambda_0}\,\log\left[\frac{\lambda_0}{b}\left(\frac{e^{c_{i0}b(T-X)} - 1}{e^{c_{i0}b(T-X)}}\right)e^{-\lambda_0 X}\right]. \tag{2.70}$$

Now, $\sigma = 0$ for $T < X$. Using Eqs. (2.69) and (2.70), we obtain for $T > X$

$$\sigma(X,T) = \frac{\lambda_0}{b}\left[-1 + \frac{e^{c_{i0}bT}\,e^{(\lambda_0 - c_{i0}b)X}}{e^{c_{i0}b(T-X)} - 1}\right]^{-1}. \tag{2.71}$$

From Eqs. (2.37) and (2.67), the concentration is

$$c(X,T) = \frac{c_{i0}\sigma(X,T)}{(\lambda_0/b)(e^{c_{i0}b(T-X)}-1)} \quad \text{for} \quad T > X \text{ and } \ c(X,T) = 0 \quad \text{for} \quad T < X. \tag{2.72}$$

The effluent concentration is

$$c(1,T) = \frac{c_{i0}\sigma(1,T)}{(\lambda_0/b)(e^{c_{io}b(T-1)}-1)} \quad \text{for} \quad T > 1 \text{ and } \ c(1,T) = 0 \quad \text{for} \quad T < 1, \tag{2.73}$$

so that

$$\frac{\partial c(1,T)}{\partial T} = -\frac{c_{io}(c_{io}b)e^{c_{io}b(T-1)}(e^{\lambda_0}-1)}{(e^{c_{io}b(T-1)}(e^{\lambda_0}-1)+1)^2}. \tag{2.74}$$

Remark 2.11 *Notice that* $\frac{\partial c(1,T)}{\partial T} < 0$ *in* (2.74) *for* $\lambda_0 > 0$. *So, filtration with increasing slope can be used to match the experimental effluent concentration that decreases in time* T.

2.5.4 Behavior of concentration and deposition in time and space

Now we show graphically the behavior of retained and dispersed particle concentration using the formulas in Section 2.5. We discuss the rate of increase or decrease in each case as well.

In the numerical examples presented in this section the values of deposited and dispersed particle concentration are obtained by solving Eqs. (2.37) and (2.32) with $\lambda(\sigma) = \max\{1 - 171\sigma, 0\}$.

The histories in time of $\sigma(X^*,T)$ and $c(X^*,T)$ at the points $X^* = 0, 0.2, 0.4, 0.6, 0.8, 1$ are shown in Figure 2.3. Notice that the values of $c(X,T)$ are 100 times smaller than $\sigma(X,T)$. Both profiles for $c(X,T)$ and $\sigma(X,T)$ increase in time, but the increase rate of $c(X,T)$ is much smaller.

On the other hand, the profiles in space of $\sigma(X,T^*)$ and $c(X,T^*)$ at the points $T^* = 0, 133, 266, 399, 532, 662$ are shown in Figure 2.4. Notice that both deposited and dispersed particle concentrations decrease in space at similar rates. The distance between the profiles of dispersed concentration of particles is smaller than that for the deposited particles; this indicates that the change in time of $c(X,T)$ is smaller than that of $\sigma(X,T)$.

We will see in Chapter 8 that the behavior of $c(X,T)$ and $\sigma(X,T)$ agrees with experimental data. However, it is not possible to reproduce with accuracy the spatial rate of decrease for $\sigma(X,T)$.

2.6 Non-constant inlet concentration

In this section we present analytical formulas for inlet concentration that varies in time. This analysis can be useful when external cake is formed at the inlet wall of the rock where the filtration process occurs. We assume that the inlet concentration $c(0,T)$ is given by

$$c(0,T) = c_i(T) = c_{io}e^{-\eta T}, \tag{2.75}$$

where c_{io} is the inlet concentration at $T = 0$ and η is positive parameter. Here the filtration function is assumed to be linear, i.e., $\lambda(\sigma) = \max\{\lambda_0 - a\sigma, 0\}$. Now, using the method described in Section 2.2 and setting

$$C_i(T) = \int_0^T c_i(\tau)d\tau, \tag{2.76}$$

we obtain

$$\sigma(0,T) = \frac{\lambda_0}{a}(1 - e^{-aC_i(T)}), \tag{2.77}$$

Moreover,

$$\sigma(X,T) = 0 \quad \text{for} \quad T < X, \tag{2.78}$$

and for $T \geq X$

$$\sigma(X,T) = \frac{\lambda_0}{a}\left[1 + \frac{e^{-aC_i(T-X)}}{1 - e^{-aC_i(T-X)}} e^{\lambda_0 X}\right]^{-1}. \tag{2.79}$$

Using Eq. (2.75), Eq. (2.79) can be rewritten as

$$\sigma(X,T) = \frac{\lambda_0}{a}\left[1 + \frac{e^{-ac_{io}\eta^{-1}(1-e^{-\eta(T-X)})}}{1 - e^{-ac_{io}\eta^{-1}(1-e^{-\eta(T-X)})}} e^{\lambda_0 X}\right]^{-1}. \tag{2.80}$$

Notice that for constant inlet concentration, i.e. for $c_i(T) = c_{io}$ for all $T \in [0, A]$, Eq. (2.79) reduces to Eq. (2.59).

In Fig. 2.5, a plot of the integral

$$h(T) = \int_0^1 \sigma(X,T)dX, \tag{2.81}$$

is shown. This is related to the pressure history.

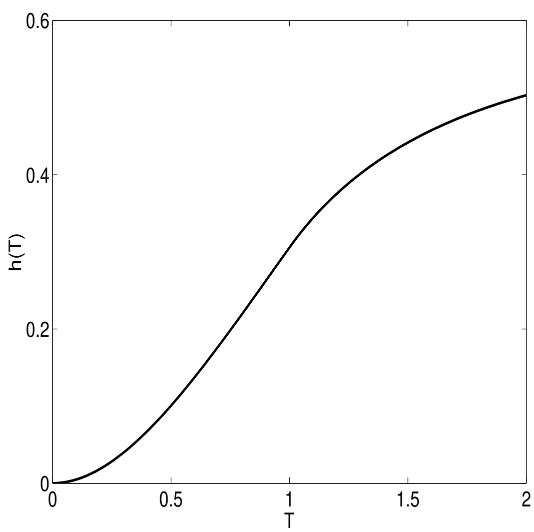

Figure 2.5: Graph of $h(T)$ in (2.81) with $\eta = 10^{-3}$, $c_{io} = 1$ and $\lambda(\sigma) = \max\{1 - 171\sigma, 0\}$.

Effluent concentration

From Eqs. (2.37), (2.77) and (2.80) we obtain the effluent concentration as

$$c(1,T) = \frac{c_{io}e^{-\eta T}}{1+(e^{\lambda_0}-1)e^{-ac_{io}\eta^{-1}(1-e^{-\eta(T-1)})}}. \tag{2.82}$$

Notice that

$$\tilde{c}(1,T) = \lim_{a\to 0} c(1,T) = c_{io}e^{-(\lambda_0+\eta T)}, \tag{2.83}$$

thus

$$\frac{\partial \tilde{c}}{\partial T}(1,T) = -\eta c_{io}e^{-(\lambda_0+\eta T)}. \tag{2.84}$$

If the filtration function is constant, i.e. $\lambda(\sigma) = \lambda_0$, then the effluent concentration is a monotone decreasing function. We obtain

$$\frac{\partial c(1,T)}{\partial T} = c_{io}e^{-\eta T}\frac{(c_{io}ae^{\eta}-\eta)(1+(e^{\lambda_0}-1)e^{-ac_{io}\eta^{-1}(1-e^{-\eta(T-1)})})-c_{io}ae^{\eta}}{(1+(e^{\lambda_0}-1)e^{-ac_{io}\eta^{-1}(1-e^{-\eta(T-1)})})^2}. \tag{2.85}$$

It possible to prove that $\frac{\partial c(1,T)}{\partial T}$ has a unique zero at $T = T_{max}$. So, the behavior of the function $c(1,T)$ with respect to time T for $T \geq 0$ is the following: $c(1,T)$ increases from $T=0$ to $T = T_{max}$, where

$$T_{max} = 1 - \frac{1}{\eta}\log\left(1+\frac{\eta}{ac_{io}}\log\left(\frac{\eta}{(c_{io}ae^{\eta}-\eta)(e^{\lambda_0}-1)}\right)\right) \tag{2.86}$$

and decreases for $T > T_{max}$. It is easy to prove that

$$\lim_{T\to\infty} c(1,T) = 0. \tag{2.87}$$

2.7 Bounds of the solution

In this section some useful bounds for the solution are derived. To do so, we restrict the filtration function $\lambda(\sigma) > 0$ to be a positive function of σ, i.e.,

$$0 < \lambda_{min} \leq \lambda(\sigma) \leq \lambda_{max}. \tag{2.88}$$

From Eqs. (2.9), (2.10),

$$\frac{\partial c}{\partial T} + \frac{\partial c}{\partial X} = -\lambda(\sigma)c. \tag{2.89}$$

Along characteristics with slope 1, this equation becomes the ODE

$$\frac{dc}{dX} = -\lambda(\sigma)c. \tag{2.90}$$

Using (2.88) and (2.90), the following inequality holds:

$$\frac{dc}{dX} \leq -\lambda_{min}c. \tag{2.91}$$

Applying Gronwall's inequality to (2.91), we obtain

$$c(X,T) \le c(0, T-X)e^{-\lambda_{min} X} \tag{2.92}$$

and

$$c(X,T) \le c(1, 1+T-X)e^{-\lambda_{min}(1-X)}. \tag{2.93}$$

In particular, setting $X = 1$ in (2.92) we obtain

$$c_e(T) < c_i(T-1). \tag{2.94}$$

Similarly using (2.33), it is possible to obtain for σ the following bound

$$\sigma(X,T) \le \sigma(0, T-X)e^{-\lambda_{min} X} \tag{2.95}$$

Denoting by $\mathcal{B}_1 = \max\limits_{T>X}\{c(0, T-X)\}$ and $\mathcal{B}_2 = \max\limits_{T>X}\{\sigma(0, T-X)\}$ we obtain from (2.92)-(2.95)

$$c(X,T) \le \mathcal{B}_1 \quad \text{and} \quad \sigma(X,T) \le \mathcal{B}_2. \tag{2.96}$$

2.8 Global solution for the direct problem

The system of equations (2.9)-(2.10) involves the filtration function $\lambda(\sigma)$. Solving this system of equation for all times for the given function $\lambda(\sigma)$ is called the *direct problem.* Numerical and analytical solutions of this system are described in Section 2.3.

Well-posedness of the direct problem

Here the well-posedness of the system (2.9)-(2.10) is studied. This system can be rewritten as

$$\frac{\partial}{\partial T}\begin{pmatrix} c \\ \sigma \end{pmatrix} + \begin{pmatrix} 1 & 0 \\ 0 & 0 \end{pmatrix}\frac{\partial}{\partial X}\begin{pmatrix} c \\ \sigma \end{pmatrix} = \begin{pmatrix} -\lambda(\sigma) & 0 \\ \lambda(\sigma) & 0 \end{pmatrix}\begin{pmatrix} c \\ \sigma \end{pmatrix}, \tag{2.97}$$

which is a quasi-linear hyperbolic system of equations. This system has two characteristic directions, which are $(dX, dT)^T = (1,1)^T$ (with speed 1) and $(dX, dT)^T = (0,1)^T$ (with speed 0), see Fig 2.2. We start the analysis by assuming that the filtration function is C^1 and $\lambda(\sigma) > 0$ for $[0,1]$.

Theorem 2.12 *There exist a unique, well-posed weak solution of* (2.9)-(2.10), (2.12) *and* (2.21) *in the infinite rectangle for C^1 boundary data $c_i(T)$, $T > 0$. This solution vanishes in the triangle in Fig. 2.2; it is C^1 in the trapezoid, where it is given by the unique solution of the ODE's* (2.33),(2.35) *and* (2.22).

Proof: We consider the system (2.97) in the triangle $\{(X,T) : 0 \le T \le X \le 1\}$. It follows from the method of characteristics described in Section 5, Chapter 2, [40] and Section 2, Chapter 5, [26], and the initial data in (2.6) that the only solution in the triangle vanishes identically.

Let us consider bounded weak solutions of (2.1), (2.2) defined near the line $X = T$ (see Fig 2.2), in the sense of [40]. Integrating (2.2) along the segments with fixed X: $0 < X \leq 1$ from $T - \epsilon$ to $T + \epsilon$, we see that

$$\lim_{\epsilon \to 0} \{\sigma(X, T + \epsilon) - \sigma(X, T - \epsilon)\} = 0.$$

Thus (2.15) holds. Performing the same integration on (2.1) yields no new information, i.e. $c(X, T)$ on $T = X$, the upper side of the trapezoid may be non-zero; in other words, there may be a shock at $T = X$.

Now, let us focus on the infinite trapezoid $\{(X, T) : 0 \leq X \leq 1,\ T \geq X \geq 0\}$. Consider the unique C^1 solution $\sigma(X, T)$, $c(X, T)$ of (2.22) and (2.33)-(2.35) in the trapezoid. Notice that (2.18), (2.17), (2.16) and (2.14) hold, therefore (2.1)-(2.2) hold and this is a C^1 solution of system (2.1)-(2.6) in the trapezoid.

In summary, the system (2.1)-(2.6) has a unique solution on the infinite rectangle. This solution has a jump along the front $X = T$, and it is the unique global weak solution of (2.1)-(2.2) under proper initial and boundary conditions and the assumption of continuous filtration function $\lambda(\sigma)$. $\square$

Remark 2.13 *Since along the front trajectory $X = T$ the deposited concentration is zero,* (2.15) *holds, we obtain the following ordinary differential equation for $c(X, X)$ along this line in the trapezoid:*

$$\frac{dc(X, X)}{dX} = -\lambda(0) c(X, X). \tag{2.98}$$

Integrating (2.98) *and using* (2.21) *at $T = 0$, we obtain*

$$c(X, X) = c_i(0)\, e^{-\lambda(0) X}. \tag{2.99}$$

Then, from (2.99) *and since $c_i(0) > 0$, we obtain that $c(X, X)$ is positive for $X > 0$; so there is indeed a shock along the characteristic $X = T$.*

Remark 2.14 *If we take the experimental data function $c_i(t)$ to be C^2 instead of C^1, then the solution σ, c of the system* (2.1)-(2.6) *is C^2 in the trapezoid. In particular, the predicted effluent concentration $c(1, T)$ is a C^2 function.*

Remark 2.15 *The triangle $\{(X, T) : 0 \leq T < X \leq 1\}$ is the range of influence of the line $\{(X, 0) : 0 \leq X \leq 1\}$ where c and σ vanish. According to Theorem 2.12, the only solution in the triangle vanishes identically. Because of the continuity of σ along lines $X =$ constant, we actually have that $\sigma = 0$ on $\{(X, T) : 0 \leq T < X \leq 1\}$.*

Piecewise C^1 filtration function

Now, we study the case when the filtration function is C^1 except at $\sigma = \sigma_1$, where $0 < \sigma_1 \leq 1$. Moreover, $\lambda(\sigma) > 0$ for $[0, \sigma_1)$ and $\lambda(\sigma) = 0$ for $[\sigma_1, 1]$, the well-posedness of the direct problem can be proved as follows.

We solve (2.22). Since $\lambda(\sigma) \geq 0$, with $\sigma(0, 0) = 0$ we obtain that $\sigma(0, T)$ is monotone non-decreasing. Moreover, recalling that $\lambda(0) > 0$ and $c_i(0) > 0$, we have $\frac{d\sigma}{dT}(0, 0) > 0$ for small T.

It follows that $\sigma(0,T) > 0$ for $T > 0$ and $\sigma(0,T)$ is monotone increasing. Now, we have two cases: either (i) $\sigma(0,T) < \sigma_1$ for $T > 0$ or (ii) $\sigma(0,T_1) = \sigma_1$, with $\sigma(0,T) < \sigma_1$ for $T < T_1$.

In the case (i), the well-posedness of the system (2.9)-(2.10), (2.12) and (2.21) is guaranteed by Theorem 2.12.

In the case (ii), Theorem 2.12 guarantees the same results for $T < T_1$. Let us consider the point $(0,T)$ with $T < T_1$; from (2.33) we obtain that σ decreases along the characteristic lines, so $\sigma < \sigma_1$ along the characteristic lines and $\lambda(\sigma) > 0$.

Applying Gronwall's inequality to (2.33) and (2.35), we obtain that c, σ are positive along the characteristic lines, thus $\lambda(\sigma) > 0$ for $T < T_1 + X$.

For $T \geq T_1$, $\lambda(\sigma(0,T)) = 0$ as $\sigma(0,T)$ is monotone increasing on $(0,T)$. From (2.22) we obtain $\sigma = \sigma_1$. It follows that the unique solution of (2.33)-(2.35) with initial data $\sigma = \sigma_1$ and $c(0,T) = c_i(T)$ is $c(X,T) = c_i(T-X)$ and $\sigma(X,T) = \sigma_1$. Using the continuous dependence theorem of ODE, we obtain that the solution is continuous near the charateristic starting in $T = T_1 + X$. Thus, we have proved:

Lemma 2.16 *The solution of the system* (2.22), (2.33)-(2.35) *is given by* (2.33) *and* (2.35) *in the trapezoidal domain* $0 \leq X \leq 1$, $0 < T \leq X + \tau$, *here* τ *can be infinite. If it is finite,* σ *is constant and equal to* σ_1 *in the trapezoid* $0 < X + \tau \leq T$ *and* $c(X,T) = c_i(X-T)$. *Also,* c *is continuous in trapezoid* $0 \leq X \leq 1$, $T > X$ *and* σ *is continuous in the infinite rectangle* $\{0 \leq X \leq 1, 0 \leq T \leq \infty\}$.

Lemma 2.17 *The solution obtained as above is a weak solution of* (2.9)-(2.10), (2.12) *and* (2.21) *in the infinite rectangle* $\{0 \leq X \leq 1, 0 \leq T \leq \infty\}$ *for* C^1 *boundary data* $c_i(T)$, $T > 0$.

Proof: Let us denote by Ω the open subset, which is the support of $C_0^1(\Omega)$ test functions φ, ψ in the infinite rectangle $\{0 \leq X \leq 1, 0 \leq T \leq \infty\}$. We need to prove that the following integrals vanish

$$\int_\Omega \{(\varphi_T + \varphi_X)c + \varphi_T \sigma dXdT \quad \text{and} \quad \int_\Omega \{(\psi_T \sigma + \lambda(\sigma)c\psi\} dXdT, \tag{2.100}$$

for all $\varphi \in C_0^1(\Omega)$ and $\psi \in C_0^1(\Omega)$.

To do so, we divide the rectangle in three parts. the first part is the triangle $\{(X,T) : 0 \leq T \leq X \leq 1\}$. The second part is the trapezoid $\{(X,T) : 0 \leq X \leq 1,\ T \leq X + T_1\}$. The third part is the infinite trapezoid $\{(X,T) : 0 \leq X \leq 1,\ T \geq X + T_1\}$. On $\{(X,T) : 0 \leq T \leq X \leq 1\} \cap \Omega$, (2.100$a$) and (2.100$b$) vanish because $\sigma = c = 0$ in this region. Now, on $\{(X,T) : 0 \leq X \leq 1,\ T \leq X + T_1\} \cap \Omega$, using the Green's Theorem and that functions c, σ are strong solution of (2.22), (2.33)-(2.35), we obtain that (2.100a) vanishes. Using an analogous argument on $\{(X,T) : 0 \leq X \leq 1,\ T \geq X + T_1\} \cap \Omega$, (2.100$a$) vanishes in this region.

On the other hand, the integral (2.100b) on $\{(X,T) : 0 \leq X \leq 1,\ T \leq X + T_1\} \cap \Omega$ is equal to the integral (2.100b) on $\{(X,T) : 0 \leq X \leq 1,\ T \geq X + T_1\} \cap \Omega$ with opposite signal, so (2.100b) vanishes in Ω. $\square$

The uniqueness is a consequence of the following

Lemma 2.18 *The solution* σ, c *of the system* (2.1)-(2.6) *is unique on the infinite rectangle* $\{0 \leq X \leq 1, 0 \leq T \leq \infty\}$.

Proof: The integral equation method described in Section 5, Chapter 2, [63] and Section 2, Chapter 5, [26], can not be used directly on the system (2.9)-(2.10). This method was applied on a quarter of a plane, where the axes were not characteristic. In our case, they are characteristic, yet data on axes are compatible, so this is not an obstacle to the usage of that method. To do so, we take the change of variables $\xi = X - aT$, with $a > 1$ and $\eta = T$. In these variables the system of equations (2.9)-(2.10) can be rewritten as

$$\frac{\partial c}{\partial \eta} + (1-a)\frac{\partial \sigma}{\partial \xi} = -\lambda(\sigma)c, \tag{2.101}$$

and

$$\frac{\partial \sigma}{\partial \eta} = \lambda(\sigma)c. \tag{2.102}$$

In these coordinate system it is possible to apply the method of [63]. □

Chapter 3

Functional equation for the filtration function

In this chapter a method for obtaining the filtration function is studied. The inverse problem consists in determining $\lambda(\sigma)$ from the effluent particle concentration history at the core outlet $c(1,T)$, and the inlet particle concentration history $c(0,T)$ that traverses the cake. The recovery method reduces to solve a functional equation, which was derived first by Bedrikovetsky et al. ([10]) under the assumption of constant injected concentration. An inverse problem associated with a similar system was studied in [20].

The quantity $c(1,T)$ is measured in laboratory experiments. The method developed here has $c(0,T)$ constant as a particular case. Because of cake formation, $c(0,T)$ is smaller than the particle concentration of the injected fluid.

In Section 3.1 we present the method for recovering the filtration function. In Section 3.2 we discuss stability issues that are important for its numerical implementation.

3.1 Recovery method

Here we describe a recovery method based on [10] and [71]. We make the following:

Assumption 3.1 *The filtration function is a nonincreasing function of σ, such that either*
i) $\lambda(\sigma) > 0$ *for* $[0,1]$ *or*
ii) $\lambda(\sigma) > 0$ *for* $[0,\sigma_1)$ *and* $\lambda(\sigma) = 0$ *for* $[\sigma_1, 1]$, *where* $0 < \sigma_1 \leq 1$.

Case (ii), $\lambda(\sigma) = 0$ after certain point σ_1 (see e.g. Section 2.5 and Fig. 3.1) is considered because this has practical uses. More precisely, this means that no deposition occurs after certain particle volume $\sigma_1 < 1$ has been deposited. To model it, we assume the following: let us consider the maximum point σ_1, where $\lambda(\sigma_1) > 0$, obtained with the method described in this section. Then if σ_1 is smaller than one, we define the filtration function as zero for $\sigma > \sigma_1$. This approximation must be accurate, if the final time in experiment measurement is large enough to consider all the deposition process (see e.g. sensitivity analysis in Chapter 7).

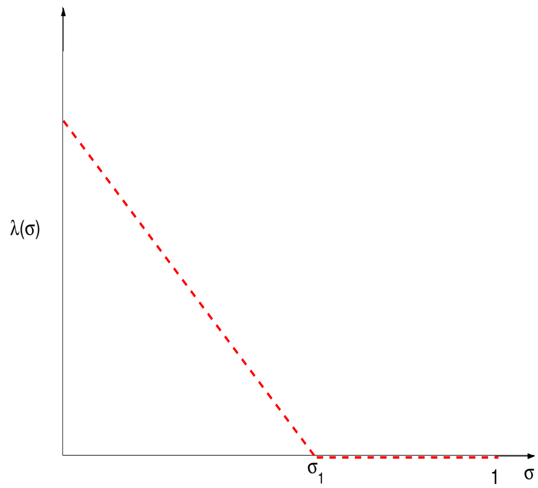

Figure 3.1: Example of filtration function

Remark 3.2 *From* (2.99) *at* $X = 1$ *we obtain*

$$c(1,1) = c(0,0)\, e^{-\lambda(0)}, \tag{3.1}$$

which will be use in Section 3.1.2 to obtain the starting value in the recovery procedure.

3.1.1 Derivation of the functional equation

It is useful to introduce the variable $z = T - 1$. Let us introduce the notation

$$c_i(z) \equiv c(0,z) > 0, \quad c_e(z) \equiv c(1, z+1) > 0 \quad \text{for} \quad z \geq 0. \tag{3.2}$$

We assume here that the experimental data c_i, c_e are C^2 functions for $0 \leq z < \infty$. Moreover, we define the function

$$\tau = C_i(z) \equiv \int_0^z c_i(s)ds, \quad \text{with} \quad 0. \leq z < \infty; \tag{3.3}$$

From (3.2) it follows that C_i in (3.3) is monotone increasing and $C_i(0) = 0$. Thus, from the implicit function theorem the inverse function $C_i^{-1}(\tau)$ exists in (3.3) and is monotone increasing.

Let us denote by

$$z = C_i^{-1}(\tau), \tag{3.4}$$

the inverse of C_i or equivalently

$$\frac{dz}{d\tau} = \frac{1}{c_i(z)}, \quad \text{with} \quad z(0) = 0. \tag{3.5}$$

Using (3.2), we define the function $C_e(z)$ as

$$C_e(z) \equiv \int_0^z c_e(s)ds, \quad \text{for} \quad 0 \leq z < \infty. \tag{3.6}$$

Let us consider the function $\Psi(\sigma)$ on $[0,1]$ or $[0,\sigma_1)$ defined in Eq. (2.13). From Assumption 3.1 and because $\Psi'(\sigma) = (\lambda(\sigma))^{-1} > 0$, there exists a function g

$$\sigma = g(\psi), \quad \text{inverse of the function} \quad \psi = \Psi(\sigma), \tag{3.7}$$

such that $g(0) = 0$. A relationship between the deposited and suspended particle concentrations at injection and exit points can be obtained by integrating Eq. (2.14) and using $\sigma(0,0) = \sigma(1,1) = 0$ (see Remark 2.15), i.e.,

$$\Psi(\sigma(0,z)) = C_i(z), \quad \Psi(\sigma(1,z)) = C_e(z). \tag{3.8}$$

Now, from (3.8) and (3.7) we obtain

$$\sigma(0,z) = g(C_i(z)) \quad \sigma(1,z) = g(C_e(z)) \quad \text{for} \quad z \geq 0. \tag{3.9}$$

Substituting the expressions in Eq. (3.9) into Eq. (2.37), we obtain the following functional equation for the function $\sigma = g(\psi)$:

$$g(C_e(z)) = \frac{c_e(z)}{c_i(z)} g(C_i(z)) \quad \text{for} \quad z \geq 0. \tag{3.10}$$

Remark 3.3 *Notice that $C_e'(z) = c_e(z)$ and $C_i'(z) = c_i(z)$ so that Eq. (3.10) may be rewritten as:*

$$g(C_e(z)) = \frac{C_e'(z)}{C_i'(z)} g(C_i(z)) \quad \textit{for} \quad z \geq 0. \tag{3.11}$$

Finally, denoting

$$D(\tau) \equiv C_e(C_i^{-1}(\tau)) \quad \text{and} \quad \theta(\tau) \equiv \frac{c_e(C_i^{-1}(\tau))}{c_i(C_i^{-1}(\tau))}, \tag{3.12}$$

Eq. (3.10) can be rewritten as

$$g(D(\tau)) = \theta(\tau) g(\tau) \quad \text{for} \quad \tau \geq 0. \tag{3.13}$$

Remark 3.4 *Notice that from* (2.94) *and the definitions in* (3.12) *we have* $0 < \theta(\tau) < 1$ *for* $\tau \geq 0$. *Moreover,* $D'(0) = \theta(0)$. *Moreover, it is possible to verify that* $D''(0) \neq 2\theta'(0)$.

The functional equation in (3.13) was studied in [71] and [72]. For constant injected concentration, $c_i(z) = c_{io}$ (3.13) reduces to Julia's equation ([72]):

$$g(D(\tau)) = D'(\tau) g(\tau) \quad \text{for} \quad \tau \geq 0. \tag{3.14}$$

The recovery method presented in [10] is based on the functional equation (3.14); a formula for the solution of (3.14) is obtained by means of an iterative procedure. In the next section an analogous formula for the solution $g(\tau)$ of (3.13) is obtained for non-constant injected concentration $c_i(T)$.

We will see that Eq. (3.10) is insufficient to solve the inverse problem; the additional value $\lambda(0)$ is needed to determine the initial value for the derivative of g, allowing to find the function $\lambda(\sigma)$. From (2.13) we obtain

$$\lambda(\sigma) = \frac{1}{\Psi'(\sigma)}, \tag{3.15}$$

and from the definition of g in (3.7) we obtain

$$\lambda(\sigma) = g^{'}(\sigma). \tag{3.16}$$

In particular $g^{'}(0) = \lambda(0)$. The initial datum $\lambda(0)$ is obtained from (3.1) and (3.2), i.e.

$$\lambda(0) = -\log(c_e(0)/c_i(0)), \tag{3.17}$$

which is well defined because c_i and c_e are positive.

Once we find the function $\sigma = g(\Psi)$ by using equation (3.11) with initial data (3.17) by solving (3.13), it is possible to find the filtration function $\lambda(\sigma)$ from Eq. (3.16). In the next section, we find the solution of the functional equation (3.13).

3.1.2 Solution of the functional equation

In this section the functional equation (3.13) is solved. We assume that the data $c_i(T)$, $c_e(T)$ is C^2, which provides sufficient smoothness for the existence of a unique C^2 solution. Sufficient conditions for the existence and uniqueness of the solution are given in [72].

Since $0 < \theta(\tau) < 1$ in Eq. (3.13) and $c_e(\tau) < 1$ for $\tau > 0$, we obtain that $D(\tau) < \tau$ for $\tau > 0$ (see Fig. 3.2). Thus, we solve the equation when $D(\tau) < \tau$ for $[0, b]$.

The following Lemma is valid ([71]).

Lemma 3.5 *Let $D : [0, b] \to [0, \infty)$ be a continuous monotone increasing function, such that $D(0) = 0$. Assume that $D(\tau) < \tau$ in $(0, b)$. Let τ_0 be a point in $(0, b)$. Consider the sequence in $[0, b]$ given by $\tau_{n+1} = D(\tau_n)$, $n = 1, 2, \dots$*

Then this sequence is monotone decreasing and it converges to 0.

Proof: Let $\tau_{n+1} = D(\tau_n) < s_n$. Since $\tau_{n+1} > 0$, $\{\tau_n\}$ is monotone decreasing and positive, so it converges to $\bar{s}$. From the continuity of D, $\tau_{n+1} = D(\tau_n)$ implies that $\bar{\tau} = D(\bar{\tau})$, so $\bar{\tau} = 0$ $\square$.

Let us define the set

$$G_0 = \{C^2[0, b] \ \text{ such that } \quad g(0) = 0\}. \tag{3.18}$$

Theorem 3.6 *Let $D : [0, b] \to [0, \infty)$ be a C^2 monotone increasing function, such that $D(0) = 0$ and $D(\tau) < \tau$ in $(0, b]$. Let $\theta : [0, b] \to (0, \infty)$ is a C^2 function, satisfying $0 < \theta(\tau) < 1$ and $\theta(0)(D^{'}(0))^2 < 1$. Furthermore consider the functional equation* (3.13) *on G_0, i.e.*

$$g\big(D(\tau)\big) = \theta(\tau) g(\tau) \quad \textit{for} \quad \tau \quad \textit{in} \quad (0, b), \tag{3.19}$$

Then the functional equation (3.19) *has a family of C^2 solutions in G_0, which differ by multiplicative constants. Moreover, the solution is uniquely defined by $g'(0)$.*

Proof: The existence of a unique C^2 solution of the functional equation (3.19) is guaranteed by Theorem 3.4.3 in [72]. Now, an iterative formula for the solution of (3.19) is presented in Theorem 5.8 in [71], which depends on an arbitrary function. Using the assumption $g'(0) \neq 0$ we find this function in next section.

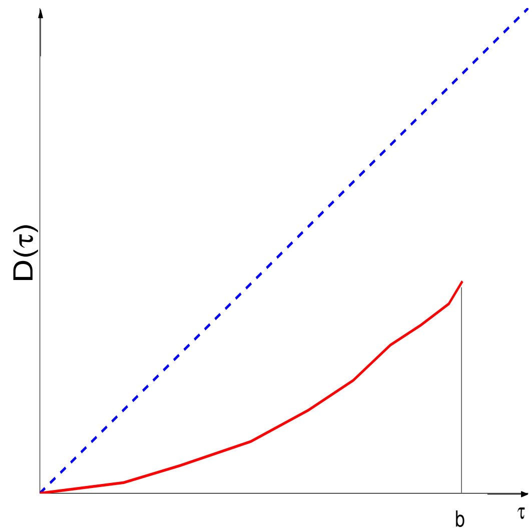

Figure 3.2: Graph of $D(\tau)$ in Lemma 3.5.

Solution of the functional equation in an interval

The functional equation (3.11) with datum (3.17) may be stated as follows: given a sufficiently smooth real-valued functions $D(\tau)$ and $\theta(\tau)$ for τ in $[0, b)$ from Section 3.1.1 for $\tau \geq 0$, with

$$D(0) = 0, \quad 0 < D'(\tau) < 1, \quad 0 < D(\tau) < \tau \quad \text{for} \quad 0 \leq \tau \leq b, \tag{3.20}$$

and

$$0 < \theta(\tau) < 1, \quad \theta^{'}(\tau) \neq 0, \quad D^{'}(0) = \theta(0) \quad \text{and} \quad D^{''}(0) \neq 2\theta^{'}(0), \tag{3.21}$$

where $1 \leq b \leq C_i(A)$. Now, from the given value $g_0' \neq 0$, we find a nonnegative function $g(\tau)$ with prescribed

$$g'(0) = g_0' \quad \text{and} \quad g(0) = 0, \tag{3.22}$$

such that

$$g(D(\tau)) = \theta(\tau)g(\tau), \quad 0 \leq \tau \leq b. \tag{3.23}$$

Let us assume that given D and θ as above, we are able to find g. We will first show that such a g is unique, by presenting an algorithm or formula for g.

Lemma 3.7 *The solution of the inverse problem* (3.20)-(3.23) *for the filtration function is unique if it exists.*

Proof: To compute $g(\tau_0)$ for any $\tau_0 > 0$, we define the two infinite sequences

$$\begin{array}{cc}
\tau_1 = D(\tau_0) & q_1 = \theta(\tau_0) \\
\tau_2 = D(\tau_1) & q_2 = \theta(\tau_1)q_1 \\
\vdots & \vdots \\
\tau_n = D(\tau_{n-1}) & q_n = \theta(\tau_{n-1})q_{n-1} \\
\vdots & \vdots
\end{array}$$

or

$$\tau_n = D^n(\tau_0) \qquad q_n = \prod_{k=0}^{n-1} \theta(\tau_k). \tag{3.24}$$

We claim that $\lim_{n\to\infty} \tau_n = 0$ monotonically. The monotonicity follows from (3.20c):

$$\tau_n = D(\tau_{n-1}) < \tau_{n-1}, \quad \text{so} \quad \tau_n < \tau_{n-1}. \tag{3.25}$$

Now, let us assume that $\tau_n \to \bar{\tau} > 0$ when $n \to \infty$. But, $\tau_n = D(\tau_{n-1})$; since D is continuous, $\bar{\tau} = D(\bar{\tau})$; Eq. (3.20a) implies that $\bar{\tau} = 0$ and the claim is established.

Notice that $\tau_1 = D(\tau_0)$ is continuous in τ_0, and so is $\tau_n = D^n(\tau_0)$. Similarly, since D' is continuous, q_n is a continuous function of τ_0. We also claim the following

Lemma 3.8 $\lim_{n\to\infty} q_n(\tau_0) = 0$ *uniformly for* $\tau_0 \in [0, c)$.

Proof: Let c be an arbitrary positive number. Since $0 < \theta(\tau) < 1$, there exist a δ and a constant ϑ, $0 < \vartheta < 1$, such that $0 < \theta(\tau) < \vartheta$ for $\tau \in [0, \delta)$. Furthermore, since $\tau_n(\tau_0)$ is continuous and $\lim_{n\to\infty} \tau_n = 0$ monotonically, there exists an index N such that $\tau_n(\tau_0) \in [0, \delta)$ for $n \geq N$. Hence

$$\tau_n(\tau_0) \in [0, \delta) \quad \text{for} \quad \tau_0 \in [0, c) \quad \text{and} \quad n \geq N. \tag{3.26}$$

We set

$$\Theta = \sup_{[0,c)} \left\{ \prod_{k=0}^{N-1} \theta(D^k(\tau)) \right\}. \tag{3.27}$$

Then from Eqs. (3.26) and (3.27) we have for $\tau_0 \in [0, c)$ and $n > N$

$$q_n(\tau_0) = \prod_{k=0}^{n-1} \theta(D^k(\tau_0)) \leq \Theta \prod_{k=N}^{N-1} \theta(D^{(k)}(\tau_0)) < \Theta \vartheta^{n-N}, \tag{3.28}$$

which shows $\lim_{n\to\infty} q_n = 0$ uniformly for $\tau_0 \in [0, c)$. $\square$

From the functional equation (3.23), it follows that

$$g(\tau_k) = g(D(\tau_{k-1})) = \theta(\tau_{k-1}) g(\tau_{k-1}) \qquad \text{or} \quad g(\tau_k) = \frac{q_k}{q_{k-1}} g(\tau_{k-1}), \tag{3.29}$$

so by repeated use of any of the two formulas above for $k = n, n-1, \cdots, 1$ we obtain

$$g(\tau_n) = g(\tau_0) \prod_{k=0}^{n-1} \theta(z_k) \quad \text{or} \quad g(\tau_n) = q_n g(\tau_0). \tag{3.30}$$

On the other hand, using Eq. (3.30), the definition of derivative, and $g(0) = 0$ from (3.22),

$$g'(0) = \lim_{n\to\infty} \frac{g(\tau_n) - g(0)}{\tau_n - 0} = \lim_{n\to\infty} \frac{g(\tau_n)}{\tau_n} \cdot \tag{3.31}$$

Substituting (3.30) in (3.31), we see that

$$g'(0) = \lim_{n\to\infty} g(\tau_0) \frac{\prod_{k=0}^{n-1} \theta(\tau_k)}{\tau_n}. \tag{3.32}$$

Thus, we obtain the solution for the functional equation (3.23) for any $\tau_0 > 0$.

$$g(\tau_0) = g_0' \lim_{n\to\infty} \frac{\tau_n}{\prod_{k=0}^{n-1}\theta(\tau_k)} \quad \text{or} \quad g(\tau_0) = g_0' \lim_{n\to\infty} \frac{\tau_n}{q_n} \cdot \tag{3.33}$$

The proof of the uniqueness theorem is complete once we show that the limit in (3.33) exists. This is proved in next theorem □.

Theorem 3.9 *(Existence): Let $D(\tau)$, $\tau \in [0,b]$ be a real nonnegative function with D' continuous, possessing the derivative D'' near 0, with D'' continuous at 0, and satisfying*

$$0 < D'(\tau) < d < 1, \quad 0 \le D(\tau) < \tau \quad \textit{for} \quad 0 \le \tau \le b; \quad D(0) = 0, \quad \textit{and} \quad D''(0) \neq 0, \tag{3.34}$$

where d is a constant. Let be θ a differentiable function such that

$$0 < \theta(\tau) < 1, \quad \theta^{'}(\tau) \neq 0, \quad \textit{for} \quad 0 \le \tau \le b, \quad D^{'}(0) = \theta(0) \quad \textit{and} \quad D^{''}(0) \neq 2\theta^{'}(0). \tag{3.35}$$

Then

(i) the functional equation $g(D(\tau)) = \theta(\tau)g(\tau)$, $0 \le \tau \le b$ with $g(0) = 0$, $g'(0) = g_0' \neq 0$ prescribed has a continuous solution, and

(ii) if D'' is continuous except at a set of τ's which does not accumulate, i.e., D'' is piecewise continuous, then g' is piecewise continuous. Also, if D'' and $\theta^{'}$ are continuous, then g' is continuous.

Proof: Let us define

$$R_n = \frac{\tau_n}{\prod_{k=0}^{n-1}\theta(\tau_k)}, \quad \rho_n = \frac{D(\tau_n)}{\theta(\tau_n)\tau_n}\cdot \tag{3.36}$$

Then

$$R_n = \frac{D(\tau_{n-1})\tau_{n-1}}{\theta(\tau_{n-1})\tau_{n-1}\prod_{k=0}^{n-2}\theta(\tau_k)} = \frac{D(\tau_{n-1})}{\theta(\tau_{n-1})\tau_{n-1}} R_{n-1} = \rho_{n-1}R_{n-1}, \tag{3.37}$$

and

$$g(\tau_0) = g_0' \prod_{n=0}^{\infty} \frac{D(\tau_n)}{\theta(\tau_n)\tau_n} \tag{3.38}$$

is the same as

$$g(\tau_0) = g_0' \prod_{n=0}^{\infty} \rho_n, \tag{3.39}$$

if this product exists. A necessary and sufficient condition for the existence of this infinite product is obtained by taking its logarithm; if the series of the logarithms converges, then the infinite product exists:

$$\sum_{n=0}^{\infty} \log \rho_n = \sum_{n=0}^{\infty} \log \frac{D(\tau_n)}{\theta(\tau_n)\tau_n} \tag{3.40}$$

is the series that will be shown to converge.

Since $\lim \tau_n = 0$, for θ is continuous and therefore uniformly continuous near 0, and because $D^{'}(0) = \theta(0) \neq 0$ from Conditions (3.34) and (3.35):

$$\rho_n = \frac{D(\tau_n)}{\theta(\tau_n)\tau_n} = \frac{\int_0^1 D^{'}(\tau_n \xi) d\xi}{\theta(\tau_n)} \tag{3.41}$$

then

$$\lim \rho_n = \frac{\int_0^1 D'(0) d\xi}{\theta(0)} = 1. \tag{3.42}$$

We know that $\lim \tau_n = 0$ monotonically, thus by further increasing N, there exists an N large enough so that for all $n > N$ we can use Taylor's formula in an interval $(0, \tau_n)$ where D'' exists. Since $D(0) = 0$, we obtain

$$D(\tau_n) = \tau_n D'(0) + \frac{\tau_n^2}{2} D''(\xi_n) \qquad \text{where} \quad 0 < \xi_n < \tau_n, \tag{3.43}$$

$$\text{and} \qquad \theta(\tau_n) = \theta(0) + \tau_n \theta^{'}(\eta_n) \qquad \text{where} \quad 0 < \eta_n < \tau_n. \tag{3.44}$$

Notice that to divide by $\theta(\tau_n)$, we need $\theta(0) \neq 0$, so, from Eqs. (3.43), (3.44) and $D^{'}(0) = \theta(0)$:

$$\rho_n = \frac{D(\tau_n)}{\theta(\tau_n)\tau_n} = \frac{\big(D'(0) + (\tau_n/2) D''(\xi_n)\big)\tau_n}{\big(D^{'}(0) + \tau_n \theta^{'}(\eta_n)\big)\tau_n} = \frac{1 + (\tau_n/2)\big(D''(\xi_n)/D'(0)\big)}{1 + \tau_n\big(\theta^{'}(\eta_n)/D^{'}(0)\big)}.$$

By further increasing N, using the continuity of $\theta^{'}$ at zero and $\theta^{'} \neq 0$, we can ensure that $|\tau_n \theta^{'}(\eta_n)| D'(0) < 1$, so that

$$\rho_n = 1 - \tau_n \frac{D''(\xi_n)/2 - \theta^{'}(\eta_n)}{D'(0)} + O(\tau_n^2).$$

Using that $\log(1 + x) = x + O(x^2)$,

$$\log \rho_n = \log \frac{D(\tau_n)}{\theta(\tau_n)\tau_n} \cong -\tau_n \frac{\big(D''(\xi_n)/2 - \theta^{'}(\eta_n)\big)}{D'(0)}. \tag{3.45}$$

Thus

$$\frac{\log \rho_n}{\log \rho_{n-1}} = \frac{\log\big(D(\tau_n)/\theta(\tau_n)\tau_n\big)}{\log\big(D(\tau_{n-1})/\theta(\tau_{n-1})\tau_{n-1}\big)} \cong \frac{-\tau_n\big(D''(\xi_n)/2 - \theta^{'}(\eta_n)\big)/D'(0)}{-\tau_{n-1}\big(D''(\xi_{n-1})/2 - \theta^{'}(\eta_{n-1})\big)/D'(0)}. \tag{3.46}$$

In (3.46) we use the fact that $D''(0) \neq 0$, $D''(0) \neq 2\theta^{'}(0)$ and that C'' and $\theta^{'}$ are continuous at zero to say that

$$\lim \frac{\log \rho_n}{\log \rho_{n-1}} = \lim \frac{\tau_n}{\tau_{n-1}} = \lim \frac{D(\tau_{n-1}) - 0}{\tau_{n-1} - 0} = D'(0) < 1, \tag{3.47}$$

from Eq. (3.20) and by the ratio criterion, this series is convergent.

Let d be a positive number between $D^{'}(0)$ and 1. From (3.47), it follows that by further increasing N, for all $n \geq N$, we have $|\log \rho_n| \leq d^n$; thus, the series (3.40) is absolutely uniformly convergent, as for all $n \geq N$ it is bounded by a geometric series and all terms are uniformly bounded for $n \leq N-1$. Thus the series converges to a continuous function, and the lemma is proven. Now if τ_n is a point where C'' is continuous, and D' is continuous at τ_n, $D^{-1}(\tau_n)$, $D^{-2}(\tau_n)$, $\cdots$,τ_0:

$$\frac{d}{d\tau_0}\log \rho_n = \left(\frac{d}{d\tau_n}\log \rho_n(\tau_n)\right)\frac{d\tau_n}{d\tau_0}\,, \tag{3.48}$$

where

$$\frac{d\tau_n}{d\tau_0} = \prod_{k=0}^{n} D'(\tau_{n-k}) \tag{3.49}$$

is continuous at τ_0 and $\frac{d}{d\tau_n}\log \rho_n(\tau_n)$ is continuous at τ_n from Eq. (3.37). We still have to show that the series with general term (3.48) is absolutely uniformly convergent near τ_0. But this is easy because $\lim_{n\to\infty}\tau_n = 0$ follows that $\lim_{n\to\infty}\theta'(\tau_n) = \theta^{'}(0)$ and $\lim_{n\to\infty}D''(\tau_n) = D^{''}(0)$. In fact, from (3.45), as $n \to \infty$, if D'' is continuous at 0 and $D''(0) \neq 0$:

$$\lim \frac{d}{d\tau_n}\log \rho_n(\tau_n) = \frac{D''(0)/2 - \theta^{'}(0)}{D'(0)}. \tag{3.50}$$

Notice that $\tau_{n-k} < \tau_0$ and the function D is monotone increasing, thus from (3.49) we obtain

$$\frac{d\tau_n}{d\tau_0} < (D'(\tau_0))^n. \tag{3.51}$$

Since $D'(\tau) < d < 1$ for $\tau \geq 0$, the series of the absolute values of the derivatives is uniformly bounded by a convergent geometric series. Thus the derivative is a continuous function, represented by the series of the derivatives.

Now that we know that the series is convergent, one verifies that the functional equation is satisfied. Once this is done, the proof of the existence theorem is complete □.

Remark 3.10 *For the Julia's equation the formula* (3.39) *reduces to*

$$g(\tau_0) = g'(0)\prod_{n=0}^{\infty}\frac{D(\tau_n)}{D'(\tau_n)\tau_n}. \tag{3.52}$$

This formula was obtained in [10].

Remark 3.11 *Once the solution g of the functional equation* (3.13) *is obtained, we can solve the direct problem* (2.1)-(2.6) *using the filtration function $\lambda(\sigma)$ determined by* (3.16) *and find $c(1,T)$. It is possible to verify, by using the method described in Section 3.1 and Theorem 3.6, that the correspondent effluent concentration function $c(1,T)$ coincides with the input data $c_e(T)$ used in the recovery procedure in (3.2b).*

Corollary 3.12 *Let $\mathcal{F}$ the set of functions such that for all $(D,\theta) \in \mathcal{F}$ the hypothesis of the Theorem* 3.9 *are valid. Let us assume that there exists a constant d_1 such that for all $(D,\theta) \in \mathcal{F}$ we have $((D''(\tau) - 2\theta(\tau))/\theta(0)) < d_1$ for all $\tau \in [0,b]$. Then solutions g of the functional equation in* (3.11) *corresponding to $(D,\theta) \in \mathcal{F}$ are uniformly bounded by $d_1 e^((1-d)^{-1})$. Moreover, the corresponding derivative functions g' are uniformly bounded by $d_1 e^(d_1/(1-d))$.*

3.2 Stabilization of the inverse problem for the filtration function

The time evolution of the hyperbolic system (2.9)-(2.10) was studied in Chapter 2, where the well-posedness of the direct problem was established. The inverse problem of determining the filtration function from the effluent concentration history was studied in Section 3.1, where we proved that problem has a unique solution. The stability of this inverse problem for non-constant inlet concentration history is studied in this section.

We state the inverse problem in the framework of operator theory. Operators are defined on an appropriate subset of Hilbert spaces where the continuous dependence of the recovered filtration function with respect to the injected and effluent concentrations is guaranteed.

We have to solve integral and differential operators that lead to ill-posed problems in several cases. Hence, we obtain sufficient conditions for our inverse problem to be well-posed in Tikhonov's sense. This study is the basis for the construction of a method for calculating numerically the approximate solution.

3.2.1 Statement of the problem

The following nonlinear nonhomogeneous hyperbolic system of equations (see Eq. (2.9) and (2.10)) simulates the filtration process in porous rock under injection of water with particles

$$\frac{\partial}{\partial T}(c+\sigma)+\frac{\partial c}{\partial X}=0, \tag{3.53}$$
$$\frac{\partial \sigma}{\partial T}=\lambda(\sigma)c, \tag{3.54}$$

with the initial condition in (2.21) and the boundary condition in (2.12). The boundary conditions consist of a given injected concentration $c_i(T)$ and a measured effluent concentration $c_e(T)$ in (3.2). The physical domain for this problem is $X \in [0,1]$, $T \in [0,A]$ with $A > 0$. Here c denotes the concentration of particles suspended in the flow and σ the concentration of retained particles in the pores.

The method for recovering the filtration function $\lambda(\sigma)$ from measurements of the injected and effluent concentration of particles, namely $c_i(z)$ and $c_e(z)$ consists on the following steps: (i) we define the functions $C_i^{-1}(\tau)$ in Eqs. (3.4) and (3.5) and $C_e(z)$ in Eq. (3.6). (ii) we obtain the solution of the nonlinear functional equation (3.13). (iii) Finally, since $\Psi(\sigma)$ is the inverse function of g in (3.13) then the filtration function $\lambda(\sigma)$ is obtained by Eq. (3.15).

Summarizing the method for obtaining the filtration function in Section 3.1 consists of the following sequence of calculations

$$\{c_i, c_e\} \to \{C_i, C_e\} \to g \to \Psi \to \lambda. \tag{3.55}$$

where "$\to$" represents a procedure to obtain output functions from the previous data. To obtain stable numerical methods to calculate the approximate solution of the filtration function, we must study the direct and inverse problem associated to Eqs. (3.6), (2.13) and (3.13). Let us introduce the following operators

$$\mathcal{A}_1 : D(\mathcal{A}_1) \subset H^1[0,A] \to L^2[0,A], \quad \mathcal{A}_1(c_e)(z) = C_e(z) = \int_0^z c_e(s)ds, \tag{3.56}$$

$$\mathcal{A}_2 : D(\mathcal{A}_2) \subset C[0,A] \to C[0,A], \quad \mathcal{A}_2(C_e)(z) = g(z), \tag{3.57}$$

where g satisfies Eq. (3.13). Let us define the operator $\mathcal{A}_3$ by

$$\mathcal{A}_3 : D(\mathcal{A}_3) \subset C[0,A] \to C[0,1], \quad \mathcal{A}_3(g) = g^{-1}, \tag{3.58}$$

where g^{-1} denotes the inverse function of g. We define the operator $\mathcal{A}_4$ by

$$\mathcal{A}_4 : D(\mathcal{A}_4) \subset L^2[0,1] \to H^1[0,1], \quad \mathcal{A}_4(\Psi)(\sigma) = \nu(\sigma), \tag{3.59}$$

where the inverse $\Psi = g^{-1}$ of the function g satisfies

$$\Psi(\sigma) = \int_0^\sigma \nu(\eta)d\eta. \tag{3.60}$$

Let us define $\lambda(\sigma) = 1/\nu(\sigma)$.

Remark 3.13 *From the corollary* 3.12 *and the method to obtain the filtration function* $\lambda(\sigma)$ *in* (3.55), *it follows that for certain classes of functions* $c_i(T)$ *and* $c_e(T)$ *described in corollary* 3.12 *the corresponding function* $\lambda(\sigma)$ *is uniformly bounded.*

We prove that the operators $\mathcal{A}_1$ and $\mathcal{A}_4$ are ill-posed. So, to obtain a conditionally well-posed problem we use the Tikhonov regularization, i.e., we obtain appropriate subsets where we guarantee the existence, uniqueness and stability of the operator equations, therefore obtaining a stable solution. To do so, we study each operator separately, finding an appropriate space to define each operator so that it has a continuous inverse. Finally, we prove that the problem of determining the filtration coefficient $\lambda(\sigma)$ from the effluent concentration $c_e(T)$ and the injected concentration $c_i(T)$ is a well-posed problem in Tikhonov's sense.

3.2.2 Well-posedness of $\mathcal{A}_1$ and $\mathcal{A}_4$

In this section we present sufficient conditions for the well-posedness of the operators $\mathcal{A}_1$ and $\mathcal{A}_4$. Since they are related with derivative operators, we summarize several results on the stabilization of the process of differentiation in Appendix E.

Well-posedness

We can see that $\mathcal{A}_1$ is an integral operator and its inverse operator is a derivative operator, while $\mathcal{A}_4$ is the derivative operator and its inverse is an integral operator.

Let us fixed the function $f_0 \in C^1[0,A]$ and let us define the subset

$$S(f_0) = \{f \in C^1[0,A] \quad \text{such as} \quad ||f - f_0||_\infty \leq r \;\; \text{and} \;\; ||f^{'} - f_0^{'}||_\infty \leq q||f - f_0||_\infty\}, \tag{3.61}$$

for some constants $r > 0$ and $q > 0$. It is easy to verify the following lemma.

Lemma 3.14 *Let $f_0 \in C^1[0, A]$ then the subset $S(f_0)$ is compact in $C[0, A]$ with the uniform norm.*

Proof: The proof is a consequence of the Arzelà -Ascoli Theorem. Notice that the family of functions in $S(f_0)$ is uniformly bounded. Moreover,

$$|f(x) - f(y)| \leq w_1|x - y|, \tag{3.62}$$

holds for all $x, y \in [0, A]$ and for all $f \in S$, where $w_1 = qr + ||f_0'||_\infty$ does not depend on f, x, y $\square$.

Let us define the subset

$$\mathcal{M}_1 = \{c_e \in C^1[0, A] : ||c_e||_\infty \leq r_1 \quad \text{and} \quad ||c_e'||_\infty \leq q_1||c_e||_\infty\} \tag{3.63}$$

for some constant $r_1 > 0$ and $q_1 > 0$. From Lemma 3.14, $\mathcal{M}_1$ is a compact subset in $C[0, A]$. The well-posedness of the operator $\mathcal{A}_1$ is a consequence of the following theorem.

Theorem 3.15 *The operator $\mathcal{A}_1 : D(\mathcal{A}_1) \subset H^1[0, A] \to L^2[0, A]$ on the subset $\mathcal{M}_1$ is well-posed in Tikhonov's sense.*

Proof: From Theorem A.6, we obtain that $\mathcal{A}_1$ is a compact operator; and from Lemma E.3 and the Lemma of Tikhonov (see Lemma A.10), we see that the inverse map of $\mathcal{A}_1$ is continuous on the subset $\mathcal{A}_1(\mathcal{M}_1)$ $\square$.

Now, we study the operator $\mathcal{A}_4$. Notice that the inverse operator $\mathcal{A}_4^{-1}$, if it is exists, is defined as an integral operator by:

$$\mathcal{A}_4^{-1} : D(\mathcal{A}_4^{-1}) \subset H^1[0, 1] \to L^2[0, 1], \quad \mathcal{A}_4^{-1}(\nu)(\sigma) = \int_0^\sigma \nu(s)ds. \tag{3.64}$$

It is known that the operator $\mathcal{A}_4^{-1}$ in (3.64) is compact and has continuous inverse on any bounded set of $H^1[0, 1]$, see Lemma E.3.

Let us denote

$$\mathcal{M}_2 = \{\nu \in C^1[0, 1] : ||\nu||_\infty \leq r_2 \quad \text{and} \quad ||\nu'||_\infty \leq q_2||\nu||_\infty\}, \tag{3.65}$$

with $r_2 > 0$ and $q_2 > 0$. The well-posedness of $\mathcal{A}_4$ is guaranteed by the following theorem.

Theorem 3.16 *The map $\mathcal{A}_4 : \mathcal{A}_4^{-1}(\mathcal{M}_2) \subset L^2[0, 1] \to H^1[0, 1]$ on the subset $\mathcal{A}_4^{-1}(\mathcal{M}_2)$ is continuous.*

Proof: From theorem A.6, we obtain that $\mathcal{A}_4^{-1}$ is a compact operator and from Lemma 3.14 and the Lemma of Tikhonov A.10 we see that $\mathcal{A}_4$ restricted to $\mathcal{A}_4^{-1}(\mathcal{M}_2)$ is continuous $\square$.

3.2.3 Well-posedness of $\mathcal{A}_2$

In [72] the stability of equation (3.11) was studied. Similar proof is presented here in the framework of the operator theory. The study of the well-posedness of $\mathcal{A}_2$ is based on Eq. (3.11). Let us consider the Banach space G_0 defined in (3.18) with the uniform norm.

Moreover, we choose for Eq. (3.11) the functions D and θ defined on $[0, b]$ satisfying the conditions (3.34) and (3.35).

Taking $s = D^{-1}(\tau)$, notice that Eq. (3.11) can be rewritten as

$$g(s) = \theta(D^{-1}(s))g(D^{-1}(s)). \tag{3.66}$$

Moreover, let us introduce the operator G on the complete space G_0 in (3.18) as

$$G : G_0 \to G_0, \quad G(g)(s) := \theta(D^{-1}(s))g(D^{-1}(s)). \tag{3.67}$$

It is possible to verify that G is continuous and $G(G_0) \subset G_0$.

Now, clearly Eq. (3.11) (or equivalently (3.66)) has a solution in G_0 if the operator G has a fixed point in G_0. This result follows from the following:

Lemma 3.17 *The operator G in* (3.67) *is contractive in G_0.*

Proof: Let g_1 and g_2 in G_0. It is possible to verify that

$$||G(g_1) - G(g_2)||_\infty \leq \max_{[0,b]}\{\theta(s)\}||g_1 - g_2||_\infty. \tag{3.68}$$

Since θ is continuous on $[0, b]$ and $0 < \theta(\tau) < 1$ for all $\tau \in [0, b]$ then there exists a constant $d < 1$ such that $\max_{[0,b]}\{\theta(s)\} < d < 1$ $\square$.

From the Lemma 3.17 above and the Banach Fixed-Point Theorem there exists a unique fixed point of the operator G in (3.67) on G_0. Notice that the result above is the same as in Lemma 3.7 and Theorem 3.9. However, with the latter result obtained using the Banach Fixed-Point Theorem, we also gain a stability condition for (3.13). The constructive proof in Lemma 3.7 is useful because it provides a procedure to determine the solution numerically.

Stability

Now we prove that Eq. (3.11) is locally well-posed. Let define the closed subset

$$\mathcal{N}_1 = \{(D, \theta) \in C^2([0, b]) \times C^2([0, b]) \quad \text{satisfying} \quad (3.34) \quad \text{and} \quad (3.35)\}. \tag{3.69}$$

Let us consider the sequences $\{D_n, \theta_n\} \subset \mathcal{N}_1$, such that $\{D_n, \theta_n\} \to \{\hat{D}, \hat{\theta}\}$ in $\mathcal{N}_1$. Let G be the operator in (3.67) defined by $\hat{D}$ and $\hat{\theta}$, and let $\hat{g}$ be the unique fixed point of G on G_0. Now, we define the family of operators in G_0 as follows

$$G_n : \mathcal{N}_1 \to \mathcal{N}_1, \quad G_n(g)(s) := \theta_n(D_n^{-1}(s))g(D_n^{-1}(s)). \tag{3.70}$$

It is possible to verify that G_n, $n = 1, 2, \ldots$ in (3.70) are continuous, $G_n(G_0) \subset G_0$ and $||G_n|| < 1$. Thus repeating the argument of Lemma (3.17), each operator G_n has a unique fixed point g_n on G_0. Moreover the following result is valid.

Lemma 3.18 *The limit $G_n \to G$ holds in G_0.*

Proof: It follows from

$$G_n g - Gg = (\theta_n - \hat{\theta})g(D_n) + \hat{\theta}(g(D_n) - g(\hat{D}))\square. \tag{3.71}$$

Finally, the following lemma is true.

Lemma 3.19 *It is valid that* $\lim g_n = \hat{g}$.

Proof: It is possible to verify that

$$||g_n - \hat{g}||_\infty \leq ||(I - G_n)^{-1}|| \;\; ||G_n - G|| \;\; ||\hat{g}||_\infty. \tag{3.72}$$

Since $||G_n|| < 1$, from the uniform boundedness principle, we obtain that $||G_n|| < \sup\{||G_n||\} = q < 1$. From Theorem 3, pag. 154 in [64] it follows that $(I - G_n)^{-1}$ exists and $||(I - G_n)^{-1}||$ is uniformly bounded by $1/(1-q)$; since $||G_n - G|| \to 0$, it follows that $||g_n - \hat{g}||_\infty \to 0$ $\square$.

Stability estimates

Let us define the subsets

$$\mathcal{M}_3 = \{c_e \in C^2[0, A] : ||c_e||_\infty \leq r_3 \quad \text{and} \quad ||c_e^{'}||_\infty \leq q_3||c_e||_\infty\}, \tag{3.73}$$

$$\mathcal{M}_4 = \{c_i \in C^2[0, A] : ||c_i||_\infty \leq r_4 \quad \text{and} \quad ||c_i^{'}||_\infty \leq q_4||c_i||_\infty\} \tag{3.74}$$

for certain constants $r_3 > 0$, $q_3 > 0$, $r_4 > 0$ and $q_4 > 0$. Moreover, we assume that for all $c_e \in \mathcal{M}_3$ and $c_i \in \mathcal{M}_4$, $c_e(z), c_i(z) > 0$ for all $z \in [0, A]$ and $c_e^{'}(z), c_i^{'}(z) \neq 0$ for $z \in [0, A]$. Let c_e and c_i in $\mathcal{M}_3$ and $\mathcal{M}_4$ respectively. Let us define C_e and C_i as in (3.56) and (3.3) respectively. Then the well-posedness of $\mathcal{A}_2$ is a consequence of the following lemma.

Lemma 3.20 *Let* C_{e1} *and* C_{e2} *in* $\mathcal{A}_1(\mathcal{M}_3)$ *and* C_{i1}, C_{i2} *in* $\mathcal{A}_1(\mathcal{M}_4)$ *such that* $C_{e1} - C_{e2} \in \mathcal{A}_1(\mathcal{M}_3)$ *and* $C_{i1} - C_{i2} \in \mathcal{A}_1(\mathcal{M}_4)$. *Let us assume that the functions*

$$D_1(z) \equiv C_{e1}(C_{i1}^{-1}(z)), \;\; D_2 \equiv C_{e2}(C_{i2}^{-1}(z)) \tag{3.75}$$

and

$$\theta_1(z) \equiv \frac{C_{e1}^{'}(C_{i1}^{-1}(z))}{C_{i1}^{'}(C_{i1}^{-1}(z))}, \quad \theta_2(z) \equiv \frac{C_{e2}^{'}(C_{i2}^{-1}(z))}{C_{i2}^{'}(C_{i2}^{-1}(z))} \tag{3.76}$$

satisfy conditions (3.34) *and* (3.35). *Let us denote by* g_1, g_2 *solutions of Eq.* (3.13) *corresponding to* (D_1, θ_1) *and* (D_2, θ_2) *respectively, i.e.,*

$$g_1(C_{e1}(z)) = \frac{C_{e1}^{'}(z)}{C_{i1}^{'}(z)} g_1(C_{i1}(z)) \quad \text{for} \quad z \geq 0, \tag{3.77}$$

$$g_2(C_{e2}(z)) = \frac{C_{e2}^{'}(z)}{C_{i2}^{'}(z)} g_2(C_{i2}(z)) \quad \text{for} \quad z \geq 0, \tag{3.78}$$

and $g_1(0) = g_2(0) = 0$ *and* $g_1^{'}(0), g_2^{'}(0) \neq 0$ *for all* $z \in [0, A]$. *Then there exist constants* v_1 *and* v_2 *that not depend of* g_1, g_2, C_{e1}, C_{e2}, C_{i1}, *and* C_{i2}, *such that*

$$\sup_{z \in [0,A]} |g_1(z) - g_2(z)| \leq v_1 \sup_{z \in [0,A]} |C_{e1}^{'}(z) - C_{e2}^{'}(z)| \tag{3.79}$$

and

$$\sup_{z \in [0,A]} |g_1(z) - g_2(z)| \leq v_2 \sup_{z \in [0,A]} |C_{i1}^{'}(z) - C_{i2}^{'}(z)|. \tag{3.80}$$

Proof: We prove here (3.79), the proof for (3.80) is similar. Let $z = C_{i1}^{-1}(\tau)$ and $z = C_{i2}^{-1}(\tau)$ be defined in Eq. (3.4). We obtain

$$|g_1(z) - g_2(z)| = |g_1(C_{i1}^{-1}(\tau)) - g_2(C_{i2}^{-1}(\tau))|. \tag{3.81}$$

Using (3.77)-(3.11) we obtain

$$|g_1(z) - g_2(z)| = \left| \frac{g_1(C_{e1}(C_{i1}^{-1}(\tau))C_{i1}'(C_{i1}^{-1}(\tau))}{C_{e1}'(C_{i1}^{-1}(\tau))} - \frac{g_2(C_{e2}(C_{i2}^{-1}(\tau))C_{i2}'(C_{i2}^{-1}(\tau))}{C_{e2}'(C_{i2}^{-1}(\tau))} \right|. \tag{3.82}$$

Taking

$$N_1 = \sup\{ \max_{[0,C_{i1}(A)]} g_1(C_{e1}(C_{i1}^{-1}(\tau)), \max_{[0,C_{i2}(A)]} g_2(C_{e2}(C_{i2}^{-1}(\tau))\}, \tag{3.83}$$

and

$$N_2 = \sup\{ \max_{[0,C_{i1}(A)]} C_{i1}'(C_{i1}^{-1}(\tau)), \max_{[0,C_{i2}(A)]} C_{i2}'(C_{i2}^{-1}(\tau))\}, \tag{3.84}$$

we obtain

$$|g_1(z) - g_2(z)| \leq N_1 N_2 \left| \frac{1}{C_{e1}'(C_{i1}^{-1}(\tau))} - \frac{1}{C_{e2}'(C_{i2}^{-1}(\tau))} \right|. \tag{3.85}$$

So, defining $N_3 = \max\limits_{[0,C_{e1}(A)]} \left\{ \frac{1}{C_{e1}'(C_{e1}^{-1}(\tau))} \right\} \times \max\limits_{[0,C_{e2}(A)]} \left\{ \frac{1}{C_2'(C_{e2}^{-1}(\tau))} \right\}$ and $t_1 = N_1 N_2 N_3$, we obtain

$$\sup_{z\in[0,A]} |g_1(z) - g_2(z)| \leq t_1 \sup_{z\in[0,A]} |C_{e1}'(z) - C_{e2}'(z)|. \tag{3.86}$$

Finally, we must prove that there exists a constant v_1 independent of C_{e1}, C_{e2}, C_{i1}, C_{i2}, g_1 and g_2 such that $t_1 \leq v_1$. Since the subsets $\mathcal{M}_3$ and $\mathcal{M}_4$ consist of uniformly bounded functions and $C'(z) \neq 0$ for all $z \in [0, A]$, there exist constants n_2 and n_3 independent of C_{i1}, C_{i2}, C_{e1} and C_{e2} such that

$$N_2 \leq n_2 \quad \text{and} \quad N_3 < n_3. \tag{3.87}$$

Now, from Corollary 3.12 (see Section 3.1) we obtain that the solutions g_1 and g_2 of Eqs. (3.77)-(3.78) respectively are continuous and uniformly bounded, i.e., there exist constants $m_1 > 0$ and $m_2 > 0$ that do not depend on C_{e1}, C_{e2}, C_{i1}, C_{i2}, g_1 and g_2 such that the following inequalities hold

$$0 \leq g_1(z) \leq m_1, \quad \text{for} \quad z \in [0, A], \tag{3.88}$$

$$0 \leq g_2(z) \leq m_2, \quad \text{for} \quad z \in [0, A], \tag{3.89}$$

for all solutions g_1 and g_2 of Eqs. (3.77)-(3.78) respectively. Let $n_3 = \max\{m_1, m_2\}$. Finally, setting $v_1 = n_1 n_2 n_3$ we obtain the inequality (3.79) $\square$.

In Section 3.1 we proved that the solution of the functional equation (3.13) exists and is unique. Thus from Lemma 3.20 we conclude that the operator $\mathcal{A}_2$ is well-posed on $\mathcal{M}_3$ and $\mathcal{M}_4$ defined in Eqs. (3.73) and (3.74).

3.2.4 Well-posedness of $\mathcal{A}_3$

The well-posedness of $\mathcal{A}_3$ is proved in the following Lemma.

Lemma 3.21 *The operator $\mathcal{A}_3$ and $\mathcal{A}_3^{-1}$ are bounded.*

Proof: The well-posedness is a consequence of the Closed Graph theorem and the fact that if $g_n \to g$ then $(g_n)^{-1} \to (g)^{-1}$ $\Box$.
From Lemma 3.21 we obtain that it is possible to obtain the inverse in a stable way.

Remark 3.22 *Notice that the stability condition of $C_e(z)$ in the operator $\mathcal{A}_1$ is valid for $C_i^{-1}(\tau)$ in* (3.4)*. Moreover, changes in $c_i(T)$ imply changes in the function $D(\tau)$ and $\theta(\tau)$ in* (3.12)*, therefore the stability with respect $c_i(T)$ follows from the well-posedness of the operators $\mathcal{A}_1$ and $\mathcal{A}_2$.*

3.2.5 Well-posedness of the inverse problem

Now, we prove that the filtration function can be obtained in a stable way from the effluent concentration using the procedure described in Section 3.1. To do so, we restrict the possible input data to a certain function class. This restriction of the feasible solution is sufficient to include many practical situations.
Let us denote by

$$\mathcal{M}_1 = \{c_e \in C^2[0, A] : ||c_e||_\infty \le r \quad \text{and} \quad ||c_e^{'}||_\infty \le q||c_e||_\infty\}, \tag{3.90}$$

for some positive constant r and q. The above mentioned result is stated in the following theorem.

Theorem 3.23 *Let $c_i(z)$ and $c_e(z)$ be the inlet and effluent concentrations respectively. Assume that c_i, c_e belong to the class of the functions S with the properties*
i) $S \subset \mathcal{M}_1$,
ii) there exist a positive number d between 0 *and* 1 *such that $0 < c_e(z) < d < 1$ for $z \in [0, A]$ and for all $c_e \in S$.*
Let c_{e1} and c_{e2} satisfy conditions (i),(ii) as well as $c_{e1} - c_{e2} \in \mathcal{M}_1$. Let us denote by λ_1 and λ_2 the filtration function obtained from c_{e1} and c_{e2} using the method described in Section 3.2.1*. Then the following inequality holds*

$$||\lambda_1(\sigma) - \lambda_2(\sigma)||_{H^1[0,1]} \le r_2 \sup_{z\in[0,A]} |c_{e1}(z) - c_{e2}(z)|. \tag{3.91}$$

Proof: Let us define Φ_1 and Φ_2 as follows

$$\Phi_1(\sigma) = \int_0^\sigma \frac{d\eta}{\lambda_1(\eta)} \quad \text{and} \quad \Phi_2(\sigma) = \int_0^\sigma \frac{d\eta}{\lambda_2(\eta)}. \tag{3.92}$$

From Remark 3.13 and Theorem 3.16 there exists a constant v_1 such that

$$\left|\left|\frac{1}{\lambda_1(\sigma)} - \frac{1}{\lambda_2(\sigma)}\right|\right|_{H^1[0,1]} \le v_1||\Phi_1 - \Phi_2||_2. \tag{3.93}$$

Since λ_1 and λ_2 are continuous positive functions then Φ_1 and Φ_1 are continuous and positive as well. Therefore we have

$$||\Phi_1 - \Phi_2||_2 < ||\Phi_1 - \Phi_2||_\infty. \tag{3.94}$$

Let us define

$$C_{e1}(z) = \int_0^z c_{e1}(\tau)d\tau \quad \text{and} \quad C_{e2}(z) = \int_0^z c_{e2}(\tau)d\tau, \tag{3.95}$$

and let g_1 and g_2 be the solutions of Eq. (3.13) corresponding to C_{e1} and C_{e2}. Now, using Lemma 3.21 there exists a constant v_2 such that

$$||\Phi_1 - \Phi_2||_\infty \leq v_2||g_1 - g_2||_\infty, \tag{3.96}$$

where g_1 and g_2 are the inverses of Φ_1 and Φ_2 respectively. From Lemma (3.20) there exists a constant v_3 such that

$$||g_1 - g_2||_\infty \leq v_3||C_{e1}^{'} - C_{e2}^{'}||_\infty. \tag{3.97}$$

Finally, from Eq. (3.93)-(3.97) we obtain

$$||\lambda_1(\sigma) - \lambda_2(\sigma)||_{H^1[0,1]} \leq \left(\sup_{\sigma\in[0,1]}(\lambda_1(\sigma)\lambda_2(\sigma)) + \sup_{\sigma\in[0,1]}(\lambda_1^{'}(\sigma)\lambda_2^{'}(\sigma))\right) v_1v_2v_3||c_{e1} - c_{e2}||_\infty. \tag{3.98}$$

From Remark 3.13 and Theorem 3.16 the functions λ and $\lambda^{'}$are uniformly bounded, thus there exist constants v_4 and v_5 that do not depend on λ_1 and λ_2 such that

$$\sup_{\sigma\in[0,1]}(\lambda_1(\sigma)\lambda_2(\sigma)) < v_4, \tag{3.99}$$

$$\sup_{\sigma\in[0,1]}(\lambda_1^{'}(\sigma)\lambda_2^{'}(\sigma)) < v_5. \tag{3.100}$$

Taking $r_2 = v_1v_2v_3v_4v_5$, we obtain (3.91) $\square$.

Chapter 4

The inverse problem for the porous rock damage function

In this chapter we study the inverse problem of determining the damage function from a given pressure history, assuming that the filtration function has already been found. The available boundary and initial conditions are also used of course.

The recovery method consists in solving an integral equation of Volterra type for the damage function $k(\sigma)$. We discuss conditions for well-posedness of the operator equation, using the methodology described in [105], [81], [29], [70], [94] and [109] for solving integral equations of the first kind.

The classical method of Tikhonov is used to reduce an ill-posed Volterra equation of the first kind into a well posed problem. Numerical implementation requires that it belongs to an appropriate subset of feasible solutions. We need to find the solution of the linear system of equations obtained by discretizing the continuous equation. Optimization and LU factorization methods are useful in finding the solution of the resulting system.

Also, regularization parameters need to be determined as an important part of the regularization methods ([34], [47], [86], [105]). To do so, the discrepancy principle and the L-curve method are used.

4.1 The integral equation

Let us subdivide the physical domain $\mathcal{D} = [0,1] \times [0,A]$ into two parts $\mathcal{D} = \mathcal{D}_+ \cup \mathcal{D}_0$, where

$$\mathcal{D}_+ = \{(X,T) \in \mathcal{D} \text{ such that } X > T\}, \tag{4.1}$$

$$\mathcal{D}_0 = \{(X,T) \in \mathcal{D} \text{ such that } X \leq T\}. \tag{4.2}$$

The behavior of $\sigma(X,T)$ in each of these two subsets is assumed to be different, i.e., $\sigma(X,T)$ is continuously differentiable in each subset, $\sigma(X,T) = 0$ in $\mathcal{D}_0$ and $\sigma(X,T) > 0$ in $\mathcal{D}_+$.

Eq. (2.11) with $m_p = 1$ can be rewritten as

$$\int_0^1 f(\sigma(X,T))dX = g(T), \quad \text{for all} \quad T \in [0,A], \tag{4.3}$$

where $f(\sigma)$ is an unknown continuous function and $g(T)$ is a given non-negative continuous function. Actually, we know the values of $\sigma(X,T_j)$ and $\Delta p(T_j)$ only for each T_j with $j = 1,\ldots,m$ and $T_j \in [0,A]$. We take $T_1 < T_2 \ldots < T_{m-1} < T_m$. Substituting these T_j, with $j = 1,\ldots,m$ in Eq. (2.11), we obtain the system of integral equations

$$\int_0^1 \frac{1}{k(\sigma(X,T_j))} dX = \Delta p(T_j), \; j = 1,\ldots,m. \tag{4.4}$$

Taking into account the notation used in Eqs. (4.3) and (4.4), we have

$$g(T_j) = \Delta p(T_j), \qquad f(\sigma(X,T_j)) = \frac{1}{k(\sigma(X,T_j))}, \quad j = 1,\ldots,m. \tag{4.5}$$

Thus, we begin the study by describing the method for finding the general solution in the continuous case. Then we show how to solve the problem for given discrete data in numerical calculations.

The physics dictates that $0 \leq \sigma < 1$ (see Chapter 2). Let us define

$$M = \max_{\mathcal{D}} \sigma(X,T). \tag{4.6}$$

Assumption 4.1 *In this work, we focus on the case where the function $\sigma(X,T)$ satisfies $\sigma(X,T) = 0$ on D_0 and the following inequalities hold*

$$-\epsilon_1 < \frac{\partial \sigma(X,T)}{\partial X} < -\epsilon_2 < 0 \tag{4.7}$$

uniformly on characteristic lines $X - T = constant$.

Assumptions 4.1 arise naturally in the physical model (see Remark 2.1). Notice that, as a consequence, the derivative $\frac{\partial \sigma(X,T)}{\partial X}$ is uniformly bounded on D_+. We know from the physics that the solution f of (4.3) must be a positive, non-decreasing continuous function. This information is very useful for finding a class of functions where Eq. (4.3) is well-posed. Thus, in order to find a function $f : [0,M] \to [0,\infty)$ that satisfies equation (4.3) using the information above, we analyze the inverse problem associated to the integral operator

$$K_\sigma \; : \; L^2[0,M] \; \to L^2[0,A], \tag{4.8}$$

defined as

$$(K_\sigma f)(T) = \int_0^1 f(\sigma(X,T)) dX, \quad \text{for} \quad 0 \leq T \leq A. \tag{4.9}$$

Thus, the problem can be formulated as the linear operator equation

$$K_\sigma f = g, \tag{4.10}$$

where K_σ is a continuous linear operator from the Hilbert space $L^2[0,M]$ to $L^2[0,A]$. We want to obtain a procedure to approximate the inverse operator K_σ^{-1}. For this purpose, the issues of existence, uniqueness and stability of Eq. (4.10) must be studied.

Typical examples satisfying Assumptions 4.1 are given by the analytical solution of the system in Eqs. (2.9), (2.10) shown in Eqs. (2.58), (2.59). The recovery strategy requires additional information about the solution such as smoothness, as well as the value of the solution at the boundaries, i.e. $f(0)$ and $f(M)$. Because $k(0) = 1$, we see that $f(0) = 1$. On the other hand, the value $f(M)$ must either be obtained from laboratory measurement or be evaluated numerically.

Using the fact that the function $\sigma(X,T)$ is continuously differentiable on $\{0 \leq X \leq 1\}$, for each T fixed, Assumption 4.1 and the implicit function theorem, it follows that it is possible to obtain the inverse function $X = \sigma^{-1}(y,T) = s(y,T)$ of $y = \sigma(X,T)$ restricted to $\mathcal{D}_+$.

Now, we reformulate the problem in Eq. (4.3) as a Fredholm integral equation of the first kind. Since $\sigma(X,T) = 0$ on $\mathcal{D}_0$, Eq. (4.3) can be rewritten as

$$\int_0^T f(\sigma(X,T))dX + \int_T^1 f(0)dX = g(T), \quad \text{for all} \quad T \leq 1, \tag{4.11}$$

and

$$\int_0^1 f(\sigma(X,T))dX = g(T), \quad \text{for all} \quad T > 1. \tag{4.12}$$

Because $\frac{\partial\sigma(X,T)}{\partial X} \neq 0$ on D_+, we can change variables $y = \sigma(X,T)$ in the first integral on the left hand side of Eqs. (4.11) and (4.12). These equations can be rewritten as

$$\int_{\sigma(T,T)}^{\sigma(0,T)} \left[-\frac{\partial\sigma}{\partial X}(s(y,T),T)\right]^{-1} f(y)dy = g(T) + (T-1)f(0), \quad \text{for all} \quad T \leq 1, \tag{4.13}$$

and

$$\int_{\sigma(1,T)}^{\sigma(0,T)} \left[-\frac{\partial\sigma}{\partial X}(s(y,T),T)\right]^{-1} f(y)dy = g(T), \quad \text{for all} \quad T > 1. \tag{4.14}$$

Using that $f(0) = 1$ we define the function

$$h(T) = \begin{cases} g(T) + (T-1) & \text{if} \quad T \leq 1; \\ g(T) & \text{if} \quad T > 1, \end{cases}$$

and write the kernel $K_\sigma(y,T)$ as

$$K_\sigma(y,T) = \begin{cases} 0 & \text{if} \quad \sigma(0,T) < y \leq M; \\ \left[-\frac{\partial\sigma}{\partial X}(s(y,T),T)\right]^{-1} & \text{if} \quad \sigma(\min\{1,T\},T) < y \leq \sigma(0,T); \\ 0 & \text{if} \quad 0 \leq y \leq \sigma(\min\{1,T\},T). \end{cases} \tag{4.15}$$

Then Eqs. (4.13) and (4.14) can be rewritten compactly as

$$(K_\sigma f)(T) = \int_0^M K_\sigma(y,T)f(y)dy = h(T), \quad \text{with} \quad T \in [0,A]. \tag{4.16}$$

A similar integral equation was obtained in [8]. Notice that the function K_σ is bounded due to Assumption 4.1 (see Eq. (4.7)). So the kernel $K_\sigma(y,T)$ belongs to $L^2([0,M] \times [0,A])$, thus K_σ is a Hilbert-Schmidt operator, and therefore K_σ defines a compact operator from $L^2[0,M]$ to $L^2[0,A]$.

Remark 4.2 *In the triangle $\{(X,T) : T \leq X \leq 1\}$, there exists no experimental information on the deposited particle concentration $\sigma(X,T)$. So, in the discretization of the integral operator K_σ the values of $\sigma(X,T)$ for $T < 1$ can be neglected. Thus, the kernel $K_\sigma(y,T)$ takes the form*

$$K_\sigma(y,T) = \begin{cases} 0 & \text{if} \quad \sigma(0,T) < y \leq M; \\ \left[-\frac{\partial\sigma}{\partial X}(s(y,T),T)\right]^{-1} & \text{if} \quad \sigma(1,T) < y \leq \sigma(0,T); \\ 0 & \text{if} \quad 0 \leq y \leq \sigma(1,T). \end{cases} \tag{4.17}$$

This simplification is useful for the numerical solution of the integral equation. However, in the theory development, we take $T \in [0,A]$.

It is easy to verify that the adjoint operator K_σ^* of K_σ is given by

$$(K_\sigma^* g)(y) = \int_0^A K_\sigma(y,T)g(T)dT, \tag{4.18}$$

where K_σ^* is defined from $L^2[0,A]$ to $L^2[0,M]$.

4.2 Conditions for existence, uniqueness and stability

In this section we show that the inverse problem given by Eq. (4.16) is not well-posed. By means of regularization methods, we transform this problem into a well-posed problem and we present an algorithm to obtain its solution.

4.2.1 Ill-posedness of the inverse problem

It is known that the inverse of a compact operator with an infinite dimensional domain is not continuous. Thus, the inverse problem given by the integral equation (4.16) is not well-posed.

To find the solution, or at least an approximation of the solution, we need to find an appropriate subset contained in a class of feasible solutions that includes additional information such as smoothness and positivity to ensure uniqueness. We choose our set of feasible solution as

$$\mathcal{F} = \{f \in L^2[0,M]; f \text{ is non-decreasing and } 0 \leq f(x) \leq B \ \text{ a.e. in } \ [0,M]\}, \tag{4.19}$$

where B is a constant that does not depend on x and f; here a.e. means "almost everywhere".

To obtain a solution of Eq. (4.16) in $\mathcal{F}$ we should keep in mind several issues. One is that the solution may not exist if the function g on the right hand side behaves too roughly. For example, since the kernel K_σ and the set of feasible solutions $\mathcal{F}$ are non-negative functions, g is necessarily a non-negative function. More precisely, we need that the function g belongs to $K_\sigma(\mathcal{F})$.

Thus, to find a solution or a quasi-solution of the ill-posed problem in (4.18) we have to define existence, uniqueness and stability aspects that are meaningful in this case. These aspects are intimately connected not only to the operator K_σ: $X \to Y$, but also to the domain space X and the image space Y. That is, well-posedness is a property of the triplet (K_σ, X, Y).

To solve approximately the inverse problem associated to Eq. (4.16) (i.e., to obtain an approximate solution), we prove that our problem is well-posed in Tikhonov's sense (see Definition A.11).

Existence and uniqueness

We denote by $(\cdot,\cdot)$ the inner product in $L^2[0, M]$, i.e.

$$(f, g) = \int_0^M f(x)g(x)dx. \tag{4.20}$$

Let us denote by

$$N(K_\sigma)^\perp = \{f \in L^2[0, M] \text{ such that } (f, g) = 0 \quad \text{for all} \quad g \in N(K_\sigma)\}, \tag{4.21}$$

where

$$N(K_\sigma) = \{h \in L^2[0, M] \text{ such that } K_\sigma h = 0\}. \tag{4.22}$$

The existence and uniqueness are guaranteed by the following

Theorem 4.3 *Let us take $X = N(K_\sigma)^\perp$ and $Y = K_\sigma(X)$. Then Eq.* (4.16) *has a solution and it is unique.*

Proof: Clearly for existence we must have $Y = K_\sigma(X)$, because with this choice the mapping $K_\sigma : X \to Y$ is surjective. The uniqueness condition is equivalent to injectivity of K_σ. This is not a serious restriction since we can take the domain X as the orthogonal complement of the null space $N(K_\sigma)$ of the operator K_σ $\square$.

Stability

Stability is a consequence of the Lemma of Tikhonov (see Lemma A.10).

Remark 4.4 *Frequently, restrictions of the form $\phi_1(x) \leq f(x) \leq \phi_2(x)$ (where $\phi_1(x)$ and $\phi_2(x)$ are given functions) are imposed to define the set of feasible solutions $\mathcal{F}$ that we are seeking. For example, in our case the feasible solutions must be the set of non-negative functions uniformly bounded by some constant B, so $\phi_1(x) \equiv 0$ and $\phi_2(x) = B$. According to Helly's choice theorem (see* [61], *page* 45*), this subset $\mathcal{F}$ of feasible solutions is compact (see* [43]*).*

Keeping in mind Remark 4.4, the following theorem holds.

Theorem 4.5 *The inverse problem in* (4.16) *is well-posed on $\mathcal{F}$ in Tikhonov's sense.*

Proof: The existence and uniqueness are guaranteed by Theorem 4.3. On the other hand, notice that the subset of feasible solutions $\mathcal{F}$ in Eq. (4.19) is contained in the domain X because if $f \in \mathcal{F}$ and $K_\sigma f = 0$ then $f \equiv 0$. Since $\mathcal{F}$ is a compact subset (see Remark 4.4) the Lemma of Tikhonov guarantees that the mapping $K_\sigma : \mathcal{F} \to Y$ is continuous and has continuous inverse $\square$.

4.2.2 Regularization method

Following the Tikhonov regularization method, we transform the integral equation of the first kind (4.16) into a well-posed Volterra-type integral equation.

The idea in the Tikhonov regularization is to define the best fit as possible solution, i.e., to find $f \in \mathcal{M}$ that minimizes the deviation $||K_\sigma f - g||$ in the $L^2[0, M]$ norm. We recall that the subset $\mathcal{M}$ is infinite dimensional and the operator K_σ is compact, so this minimization problem is ill-posed. Thus, we need to penalize the deviation in the sense of optimization theory, that is, we must obtain a solution by minimizing Tikhonov's functional

$$\Phi_\alpha(f) = ||K_\sigma f - h||^2 + \alpha||f||^2, \tag{4.23}$$

with $f \in L^2[0, M]$ and $\alpha > 0$. Here the term $||f||^2$ is used as a penalization for the square error $||K_\sigma f - h||^2$. This is a way for regularizing the ill-posed problem in (4.16). The existence of the optimal f is guaranteed by the following theorem.

Theorem 4.6 *Let $K : X \to Y$ be a linear bounded operator between Hilbert spaces and $\alpha > 0$. Then the Tikhonov functional Φ_α has a unique minimum $f_\alpha \in X$. This minimum f_α is the unique solution of the normal equation*

$$\alpha f_\alpha + K^* K f_\alpha = K^* h. \tag{4.24}$$

Theorem 4.6 remains valid on the subset $\mathcal{F}$ (see [105], page 165), and the solution of the optimization problem over the subset $\mathcal{F}$ is given by

$$\alpha f_\alpha + K_\sigma^* K_\sigma f_\alpha = K_\sigma^* h. \tag{4.25}$$

The solution of Eq. (4.25) can be rewritten as $f_\alpha = R_\alpha g$, with the regularization operator defined as

$$R_\alpha : Y \to X, \qquad R_\alpha = (\alpha I + K_\sigma^* K_\sigma)^{-1} K_\sigma^*. \tag{4.26}$$

Eq. (4.25) is a well-posed Volterra-type integral equation. Moreover, $f_\alpha \to f$ as $\alpha \to 0$, in the norm of the Hilbert space X.

We will see that the term $||f||^2$ for penalizing the Tikhonov functional in (4.23) is not sufficient for regularizing the inverse problem in (4.16). In Section 4.2.4, we introduce another penalization function that solves this difficulty.

Now we present some useful methods for estimating the regularization parameter α.

4.2.3 Choice of regularization parameter value

To solve the optimization problem in the regularization method, it is necessary to estimate the regularization parameter α in Eq. (4.23). There are many strategies in order to guarantee optimal convergence of the regularized solution starting from data polluted by errors ([66], [70], [95], [86] and [105]). In this work we combine the discrepancy principle and the L-curve methods for choosing the regularization parameter value. In this way we show how to obtain the approximate solution when the tolerance of the possible solution is specified.

The difficulty of the discrepancy principle method is that we need to know a priori information about the deficiency of the possible solution. Another useful tool is the L-curve method, which does not require a priori tolerance specification.

So, the strategy is the following. First, we obtain an approximate initial solution, fixing a prescribed analytical expression for the solution and estimating the deficiency of the possible solution. Here we choose a regularization parameter using the L-curve method. Second, we calculate a solution by Tikhonov regularization using the discrepancy principle for estimating the regularization parameter with previously specified tolerance.

Remark 4.7 *The choice of the prescribed analytical expression for the solution is equivalent to the projection method for regularization. So, the problem of obtaining the approximate solution is transformed by regularization into a parameter estimation problem.*

The discrepancy principle

This section is devoted to a posteriori choices of the regularization parameter α. We will show how to determine an optimal value of the parameter by the discrepancy principle, which is based on the Tikhonov regularization method.

We consider again the linear compact operator K_σ in Eq. (4.16), which is injective between the Hilbert space X and Y. Notice that by construction K_σ has a dense range. We have seen that the family of operators R_α in Eq. (4.26) defines regularization operators that approximate the unbounded inverse of K_σ on $K_\sigma(X)$.

The following theorem will be needed when discussing the discrepancy principle.

Theorem 4.8 *Let $K : X \to Y$ a compact linear operator with the injectivity property. Let $h \in Y, \alpha > 0$, and f_α be the unique solution of the equation*

$$\alpha f_\alpha + K^* K f_\alpha = K^* h. \tag{4.27}$$

Then f_α depends continuously on h and α. The mapping $\alpha \to ||f_\alpha||$ is monotone nonincreasing and $\lim_{\alpha\to\infty} f_\alpha = 0$. The mapping $\alpha \to ||Kf_\alpha - h||$ is monotone nondecreasing and $\lim_{\alpha\to 0} K f_\alpha = h$. If $K^*h \neq 0$, then strict monotonicity holds in both cases.

Notice that the operator K_σ defined in (4.16) satisfies the hypotheses of the above theorem. We wish to approximate the solution of Eq. (4.16) for a given right hand side h^δ with a known error level from the unknown exact function h, i.e., satisfying

$$||h^\delta - h|| \leq \delta. \tag{4.28}$$

Now, using a perturbed right hand side, we want to construct a reasonable approximation $f_{\alpha(\delta)}$ to the exact solution of Eq. (4.16). Finding the regularization parameter from a priori δ leads us to the discrepancy principle as follows.

We compute the value $\alpha(\delta) > 0$ such that the corresponding Tikhonov solution $f_{\alpha(\delta)}$ of Eq.(4.18), i.e., the minimum of the Tikhonov functional in Eq. (4.23), satisfies the equation

$$||K_\sigma f_{\alpha(\delta)} - h^\delta|| = \delta. \tag{4.29}$$

Notice that this choice of α by the discrepancy principle guarantees that, on one side, the error between the regularization solution and the known value h^δ is equal to δ and, on the other side, that α is not too small.

Equation (4.29) is uniquely solvable provided that the inequalities $||h^\delta - h|| \leq \delta < ||h^\delta||$ hold, because by Theorem 4.8, the following inequalities hold

$$\lim_{\alpha\to\infty} ||K_\sigma f_\alpha - h^\delta|| = ||h^\delta|| > \delta, \tag{4.30}$$

$$\lim_{\alpha\to 0} ||K_\sigma f_\alpha - h^\delta|| = 0 < \delta. \tag{4.31}$$

Furthermore, the mapping $\alpha \to ||K_\sigma f_\alpha - h^\delta||$ is continuous and strictly increasing.

Thus the determination of $\alpha(\delta)$ is equivalent to the problem of finding the zero of the monotone function from $\mathbb{R}^+$ to $\mathbb{R}^+$:

$$\Phi(\alpha) = ||K_\sigma f_\alpha - h^\delta||^2 - \delta^2, \quad \text{(for fixed } \delta). \tag{4.32}$$

So, it possible to carry out the computation by Newton's method as follows.

We recall that in [70] it is shown that the derivative of the mapping $\alpha \to f_{\alpha(\delta)}$ is given by the solution of the equation

$$(\alpha I + K_\sigma^* K_\sigma)\frac{d}{d\alpha} f_\alpha = -f_\alpha. \tag{4.33}$$

This equation can be rewritten as

$$||h - K_\sigma f_\alpha||^2 = (h - K_\sigma f_\alpha, h) - (K_\sigma^*[h - K_\sigma f_\alpha], f_\alpha) = ||h||^2 - (f_\alpha, K_\sigma^* h) - \alpha||f_\alpha||^2, \tag{4.34}$$

hence we get

$$\Phi(\alpha) = ||h||^2 - (f_\alpha, K_\sigma^* h) - \alpha||f_\alpha||^2 - \delta^2, \tag{4.35}$$

and

$$\frac{d}{d\alpha}\Phi(\alpha) = -(\frac{df_\alpha}{d\alpha}, K_\sigma^* h) - ||f_\alpha||^2 - 2\alpha Re(\frac{df_\alpha}{d\alpha}, f_\alpha), \tag{4.36}$$

where the derivative $\frac{df_\alpha}{d\alpha}$ is given by Eq. (4.33). Thus, we set the actual regularization parameter α as the limit of the iterative procedure

$$\alpha_{k+1} = \alpha_k - \left(\frac{d}{d\alpha}\Phi(\alpha^k)\right)^{-1} \Phi(\alpha^k). \tag{4.37}$$

From the previous facts it is possible to prove that the parameter α satisfies:

$$\alpha(||f_{\alpha(\delta)}|| - \delta) \leq ||K_\sigma||^2 \delta. \tag{4.38}$$

Thus we may use the following starting value α for Newton's iteration in (4.37)

$$\alpha_0 = \frac{||K_\sigma||^2 \delta}{||f_{\alpha(\delta)}|| - \delta}, \tag{4.39}$$

and we find a zero of the function $\Phi(\alpha)$ in (4.32).

The L-curve method

The L-curve method is broadly discussed in [53] and [54]. Moreover, useful tools in the Matlab package are available, see [55]. Here we mention some fundamental ideas in the L-curve method.

The method consists on obtaining a so-called L-curve and estimating a regularization parameter as the point of maximum curvature. Such a curve is a log-log plot of the norm of the regularized solution versus the norm of the corresponding residual norm. It is a convenient graphical tool for displaying the trade-off between the size of a regularized solution and its fit to a given data, as the regularization parameter varies.

The L-curve gives insight into the regularizing properties of the underlying regularization method, and it is an aid in choosing an appropriate regularization parameter for the given data. Now, we summarize the main properties of the L-curve.

The L-curve is parametrized by the regularization parameter, i.e.,

$$\{\log(||Ax_\alpha - b||), \log(||L(x_\alpha - x_0)||); \quad \alpha \in \mathbb{R}^+\}, \tag{4.40}$$

where the matrices A and L represent a discretized version of Tikhonov's functional. Here x_0 is a given reference value.

In many application, such a curve takes a concave form. The procedure is to estimate the optimal value of the regularization parameter so that it corresponds to the point of the curve where its curvature maximizes. To do so, we use a simple one-dimensional optimization procedure without constrains.

4.2.4 Solution in Sobolev spaces

In previous sections we introduced integral equations of the first kind, which are defined by the linear compact operator K_σ: $X \to Y$, with $X \subset L^2[0,M]$ and $Y \subset L^2[0,A]$. These subspaces are chosen to select an adequate metric to measure the error on the right hand side of Eq. (4.16) and to obtain an approximate solution in the subset of feasible solutions.

However, more flexibility in the choice of the solutions space X is necessary, because additional regularity properties of the exact solution are known a priori. Moreover, the penalty term in the functional (4.23) guarantees only a bounded solution, while we know that feasible solutions are differentiable.

Because of these facts, Tikhonov suggested incorporating the derivative into the penalty term in (4.23), where the derivative $\frac{d}{dx}f = f'$ is taken in the weak sense, as we explain now.

Definition 4.9 *A function $\phi \in L^2[0,M]$ is said to have a weak derivative $\phi' \in L^2[0,M]$ if*

$$\int_0^M \phi\psi' dx = -\int_0^M \phi'\psi dx, \tag{4.41}$$

for all $\psi \in C^1[0,M]$, with $\psi(0) = \psi(M) = 0$.

By introducing positive differentiable functions $q_0, \dots, q_p$ in the minimization, we replace the functional $\Phi_\alpha(f)$ in Eq. (4.23) by the functional

$$\overline{\Phi_\alpha}(f) = ||K_\sigma f - h||^2 + \alpha(||q_o^{1/2} f||^2 + ||q_1^{1/2}\frac{d}{dx}f||^2), \tag{4.42}$$

or in more general form as

$$\overline{\Phi_\alpha}(f) = ||K_\sigma f - h||^2 + \alpha \int_0^M \sum_{r=0}^{p} q_r(x) \left(\frac{d^r f}{dx^r}(x) \right)^2 dx. \tag{4.43}$$

Based on the previous discussion, we show how to find the solution in the Sobolev space $H^1[0, M]$ with inner product

$$(\phi, \psi) = \int_0^M (\phi(x)\psi(x) + \phi^{'}(x)\psi^{'}(x))dx. \tag{4.44}$$

Now, the integral equation of first kind in (4.16) is interpreted as an integral operator with smooth kernel mapping $H^1[0, M]$ on $L^2[0, A]$. All the theory on regularization, including convergence and regularity, remains applicable in this setting. This application is summarized in the following theorem.

Theorem 4.10 *Consider a linear compact operator $K_\sigma : X \subset H^1[0, M] \to K_\sigma(X)$. Then the unique solution f_α that minimizes the functional in Eq.* (4.42) *belongs to $C^2[0, M]$ and satisfies the integro-differential equation*

$$\alpha(f_\alpha - f_\alpha^{''}) + K_\sigma^* K_\sigma f_\alpha = K_\sigma^* h, \tag{4.45}$$

and the boundary condition

$$f_\alpha^{'}(0) = f_\alpha^{'}(M) = 0, \tag{4.46}$$

with $q_o = q_1 \equiv 1$.

Finally, the problem of finding a regularized solution f_α of Eq. (4.42) reduces to finding a solution of the integro-differential equation Eq. (4.45) satisfying the condition

$$f_\alpha(0) = f_1 \quad \text{and} \quad f_\alpha(M) = f_2, \tag{4.47}$$

where f_1 and f_2 are known values.

Remark 4.11 *We can obtain the values of $f_\alpha(0)$ and $f_\alpha(M)$ either from laboratory experiments or by some numerical method. Since no particle deposition σ occurs at time zero and therefore no formation damage exists in the porous rock, we assume that $f_\alpha(0) = 1$. In practice the values of $f_\alpha(M)$ can be estimated by the method of regularization by parametrization presented in Section* 4.4.

Notice that it is possible to obtain a similar theorem in a more general case i.e., on $H^p[0, M]$. In such a case Eq. (4.45) becomes the following

$$\alpha \sum_{j=0}^{p} (-1)^j \frac{d^j}{dx^j} \left[q_j \frac{d^j f_\alpha}{dx^j} \right] + K_\sigma^* K_\sigma f_\alpha = K_\sigma^* h, \tag{4.48}$$

with adequate boundary conditions. This general case must be used to obtain more smoothness in the solution if additional conditions are needed to stabilize the regularized solution. To choose the higher order derivative terms in Eq. (4.43), we need to determine the "degree of ill-posedness" of the operator K_σ, see [92] and [102] for examples.

4.3 Collocation method for the integral equation

In this section we describe a numerical algorithm for obtaining the approximate solution of the integro-differential equation (4.45) in the space $H^1[0,M]$. Similar procedures are needed for obtaining solutions in most Sobolev spaces.

In the following paragraphs we develop a procedure to calculate an approximation of the function $f:[0,M]\to[0,\infty)$ in Eq. (4.25). To do so, we discretize the integral by means of a quadrature formula, with an appropriate non-uniform partition of interval $[0,M]$. Thus, the continuous linear problem is transformed into solving a linear system of equations.

4.3.1 Formulation

Eq. (4.25) can be rewritten as

$$\alpha f_\alpha(t)+\int_0^A K_\sigma(t,y)\left[\int_0^M K_\sigma(s,y)f_\alpha(s)ds\right]dy=\int_0^A K_\sigma(t,y)h(y)dy, \tag{4.49}$$

or

$$\alpha f_\alpha(t)+\int_0^A\int_0^M K_\sigma(t,y)K_\sigma(s,y)f_\alpha(s)dsdy=\int_0^A K_\sigma(t,y)h(y)dy. \tag{4.50}$$

Introducing the notation

$$\bar{K}(t,s)=\int_0^A K_\sigma(t,y)K_\sigma(s,y)dy, \qquad H(t)=\int_0^A K_\sigma(t,y)h(y)dy, \tag{4.51}$$

we can rewrite Eq. (4.50) as

$$\alpha f_\alpha(t)+\int_0^M \bar{K}(t,s)f_\alpha(s)ds=H(t), \tag{4.52}$$

where $t,s\in[0,M]$ and $y\in[0,A]$.

4.3.2 Numerical algorithm

This section is devoted to describing the numerical algorithm for solving Eqs. (4.45) and (4.52). We emphasize implementation issues in computer programming. Methods and examples can be found in [105], [29], [109] [107], [98], [4] and [92].

Here the problem of obtaining an approximate solution of the integral equation (4.52) is reduced to solving a linear system of equations, which can be obtained by the collocation method. To do so, we discretize the operator K_σ in (4.16) and the adjoint K_σ^* in (4.18). Finally, a discretization of $K_\sigma^*K_\sigma$ is obtained and used for solving (4.25).

Discretization of the operator K_σ

We take a partition of the interval $[0,A]$ as

$$y_1=0, y_2=\delta,\dots,y_{2r+1}=2r\delta, \text{ with } \delta=A/2r, \tag{4.53}$$

where r is some positive integer. Taking the kernel K_σ in (4.15) and using an appropriate quadrature formula we obtain

$$\int_0^M K_\sigma(s, y_l) f_\alpha(s) ds \approx \sum_{j=1}^{m_s} \omega_j K_\sigma(s_j, y_l) f_\alpha(s_j), \tag{4.54}$$

with $l = 1, \ldots, 2r + 1$; here ω_j, with $j = 1, \ldots, m_s$ are weights to be determined.

Now we show how to calculate the weight vector $W = (\omega_j)$ and the values $S = (s_j)$ with $j = 1, \ldots, m_s$. Since the kernel $K_\sigma(y, T)$ is non-zero in the range of $\sigma(1, T)$ to $\sigma(0, T)$ for $T \geq 1$ and from $\sigma(T, T)$ to $\sigma(0, T)$ for $T < 1$ it is necessary to use a non-uniform partition of the interval $[0, M]$ as follows (see Fig. 4.1).

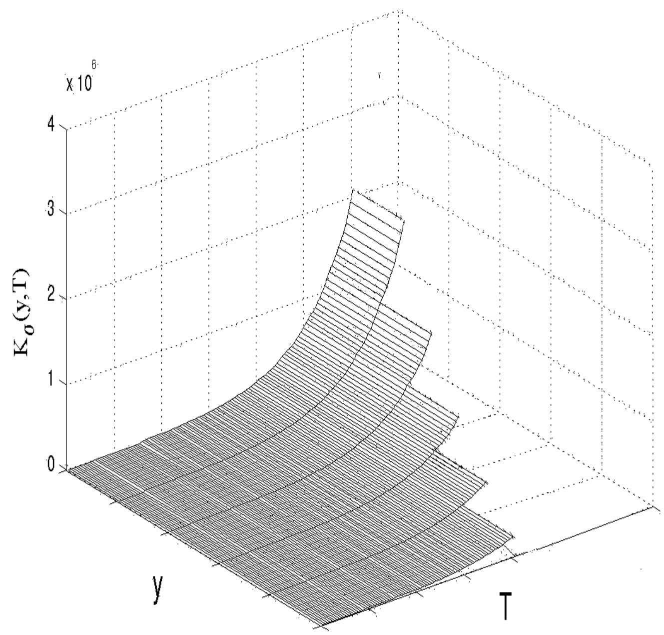

Figure 4.1: Graph of the kernel $k_\sigma(y, T)$

Remark 4.12 *Notice that kernel $K_\sigma(s, T)$ has discontinuities on the curves $s = \sigma(0, T)$ and $s = \sigma(1, T)$, see Section 4.1. Thus, with a non-uniform partition in Eq.(4.58) we guarantee that the integral partition takes into account all possible discontinuities. If a uniform partition were used, its accuracy would be reduced to first order at the discontinuity curves; this would force us to use an extremely fine grid.*

Now, we build a non-uniform partition of the interval $[0, M]$, based on the discontinuity points of the kernel. Let us denote the vector

$$z = [\sigma(1, y_1), \sigma(0, y_1), \sigma(1, y_2), \sigma(0, y_2), \ldots, \sigma(1, y_{2r+1}), \sigma(0, y_{2r+1})], \tag{4.55}$$

whose components $\sigma(1, y_j), \sigma(0, y_j)$, with $j = 1, \ldots, 2r+1$ corresponds to the points where the kernel $K_\sigma(s, T)$ in (4.15) has discontinuities in s.

Now, by sorting in increasing order the components of the vector z we get a new vector

$$\bar{z} = [a_1, \ldots, a_{4r+2}], \tag{4.56}$$

such that $a_1 \leq a_2 \leq \ldots < a_{4r+2} = M$ holds. Now, let us define by io the index of the last component a_{io} of the vector $\bar{z}$ such as $a_{io} = 0$. So, we obtain the vector

$$\bar{p} = [a_{io}, a_{io+1}, \ldots, a_{4r+2}], \tag{4.57}$$

which we assume to have n_s components. Finally, the components of the vector $\bar{p}$ determine a non-uniform partition of $[0, M]$. Using this partition, the integral in Eq. (4.54) can be rewritten for $q = 1, \ldots, 2r+1$ as

$$\begin{aligned}\int_0^M K_\sigma(s, y_q) f_\alpha(s) ds &= \int_{a_{io}}^{a_{io+1}} K_\sigma(s, y_q) f_\alpha(s) ds + \int_{a_{io+1}}^{a_{io+2}} K_\sigma(s, y_q) f_\alpha(s) ds + \ldots \\ &+ \int_{a_{4r+1}}^{a_{4r+2}} K_\sigma(s, y_q) f_\alpha(s) ds.\end{aligned} \tag{4.58}$$

Now, each integral on the right hand side of (4.58) can be approximated separately. To do so, fix m_l, taking $\beta_l = (a_{l+1} - a_l)/2m_l$, and

$$s_1 \equiv a_l, s_2 = a_l + \beta_l, \ldots, s_{2m_l+1} = a_l + 2m_l\beta_l \equiv a_{l+1}. \tag{4.59}$$

So, an arbitrary integral can be approximated using Simpson's integration formula by

$$\int_{a_l}^{a_{l+1}} K_\sigma(s, y_q) f_\alpha(s) ds \approx \sum_{j=1}^{2m_l+1} B_j^l K_\sigma(s_j, y_q) f_\alpha(s_j), \tag{4.60}$$

with $q = 1, \ldots, 2r+1$ and $l = io, io+1, \ldots, 4r+1$. The quadrature integration weights B_j^l are given in [70] and [106]:

$$B_1^l = B_{2m_l+1}^l = \beta_l/3, B_2^l = B_4^l = \ldots = B_{2m_l}^l = 4\beta_l/3, \quad B_3^l = B_5^l = \ldots = B_{2m_l-1}^l = 2\beta_l/3.$$

Now (4.58) can be approximated using (4.60) as follows:

$$\begin{aligned}\int_0^M K_\sigma(s, y_q) f_\alpha(s) ds &\approx \sum_{j=1}^{2m_{io}+1} B_j^{io} K_\sigma(s_j, y_q) f_\alpha(s_j) + \ldots + \sum_{j=1}^{2m_l+1} B_j^l K_\sigma(s_j, y_q) f_\alpha(s_j) + \ldots \\ &+ \sum_{j=1}^{2m_{4r+1}+1} B_j^{4r+1} K_\sigma(s_j, y_q) f_\alpha(s_j).\end{aligned} \tag{4.61}$$

The next step in writing Eq. (4.61) similarly to Eq. (4.54) is grouping the repeated nodes s_j in (4.61); the new weights are obtained by adding $B_{2m_l+1}^l$ and B_1^{l+1}.

More exactly the weights $W = (\omega_j)$ with $j = 1, \ldots, m_s$ are calculated as follows. First we introduce the vector $\overline{W}$ by taking all the weights in (4.61) as:

$$\overline{W} = [B_1^{io}, B_2^{io}, \ldots, B_{2m_{io}+1}^{io}, \ldots, B_1^l, B_2^l, \ldots, B_{2m_l+1}^l, \ldots,$$
$$B_1^{4r+1}, B_2^{4r+1}, \ldots, B_{2m_{4r+1}+1}^{4r+1}], \tag{4.62}$$

with $2\sum_{q=io}^{4r+1} m_q + (n_s - 1)$ components. Second, we drop the component B_1^l of the vector $\overline{W}$ for all subindexes $l = io, io+1, \ldots, 4r+1$ and we set $B_{2m_l+1}^l = B_{2m_l+1}^l + B_1^{l+1}$, for each $l = io, io+1, \ldots, 4r$, namely,

$$W = [B_2^{io}, \ldots, B_{2m_1+1}^{io} + B_1^{io+1}, \ldots, B_2^l, \ldots, B_{2m_l+1}^l + B_1^{l+1}, \ldots,$$
$$B_{2m_{4r}+1}^{4r} + B_1^{4r+1}, B_2^{4r+1}, \ldots, B_{2m_{4r+1}+1}^{4r+1}], \tag{4.63}$$

with $m_s = 2\sum_{q=io}^{4r+1} m_q - 1$ components.

We derive the values s_j with $j = 1, \ldots, m_s$ on the right hand side of Eq. (4.54), which are the values that correspond to the products $\omega_j K_\sigma(s_j, y_q) f(s_j)$ as follows: first we introduce the vector of nodes in (4.61) as:

$$\overline{S} = [a_{io}, a_{io} + \beta_1, \ldots, a_{io} + 2m_1\beta_1, \ldots, a_l, a_l + \beta_l, \ldots, a_l + 2m_l\beta_l, \ldots,$$
$$a_{4r+1}, a_{4r+1} + \beta_{4r+1}, \ldots, a_{4r+1} + 2m_{4r+1}\beta_{4r+1}], \tag{4.64}$$

with $2\sum_{q=io}^{4r+1} m_q + (n_s - 1)$ components. Second, we drop the component a_l of the vector $\overline{S}$ for all subindexes $l = io, io+1, \ldots, 4r+1$. We obtain the vector $S = (s_j)$:

$$S = [a_{io} + \beta_1, \ldots, a_{io} + 2m_1\beta_1, \ldots, a_l + h_l, \ldots, a_l + 2m_l\beta_l, \ldots,$$
$$a_{4r+1} + \beta_{4r+1}, \ldots, a_{4r+1} + 2m_{4r+1}\beta_{4r+1}] \tag{4.65}$$

with m_s components. Let us define the matrix $C = (a_{qj})$

$$a_{qj} = \omega_j K_\sigma(s_j, y_q), \tag{4.66}$$

where $q = 1, \ldots, 2r+1$ and $j = 1, \ldots, m_s$. The weights ω_j are defined in (4.63) and the nodes s_j are defined in (4.65).

Finally, the integral in Eq. (4.54) is discretized as

$$\int_0^M K_\sigma(s, y_q) f_\alpha(s) ds \approx \sum_{j=1}^{m_s} a_{qj} f_\alpha(s_j), \tag{4.67}$$

where $s_1, \ldots, s_{m_s}$ are components of the vector S in Eq. (4.65) and $q = 1, \ldots, 2r+1$.

Discretizing the adjoint operator K_σ^* with the operator K_σ

We need to compute $K_\sigma^* K_\sigma$. To do so, the product of the operators $K_\sigma^* K_\sigma$ is approximated as the product of two matrices by using an appropriate integration formula.

The second term on the left hand side of Eq. (4.49) can be approximated as follows

$$\int_0^A K_\sigma(t_k, y)\left[\int_0^M K_\sigma(s, y)f_\alpha(s)ds\right]dy \approx \int_0^A K_\sigma(t_k, y)\sum_{q=1}^{m_s}\omega_q K_\sigma(s_q, y)f_\alpha(s_q)dy, \qquad (4.68)$$

hence, using again Simpson's integration formula we obtain

$$\int_0^A K_\sigma(t_k, y)\sum_{q=1}^{m_s}\omega_q K_\sigma(s_q, y)f_\alpha(s_q)dy \approx \sum_{j=1}^{2r+1} A_j K_\sigma(t_k, y_j)\sum_{i=1}^{m_s}\omega_q K_\sigma(s_q, y_j)f_\alpha(s_q), \qquad (4.69)$$

where s, t are given in Eq. (4.65) and $y_1 = 0, y_2 = \delta, \ldots, y_{2r+1} = 2r\delta$. The quadrature integration weights are given by

$$A_1 = A_{2r+1} = \delta/3,\ A_2 = A_4 = \ldots = A_{2r} = 4\delta/3, \quad A_3 = A_5 = \ldots = A_{2r-1} = 2\delta/3. \quad (4.70)$$

Setting $b_{kj} = A_j K_\sigma(t_k, y_j)$ and $a_{jq} = w_q K_\sigma(s_q, y_j)$, we see that Eq. (4.68) can be rewritten as

$$\int_0^A K_\sigma(t_k, y)\left[\int_0^M K_\sigma(s, y)f_\alpha(s)ds\right]dy \approx \sum_{q=1}^{m_s}\left(\sum_{j=1}^{2r+1} b_{kj}a_{jq}\right)f_\alpha(s_q), \qquad (4.71)$$

or in a simplified form

$$\int_0^A K_\sigma(t, y)\left[\int_0^M K_\sigma(s, y)f_\alpha(s)ds\right]dy \approx BCf_\alpha, \qquad (4.72)$$

where the matrix $B = (b_{kj})$ has m_s rows and $2r+1$ columns and $C = (a_{jq})$ has $2r+1$ rows and m_s columns.

Notice that the matrix A is the discretization of the operator K_σ in Eq. (4.16) and the matrix B is the discretization of the adjoint operator K_σ^* in Eq. (4.18). So, since the inverse problem (4.18) is ill-posed, we know that these matrices are ill-conditioned. Thus, to solve a discretization of the integral equation (4.52), Tikhonov regularization for matrices is needed, see Section A.4.2.

Discretized version of the integral equation

Now using the discretization of the operator and of its adjoint we derive the linear system that is the discretized version of the integral equation (4.52).

The right hand side on Eq. (4.52) is given by

$$H(t_k) = \int_0^A K_\sigma(t_k, y)h(y)dy \approx \sum_{j=1}^{2r+1} A_j K_\sigma(t_k, y_j)h(y_j), \qquad (4.73)$$

where $t = (t_k)$, with $k = 1, \ldots, m_s$ are given in Eq. (4.65), with $A_1, \ldots, A_{2r+1}$ in Eq. (4.70) and $y_1 = 0, \ldots, y_{2r+1} = 2r\delta$ are given in (4.53).

Notice that Eq. (4.73) can be rewritten as

$$\int_0^A K_\sigma(t, y)h(y)dy \approx Bh, \qquad (4.74)$$

where $h = [h(y_1), \ldots, h(y_{2r+1})]$. Denoting by I_{m_s} the identity square matrix of order m_s, we obtain a discretized version of Eq. (4.52) as

$$(\alpha I_{m_s} + BC) f_\alpha = Bh. \tag{4.75}$$

Setting $E = \alpha I_{m_s} + BC$, $y = Bh$ and denoting

$$\begin{aligned} f_\alpha = f_\alpha(S) = [&f_\alpha(a_{io} + \beta_1), \ldots, f_\alpha(a_{io} + 2m_1\beta_1), \ldots, f_\alpha(a_l + \beta_l), \ldots, f_\alpha(a_l + 2m_l\beta_l), \ldots, \\ &f_\alpha(a_{4r+1} + \beta_{4r+1}), \ldots, f_\alpha(a_{4r+1} + 2m_{4r+1}\beta_{4r+1})], \end{aligned} \tag{4.76}$$

we obtain a linear system

$$E f_\alpha = y. \tag{4.77}$$

Fixing the value of the parameter α and solving system (4.77), we obtain the discrete approximation of the regularized solution of Eq. (4.49).

Numerical algorithm for the Discrepancy principle

In this Section we describe the computer implementation of the discrepancy principle for estimating the regularization parameter. It is based on the discretization of Eq. (4.52). Thus, we take into account that solving Eq. (4.16) is equivalent to solving the linear system

$$C f_\alpha = h, \tag{4.78}$$

where the matrix C is calculated in Eq. (4.66) and the vector h is given. Using the Tikhonov regularization method, we arrive to a regularized linear system in Eq. (4.77). Notice that the complete regularized solution can be obtained when we have estimates for the regularization parameter α.

When we know the error δ between the "true" value of the vector h and the measured value h^δ, it is possible to use the discrepancy principle. Now, we describe the implementation procedure of the discrepancy principle (see Section 4.2.3) as follows. We find a regularization parameter as the zero of the function $\Phi(\alpha)$ in Eq. (4.32). The procedure begins by fixing a value δ such that

$$||C f_\alpha^\delta - h^\delta|| \leq \delta < ||h^\delta||, \tag{4.79}$$

where f_α^δ is as in Eq. (4.76) an approximation of the solution and $h^\delta = (h(a_{io+1}), \ldots, h(a_{4r+2}))$ are given values. The regularization parameter α is determined by discrepancy principle, i.e., α is the zero of the function (see Section 4.2.3):

$$\Phi(\alpha) = ||C f_\alpha - h||^2 - \delta^2. \tag{4.80}$$

To find the zero of Eq. (4.80), we use Newton's method. So, we start by fixing ϵ and selecting an appropriate starting initial value for the parameter α for the iterative procedure as

$$\alpha_0 = \frac{||C||\delta}{||C f_\alpha^\delta - \delta||}. \tag{4.81}$$

We continue and determine the quantities f_{α_k} as the solution of the linear system

$$E f_{\alpha_k} = Bh. \tag{4.82}$$

Then, $\frac{df_{\alpha_k}}{d\alpha}$ is calculated as the solution of

$$E\frac{df_{\alpha_k}}{d\alpha}(\alpha_k) = f_\alpha, \tag{4.83}$$

and

$$\frac{d\Phi}{d\alpha}(\alpha_k) = -(\frac{df_{\alpha_k}}{d\alpha}(\alpha_k), Bh) - (f_{\alpha_k}, f_{\alpha_k}) - 2\alpha_k(\frac{df_{\alpha_k}}{d\alpha}(\alpha_k), f_{\alpha_k}), \tag{4.84}$$

where $(\cdot,\cdot)$ denotes the inner product of two vectors.

Finally, we obtain a new value α_{k+1} using Eq. (4.37). We continue the iterative procedure until the acceptable tolerance ϵ is reached, i.e., $|\alpha_{k+1} - \alpha_k| < \epsilon$ holds.

In the numerical example presented in Section 4.5 to test the discrepancy principles we take f_α^δ as the exact value of the solution, $h = Cf_\alpha^\delta$ and h^δ as a data function polluted by error.

Solution of the integro-differential equation

This section is devoted to the discretization of the integro-differential equation (4.45). As in the discretization of Eq. (4.24), we take a nonuniform partition of the interval $[0, M]$.

We indicate such a partition by its mesh points s_k with $k = 1, \dots, m_s$ as in Eq. (4.65). Setting the points $s_0 = 0$ and $s_{m_s+1} = s_{m_s} + d_{m_s+1}$, where $d_{m_s+1} = s_{m_s} - s_{m_s-1}$, we obtain for $k = 0, \dots, m_s$:

$$d_k = s_{k+1} - s_k, \quad \text{where} \quad d_k \neq d_{k+1}. \tag{4.85}$$

So, in this case Eq. (4.45) is approximated by a system of linear equations for the unknowns f_k, $k = 1, \dots, m_s$, of the form (see [105], pag 78):

$$-\frac{\alpha q_1(s_k)}{d_k d_{k-1}} f_{k+1} - \frac{\alpha q_1(s_{k-1})}{d_{k-1}^2} f_{k-1} + \left(\frac{\alpha q_1(s_k)}{d_k d_{k-1}} + \frac{\alpha q_1(s_{k-1})}{d_{k-1}^2} + \alpha q_0(s_k)\right) f_k +$$
$$\sum_{l=1}^{m_s}\left(\sum_{j=1}^{2r+1} b_{kj} a_{jl}\right) f_l = y_k, \quad \text{where} \quad y_k = \sum_{j=1}^{2r+1} b_{kj} h_j, \tag{4.86}$$

with $k = 1, \dots, m_s$. The values of $f(0)$ and $f(M)$ are given, see Remark 4.11. So in system (4.86) we set

$$f_0 = f(0) \quad \text{and} \quad f_{m_s+1} = f(M). \tag{4.87}$$

Let us use the notation $\bar{f} = (f(s_1), \dots, f(s_{m_s}))$. Now we rewrite the system (4.86) as

$$(\alpha V + BC)\bar{f} = \bar{y}, \tag{4.88}$$

where C and B represent the discretization of the operator K_σ and of its adjoint K_σ^* respectively; the matrix $V = (V_{ij})$ is given by the formulae:

$$V_{12} = -\frac{q_1(s_2)}{d_2 d_1}, \tag{4.89}$$

$$V_{qq} = \frac{q_1(s_q)}{d_q d_{q-1}} + \frac{q_1(s_{q-1})}{d_{q-1}^2} + q_0(s_q), \quad \text{with} \quad q = 1, \dots, m_s, \tag{4.90}$$

$$V_{q,q-1} = -\frac{q_1(s_{q-1})}{d_{q-1}^2}, \quad V_{q,q+1} = -\frac{q_1(s_q)}{d_q d_{q-1}}, \quad \text{with} \quad q = 2, \dots, m_s - 1, \tag{4.91}$$

$$V_{m_s,m_s-1} = -\frac{q_1(s_{m_s})}{d_{m_s}}; \tag{4.92}$$

the other elements of this matrix are zero. We obtain the values of the vector $\bar{y} = (\bar{y}_1, \dots, \bar{y}_{m_s})^T$ as follows:

$$\begin{aligned} \bar{y}_1 &= y_1 + \frac{\alpha q_1(s_0)}{d_0^2} f_0, \quad \bar{y}_k = y_k, \quad \text{for} \quad k = 2, \dots, m_s - 1, \\ \bar{y}_{m_s} &= y_{m_s} + \frac{\alpha q_1(s_{m_s})}{d_{m_s} d_{m_s-1}} f_{m_s+1}. \end{aligned} \tag{4.93}$$

Inversion operation

As we have seen in the previous section, we need to calculate the inverse $X = \sigma^{-1}(y, T)$ of the function $y = \sigma(X, T) = s(y, T)$. This problem is equivalent to finding a zero of the function $G(X) = \sigma(X, T) - y$ in the interval $[0, 1]$ for given values of y and T. In Section 4.1 we proved the existence of a unique zero of such a function on D_+.

In practice, $\sigma(X, T)$ is given at discrete points (X_i, T_j), with $i = 1, \dots, n$ and $j = 1, \dots, m$. Since $\sigma(X, T)$ is well behaved in D_+, we can use two-dimensional interpolation to obtain the value of this function at any point $(X, T) \in D_+$.

Now we seek a zero X^* using Newton's method, i.e, we obtain a solution of the iterative procedure:

$$X^{k+1} = X^k - \left(\left. \frac{\partial \sigma(X, T)}{\partial X} \right|_{X = X^k} \right)^{-1} \sigma(X^k, T), \quad \text{with} \quad k = 0, 1, \dots \tag{4.94}$$

with (X^0, T) given in D_+.

4.4 Regularization by parametrization

In the previous section we described a general procedure for finding the solution of Eq. (E.1). Continuity was one of the assumptions about the unknown function $f(\sigma)$; however, we do not know the analytical structure of the solution. This situation led to an ill-posed problem that was solved using the Tikhonov regularization method.

In this section we prescribe an analytical expression for the function $f(\sigma)$ in Eq. (4.3) that depends only on a few parameters, or equivalently we project the function $f(\sigma)$ on a finite dimensional subspace V_n. Even in this finite dimension formulation, we still have an ill-posed problem, but the procedure to obtain an approximate solution reduces to estimating a finite number of parameter values. Here we do not need a priori information on the deficiency of the solution δ.

We assume that the solution of Eq. (4.3) is given by the polynomial expression:

$$f(\sigma) = 1 + \theta_1 \sigma + \theta_2 \sigma^2 + \dots + \theta_n \sigma^n, \tag{4.95}$$

where $\theta_1, \theta_2, ..., \theta_n$ are parameters to be determined. The formula above is equivalent to taking the formation damage function in Eq. (2.11) as

$$k(\sigma) = (1 + \theta_1\sigma + \theta_2\sigma^2 + ... + \theta_n\sigma^n)^{-1}. \tag{4.96}$$

Let us denote the moments of σ by

$$S_k(T) = \int_0^1 (\sigma(X,T))^k dX. \tag{4.97}$$

Then Eq. (4.3) can be rewritten as

$$1 + \theta_1 S_1(T) + \theta_2 S_2(T) + ... + \theta_n S_n(T) = g(T) \quad \text{for all} \quad T \in [0, A]. \tag{4.98}$$

Since the values of $S_1(T), \ldots, S_n(T)$ and $g(T)$ for T equal to $T_1, T_2, \ldots, T_m \in [0, A]$ are known, the problem of finding the solution of Eq. (4.3) reduces to estimating the parameters $\theta_1, \theta_2, ..., \theta_n$ by finding the "best" solution of the linear system of equations

$$C\bar{x} = \bar{y}, \tag{4.99}$$

where the matrix C with m rows and n columns is given by

$$C_{qj} = S_j(T_q), \tag{4.100}$$

with $q = 1, \ldots, m$ and $j = 1, \ldots, n$; we are using the notation $\bar{y} = (\bar{y}_1, \ldots, \bar{y}_n)$ where

$$\bar{y}_q = g(T_q) - 1, \quad \text{with} \quad q = 1, \ldots, n \quad \text{and} \quad \bar{x} = (\theta_1, \ldots, \theta_n). \tag{4.101}$$

Now, the solution $\bar{x}$ of the linear system (4.99), which is a discrete ill-posed problem, can be found using the Tikhonov regularization method (see Section A.4.2 and Eq. (A.35)), i.e.,

$$\bar{x}_\alpha = argmin\{||C\bar{x} - \bar{y}|| + \alpha^2||L(\bar{x} - \bar{x}_0)||\}, \tag{4.102}$$

where the matrix L represents a discretization of the derivative operator, α is the regularization parameter and $\bar{x}_0$ is a prescribed reference value. In this case, the L-curve method is used to estimate a value of the regularization parameter. Notice that the discretized operator can be chosen appropriately to obtain a smooth approximation of the solution.

Estimation of the initial guess

It is known that the family of regularized solution converges to the solution if the selected initial guess is close enough to the solution. So, an estimate of this value is essential. To find it, there exist many strategies. Here we mention some possibilities:

1. The initial value f_0 may be obtained as the best physical estimate based on semi-empirical considerations.

2. Additional information on the solution must be used such as boundedness, smoothness and monotonicity as well as values of the solution at the boundary of the physical domain

3. Reduction of the problem to simple cases where it is possible to obtain an appropriate initialization.

4.5 Applications of the algorithm

In this section we show the numerical results of the regularization methods presented in Sections 4.3.2 and 4.4. The regularization procedures are tested with synthetic data, which is obtained by fixing the parameters in the analytical solution described in Section 2.2. Moreover, random perturbations are added to simulate the observational data. We discuss the method of regularization by parametrization and the collocation method applied to the integral equation in (4.3).

4.5.1 Synthetic data

To illustrate the validity of the algorithm proposed in Sections 4.3.2 and 4.4, we study an example of solving the inverse problem (E.1) in a situation where the exact solution is known.

Let us take $\sigma(X,T)$ given by Eqs. (2.58), (2.59), fixing the parameters: $c_{io} = 2$, $\lambda_0 = 1$, $a = 2$ and $T_{max} = A = 2$. Assume the permeability is given by (4.96) with $n = 3$, i.e.,

$$k(\sigma) = (1 + \theta_1\sigma + \theta_2\sigma^2 + \theta_3\sigma^3)^{-1}. \tag{4.103}$$

Thus, we seek the solution of Eq. (4.3), or equivalently, the values of the parameters θ_1, θ_2 and θ_3 are estimated from the data obtained by adding noise to the exact values.

In the following we describe the method used to create the synthetic data. First, the values of the parameters θ_1, θ_2 and θ_3 are chosen. Second, we calculate the right hand side of (4.3). Third, we simulate the experimental data by adding random error to the right hand side of (4.3) ([103]). Thus, we obtain:

$$g^\delta(T_j) = \int_0^1 (k(\sigma(X,T_j)))^{-1} dX \pm \delta\nu, \quad \text{for} \quad T_j \in [0, A] \quad \text{with} \quad j = 1, \dots, m, \tag{4.104}$$

where ν represents the standard Gaussian random variable with zero mean and unit standard deviation. In this study, we use the relative error τ to define the standard deviation, i.e., $\delta = \tau g(T_j)$.

In the example studied in next section we take the permeability reduction as

$$k(\sigma) = (1 + 30\sigma + 20\sigma^2 + 10\sigma^3)^{-1}. \tag{4.105}$$

Two numerical experiments to recover $k(\sigma)$ are presented taking the relative error τ of the simulated data as 0.01 and 0.05. Both cases are solved with two grid size discretizations, which generate matrices with order $N = 210$ and $N = 420$. In these experiments, the influence of the relative error and of the grid size are studied. Moreover, the effects of penalizers with various derivative orders on the regularized solution are considered.

4.5.2 Numerical results and discussion

The method developed in Sections 4.3.2 and 4.4 involves the calculation of the regularization parameter α. For an appropriate choice of this parameter each method is relatively

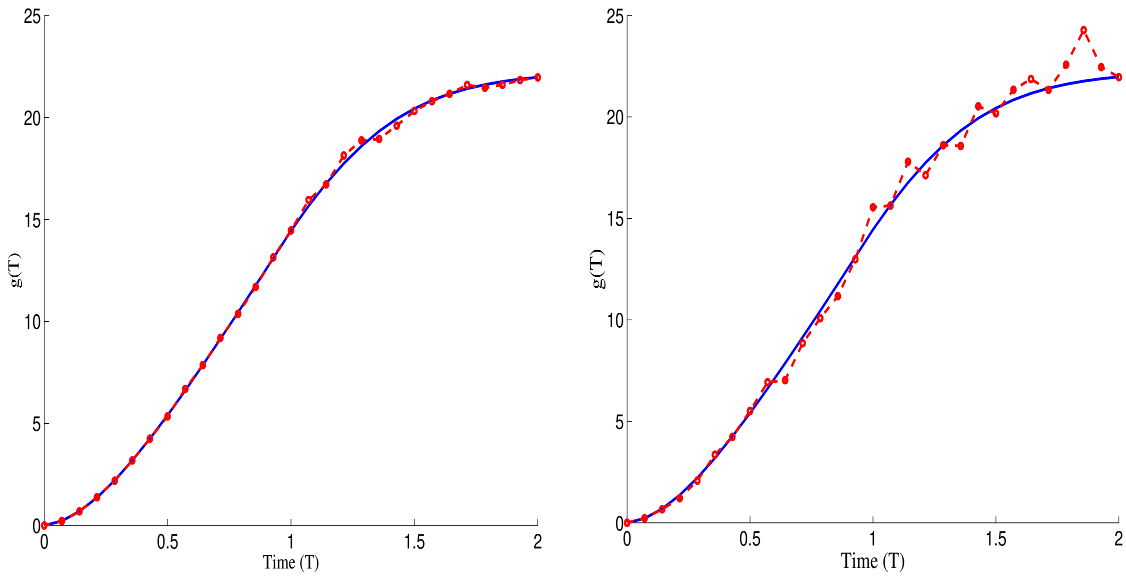

a) relative error $\tau = 0.01$. b) relative error $\tau = 0.05$

Figure 4.2: Right hand side of (4.104) with different relative error. Dashed line with circles: perturbed solution. Solid line: exact solution

stable with respect to data perturbations, so that both are reasonable computational methods. However, the sensitivity of the several solution methods to the perturbations are quite different. We examine several numerical examples illustrating this behavior. The Picard condition can be used to choose the "best" solution in the collocation method ([109] and [53]).

In the first numerical experiment we take small relative error $\tau = 0.01$ (see Fig. 4.2a). We start by examining the numerical solution obtained by minimizing the penalized functional without derivatives, i.e, by using as the penalizing functional the norm of the function. In Fig. 4.3 the solution of (4.23) obtained by the collocation method (see Section 4.3) is shown. Indeed, the solution using regularization by parametrization without the regularization term is shown, i.e., we minimize (4.102) with $\alpha = 0$ (see Section 4.4).

Notice that when the norm of the function is used as penalization (see Eq. (4.23)), then the regularized solution has large oscillations around the exact solution. This behavior suggests using the derivative to smooth the regularized solution, i.e., to use Eq. (4.42) to recover the solution more accurately.

On the other hand (see Fig. 4.3*a*), the numerical solution obtained with the method of regularization by parametrization apparently gives an accurate solution. However, when no regularization is used, the sensitivity of the solution with respect to the experimental error increases. For example, in Fig. 4.3*b* we show the regularization by parametrization solution with $\alpha = 0$, $\tau = 0.05$; notice that the regularized solution changes with respect to the exact solution when τ increases, because the norm of the difference between the regularized solution and the "true" solution is proportional to τ (see Section A.4.1).

Now, we present the result when a regularization term with first order derivative is added. The discussion clarifies the influence of the order of the derivative and of the grid size on the

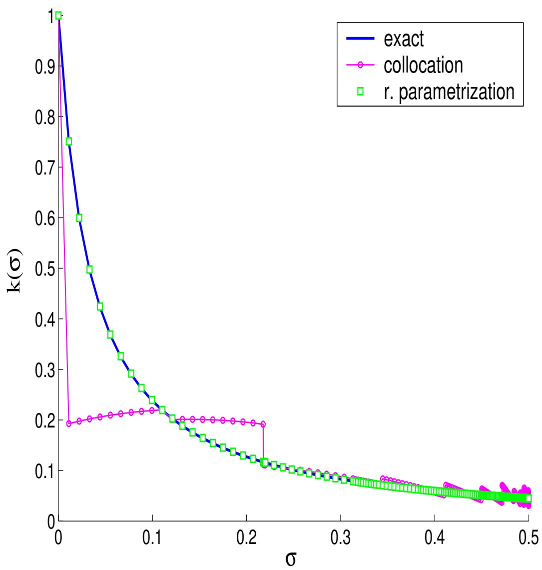

a) relative error $\tau = 0.01$.

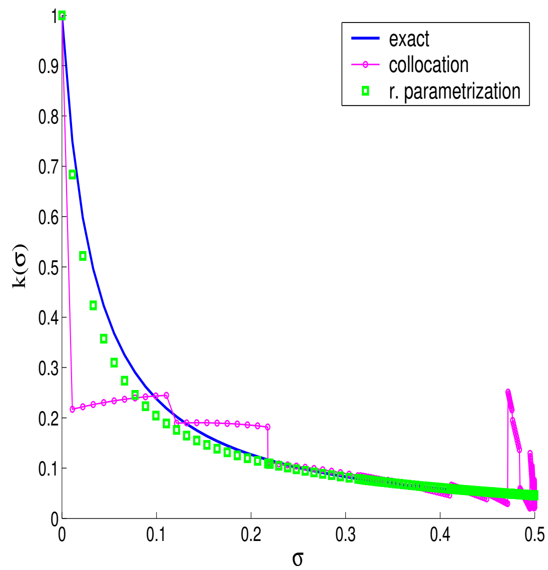

b) relative error $\tau = 0.05$

Figure 4.3: Solid line: exact solution. Solid line with circles: regularized solution by collocation method. Squares: solution with regularization by parametrization.

accuracy of the solution.

In Figs 4.4 the solution obtained by the method of regularization by parametrization is shown. The regularization parameter α is estimated by the L-curve method and by the discrepancy principle. Moreover, the solution obtained by solving the integral equation through the collocation method is shown, with α estimated by the discrepancy principle. Here the relative error in (4.104) is chosen as $\tau = 0.01$. Notice that the three solutions are reasonable approximations of the exact solution. Moreover, more accurate solutions are obtained by refining the grid in the collocation method.

In the numerical experiments with the method of regularization by parametrization, the matrices L_1 and L_2 in Eq. (4.106) are used in the regularizing term (see Eq. (4.102)), where

$$L_1 = \begin{pmatrix} 1 & -1 & & & \\ & 1 & -1 & & \\ & & \cdots & \cdots & \\ & & & 1 & -1 \end{pmatrix}, \quad L_2 = \begin{pmatrix} 1 & -2 & 1 & & & \\ & 1 & -2 & 1 & & \\ & & \cdots & \cdots & \cdots & \\ & & & 1 & -2 & 1 \end{pmatrix}. \tag{4.106}$$

These matrices represent discretized versions of the derivative operator of first and second order respectively. So, we use them to stabilize the least square solution. The choice of order of the derivative matrix L in (4.102) depends on the degree of the ill-posed problem (see 4.2.4). More exactly, to obtain singular values with higher decrease rate higher order derivative operators are required ([53]). In the example treated here, the regularized solutions obtained from the matrices L_1 and L_2 are close to the exact solution. More accurate and stable solution are obtained using L_2.

The second case consists on recovering the same solution with larger relative error, i.e., with $\tau = 0.05$ (see Fig. 4.5). In this case, the regularized solution changes significantly

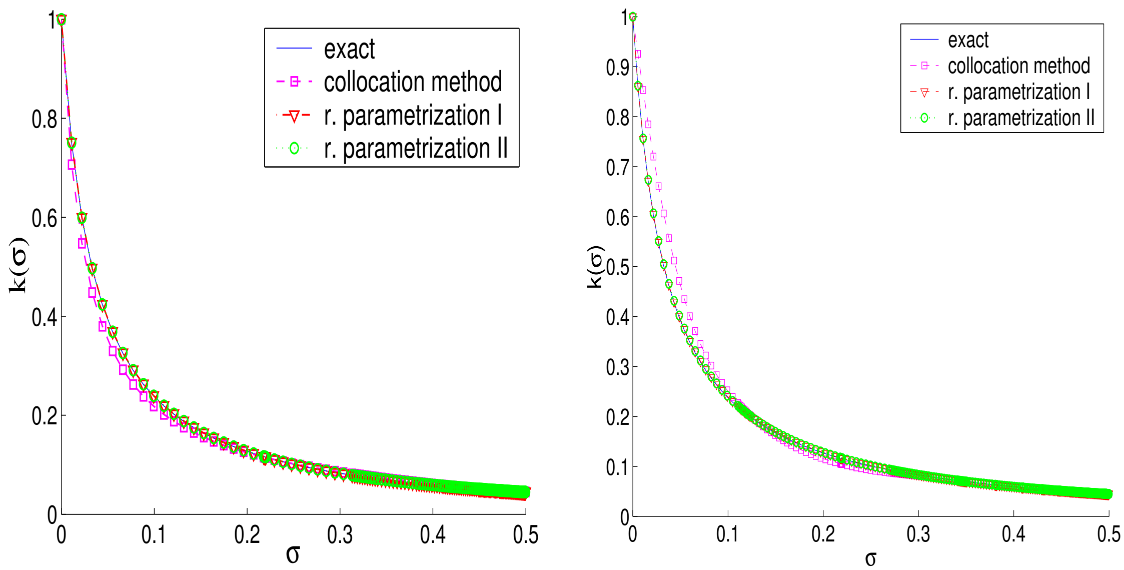

a) Regularized solution with grid discretization size $N = 210$ $\alpha_{dpc} = 1.35 \times 10^{-4}$ $\alpha_l = 1.54 \times 10^{-8}$, $\alpha_{dp} = 0$.

b) Regularized solution with grid discretization size $N = 420$ $\alpha_{dpc} = 1.84 \times 10^{-4}$ $\alpha_l = 2.92 \times 10^{-8}$ $\alpha_{dp} = 0$.

Figure 4.4: Regularized solution with $\tau = 0.01$. Solid line: exact solution. Squares: regularized solution from collocation method with discrepancy principle (α_{dpc}). Triangles: solution from regularization by parametrization method with L-curve (α_l). Circles: solution from regularization by parametrization with discrepancy principle (α_{dp}).

relative to the exact solution when the value of τ is increased. In Fig. 4.2b the right hand side $g(T)$ of the equation (4.104) and this function polluted with noise are shown.

We can see in Figs. 4.4 and 4.5 that the approximate solution is sensitive to the relative error τ. Moreover, it is possible to see that in both methods more accuracy is obtained by refining the grid discretization.

4.5.3 Condition number

Several numerical reasons can be given to explain why the solution with higher order derivative in the regularization term produces more stable solutions. Our study is based on the condition number of the discretized matrices. In Table 4.1, the condition numbers of the discretized matrices for different grid sizes and relative errors are shown. From columns 1 and 2, we see that the condition number decreases considerably when a penalizing term is added.

In Table 4.1, e_1, e_2 and e_3 represent the relative error of the regularized solution relative to the exact solution for the collocation method and the regularization by parametrization method. Moreover, the regularization parameter is calculated through both the discrepancy principle and the L-curve method. Here $cond_1$ and $cond_{1r}$ are the condition numbers of the discretized matrices with and without the regularization term, respectively. The regularization parameter α_{dpc} corresponds to the collocation method with the discrepancy principle

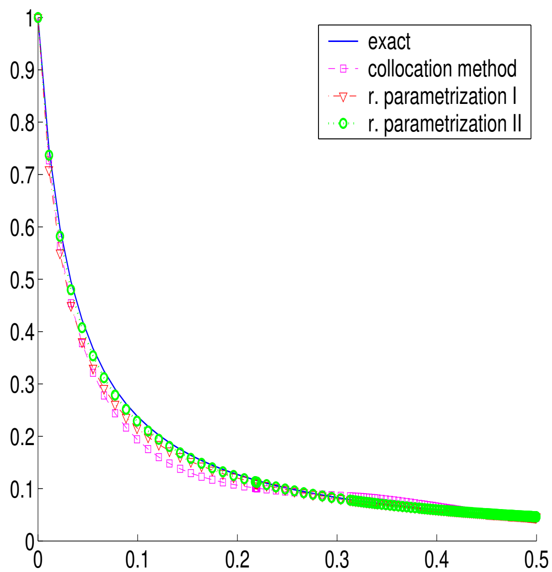

a) Regularized solution with
grid discretization size $N = 210$
$\alpha_{dpc} = 2.47 \times 10^{-4}$ $\alpha_l = 1.54 \times 10^{-8}$,
$\alpha_{dp} = 0$.

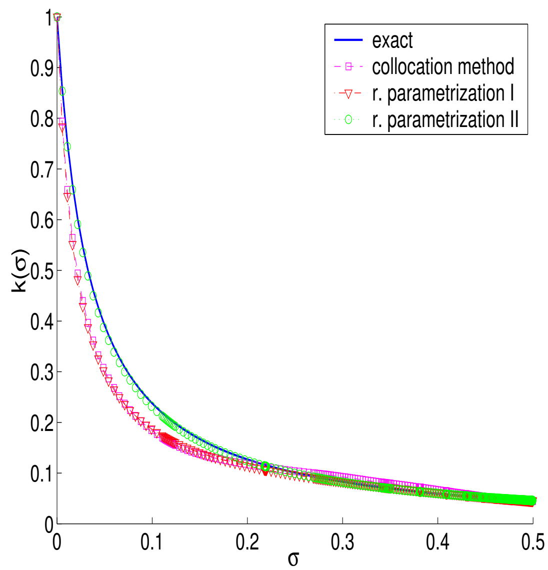

b) Regularized solution with
grid discretization size $N = 420$
$\alpha_{dpc} = 1 \times 10^{-4}$ $\alpha_l = 2.92 \times 10^{-8}$
$\alpha_{dp} = 0$.

Figure 4.5: Regularized solution with $\tau = 0.05$. Solid line: exact solution. Squares: regularized solution from collocation method with discrepancy principle (α_{dpc}). Triangles: solution from regularization by parametrization method with L-curve (α_l). Circles: solution from regularization by parametrization with discrepancy principle (α_{dp}).

and α_l to the regularization by parametrization through the L-curve method.

We see that the matrix condition number depends weakly on the relative error τ and on the grid size of the discretization N, but strongly on the regularization term. Notice that by refining the size of the discretization (see Table 4.1, columns 7-10) by a factor of two, the matrix condition number increases approximately by 10. This is so because the discretization with very fine grid size is a better approximation to the continuous inverse problem, which is ill-posed.

The regularization parameters (Table 4.1, columns 11 and 12) are different in each method. These examples suggest that, beyond a certain discretization size, the regularized solution shows no significant improvement. Moreover, the regularization parameter shows little sensitivity to the grid size N and is more sensitive to changes in the relative error τ.

4.5.4 The Picard condition

In Section 4.2, the existence and uniqueness of the solution of the integral equation in (4.3) is proved. However, the numerical algorithms presented here provide more than one solution, depending on the method used to solve the problem. Several tools have been developed to solve the loss of uniqueness in the numerical methods ([44] and [109]). One way is to add constraints in the optimization of the Tikhonov functional by taking advantage of properties of the solution that lead to uniqueness. Such tools will be successfully used for the nonlinear

Table 4.1: Condition number of the discretized matrices.

	N	τ	e_1	e_2	e_3	$cond_1$	$cond_{1r}$	$cond_2$	$cond_{2r}$	α_{dpc}	α_l
1	210	0.01	0.17	0.01	0.01	1×10^{21}	8×10^7	7×10^5	3×10^3	1×10^{-4}	1×10^{-8}
2	420	0.01	0.18	0.01	0.01	9×10^{21}	3×10^8	7×10^5	4×10^3	1×10^{-4}	3×10^{-8}
3	210	0.05	0.5	0.05	0.06	1×10^{21}	8×10^7	7×10^5	3×10^3	2×10^{-4}	2×10^{-8}
4	420	0.05	0.68	0.05	0.06	9×10^{21}	4×10^8	7×10^5	4×10^3	2×10^{-4}	3×10^{-8}

studies in Chapter 5.

In the linear case the unique solution can be found with simpler techniques that use the singular value decomposition (SVD). The solution can be estimated as presented in this work by adding a condition for choosing a reasonable solution. In [109], uniqueness of the solution is guaranteed by restricting the class of the solutions allowed or specifying a particular expansion in the SVD for the solution. More exactly, they choose the solution that satisfies the discrete Picard condition (see Section A.4.3).

This procedure is related to the sensitivity analysis, in the sense that it is hoped that the choice of the best method for estimating the regularization parameter α leads to the most likely solution from the statistical point of the view. For example, in [110] it is proved that the L-curve method is not statistically appropriate. However, the discrepancy principle has a statistical justification.

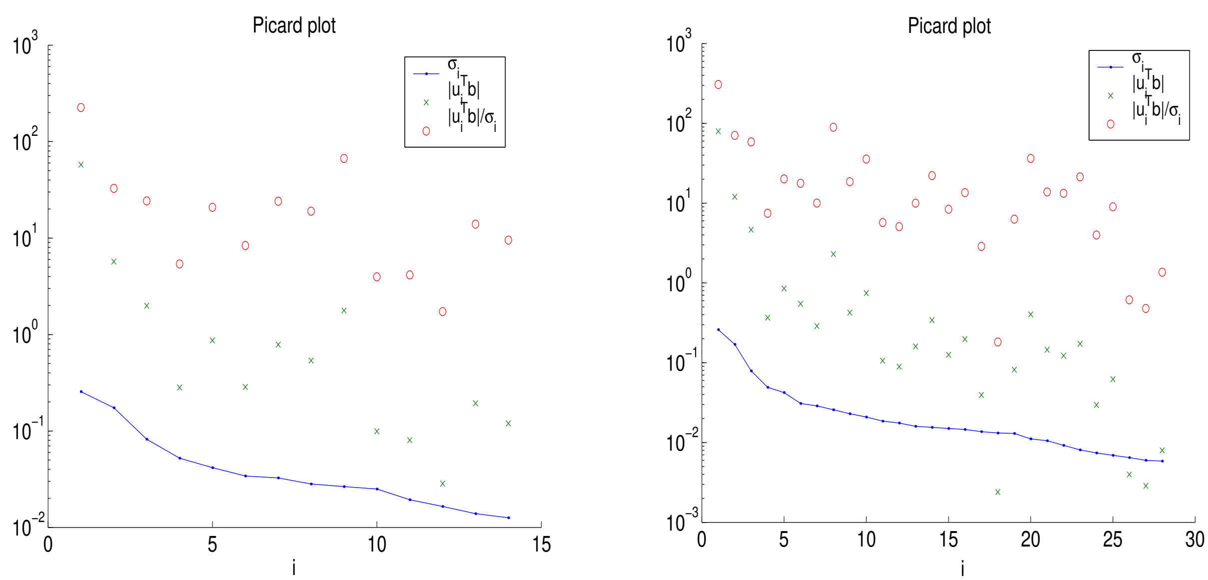

a) Unperturbed right-hand side with $N = 210$. b) Perturbed right-hand size with $N = 420$.

Figure 4.6: Picard condition in collocation method for $\tau = 0.01$. Vertical logarithmic scale.

So, in practical situations, it is advisable to use the discrepancy principle, but to use the L-curve method instead, when the value of the solution deficiency δ in (4.28) is not known.

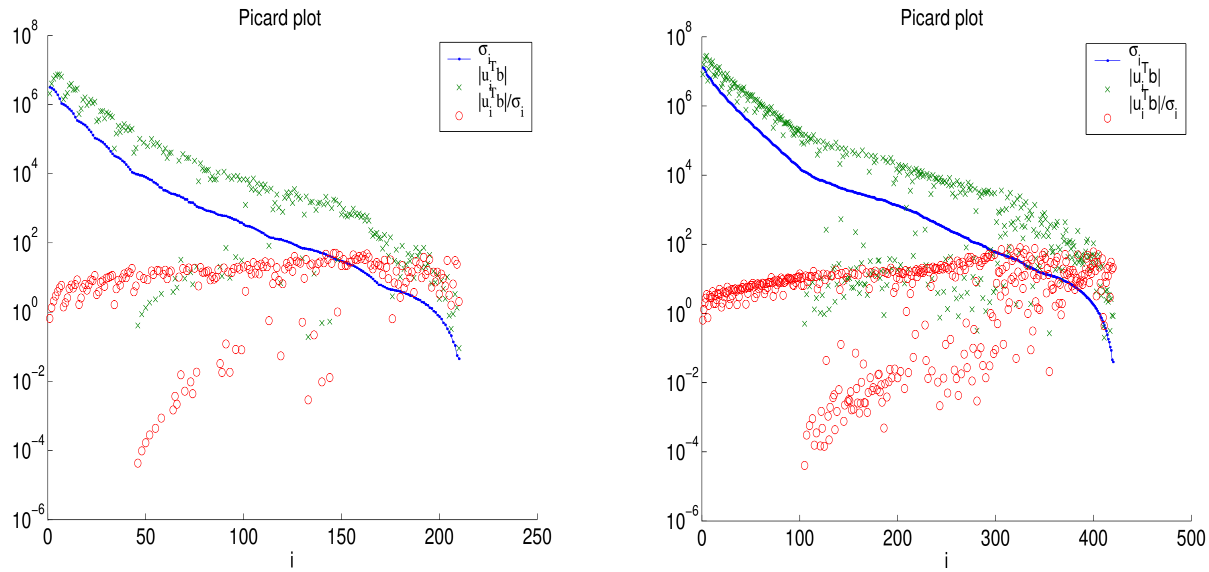

a) Unperturbed right hand side with $N = 210$. b) Perturbed right hand size with $N = 420$.

Figure 4.7: Picard condition in collocation method, $\tau = 0.01$. Vertical logarithmic scale.

The first step in the regularization is to verify the discrete Picard condition. This enables us to evaluate the discretization of the continuous problem and to choose the best solution is certain cases. It is known that this condition is sensitive to several factors (see Section A.4.3). To show this sensitivity, we study two examples, considering the cases $N = 210, 420$ and $\tau = 0.01$ for the collocation method, taking unperturbed and perturbed right-hand sides. In Fig. 4.6 the Picard condition for the system (4.78) is shown and in Fig. 4.7 the case of the system (4.77).

In Fig. 4.6a, we can see that none of the Fourier coefficients $|u_i^T b|$ for the unperturbed problem are smaller than the singular value σ_i. However, when the order of the matrix C in (4.78) increases (see Fig. 4.6b), certain Fourier coefficients satisfy this condition. Notice, that in both cases the Fourier coefficient curves can be approximated accurately by a linear trend. Hence, one possible regularization strategy is to increase the matrix order, which implies in providing more information on the right hand side of the system (4.78), or to change the discretization. However, in spite of the fact that the Picard condition is not satisfied, we obtain an accurate regularized solution, therefore we evaluate another case where the regularization is taken into account (see Fig. 4.5).

Now we study the Picard condition in the case that the regularization has been applied, i.e. to the system (4.77). In Fig. 4.7, we can see that most of the Fourier coefficients $|u_i^T b|$ for the unperturbed problem are smaller than the singular value σ_i (see Fig. 4.7a), although many singular values and Fourier coefficients would be affected by rounding errors. On the other hand, for the perturbed problem (see Fig. 4.7b), we see that with fine discretization, many more Fourier coefficients $|u_i^T b|$ are smaller than the singular value σ_i, comparing to the unperturbed case. We also see that in both cases the Fourier coefficient curves can be approximated accurately by linear trend with small slope decreasing to zero faster than the singular values. This indicates that the perturbed and unperturbed right hand sides satisfy the discrete Picard condition in the system (4.77), i.e., in average the Fourier coefficients are smaller than the singular values.

Thus, these facts suggest that an alternative regularization method for this problem is to damp the components for which the perturbation dominates, and leave the remaining components intact. Indeed, in the collocation method we need to choose the regularization parameter with large discretization grid size and then use the SVD expansion to filter the small singular values.

Another source of errors is the Singular Value Decomposition (SVD) itself, which we do not study in detail here, so the influence on the regularization parameter is a topic for further work.

In next section we prove that the behavior of the regularized solution in the above numerical examples occurs in general, i.e., the regularized solution converges to the "true" solution penalized with first order derivative.

4.6 Convergence results

In this section we prove stability results for the general linear equation (4.16). The numerical examples in the previous section suggest that it is possible to stabilize the integral equation of the first kind using only first derivative penalizing functionals (see Section 4.3). We will see that this is an intrinsic property of the operator kernel.

First we present preliminary concepts and lemmas to be used in the sequel.

4.6.1 Preliminaries

The Tikhonov regularization for solving the integral equation of the first kind in (4.16) is used (see section 4.3). Basically, the method reduces to minimizing the functional

$$\Phi_\alpha(f) = ||Kf - g||^2 + \alpha||Lf||, \tag{4.107}$$

where L represents an unbounded, self-adjoint linear operator. For example in the numerical experiment in previous section we took

$$Lf = \frac{df}{dx}. \tag{4.108}$$

With this choice we obtain good numerical results (see Section 4.5 for details). In this section we prove that taking one derivative in the penalizing functional $||Lf||$ we guarantee that the regularized solution f_α of Eq. (4.107) converges in L^2-sense to the "true" solution $K^\dagger g$ (see Section A.3.1 for the definition of $K^\dagger$).

Now, we present the main concepts and definitions for explaining the convergence result. We assume that we have a Fredholm integral equation of the first kind on $[0,1]$

$$\int_0^1 k(x,t)f(x) = g(t), \tag{4.109}$$

where $k \in L^2([0,1]^2)$ and $f \in L^2[0,1]$.

Remark 4.13 *Equation* (4.16) *can be reduced to an equation of the form* (4.109) *by a trivial change of variables.*

We regularize Eq. (4.109) by using the Hilbert scale (see section A.2) $(X_s)_{s\in\Re}$, which is induced by the operator $L : D(L) \subset L^2[0,1] \longrightarrow L^2[0,1]$ defined by

$$Lf = \sum_{n=1}^{\infty} n(f, v_n)v_n, \tag{4.110}$$

where $v_n(s) = \sqrt{2}\sin(n\pi s)$ and $(\cdot,\cdot)$ is the inner product in $L^2[0,1]$. We take

$$D(L) = \{f \in H^1[0,1] : f(0) = f(1) = 0\}. \tag{4.111}$$

Notice that Eq. (4.110) is the spectral representation of the operator L in (4.108) with $D(L)$ defined in (4.111). Moreover, the operator L defined in this way is injective.

It is possible to show ([92]) that for $s > 0$ we have a Hilbert scale defined as:

$$X_s = D(L^s) = \left\{f \in H^s[0,1] : f^{2e}(0) = f^{2e}(1) = 0, e = 0,1,\ldots,\left[\frac{s}{2} - \frac{1}{4}\right]\right\}, \tag{4.112}$$

and the inner product in X_s is given by

$$(f,g)_k = (L^k f, L^k g) = \pi^{-2k}\left(\frac{d^k f}{dx^k}, \frac{d^k g}{dx^k}\right). \tag{4.113}$$

4.6.2 Auxiliary lemmas

Lemma 4.14 *There exist $b \geq 0$ and $d > 0$ such that*

$$||Lf|| \geq d||f||_b. \tag{4.114}$$

Proof: By definition we have $||f||_s = ||L^s f||$, so Eq. (4.114) holds taking $d = 1$ and $b = 1$ $\square$. Moreover, the following lemma is valid.

Lemma 4.15 i) *Let $K : L^2[0,1] \to L^2[0,1]$ be a linear operator defined as*

$$Kf := \int_0^1 k(x,\cdot)f(x)dx; \tag{4.115}$$

ii) *let $s_1(t)$ and $s_2(t)$ be monotone increasing continuous functions such as*

$$0 \leq s_1(t) \leq s_2(t) < 1 \quad on \quad [0,1], \tag{4.116}$$

iii) *let $S(x,t)$ be a continuous function strictly positive on $s_1(t) \leq x \leq s_2(t)$ with $t \in [0,1]$.*

Assume that the kernel is given by $k(x,t) = \begin{cases} 0 & s_2(t) \leq x \leq 1; \\ S(x,t) & s_1(t) < x < s_2(t); \\ 0 & 0 \leq x \leq s_1(t). \end{cases}$

Then there exists a constant $c > 0$ such that

$$||Kf|| \geq c||f||_{-1}, \tag{4.117}$$

where

$$||f||_{-1}^2 = \sum_{j=1}^{\infty} \frac{|(f, e_j)|^2}{j^2}. \tag{4.118}$$

Proof: Let $e_j(t) = \sqrt{2}sin(\pi jt)$, with $j = 0, 1, \ldots$, be an orthonormal basis of $D(L)$ in (4.111). We have for $f \in D(L)$

$$f = \sum_{j=1}^{\infty}(f, e_j)e_j. \tag{4.119}$$

The following Parseval equality holds

$$||Kf||^2 = \sum_{j=1}^{\infty}\sum_{q=1}^{\infty}(f, e_q)(f, e_j)(Ke_q, Ke_j), \tag{4.120}$$

and the Parseval inequality holds

$$||Kf||^2 \geq \sum_{j=1}^{\infty} |(f, e_j)|^2||Ke_j||^2. \tag{4.121}$$

Set $n_1 = \max\limits_{[0,A]}\{s_2(t)\}$,

$$\gamma_1 = \min_{(x,t)\in[0,n_1]\times[0,1]} S(x, t) > 0, \quad \gamma_2 = \max_{(x,t)\in[0,n_1]\times[0,1]} S(x, t) > 0 \tag{4.122}$$

and

$$D_j(t) = cos(js_1(t)\pi) - cos(js_2(t)\pi), \tag{4.123}$$

we obtain

$$\frac{\sqrt{2}\gamma_1}{j\pi}D_j(t) \leq Ke_j(t) \leq \frac{\sqrt{2}\gamma_2}{j\pi}D_j(t). \tag{4.124}$$

If $D_j(t) > 0$

$$Ke_j(t)^2 \geq \frac{2\gamma_1^2}{j^2\pi^2}D_j(t)^2. \tag{4.125}$$

or if $D_j(t) < 0$

$$Ke_j(t)^2 \geq \frac{2\gamma_2^2}{j^2\pi^2}D_j(t)^2. \tag{4.126}$$

As $D_j(t)$ changes sign at a finite number of points we conclude from Eqs. (4.125) and (4.126) that

$$\int_0^1 Ke_j(t)^2dt \geq \frac{2\gamma_1^2}{j^2\pi^2}\int_0^1 D_j(t)^2dt. \tag{4.127}$$

As $\int_0^1 D_j(t)^2 dt > D > 0$ holds uniformly for some D, we obtain

$$||Ke_j||^2 \geq \frac{2\gamma_1^2}{j^2\pi^2} D. \tag{4.128}$$

Thus

$$||Kf||^2 \geq \frac{2D\gamma_1^2}{\pi^2} \sum_{j=1}^{\infty} \frac{|(f, e_j)|^2}{j^2}. \tag{4.129}$$

□

4.6.3 Convergence of the regularized solution

Now, we can prove that the regularized solution of Eq. (4.16) in Section 4.1 converges to the least square solution $K^{\dagger}g$ penalized with a first derivative term. We show that this is a particular case of the family of operators treated in Lemma 4.15. Let us choose $\alpha = \alpha(\delta, y)$ by the discrepancy principle, i.e., satisfying Eq. (A.25). Then the following theorem is valid

Theorem 4.16 *Let $K : X \to Y$ be a compact linear operator, satisfying the assumptions in lemma* 4.15. *Let $\hat{x}$ be the generalized solution belonging to the set $M_\rho = \{x \in D(L) : ||Lx|| < \rho\}$. Then the regularized solution $\tilde{x}_\alpha$ satisfies*

$$||\hat{x} - \tilde{x}_\alpha|| \leq 2\rho^{1/2}(\delta/c)^{1/2}, \tag{4.130}$$

where $c = \sqrt{2D}\gamma_1/\pi$.

Proof: It follows from the application of Theorem A.22 and Lemmas 4.14 and 4.15 □.

Remark 4.17 *Notice that if $\delta \to 0$ when $\alpha \to 0$ then $\tilde{x}_\alpha \to \hat{x}$.*

Now it is easy to see that the operator defined in Eq. (4.16) is a particular case of the class defined in lemma 4.15. It is enough to use the change of variables $t = T/A$ and $x = y/M$ in the integral equation (4.16) and to choose:

$$s_1(t) = \sigma(1, t)/M, \quad s_2(t) = \sigma(0, t)/M \tag{4.131}$$

and

$$S(x, t) = \left(\frac{\partial \sigma}{\partial x}(s(x, t), t)\right)^{-1}. \tag{4.132}$$

With these new variables, the operator K_σ in (4.16) satisfies the assumptions of Lemma 4.15. Therefore the convergence result obtained here is valid for the operator K_σ.

Chapter 5

Recovery of the permeability reduction and filtration functions from concentration and pressure histories

In this chapter we formulate the inverse problem of determining the permeability reduction and filtration functions from the laboratory experimental measurements. The pressure drop and effluent concentration histories are measured. Basically, the recovery method consists in optimizing functionals which relate changes in the unknown functions to changes in measured outputs from the filtration experiments. The existence, uniqueness and stability issues for nonlinear ill-posed problems are treated. The practical importance of recovering the permeability reduction and filtration functions is that these functions are used for the simulation of injectivity in wells.

5.1 Preliminaries

A broad class of ill-posed inverse problems involves the recovery of distributed coefficients in systems of differential equations, see for example [30] and [46]. The first part of the direct problem is an equation

$$\mathcal{A}(\theta)u = q, \tag{5.1}$$

where $\mathcal{A}$ refers to a differential operator defined on an appropriate domain Ω and equipped with suitable boundary and/or initial conditions. Here θ represents a parametrization of unknown functions to be determined from the measurement b of the solution of (5.1).

Remark 5.1 *In our study $\mathcal{A}$ represents the evolutionary operator given by the system of equations* (2.9)-(2.10)*, with $u = (c, \sigma)$ and $q = 0$. The boundary and initial conditions are given in equations* (2.12)*,* (2.21) *and* (2.22)*.*

Let the operator Q indicate the projection onto the locations in Ω to which the data are associated. Thus, the data are viewed as a nonlinear function of the model:

$$b = Q(\mathcal{A}(\theta))^{-1}q + \epsilon, \tag{5.2}$$

where ϵ is the measurement noise. To calculate $(\mathcal{A}(\theta))^{-1}$ in (5.2), we need to be able to solve the forward problem (5.1) by a stable numerical method. Moreover an appropriate parametrization θ must be chosen.

In the nonlinear case, in general, there is no unique parametrization θ that generates the measured data. Moreover, even in the absence of noise, the recovered θ does not depend continuously on such data ([5], [31]). Therefore, a regularization procedure must be used to recover a smooth solution of the regularized problem that is at least locally unique.

Here we discuss the identification problem of the unknown parameters θ from certain observations b in distributed systems, for θ belonging to certain admissible subset Q_{ad}. Now, the problem of recovering $\theta \in Q_{ad}$ in (5.2) can written as an unconstrained, linear or nonlinear least squares problem, i.e.,

$$\min_{\theta \in Q_{ad}} ||Q(\mathcal{A}(\theta))^{-1}q - b||^2 + \alpha||W(\theta - \theta_0)||^2, \tag{5.3}$$

where W typically is a weighting matrix involving discretized derivatives, i.e., a stabilizing functional which does not depend on θ, while θ_0 is a reference model and α is the regularization parameter. For instance, in the linear case we used the matrices in (4.106).

The optimization problem (5.3) obtained in this way is typically very large and incurs in several numerical difficulties. So, additional information about the solution is needed. This information is included in the subset Q_{ad} and in the point θ_0.

Several minimization methods for obtaining approximate solutions of (5.3) generate sequences of iterates where for a given current iterate θ, an update of the form $\theta \leftarrow \theta + \beta\delta\theta$ is subsequently carried out, and the process is repeated to convergence. The correction $\delta\theta$ is obtained either by linearizing the expression under the norm in (5.3) and solving a linear least squares problem

$$(J^T J + \alpha W^T W)\delta\theta = J^T(g - \mathcal{A}(\theta)) - \alpha W^T W(\theta - \theta_0), \tag{5.4}$$

where $J = J(\theta) = \frac{\partial \mathcal{A}(\theta)}{\partial \theta}$ is the sensitivity matrix, or by solving some quadratic function obtained by approximating the Hessian of the objective function ([23] and [24]). Thus the role of the matrix W in (5.3) is to provide a stable way of calculating the advance $\delta\theta$, which is very useful when the matrix J has high condition number.

The parameter θ is calculated by taking into account certain restrictions for determining the increment $\delta\theta$ in a stable way. In general, the physical solution has bounds that are used for defining the subset Q_{ad} with an appropriate structure for guaranteeing the convergence of the optimization procedure to the "true" solution.

A number of questions arise when attempting to carry out this approach in practice, including the scaling of W and the calculation of the regularization parameter α. We examine these issues in the context of inverse problems appearing in the filtration process of injection of water with particles.

5.2 Least square solution

The system (2.9)-(2.10) involves the filtration function $\lambda(\sigma)$. On the other hand, Darcy's law (2.11) depends on the permeability reduction function $k(\sigma)$. The inverse treatment of these equations is simplified by assuming that $\lambda(\sigma)$ and $k(\sigma)$ depend on a finite number of parameters ([10]).

One approach to recover these functions referred previously is to choose a least squares solution, which formulates the inverse problem as an optimization problem. The parameters leading to a solution of the evolutionary differential equation that best matches the experimental measurements are sought.

However, is not evident that the solution of the optimization problem solves the original inverse problem. So, uncertainty analysis is necessary to predict the most probable set of optimum parameters. In the sensitivity analysis, the lack of explicit solutions of the so-called direct problem for different parametrizations of $\lambda(\sigma)$ is an obstacle.

For the validation of the method several numerical experiments are used. Other applications can be found in [28], [22], [31], [5] and [18].

5.3 Parametrization

Several types of parametrization are analyzed in order to find which one produces the best fit between experimental data and the output predicted by the model.

The choice of parameters and their ranges depend on the physical properties of the filtration process. Thus, for permeability reduction we take $k(\sigma)$ with n parameters

$$k(\sigma) = (1 + \theta_1\sigma + \theta_2\sigma^2 + \theta_3\sigma^3 + \ldots + \theta_n\sigma^n)^{-1}. \tag{5.5}$$

For the filtration function the following parametrizations are considered, using θ_j with $j > n$:
a) $\lambda(\sigma) = \max\{\theta_{n+1} + \theta_2\sigma + \theta_3\sigma^2 + \ldots + \theta_N\sigma^{N-n-1}, 0\}$, with $N > n$
b) $\lambda(\sigma) = \theta_{n+1}e^(- \theta_{n+2}\sigma)$,
c) $\lambda(\sigma) = \theta_{n+1} - \theta_{n+2}e^(- \theta_{n+3}\sigma)$.
In (a) the parameters θ_j, $j = n+1, \ldots, N$ are assumed to have variable sign. In cases (b) and (c) the parameters have positive sign. We also impose some additional conditions such as monotonicity (decreasing or increasing), and positivity of the unknown function $k(\sigma)$ and $\lambda(\sigma)$. Another unknown function that arises in the problem due to the heterogeneity of the clean rock is the absolute permeability spatial distribution, which can be determined separately from Darcy's law. We assume here that the parameters θ have values in a compact set given by the box:

$$\Omega = \underline{\theta}_j \leq \theta_j \leq \overline{\theta}_j, \quad \text{for} \quad j = 1, \ldots, N. \tag{5.6}$$

Remark 5.2 *Denoting the function $f(\sigma) = 1/k(\sigma)$, we define a one to one map of $f(\sigma)$ and $\lambda(\sigma)$ into the set of parameters $\theta \in \Omega$, such that for all parametrizations θ of $f(\sigma)$ and $\lambda(\sigma)$ the convergence in parameter space $\mathbb{R}^N$ implies the uniform convergence of the functions $f(\sigma), \lambda(\sigma)$ in the H^1 norm.*

Remark 5.3 *Since the solution σ and c of the system* (2.9) *and* (2.10) *obey ordinary differential equations along characteristic lines (see Remark* 2.2*), the continuity of the solution is a consequence of the theorem on ODE solution continuity with respect to parameter changes (see [62], pag.* 91*). So the maps*

$$\theta \to \sigma(X, T; \theta), \quad \theta \to c(X, T; \theta) \tag{5.7}$$

are continuous.

Remark 5.4 *Synthetic data are used in order to calibrate the model and to test the algorithm. These data are obtained for certain parameters by solving the direct problem given by the system of equations* (2.9), (2.10) *and* (2.11). *So, the pressure drop history at different points in the core as well as the effluent concentration history are obtained, and random errors are added to these histories for simulating the observational data.*

5.4 Filtration function from effluent concentration

In this section we describe the method for recovering the filtration function from the effluent concentration history. The well posedness is discussed, as well as some numerical examples of the recovery method.

5.4.1 Well-posedness of the inverse problem

The operator theory framework is used to study the well-posedness of the inverse problem of determining the filtration function from the effluent concentration. The stability and convergence result obtained here are based on [16], [33], [67] and [25]. We choose

$$D(G^c) = \{\lambda \in H^2[0,1], \quad \text{such that} \quad \lambda > \gamma_1\}, \tag{5.8}$$

with γ_1 constant. Let us define the nonlinear operator

$$G^c : D(G^c) \subset H^2[0,1] \to L^2[0,A], \quad G^c(\lambda) = c(1,\cdot\,;\lambda), \tag{5.9}$$

where λ represents the filtration function and $c(1,\cdot\,;\lambda)$ is the effluent concentration obtained from the solution of the system (2.9)-(2.10), with boundary and initial condition given in (2.12) and (2.21). From the well-posedness of the direct problem, we have that for each λ there exist a unique function $c(1,\cdot\,;\lambda)$; so the operator in (5.9) is well-defined. Notice that the domain $D(G^c)$ is closed and convex, therefore it is weakly closed.

Let us denote by

$$\mathcal{M} = \{\lambda \in H^2[0,1] \quad \text{such that} \quad \gamma_2 < \lambda < \gamma_3\}, \tag{5.10}$$

where γ_3 is constant. From now on, we take in $\mathcal{M}$ the uniform norm, which is possible because $H^2[0,1]$ is compactly embedded in $C^1[0,1]$

Thus the following theorem is valid:

Theorem 5.5 *The following assertions are valid.*

i) Let λ be represents the filtration function and $c(1,\cdot\,;\lambda)$ is the solution of the system (2.9)-(2.10)*, with boundary and initial condition given in* (2.12) *and* (2.21)*. Let $\kappa \geq 0$ and the domain*

$$D(G^c) = \{\lambda \in H^{2+\kappa}[0,1] \quad \textit{such that} \quad \lambda > \gamma_2\}. \tag{5.11}$$

Then the (nonlinear) operator

$$G^c : D(G^c) \subset H^{2+\kappa}[0,1] \to L^2[0,A], \quad G^c(\lambda) = c(1,\cdot\,;\lambda), \tag{5.12}$$

is continuous and injective.

ii) Let $D(G^c)$ *be as in* (5.8). *Then the operator in* (5.9) *is weakly closed and compact.*

iii) The map $G^c : \mathcal{M} \to G^c(\mathcal{M})$ *is continuous and has continuous inverse.*

Proof: (i) Let $\lambda_n \to \lambda$ in $H^{2+\kappa}[0,1]$ with $\kappa \geq 0$. Since $H^{2+\kappa}[0,1]$ is compactly imbedded in $C^1[0,1]$ then $\lambda_n \to \lambda$ uniformly in $C^1[0,1]$. From Remark 5.3 follows that $G^c(\lambda_n) \to G^c(\lambda)$ in $L^2[0,A]$. The injectivity is a consequence of the uniqueness of the solution of the system of equations (2.9) and (2.10).

(ii) Let $\{\lambda_n\}$ be a sequence in $D(G^c)$ converging weakly in $H^2[0,1]$ towards λ. Since $D(G^c)$ is weakly closed $\lambda \in D(G^c)$ and since $H^2[0,1]$ is compactly embedded in $C^1[0,1]$, then $\lambda_n \to \lambda$ in $C^1[0,1]$. By (i) $G^c(\lambda_n) \to G^c(\lambda)$ in $L^2[0,A]$. Thus, we proved that G^c is compact and hence weakly closed.

(iii) Notice that G^c is continuous in $\mathcal{M}$ by (i) and $\mathcal{M}$ is a compact subset of $C[0,1]$ (see Lemma E.1), then (iii) is a consequence of the Lemma of Tikhonov $\square$.

Remark 5.6 *From (ii) in Theorem* 5.5 *and Theorem A.*18*, the inverse problem of determining the filtration function* λ *in* $G^c(\lambda) = b$*, with given* $b = c_e^{data}(\cdot)$ *is an ill-posed problem.*

5.4.2 Implementation

Here we assume that the filtration function $\lambda(\sigma)$ is well-behaved, i.e., continuously differentiable. Moreover, from Remark 5.2 there exists a correspondonce between the filtration function λ and its parametrization θ. So, from now on we denote $c(1,T;\lambda)$ by $c(1,T;\theta)$.

An algorithm that allows the recovery of the filtration function $\lambda(\sigma)$ from the effluent concentration $c_e^{data}(T)$ is presented in Chapter 3. This method has some instabilities, which are treated in Section 3.2. However, optimization is a more robust recovery method. It consists on finding the filtration function that minimizes the cost function

$$F^c(\theta) = \int_0^A (c(1,T;\theta) - c_e^{data}(T))^2 dT, \tag{5.13}$$

where θ is a certain parametrization of λ; $c_e^{data}(T)$ represents the available information and $c(1,T;\theta)$ is a solution of the system (2.9)-(2.10). Therefore, the value of $F^c(\theta)$ is obtained after the system (2.9) and (2.10) has been solved for the fixed value θ. The optimization algorithms used for minimizing the nonlinear function $F^c(\theta)$ are discussed in Appendix D.

Remark 5.7 *Let an appropriate parametrization of* λ *be denoted by* $\theta \in \Omega$ *; the operator in* (5.9) *can be rewritten as*

$$G^c : \Omega \subset \mathbb{R}^N \to L^2[0,A], \quad G^c(\theta) = c(1,\cdot\,;\theta). \tag{5.14}$$

Now, the problem of recovering the filtration function is equivalent to solving the nonlinear operator equation

$$G^c(\theta) = b, \tag{5.15}$$

where $b = c_e^{data}(T)$ *is given.*

Using Remarks 5.2 and 5.3, Theorem 5.5 can be rewritten in terms of the filtration function parametrization in the following lemmas.

Lemma 5.8 *Let* $c(1, \cdot\,; \theta)$ *be the effluent concentration obtained by solving* (2.9) *and* (2.10) *for a filtration function* $\lambda(\sigma)$. *Then the map* $G^c : \theta \to c(1, \cdot\,; \theta)$ *is continuous and injective.*

Lemma 5.9 *The nonlinear operator in* (5.14)*, restricted to the compact set* Ω *in* (5.6) *is continuous and one to one.*

Lemma 5.10 *The inverse map of the function in* (5.14)*, restricted to the compact* Ω *set in* (5.6)*, is continuous.*

Notice that the functional in (5.13) can be rewritten as

$$F^c(\theta) = ||G^c(\theta) - b||_2^2, \tag{5.16}$$

where b denotes the effluent concentration history. The existence and uniqueness of the solution of the inverse problem in (5.13) follows from the next theorem

Theorem 5.11 *There exist a unique solution of the optimization problem*

$$\min_{\theta \in \Omega} F^c(\theta). \tag{5.17}$$

Proof: Since the function F^c is continuous and injective on the compact set Ω, using the theorem of Weierstrass ([73]) we obtain that F^c has an unique minimum on Ω $\square$.

In the nonlinear case, the Lemma of Tikhonov provides a way to stabilize certain ill-posed inverse problems, however it leads neither to a quantitative stability estimate nor to a procedure for obtaining the solution. Thus, we tested three optimization procedures for solving nonlinear inverse problems.

Numerical results and discussion

The Quasi-Newton method with line search (see Appendix D) is the first algorithm implemented for finding the minimum of the cost function (5.13) in this work. This method has been extensively used for solving ill-posed problems ([5], [49] and [87]). Figures 5.1 and 5.2 show the plots of predicted and prescribed effluent concentration. The prescribed effluent concentration is obtained from synthetic data with perturbation error of 5%.

In Fig. 5.1a we show the recovered two-parameter linear filtration function $\lambda(\sigma) = \max\{\theta_1 + \theta_2\sigma, 0\}$ at each iteration of the algorithm. In Fig. 5.1b the dashed line represents the effluent concentration predicted by the model and the solid line with circles represents the synthetic data.

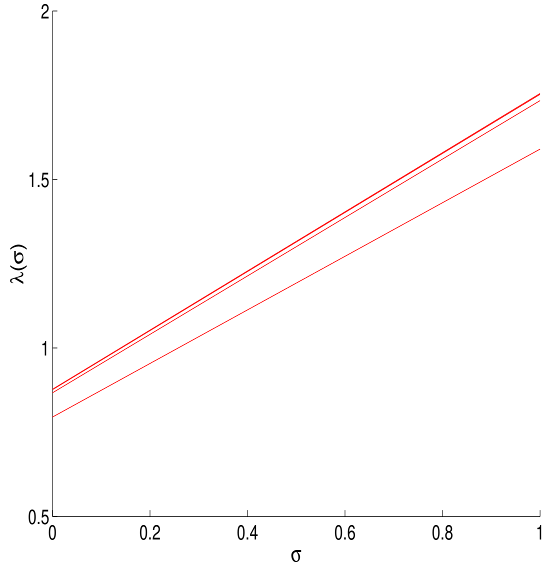

a) Recovered filtration function.

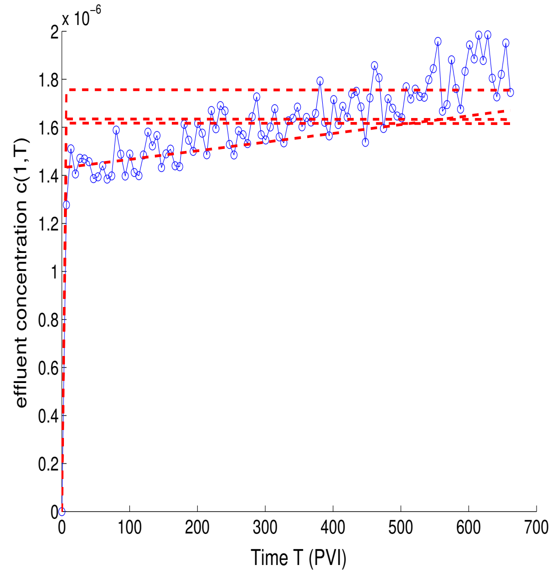

b) Effluent concentration $c(1,T)$ in fraction units.

Figure 5.1: Iterate solutions recovering filtration function $\lambda(\sigma) = \max\{1 - 171\sigma, 0\}$. In (b) Solid line with circles: data perturbed with 5% noise. Dashed lines: iterates.

The Quasi-Newton method in this case converges in five iterations. However, the recovered filtration function is not accurate. The filtration function obtained is unphysical because only increasing effluent concentrations should arise from decreasing filtration functions, according to Remarks 2.10-2.11. So, this example shows that parameter restrictions are needed to recover correctly the unknown filtration functions with this method, i.e., appropriate bounds on θ_1 and θ_2 must be added in the optimization procedure to guarantee that the solution lies in the set of feasible solutions.

An optimization technique that performs the minimization of a nonlinear function with box constraints is needed. The projected gradient method with box constraints is used, see [69], [82], [36] and [19] for details of the method. This method has been successfully employed in many practical inverse problems, see e.g. [18].

The program "EASY" implements the above mentioned technique for optimizing the functional (5.13) with box constraints on the parameter θ. In the calibration of the "EASY" program, several numerical experiments were carried out for finding the optimum set of parameters. Moreover, scales for the independent variables were taken into account, as well as properties of the solution such as positivity and monotonicity, accuracy of the solution and compatibility of initial parameter guess.

The large-scale interior reflective Newton method was also used for recovering the filtration function. This algorithm is available in Matlab's optimization toolbox.

The recovered filtration functions are shown in Fig. 5.2a . The recovered filtration functions are $\lambda(\sigma) = \max\{1.05 - 235\sigma, 0\}$ for Matlab algorithm and $\lambda(\sigma) = \max\{0.99 - 179\sigma, 0\}$ for the "EASY" algorithm, with relative errors of 3.6% and 0.2% respectively. As opposed to the numerical result using the Quasi-Newton method, these procedures recover

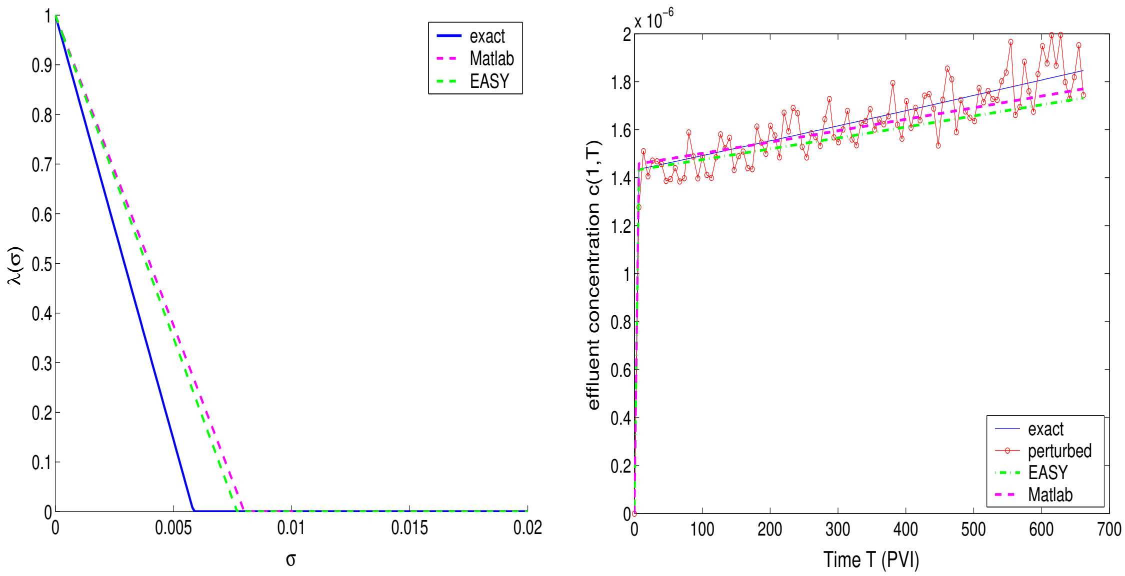

a) Recovered filtration functions.

b) Effluent concentration $c(1, T)$ in fraction units.

Figure 5.2: Approximate solution with filtration function $\lambda(\sigma) = \max\{1 - 171\sigma\}$.

accurately the prescribed filtration function. The relative error of the estimated parameter θ_2 is 37% using the Matlab algorithm and 5.2% using the EASY algorithm; the estimated error in the parameter θ_1 is 2% with Matlab and 5% with "EASY". Both methods predict the true sign of the filtration function slope; this recovery was possible, in part, because we set the box constraint for the parameter slope θ_2 as $[-1000, 0]$.

Notice that the filtration function slope value θ_2 differs from the exact value much more than the parameter θ_1. This disagreement is due to the low sensitivity of the effluent concentration with respect to the slope parameter (see Section 2.5). The choice of the "best" approximation requires sensitivity analysis, which is discussed in Chapter 7.

In Fig. 5.2*b*, the unperturbed effluent concentration and perturbed effluent data with 5% error is shown. Moreover, the predicted effluent concentration using the Matlab and "EASY" algorithms are shown. Notice that both procedures predict well the effluent concentration history.

5.5 Permeability reduction and filtration functions from pressure distribution history

Here the recovery method to obtain the permeability reduction and filtration functions from pressure distribution history is discussed. The well-posedness of the inverse problem is studied. Moreover, the implementation of the recovery method based on the parametrization of the functions is described. The inverse problem is write in terms of a nonlinear operator. This operator relating the permeability reduction and filtration functions with the pressure drop histories is based on (2.11).

5.5.1 Well-posedness of the inverse problem

In this section we study the well-posedness of the inverse problem. We prove that the inverse problem is ill-posed and a regularization of the problem is found. Assuming that $k(\sigma)$ is strictly positive, we can define the function

$$f(\sigma) = 1/k(\sigma). \tag{5.18}$$

We find a feasible set for the solution $(f(\sigma), \lambda(\sigma))$, where the inverse problem has a unique solution and such that small perturbations of experimental pressure history produce small parameter variations. We choose

$$D(G^p) = \{(f, \lambda) \in H^1[0,1] \times H^2[0,1], \quad \text{such that} \quad f > \bar{f}_1, \quad \lambda > \bar{\lambda}_1\}, \tag{5.19}$$

where $\bar{f}_1$ and $\bar{\lambda}_1$ are positive constants. Let us define on $D(G^p)$ the nonlinear operator

$$G_l^p(f, \lambda) = \int_{X_l}^{X_{l+1}} f(\sigma(X, \cdot\,; \lambda))dX, \quad \text{with} \quad l = 1, \ldots, m_p. \tag{5.20}$$

Furthermore, we define

$$G^p : D(G^p) \subset H^1[0,1] \times H^2[0,1] \to (L^2[0, A])^{m_p}, \tag{5.21}$$

$$G^p(f, \lambda) = \left(G_1^p(f, \lambda), \ldots, G_{m_p}^p(f, \lambda)\right), \tag{5.22}$$

where f is defined in (5.18), λ is the filtration function and $\sigma(X, \cdot\,; \lambda)$ is the solution of the system (2.9)-(2.10). From the well-posedness of the direct problem we have that for each λ there exist a unique piecewise C^1 solution $\sigma(X, \cdot\,; \lambda)$, moreover since I is an integrable function the operator in (5.22) is well-defined. Notice that the domain $D(G^p)$ is closed and convex, therefore it is weakly closed.

Let us restrict the class of feasible solutions so that the nonlinear functional $G^p(f, \lambda)$ is continuous and injective. Then, Tikhonov's Lemma can be used to prove the stability of the ill-posed problem. More precisely, let us denote the subsets

$$\mathcal{F}_1 = \{f \in C^1[0,1] \quad \text{such that} \quad 0 \leq f \leq r_1 \quad \text{and} \quad 0 < f' \leq r_2\}, \tag{5.23}$$

$$\mathcal{F}_2 = \{\lambda \in H^2[0,1] \quad \text{such that} \quad r_3 \leq \lambda \leq r_4\}, \tag{5.24}$$

where r_1, r_2, r_3 and r_4 are constants.

Let us define $\mathcal{F} = \mathcal{F}_1 \times \mathcal{F}_2$. From Lemma E.1, $\mathcal{F}_1$ and $\mathcal{F}_2$ are compact subsets of $C[0,1]$; thus by Theorem 6 of [64], the subset $\mathcal{F}$ is compact in $C[0,1] \times C[0,1]$. From now on, we take in $\mathcal{M}$ the uniform norm, which is possible because $H^1[0,1]$ and $H^2[0,1]$ are compactly embedded in $C[0,1]$. The following theorem holds.

Theorem 5.12 *The following assertions are valid.*

i) Let λ represent the filtration function and $\sigma(X, T; \lambda)$ be the solution of the system (2.9)-(2.10)*, with initial and boundary conditions given in* (2.21) *and* (2.6)*. Let $\kappa \geq 0$ and the domain*

$$D(G^p) = \{(f, \lambda) \in H^{1+\kappa}[0,1] \times H^{2+\kappa}[0,1] \quad \textit{such that} \quad f > \bar{f}_2, \quad \lambda > \bar{\lambda}_2\}. \tag{5.25}$$

Then the (nonlinear) operator

$$G^p : D(G^p) \subset H^{1+\kappa}[0,1] \times H^{2+\kappa}[0,1] \to (L^2[0,A])^{m_p} \tag{5.26}$$

with G^p defined in (5.22) is continuous and injective on $\mathcal{F}$.

ii) Let $D(G^p)$ as in (5.19). Then the operator G^p in (5.22) is weakly closed and compact.

iii) The map $G^p : \mathcal{F} \to G^p(\mathcal{F})$ is continuous and has continuous inverse.

Proof: (i) From Remark 5.3 the map $\lambda \to \sigma(X,T;\lambda)$ is continuous. Now, let $\{f_n, \lambda_n\}$ be a sequence such that $(f_n, \lambda_n) \to (f, \lambda)$ in $H^{1+\kappa}[0,1] \times H^{2+\kappa}[0,1]$, with $\kappa \geq 0$. Since $H^{1+\kappa}[0,1]$ and $H^{2+\kappa}[0,1]$ are compactly embedded in $C[0,1]$ then $f_n \to f$ and $\lambda_n \to \lambda$ uniformly. It follows that $f_n(\sigma(X,T;\lambda_n)) \to f(\sigma(X,T;\lambda))$ uniformly and, by Theorem 5, page. 314 in [73], the sequence

$$g_n(T) = G_l^p(f, \lambda_n)(T) = \int_{X_l}^{X_{l+1}} f_n(\sigma(X,T;\lambda_n))dX \quad \text{with} \quad l = 1, \ldots, m_p, \tag{5.27}$$

consists of continuous functions and $g_n \to g$ uniformly in $C[0,A]$. As a consequence

$$\int_{X_l}^{X_{l+1}} f_n(\sigma(X,\cdot\,;\lambda_n))dX \to \int_{X_l}^{X_{l+1}} f(\sigma(X,\cdot\,;\lambda))dX \quad \text{with} \quad l = 1, \ldots, m_p, \tag{5.28}$$

uniformly as $n \to \infty$ in the $L^2[0,A]$ sense. Finally, the operator in (5.22) is continuous.

Now, we show that the map G^p is injective on $\mathcal{F}$. Taking $(f,\lambda) \in \mathcal{F}$ such that $G^p(f,\lambda) = 0$ then

$$\int_{X_l}^{X_{l+1}} f(\sigma(X,T;\lambda_n))dX = 0 \quad \text{for all} \quad l = 1, \ldots, m_p \quad \text{and} \quad T \in [0,A]. \tag{5.29}$$

From (5.23) and (5.29) we obtain that

$$f(\sigma(X,T;\lambda_n)) = 0 \quad \text{almost everywhere in} \quad [0,1] \times [0,A]. \tag{5.30}$$

Since $\sigma \in [0,1]$, $f = 0$ almost everywhere in $[0,1]$; moreover, as f is an increasing function, then $\sigma(X,T,\lambda) = 0$ almost everywhere, and from (2.9) and (2.10) we conclude that $\lambda = 0$.

(ii) Let $\{f_n, \lambda_n\}$ be a sequence in $D(G^p)$ converging weakly in $H^1[0,1] \times H^1[0,1]$ to (f,λ). Since $D(G^p)$ is weakly closed $(f,\lambda) \in D(G^p)$ and since $H^1[0,1]$ and $H^2[0,1]$ are compactly embedded in $C^1[0,1]$, then $(f_n, \lambda_n) \to (f,\lambda)$ in $C^1[0,1]$. By (i) $G^p(f_n,\lambda_n) \to G^p(f,\lambda)$ in $(L^2[0,A])^{m_p}$. Thus, we have proved that G^p is compact and also weakly closed.

(iii) It follows from (i) and the Lemma of Tikhonov $\square$.

Remark 5.13 *Let h be a given function. From (ii) in Theorem 5.12 and Theorem A.18, the inverse problem of determining the permeability reduction and filtration functions in $G^p(f,\lambda) = h$ is an ill-posed problem.*

5.5.2 Implementation

The equation (2.11) relates the pressure distribution history to the permeability reduction $k(\sigma)$. If we take into account that σ is obtained by solving both equations (2.9)-(2.10), then Eq. (2.11) depends on the filtration function as well.

We need to recover the permeability reduction and filtration functions. We do so for the parametrization

$$k(\sigma) = (1 + \theta_1 \sigma + \theta_2 \sigma^2)^{-1} \tag{5.31}$$

and

$$\lambda(\sigma) = \max\{\theta_3 + \theta_4 \sigma, 0\}. \tag{5.32}$$

The relationships between the permeability reduction function, filtration function and pressure distribution history can be written in terms of a nonlinear functional. To do so, let us use the notation of $\Delta p^l(T;\theta)$ with $l = 1, \ldots, m$, defined from (2.7). We recover θ by minimizing the nonlinear functional

$$F^p(\theta) = \sum_{l=1}^{m} \int_0^A \left(\Delta p^l(T;\theta) - \Delta p^l_{data}(T)\right)^2 dT, \tag{5.33}$$

where $\Delta p^l_{data}(T) = p(X_{l+1}, T) - p(X_l, T)$ is given. Here $\theta = (\theta_1, \theta_2, \theta_3, \theta_4)$ is defined in (5.31) and (5.32). Notice that the value of $F^p(\theta)$ is calculated by solving the system (2.9)-(2.10) first.

Remark 5.14 *Denoting $G^p(\theta) = (G^p_1(\theta), \ldots, G^p_{n-1}(\theta))$, we see that F^p in Eq.* (5.33) *can be rewritten as*

$$F^p(\theta) = \sum_{i=1}^{m} ||G^p_i(\theta) - h_i||_2^2, \tag{5.34}$$

where $h_i(T)$ denotes the pressure drop history from the experiment.

Taking into account Remarks 5.2 and 5.14, it is possible to guarantee the existence of a minimizer for the functional in (5.33).

Remark 5.15 *Analogously to Theorem* 5.11 *we can prove that there exists a solution of the optimization problem*

$$\min_{\theta \in \Omega} F^p(\theta). \tag{5.35}$$

Moreover, we can add restrictions to guarantee the existence of a unique solution. Let us denote by f_θ the parametrization corresponding to the parameter θ, which we assume to be one to one. Now, from (i) in Theorem 5.12*, the functionals G^l_p, with $l = 1, \ldots, m$ on the subset*

$$\bar{\Omega} = \{\theta \in \Omega \quad \text{such that} \quad f_\theta \in \mathcal{F}_1\}, \tag{5.36}$$

are injective. So, by restricting the minimization of F^p to $\bar{\Omega}$ we guarantee the uniqueness of the solution.

Numerical results and discussion

In this section we present several numerical examples where the functional equation in (5.33) is minimized. The Matlab package and the "EASY" program are used. A set of synthetic pressure drops for five consecutive rock segments and synthetic effluent concentration data are created by using a perturbation error of 1% and 5%. The "exact" permeability reduction and filtration functions are prescribed as

$$k(\sigma) = (1 + 300\sigma + 100\sigma^2)^{-1}, \quad \lambda(\sigma) = \max\{1 - 171\sigma, 0\}. \tag{5.37}$$

The permeability reduction function recovered for noisy data is shown in Fig. (5.3a). On the other hand, the experimental pressure drops Δp_i for five segments in the core and the predicted pressure drops are shown in Fig. (5.3b).

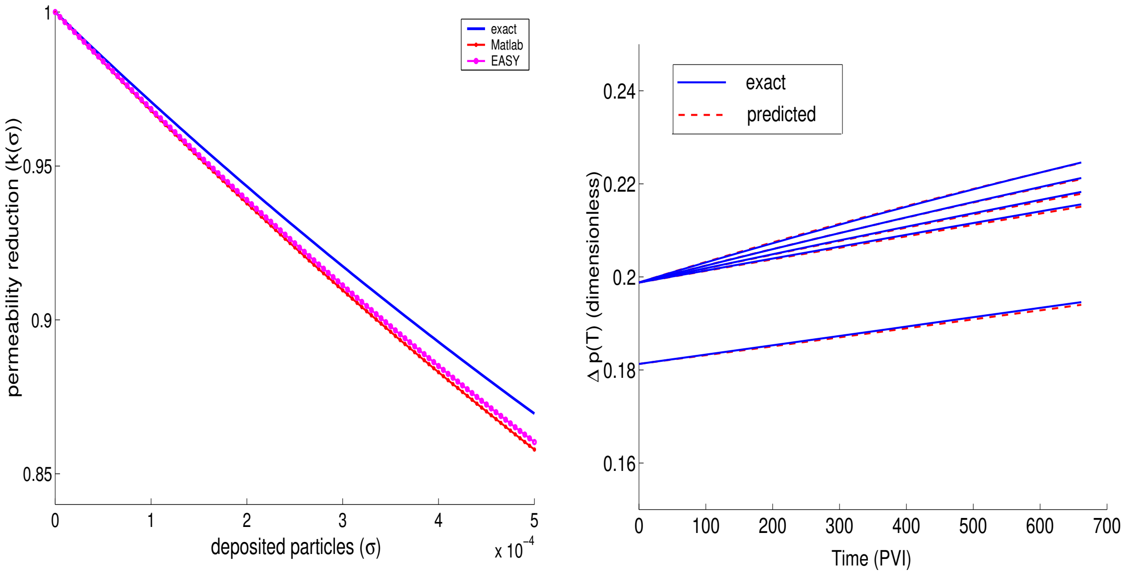

a) Permeability reduction. b) Pressure drops

Figure 5.3: Recovered functions with 5% perturbation error.

The pressure drops $\Delta p_i(T, \theta)$ are recovered with relative errors of 1.8%, 2.5%, 1.9%, 2.5% and 2.4% in the five core segments respectively. The relative errors for the recovered permeability reduction function are 0.8% with "EASY" and 0.78% with Matlab. The recovered filtration functions are $\lambda(\sigma) = 0.95 + 0.0\sigma$ with Matlab and $\lambda(\sigma) = 0.89 - 172\sigma$ with "EASY", with 2.7% and 11.5% relative errors respectively. The effluent concentrations are recovered with relative errors of 14% with "EASY" and 28% with Matlab.

Notice that the permeability reduction function is recovered accurately with both Matlab and "EASY", and the corresponding pressure drop histories are predicted well. However, the recovered filtration function is not accurate with Matlab, and the predicted effluent concentration history is less accurate than the pressure drop histories, with both optimization methods.

To study the sensitivity of the model parameters to the noise in the experimental data, we repeat the above experiment with 1% perturbation error. We see that these functions are recovered more accurately.

The pressure drops $\Delta p_i(T,\theta)$ are recovered with 1.2%, 1.1%, 1.0%, 0.8% and 1.0% of relative error, in the five core segments respectively. The relative errors for the recovered permeability reduction function are 1.7% with "EASY" and 0.9% with Matlab. The filtration functions recovered are $\lambda(\sigma) = 0.92 + 0.0\sigma$ with Matlab and $\lambda(\sigma) = 0.67 - 58\sigma$ with "EASY", with 4.6% and 31% relative error respectively. The effluent concentrations are recovered with 7% with "EASY" and 25% with Matlab.

Since the perturbation error is smaller, the permeability function is recovered with smaller relative error than in the 5% perturbation error case. Moreover, behavior similar to that in the previous case is obtained, i.e., the permeability reduction function is recovered accurately with both procedures, while the filtration function is not. This fact indicates that to recover the filtration function accurately, other factors must be considered in the functional to be minimized, e.g., to take into account the effluent concentration. To solve these difficulties we propose a recovery method where both permeability reduction and filtration functions are recovered accurately (see Section 5.6).

Although 'EASY" and Matlab optimization procedures have comparable recovery skill for the permeability reduction function, we observe the first one finds the optimum faster than the second subroutine, therefore the "EASY" program enables us to test more initial guesses and to study the sensitivity of the model parameters with greater efficiency. The selection of the "true" solution from several local minimum solutions is done using the sensitivity analysis, which examines all the possible local minima and finds the most probable solution. Sensitivity analysis is presented in Chapter 7.

5.6 The recovery method

In Sections 5.4 the inverse problem of recovering the filtration function from the effluent concentration history was studied. On the other hand, in Section 5.5 the recovery of the permeability reduction function from pressure drop histories was presented. None of these methods recovers well both functions, so we present a more complete method that determines accurately the permeability reduction and filtration functions from the pressure drop and effluent concentration histories at the same time. To do so, we use the results obtained in Sections 5.4 and 5.5.

Remark 5.16 *Since the nonlinear operators G^c and G^p satisfy the hipothesis of Theorem A.18, the recovery of the permeability reduction and filtration functions are nonlinear locally ill-posed problems. Hence, the Regularization of Tikhonov is used to find stable solutions. The regularized solution is determined as the minimizer over $D(G^p) \times D(G^c)$ of the functional*

$$(f,\lambda) \to F^c(\theta) + F^p(\theta) + \alpha_c||\lambda - \lambda^*||^2_{H^1[0,1]} + \alpha_p||f - f^*||^2_{H^1[0,1]}. \tag{5.38}$$

Since G^p and G^c are weakly closed, stability and convergence follow from Theorem A.20 and A.21.

Neglecting the interaction between the parameters, i.e., by assuming that they are uncorrelated, we obtain

$$||f - f^*||^2_{H^1[0,1]} \approx l_1(\theta_1 - \theta_1^*)^2 + l_2(\theta_2 - \theta_2^*)^2 \tag{5.39}$$

and

$$||\lambda - \lambda^*||^2_{H^1[0,1]} \approx l_3(\theta_3 - \theta_3^*)^2 + l_4(\theta_4 - \theta_4^*)^2, \tag{5.40}$$

where l_i, $i = 1, \ldots, 4$ are certain constants. Thus, from Eqs. (5.39)-(5.40), we see that the penalization functional can be written in terms of the parameters θ. Using this fact, we propose a method that consists in recovering the permeability reduction and filtration functions by minimizing the cost function

$$H_{\alpha_p,\alpha_c}(\theta) = w_c F^c(\theta) + w_p F^p(\theta) + \alpha_p(\theta_1^2 + \theta_2^2) + \alpha_c(\theta_3^2 + \theta_4^2), \tag{5.41}$$

where F^c and F^p are defined in Eqs. (5.13), (5.33) respectively. Here w_p and w_c are certain positive weights which add to 1, and α_c and α_p represent regularization parameters. The ranges of the parameters θ_k are given in (5.6).

To test the recovery method, a set of synthetic data is generated. We add to the synthetic data a perturbation error of 1% and 5%. We call the first data "clean data" and the second "noisy data". We study three recovery cases based on Eq. (5.41), with different w_i and α_i: Case I: $w_p \approx 1$ and $w_c \approx 0$, Case II: $w_p \approx 0$ and $w_c \approx 1$ and Case III: $w_p \approx w_c$. Case I means that we have given more importance to the pressure drop histories, which was studied in Section 5.5. On the other hand, in Case II we give more weight to the effluent concentration history, which was treated in Section 5.4.

We see that in Case I the recovered permeability reduction function $k(\sigma)$ is obtained accurately, but the recovered filtration function $\lambda(\sigma)$ is not. In Case II we recover $\lambda(\sigma)$ appropriately, but we do not obtain $k(\sigma)$ accurately. These results show that for appropriate recovery, it is important to use both experimental data histories, pressure drops and effluent concentration histories.

Now, we present numerical experiments with clean and noisy data for Case III, i.e., where both experimental data are used, with similar importance level. Figure 5.4 shows the recovered permeability reduction and the filtration function, without penalizing ($\alpha_c = 0$ and $\alpha_p = 0$). The corresponding synthetic pressure drops $\Delta p^l(t)$ for the five segments in the core and the predicted pressure drops are shown in Fig. 5.5. (Fig 5.6 is added to clarify Fig. 5.5*b*). Moreover, Fig. 5.7 contains the effluent concentration predicted in the same numerical experiment.

The recovered permeability reductions have relative errors of 0.6% and 0.7% for clean and noisy data respectively. The predicted pressure drops $\Delta p^l(t,\theta)$ have relative errors of 1.1%, 1.2%, 1.0%, 1.1% and 1.1% for clean data and 1.7%, 2.6%, 1.9%, 2.6% and 2.4% for noisy data. Notice that the predicted and exact histories are very close despite the perturbation error. The recovered filtration functions are $\lambda(\sigma) = \max\{0.99 - 170\sigma, 0\}$ for clean data and $\lambda(\sigma) = \max\{0.99 - 179\sigma, 0\}$ for noisy data, with relative errors of 0.03% and 0.2% respectively. The recovered filtration function from the clean data is indistinguishable from the prescribed function, see Fig. 5.4*b*. The predicted effluent concentrations have relative errors of 1.1% and 3.7% for clean and noisy data respectively. So, we see that for both clean and noisy data the permeability reduction and filtration function are recovered accurately, with smaller relative errors for clean data, as expected in this experiment.

Using the "EASY" program, we found that the recovered solution is sensitive to the initial guess, to the box bounds in Eq. (5.6) and to the noise added to the synthetic data (see examples in Chapter 7). Taking into account this sensitivity and the physical properties of the

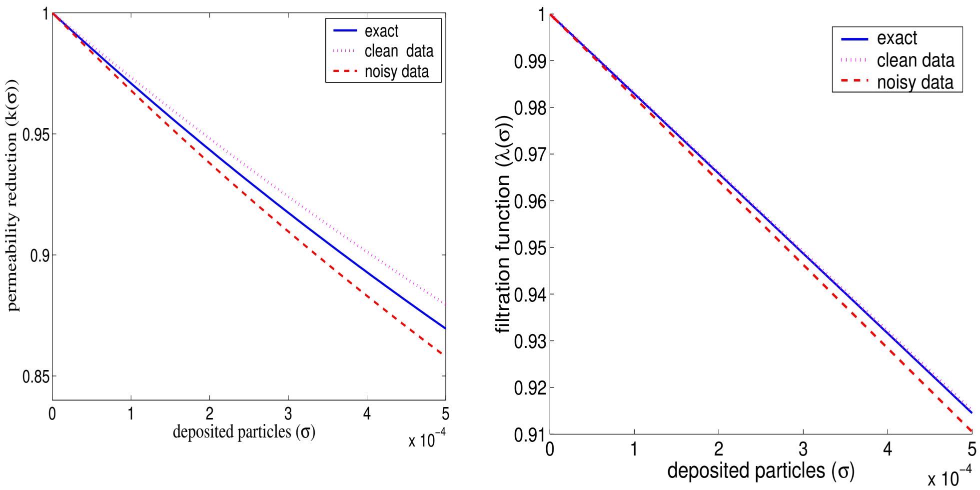

a) Permeability reduction b) Filtration function

Figure 5.4: Recovered functions for clean and noisy synthetic data.

permeability reduction and filtration functions we choose the box constraints appropriately, e.g. the parameters θ_1 and θ_2 are taken positive, the slope θ_4 in $[-1000, 0]$ and θ_3 in $[0, 2]$, see Eqs. (5.31)-(5.32).

Moreover, in order to remedy the ill-posedness of the problem we utilize non-zero penalization parameters α_p and α_c in Eq. (5.41). To estimate good values for these parameters, we made experiments with large values and then we reduced them until an adequate stabilization was obtained. In our case, $\alpha_p = \alpha_c = 10^{-9}$ were adequate. This is a practical solution, however a careful determination of α_p and α_c can be done based on the noise statistics.

Our tests show that a more stable solution is obtained in the presence of the penalization term, i.e. pressure drop changes in solutions obtained with penalization do not produce significative changes in the recovered functions. Moreover, the relative error in the recovered permeability reduction function was 0.4% for the clean data and 0.3% for the noisy data. The recovered filtration functions have relative errors of 0.03% and 0.1% for the clean and noisy data respectively. Notice that the penalization term yields no significant accuracy improvement; however, because among equally inaccurate approximate solutions we prefer the stable ones, a penalizing term such as that in Eq. (5.41) is used. These observations require the sensitivity analysis, which we include in Chapter 7.

From the numerical examples based on synthetic data, we conclude that the recovery method described here is appropriate for finding the permeability reduction and filtration functions from experimental data.

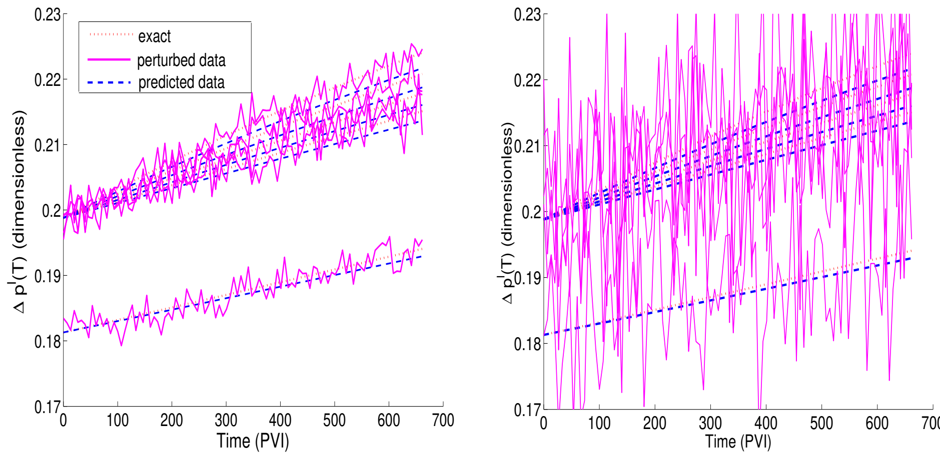

a) Clean data b) Noisy data

Figure 5.5: Pressure drop histories from synthetic data.

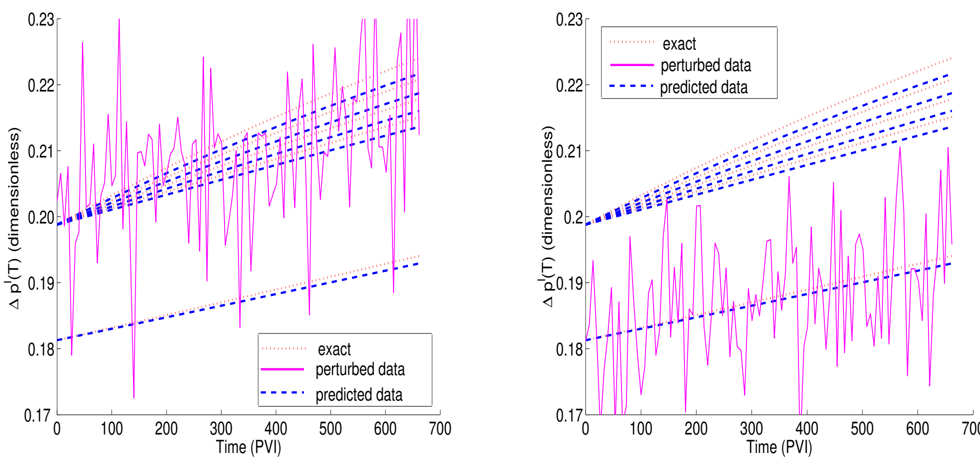

a) Perturbed data in core segment 4 b) Perturbed data in core segment 5

Figure 5.6: Pressure drop histories for noisy data. Vertical scale as in Fig. 5.5*a*.

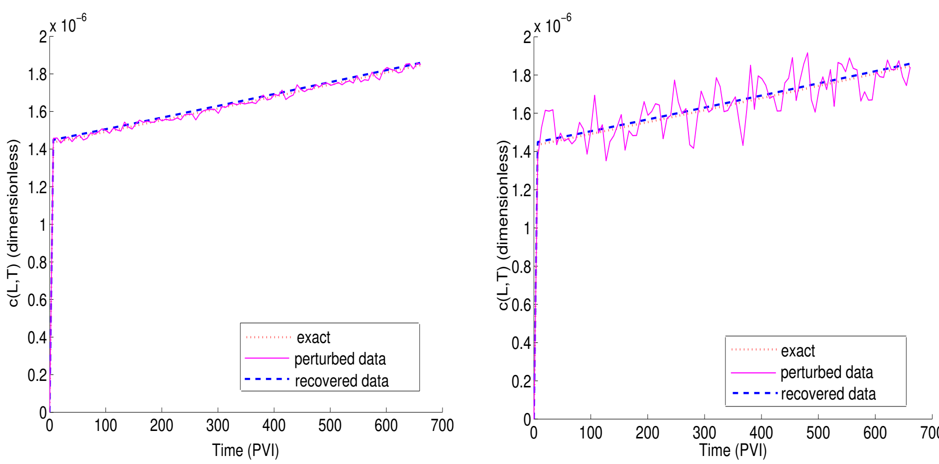

a) Clean data b) Noisy data

Figure 5.7: Synthetic predicted and perturbed effluent concentration.

Chapter 6

Filtration function from particle deposition

In this chapter we discuss the inverse problem of determining the filtration function from the particle deposition given at a grid in space time. Some aspects about methods for solving this inverse problem are analyzed. However, we do not develop all the details.

In sophisticated engineering experiments, the particle deposition can be estimated at a finite number of points and times (X_l, T_j), $l = 1, \ldots, n$, $j = 1, \ldots, m$. The deposition $\sigma(X,T)$ at any (X,T) can be obtained by interpolation. In theory we assume that $\sigma(X,T)$ is given at all points and times of the physical domain.

6.1 Recovery methods

We assume that the filtration function is a well-behaved function. Now, we summarize some methods that allow to recover the filtration function from the particle deposition distribution history. The general features of such methods are discussed and a procedure for the numerical implementation is shown as well.

6.1.1 Method I. Direct formulation

From Eq. (2.10), the filtration function can be recovered from the particle deposition $\sigma(X,T)$ as follows:

$$\lambda(\sigma(X,T)) = \frac{1}{c(X,T)} \frac{\partial \sigma}{\partial T}(X,T). \tag{6.1}$$

Now, from (2.37) we obtain

$$\frac{1}{c(X,T)} = \frac{1}{c_i(T)} \frac{\sigma(0, T-X)}{\sigma(X,T)}, \quad \text{for} \quad T > X. \tag{6.2}$$

Introducing (6.2) into (6.1) we obtain

$$\lambda(\sigma(X,T)) = \frac{1}{c_i(T)} \frac{\sigma(0, T-X)}{\sigma(X,T)} \frac{\partial \sigma}{\partial T}(X,T), \quad \text{for} \quad T > X. \tag{6.3}$$

So, theoretically, Eq. (6.3) defines a method for calculating the filtration function $\lambda(\sigma)$ for $\sigma > 0$. However, this method does not provide the value $\lambda(0)$. A possibility to obtain $\lambda(0)$ requires an approximation, i.e., assuming that near zero the filtration function is almost constant then from (2.54) and data at several times $T_1, \ldots, T_m$ the value of $\lambda(0)$ can be estimated by the formula

$$\lambda(0) = \sigma(0,1)/c_i(1). \tag{6.4}$$

The main numerical difficulty of this recovery method is the calculation of the derivative $\frac{\partial \sigma}{\partial T}(X,T)$ in (6.2), which cannot be done reliably.

6.1.2 Method II. Integral equation

Now, an integral equation relating particle deposition and filtration function is obtained from (2.9) and (2.10). To do so, we rewrite Eq. (2.31) as a Volterra integral equation of the first kind. We set $M = \max_{T>X} \sigma(0, T-X), \quad m = \min_{T>X} \sigma(X,T)$,
and

$$K(\eta, T, X) = \begin{cases} 0 & \text{if} \quad \sigma(0, T-X) < \eta \leq M; \\ 1/\eta & \text{if} \quad \sigma(X,T) < \eta \leq \sigma(0, T-X); \\ 0 & \text{if} \quad m \leq \eta \leq \sigma(X,T). \end{cases}$$

Equation (2.31) can be rewritten as

$$\int_m^M \frac{K(\eta, X, T)d\eta}{\lambda(\eta)} = X. \tag{6.5}$$

Now, assuming that $\lambda(\eta) > 0$, we define

$$f(\eta) := 1/\lambda(\eta) \quad \text{and} \quad g(X) := X, \tag{6.6}$$

we obtain from (6.5) that

$$\int_m^M K(\eta, X, T) f(\eta) d\eta = g(X). \tag{6.7}$$

Notice that Eq. (6.7) is valid on each characteristic line $T - X = const$ (see Section 2.2). Thus, taking a parameter $T = const + X$, the kernel $K(\eta, X, T) = K(\eta, X, const + X)$ depends only on X and η. This means that along each characteristic line we have a Volterra integral equation of the first kind.

Remark 6.1 *To avoid the singularity of the kernel $K(\eta, X, T)$ at $\eta = 0$ we restrict $(X,T) \in [0,1] \times [T_1, A]$ where T_1 and A are positive constants. In this way, we do not consider the region $T \leq X$, where $\sigma = 0$. More precisely, the integration is valid along the region spanned by characteristic lines $X - T = \tau$, with $\tau > 0$.*

Finally, by solving the integral equation (6.7) we obtain the filtration function from the particle deposition. Notice that the kernel K in Eq. (6.7) is similar to the kernel in Eq. (4.15). So the results of the existence, uniqueness and stability obtained for (4.16) can be generalized to this case.

6.1.3 Method III. Functional equation

From Eq. (2.14) we obtain for $z \geq 0$

$$\frac{\partial \Psi(\sigma(0,z))}{\partial T} = c(0,z), \quad \text{for} \quad \sigma \text{ in } [0, \sigma_1) \tag{6.8}$$

and

$$\frac{\partial \Psi(\sigma(1,z))}{\partial T} = c(1,z), \quad \text{for} \quad \sigma \text{ in } [0, \sigma_1). \tag{6.9}$$

Using Eq. (2.37) we obtain

$$\frac{\sigma(1,z)}{\sigma(0,z-1)} = \frac{c(1,z)}{c(0,z-1)} \quad \text{for} \quad z \geq 1\cdot \tag{6.10}$$

Now, denoting by

$$g(\sigma) = \frac{\partial \Psi(\sigma)}{\partial T}, \tag{6.11}$$

$$D_e(z) = \sigma(1,z) \quad \text{and} \quad D_i(z) = \sigma(0, z-1), \tag{6.12}$$

we obtain from Eqs. (6.8)-(6.11) the functional equation for g

$$g(D_e(z)) = \frac{D_e(z)}{D_i(z)} g(D_i(z)) \quad \text{for} \quad z \geq 1. \tag{6.13}$$

Notice that Eq. (6.13) is similar to Eq. (3.11), therefore a procedure analogous to that Chapter 3 can be developed to solve Eq. (6.13). We can see that (6.13) utilizes only the particle deposition data at two locations.

Eq. (6.13) is insufficient to solve the inverse problem; the additional values $\lambda(0)$ and $\lambda'(0)$ are needed to determine the initial value for the derivative of g, which is essential to determine the solution of Eq. (6.13).

Once we have determined g from (6.13) the filtration function can be calculated from

$$\lambda(\sigma) = \frac{1}{g(\sigma)} \frac{\partial \sigma}{\partial T}. \tag{6.14}$$

6.1.4 Method IV. Optimization method

In this section we present an alternative method for calculating the filtration function from the particle deposition. The procedure consists in optimizing a functional on an appropriate compact subset Ω. Thus, we start by parametrizing the filtration function, for instance as $\lambda(\sigma) = \theta_1 + \theta_2 \sigma$ and then we estimate the parameter values $\bar{\theta}$ as

$$\bar{\theta} = \min_{\theta \in \Omega} \sum_{i=1}^{n} \sum_{j=1}^{m} (\sigma(X_i, T_j; \theta) - \sigma_{data}(X_i, T_j))^2. \tag{6.15}$$

Here $\sigma(X_i, T_j, \theta)$ is calculated solving the system of equations (2.9)-(2.10), and $\sigma_{data}(X_i, T_j)$ represents the experimental data. To obtain stable solution, a penalization term is added to the right hand side of (6.15).

This method differs from the others because it is more robust and allows modifications in the forward problem (2.9) and (2.10) without substantial modifications in the recovery procedure. Using the methodology developed in Section 5.4.1 we can prove that the inverse problem presented in this subsection is well-posed in the sense of Tikhonov.

Chapter 7

Sensitivity analysis

Sensitivity analysis permits to identify the "best" models when the number of parameters to be identified is relatively large and there does not exist a unique solution of the inverse problem. The Gauss-Newton method may become unstable due to correlation effects between the parameters. It is known that for the identification of complex constitutive law parameters, the inverse problem becomes ill-conditioned. Stability analysis is necessary in order to understand the reasons for the instability and to propose a stabilization method.

Once the optimal set of parameters is obtained, it may be interesting to study the stability of the inverse analysis. The computation of the sensitivity matrix allows studying the stability of the proposed inverse method ([103]).

One can see that stability analysis method is based on first order approximations and that the inequality holds only for small perturbations. So, this method is able to indicate whether a parameter can be identified accurately or not.

Some parameters may be determined with large uncertainty due to lack of sensitivity of the measurements. This means that the experiment is not adequate to determine these parameters. Uncertainty may also be caused by large correlation effect between some parameters. If some parameters are highly correlated, the function which we minimize shows a valley close to the optimum, rather than a single minimum.

Set $F(\theta) = Q(\mathcal{A}(\theta))^{-1}q$ and $\alpha = 0$ in Eq. (5.3). The parameter identification problem without penalization reduces to

$$\min_{\theta \in Q_{ad}} ||F(\theta) - b||^2, \tag{7.1}$$

or in a more general way to

$$\min_{\theta \in Q_{ad}} (F(\theta) - b)^T D(F(\theta) - b), \tag{7.2}$$

where D is certain weighting matrix. By definition we set

$$||F(\theta) - b||_D^2 = (F(\theta) - b)^T D(F(\theta) - b), \tag{7.3}$$

so Eq. (7.2) can be rewritten as

$$\min_{\theta \in Q_{ad}} ||F(\theta) - b||_D^2. \tag{7.4}$$

7.1 Sensitivity coefficients

Sensitivity analysis in (7.1) is carried out to obtain information about the parameter identification. To do so, the sensitivity coefficient with respect to a parameter as a function of time and observation location is used. The sensitivity coefficient is defined by (e.g, [103],[104]):

$$F_{\theta_i}(T, X; \theta) = \frac{\partial F(T, X; \theta)}{\partial \theta_i}, \tag{7.5}$$

where T is the time, X is the coordinate of the observation location, θ_i is the i-th parameter in the n-dimensional parameter vector θ and F is a function that depends on the state variables T and X.

Because the values of the parameters θ may vary over several orders of magnitude for a given observation location X, a dimensionless sensitivity coefficient was used to compare various model parameters:

$$S_{\theta_i}(T) = \frac{\partial(\ln F)}{\partial(\ln \theta_i)}, \tag{7.6}$$

or

$$S_{\theta_i}(T) = \frac{F(T, X, \theta_1, \ldots, \theta_i + \Delta\theta_i, \ldots, \theta_n) - F(T, X, \theta_1, \ldots, \theta_i, \ldots, \theta_n)/F(T, X, \theta)}{\Delta\theta_i/\theta_i}, \tag{7.7}$$

where $\Delta\theta_i$ is a small perturbation of parameter θ_i near its basic value.

Now using Taylor's formula the dimensionless sensitivity coefficient can be rewritten as

$$S_{\theta_i}(T) = \frac{\theta_i}{F(T, X, \theta)} \frac{\partial F(T, X, \theta)}{\partial \theta_i}. \tag{7.8}$$

Following the same methodology as in [103], the dimensionless sensitivity coefficient is plotted as a function of the observation time for each possible set of model parameters θ at a given position X to form a sensitivity curve. From this curve we infer the possible effect of proposed recovery designs on parameter identification quality.

7.2 Interrelationship between parameters

A useful tool for studying the correlation between the parameters θ_i, with $i = 1, \ldots, n$ is the correlation coefficient matrix $corr(\theta) = (a^*_{ij})$. This matrix is defined from the covariance matrix $cov(\theta) = (a_{ij}) \approx e^2(J^T J)^{-1}$, where e is the observation error variance, and $J = \partial F(\theta)/\partial\theta$ and J^T are the sensitivity matrix and its transpose, respectively.

$$a^*_{ij} = a_{ij}/\sqrt{a_{ii}a_{jj}}. \tag{7.9}$$

The correlation matrix can be used to obtain the optimum number of parameters in the model. To do so, we choose the number of parameters that guarantees small correlation coefficients.

7.3 Sensitivity of the optimal solution

Now we obtain relationships between small variations in the experimental parameters and in the optimal set of parameters (for details see [39], [7]).

The optimal set of parameter is defined by the following relation:

$$\frac{\partial F(\theta)^T}{\partial \theta} D(F(\theta) - b) = 0. \tag{7.10}$$

If the experimental data b is replaced by a perturbed experimental data $b+\delta b$, one can denote the perturbed optimal set of parameters by $\theta + \delta\theta$ and the following relationship holds:

$$\frac{\partial F(\theta)^T}{\partial \theta} D \left(F(\theta) + \frac{\partial F(\theta)}{\partial \theta}\delta\theta - b - \delta b \right) \approx 0. \tag{7.11}$$

Finally, one can prove that

$$|\delta\theta_k| \leq \sqrt{G_{kk}}||\delta b||_D, \tag{7.12}$$

where

$$G = \left(\frac{\partial F(\theta)^T}{\partial \theta} D \frac{\partial F(\theta)}{\partial \theta} \right)^{-1}. \tag{7.13}$$

This analysis is based on first order approximation so that the inequality (7.12) holds only for small perturbations.

7.4 Sensitivity analysis for effluent concentration

In this section the sensitivity analysis is studied when we have an analytical solution for the effluent concentration. The analysis of the sensitivity coefficient is used to study the effect of small variations of the effluent concentration $c(1,T)$ on the recovered parameters. Moreover, it is possible to determine when the parameter can be identified well using the model.

We start by generating synthetic data with 5% perturbation error in $c(1,T;\theta)$. Then, the recovered function $\lambda(\sigma) = \max\{\theta_3 + \theta_4\sigma, 0\}$ is obtained by minimizing the cost function in (5.13). We continue and fix a feasible parameter set given by $0 \leq \theta_4 \leq 2$ and $-300 \leq \theta_4 \leq 0$; and we set the physical domain for (X,T) as $[0,1] \times [0,A]$. Then we try to recover the prescribed value $(1,-171)$, starting from different initial guesses of the parameters (θ_3, θ_4), namely, $(0.01,-30)$, $(0.5,-100)$, $(0.09,-17)$ and $(1.5,-200)$.

Minimizing runs are carried until a relative error smaller than 1% is reached. Then, we check if the model parameters attain the prescribed value. Different initial guesses lead to similar end values, which are close to the true parameter values with relative errors smaller than 0.01% for θ_3 and 0.4% for θ_4. The results show that within the limited number of trials conducted, the performance function has a unique minimum within the selected range of parameter space.

The dimensionless sensitivity coefficients for linear filtration function for $T > X$ are given by

$$S_{\theta_3} = \frac{-\theta_3 e^{c_{io}\theta_4(T-X)} e^{\theta_3 X}}{1 + e^{c_{io}\theta_4(T-X)}(e^{\theta_3 X} - 1)}, \quad S_{\theta_4} = \frac{c_{io}\theta_4(T-X) e^{c_{io}\theta_4(T-X)}(e^{\theta_3 X} - 1)}{1 + e^{c_{io}\theta_4(T-X)}(e^{\theta_3 X} - 1)}. \tag{7.14}$$

From (7.14) we obtain

$$S_{\theta_3}/S_{\theta_4} = -\frac{\theta_3 e^{\theta_3 X}}{c_{io}\theta_4(e^{\theta_3 X}-1)(T-X)}. \tag{7.15}$$

Thus from (7.15), we can see that in general, S_{θ_3} is different from S_{θ_4}, therefore θ_3 and θ_4 are not equally sensitive. However, notice that S_{θ_4} is linearly increasing in time for $0 < \theta_3 X < 1$, while S_{θ_4} tends to $-\theta_3 e^{\theta_3 X}$ when time increases. Therefore, for identifying accurately the values in the two-parameter model, the experiment has to be carried out for large enough times. Let us denote

$$q = \frac{\theta_3}{e^{-\theta_4 c_{io} T} + e^{\theta_3}}. \tag{7.16}$$

From Eq. (7.14) and the above mentioned restriction on the parameters θ_3, θ_4, X and T, we obtain the following inequality

$$|S_{\theta_3}| \geq q. \tag{7.17}$$

From (7.16) and (7.17) it follows that $\Delta\theta_3/\theta_3 < q^{-1}\Delta c(1,T)/c(1,T)$. Notice that if $c_{io}\theta_4 T$ is small, then the sensitivity of the parameter θ_3 depends essentially on time and θ_3. Since $c_{io} \approx 10^{-6}$, then for times T smaller than 10^4 PVI and for $\theta_4 \approx 10^2$, $c_{io}\theta_4 T$ is small. This shows there exist a certain region where the correlation between θ_3 and θ_4 is small, therefore these two parameters are a good choice in some cases.

7.5 Sensitivity analysis for the pressure drops

An analysis similar to that of previous section is carried out to recover the filtration function and the permeability reduction from the pressure drop histories.

We recover the functions $k(\sigma) = (1+\theta_1\sigma+\theta_2\sigma^2)^{-1}$ and $\lambda(\sigma) = \theta_3 + \theta_4\sigma$ from five pressure drop histories $\Delta p^1_{data}(T)$, $\Delta p^2_{data}(T)$, $\Delta p^3_{data}(T)$, $\Delta p^4_{data}(T)$ and $\Delta p^5_{data}(T)$ by minimizing the cost function in (5.33). We start by generating synthetic data with 5% perturbation error in the pressure drop histories. The feasible parameter set given by $0 \leq \theta_1 \leq 1000$, $0 \leq \theta_2 \leq 1000$, $0 \leq \theta_3 \leq 2$ and $-300 \leq \theta_4 \leq 0$ is explored. Then we try to recover the prescribed value $(300, 100, 1, -171)$, starting from different initial guesses of the parameter vector $(\theta_1, \theta_2, \theta_3, \theta_4)$, i.e., $(10, 15, 0.9, -40)$, $(5, 33, 0.45, 0)$, $(115, 333, 0.1, -10)$ and $(1, 1, 1.5, -200)$.

The synthetic pressure drop histories are recovered with relative errors smaller than 2.6%. The recovered parameter are $(284, 247, 1.12, -276)$, $(333, 347, 0.9, -237)$, $(385, 231, 0.6, -39)$ and $(356, 987, 0.8, -206)$ for each of the above mentioned cases respectively. Notice that different initial guesses lead to different parameter values. The parameters θ_1 and θ_3 are predicted more accurately than θ_2 and θ_4.

Then, from previous results we see that the pressure drop histories are predicted accurately, but the parameters θ are not. However, the recovered permeability reduction function is obtained accurately, with relative error smaller than 2% for all cases. We see that there exist several parameters which give good approximation of the solution. Thus, we have the situation of parameter non-uniqueness.

In order to choose appropriate physical bounds for the parameters, several laboratory experiments should be carried out. For example, in the set of experimental data studied in Chapter 8, we see that two parameters in the permeability reduction function were needed to predict well the pressure drop histories. One possible way of obtained unique parameters is described in Remark 5.15, i.e., additional nonlinear constraints must be used in the optimization of the functional in (5.33). Another way to obtain parameter uniqueness is to choose an appropriate penalization of the functional; this method was presented in Section 5.6.

Other useful information can be extracted from the analysis of the sensitivity matrix. The correlation between the parameters cannot be obtained accurately by means of (7.9) because the matrix $J^T J$ has large condition number. This shows the high degree of ill-posedness of this nonlinear inverse problem.

The above mentioned numerical examples do not encourage us to use fewer parameters in the model. So, other indicators must be used. More precisely, the sensitivity coefficients of θ_1, θ_2, θ_3 and θ_4 and their behavior for large time T are used.

We set $\Phi_1(T) = 1 - e^{c_{io}\theta_4 T}$ and $\Phi_2(T) = 1 - \Phi_1$ and

$$I_1 = -\frac{1}{\theta_4} \log \left(e^{\theta_3(x_l - x_{l+1})} \frac{e^{\theta_3 x_{l+1}} - 1 + e^{-c_{io}\theta_4 T}}{e^{\theta_3 x_l} - 1 + e^{-c_{io}\theta_4 T}} \right), \tag{7.18}$$

$$I_2 = \int_{x_l}^{x_{l+1}} \frac{dX}{(1 + \Phi_2(T)(e^{\theta_3 X} - 1))^2}. \tag{7.19}$$

The pressure drops in (x_l, x_{l+1}) are given for $T >> X$ by

$$H^l(T;\theta) = \Delta p^l(T, \theta_1, \theta_2, \theta_3, \theta_4) = 1 + \theta_1 I_1 + \theta_2 \frac{\theta_3^2 (1 - \Phi_2(T))^2}{\theta_4^2} I_2, \tag{7.20}$$

From (7.20) we obtain

$$\frac{\partial H^l(T;\theta)}{\partial \theta_1} = I_1, \quad \frac{\partial H^l(T;\theta)}{\partial \theta_2} = \frac{\theta_3^2 (1 - \Phi_2(T))^2}{\theta_4^2} I_2, \tag{7.21}$$

$$\frac{\partial H^l(T;\theta)}{\partial \theta_3} = \theta_1 \frac{\partial I_1}{\partial \theta_3} + 2\theta_2 \frac{\theta_3 (1 - \Phi_2(T))^2}{\theta_4^2} I_2 + \theta_2 \frac{\theta_3^2 (1 - \Phi_2(T))^2}{\theta_4^2} \frac{\partial I_2}{\partial \theta_3}, \tag{7.22}$$

$$\frac{\partial H^l(T;\theta)}{\partial \theta_4} = \theta_1 \frac{\partial I_1}{\partial \theta_4} + 2\theta_2 \theta_3^2 \frac{\partial}{\partial \theta_4} \left(\frac{(1 - \Phi_2(T))^2}{\theta_4^2} I_2 \right). \tag{7.23}$$

Finally, from (7.8) and (7.21)-(7.23), the sensitivity coefficients are

$$S_{\theta_i} = \frac{\theta_i}{H^l(T;\theta)} \frac{\partial H^l(T;\theta)}{\partial \theta_i}, \quad i = 1, 2, 3, 4. \tag{7.24}$$

We see that S_{θ_1}, S_{θ_2}, S_{θ_3} and S_{θ_4} depend strongly and nonlinearly on θ_1, θ_2, θ_3 and θ_4.

Now, we suggest a region where the parameters θ_1 and θ_2 have small correlation. To do so, we study first the behavior of the sensitivity coefficients when T is large. Notice that

$$\mathcal{V}_1 = \lim_{T \to \infty} I_1 = -\frac{1}{\theta_4} \log \left(e^{\theta_3(x_l - x_{l+1})} \right), \tag{7.25}$$

$$\mathcal{V}_2 = \lim_{T \to \infty} I_2 = \int_{x_l}^{x_{l+1}} \frac{dX}{(1 + (e^{\theta_3 X} - 1))^2}, \tag{7.26}$$

$$\mathcal{V}_3 = \lim_{T\to\infty} H^l(T;\theta) = 1 + \theta_1\mathcal{V}_1. \tag{7.27}$$

Using (7.24)-(7.27) we obtain

$$\lim_{T\to\infty} S_{\theta_1} = \frac{\theta_1\mathcal{V}_1}{1+\theta_1\mathcal{V}_1} \tag{7.28}$$

and

$$\lim_{T\to\infty} S_{\theta_2} = 0. \tag{7.29}$$

Using (7.28)-(7.29) and (7.21), we obtain that for θ_3/θ_4 small or constant, S_{θ_1} and S_{θ_2} depend only of θ_1 and θ_2 respectively. In this case the parameters θ_1 and θ_2 have a region where their correlation is small. Thus, the parameters θ_1 and θ_2 can be identified well for large times.

Chapter 8

Validation of the model from experimental measurements

In this chapter we use the experimental data of Al Abduwani et al. (2003) ([1]) to investigate the validity of the model described by the equations (2.9)-(2.10) and Darcy's law. This model was established first by Herzig et al. (1970) ([60]) and has been used for almost forty years for modeling deep bed filtration. In the validation, the tools developed in this work are used, i.e., the direct problem, the inverse problem methods and the sensitivity analysis for finding the best empirical functions parameters. The experimental dataset is described in appendix C.

The output data measured in laboratory experiments are presented. Moreover, the match between model and experimental data is described. We can see that the recovered parameters model using the pressure drop histories do not predict accurately the particle deposited at end time in any of the five experiments analized. On the other hand, when pressure drop histories are predicted accurately, the effluent concentration is not. We explain the reason for these facts at the end of this chapter.

8.1 Experimental methodology

In order to simulate produced water re-injection and to investigate the relationship between filtration and particle deposition, six static filtration experiments were conducted in the laboratory on Bentheim sandstone, using hematite particles to construct the synthetic water to be injected. In these experiments, different hematite concentrations and injection flow rates were used. The salinity of the water was kept constant by using doubly distilled water; the acidity was controlled and kept constant at a pH value of 5.0 ± 0.1. A monodisperse selection of hematite particles was not possible, and instead a very narrow band of size dispersion was allowed (1.0 to 5.0 μm), with the majority of the particles having a size of 2.0 μm. Thus, the ratio of average pore throat diameter to average hematite particle diameter was 7.5.

Moreover, in these experiments the effluent concentration history of particles was measured. This characterization of the effluent sample was either done on-line with a laser diffraction unit or at a later stage using chemical analysis - Atomic Adsortion Spectroscopy

(AAS). The pressure drop histories were measured at seven points. The new addition described in [1] is the introduction of post-mortem diagnosis, i.e. the final particle deposition is measured by utilizing both chemical and visual analysis. This establishes a reliable deposition profile along the core - a major advancement, providing redundant data for the inverse problems, which is especially useful for testing the validity of the available heuristic model in the literature.

One of these data sets was rejected because of experimental error. Analysis of the other five experiments led to analogous results, and therefore we describe only one experiment here.

Pressure history was measured within 10% error. The post-mortem deposition profile has a very low error margin: ± 2.5%. The essential part of the data follows in Table C.1 (see Appendix C), where the properties of the core, the flow and the injected particle concentration are presented.

Because the rock core is not perfectly homogeneous in practice, the absolute permeability spatial distribution $k_0(x)$ must be determined from Darcy's law. To do so, at the beginning of the experiment, clean water is injected and the pressure drop is measured between several points x_l of the core. We estimate the absolute permeability k_0^l in each of the five segments of the core as follows: from Darcy's law (or Eq. (2.3) with $k(0) = 1$) we have $k_0^l = q\mu L\mathcal{A}/\Delta p^l$, where q is the average flow rate, $\mathcal{A}$ is the area of the transversal section, μ is the dynamic viscosity, L is the core length, and Δp^l is the pressure drop at time zero; the length of each segment is shown in Table C.3 (see Appendix C); this information determines all $k_0^l(x)$ for each experiment.

Data are further preprocessed because the flow $U(t)$ is not exactly constant. This complication is resolved by a time dependent scaling so that the nondimensional time unit is the number of porous volumes injected (P.V.I.).

8.2 Results and discussion

Here the validity of the model based on the experimental data in Section 8.1 is studied. To do so, we use the recovery method described previously and we show that there are cases when either the pressure drop or the effluent concentration histories are predicted accurately, but not at the same time. Moreover, the new data, namely the deposition distribution, are predicted with gross inaccuracy. The reason of this fact will be explained.

Using the methodology described in Section 5.6, we recover the permeability reduction function

$$k(\sigma) = (1 + \theta_1\sigma + \theta_2\sigma^2)^{-1}, \tag{8.1}$$

and the filtration function

$$\lambda(\sigma) = \max\{\theta_3 + \theta_4\sigma, 0\}, \tag{8.2}$$

by minimizing the functional in Eq. (5.41). Two studies are carried out, in the first one taking $w_p \approx 1$ and $w_c \approx 0$ and in the second one taking $w_p \approx w_c$. We show that in both cases, the model does not predict accurately the experimental data.

8.2.1 First study

Here, we recover the permeability reduction and filtration functions, minimizing the functional in Eq. (5.41), with $w_p \approx 1$ and $w_c \approx 0$ (Case I).

The results are presented in Table 8.1, where e_1, e_2, e_3, e_4 and e_5 are the relative errors between the predicted pressure drops and the experimental data in each segment.

Table 8.1: Recovered permeability reduction function $k(\sigma) = (1+\theta_1\sigma+\theta_2\sigma^2)^{-1}$ and filtration function function $\lambda(\sigma) = \theta_3 + \theta_4\sigma$.

	θ_1	θ_2	θ_3	θ_4	$e_1(\%)$	$e_2(\%)$	e_3 (%)	$e_4(\%)$	$e_5(\%)$
Exp. 1	230	0.0	9.68	-0.84	0.83	1.2	1.7	1.5	1
Exp. 2	200	327	6.52	-0.0	0.9	1.9	1.7	2.2	1.7
Exp. 3	166	583	9.12	-2.17	10	1.2	2.6	2	2
Exp. 4	561	1526	15	-2.1	1.9	5.9	3.5	4	4.5
Exp. 5	130	139	2	0.0	1.9	1.0	0.8	1.0	1.4

Figures (8.1*a*), (8.2*a*), (8.3*a*), (8.4*a*) and (8.5*a*) present the plots of the experimental data and the absolute values of the predicted pressure drops for five experiments. In this figure, the highest experimental pressure drop corresponds to the first segment, and it has increasing trend. In the segments 2-4 the pressure drop histories have smaller values that are almost constant. The smallest value is measured in the last segment.

A remark on the experimental pressure drop histories shown in Fig. (8.1*a*): we see that the pressure drops in core segments 3 through 5 are essentially independent of time. This means that there is basically no deposition in these core segments. Therefore, there is no useful information contained in these three pressure drop histories. This fact suggests that the core segments where pressure is measured should be shorter.

On the other hand, in Figures (8.1*b*), (8.2*b*), (8.3*b*), (8.4*b*) and (8.5*b*) the recovered and experimental particles deposited at the end time of the experiment are shown. We can see that the predicted deposited particle distribution does not match accurately the experimental data in any of the five experiments, mainly at the beginning of the core.

Summarizing, in this example the predicted pressure drop is accurate, while the predicted final deposition distribution is not. In this case the predicted effluent concentration has gross inaccuracy, so we do not plot it.

8.2.2 Second study

Here, we recover the permeability reduction function and the filtration function, minimizing the functional in Eq. (5.41), with $w_p \approx w_c$ (Case III). The results for the experiment 1 is shown; the behavior in the experiments 2, 3, 4 and 5 is similar. The results are presented in Table 8.2, where e_1, e_2, e_3, e_4 and e_5 are the relative errors between the predicted and experimental pressure drops in each segment. The value e_c is the relative error of the effluent concentration approximation.

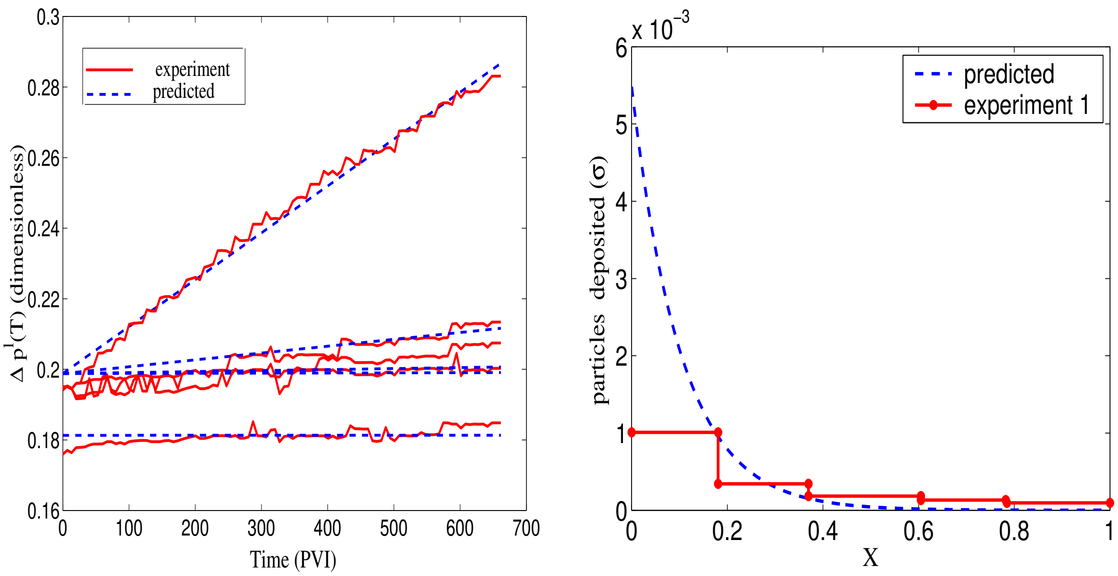

a) Pressure drop. b) Particle deposition at end time.

Figure 8.1: Experiment 1.

Table 8.2: Recovered permeability reduction $k(\sigma) = (1+\theta_1\sigma+\theta_2\sigma^2)^{-1}$ and filtration function $\lambda(\sigma) = \max\{\theta_3 + \theta_4\sigma, 0\}$ (recovery Case III), as well as relative errors in predicted pressure drops in the segments and in predicted effluent concentration.

	θ_1	θ_2	θ_3	θ_4	$e_1(\%)$	$e_2(\%)$	$e_3(\%)$	e_4 (%)	e_5 (%)	e_c (%)
Exp. 1	361	101	0.73	-148	15	2.8	4.0	5.0	4.7	4.8

In Experiment 1, we observe that the pressure drops are predicted accurately (relative error smaller than 5.0%) in segments 2 through 5, while it is higher (15%) in segment 1. Moreover, we see that the particle deposition predicted by the model does not match the experimental data. The highest deposition rate is measured in the first segment, where the water with particles is injected, while it is smaller in the other segments (see Fig. 8.1*b*). The main difference is observed in the first segment of the core, where the deposition is higher. Hence the main difference cannot be explained as resulting from noise. In Fig. 8.6, the smooth curve interpolating the experimental effluent concentration data is found in [1]. The significance of the discrepancy at early times between the predicted and interpolated curves in Fig. 8.6 is unclear.

In this case, the predicted effluent concentration is accurate, but the predicted distribution deposition is not.

8.2.3 Results

Other studies with different weights were carried out without improvements in the results. Thus from the previous facts, there exists a certain incompatibility in the model that prevents

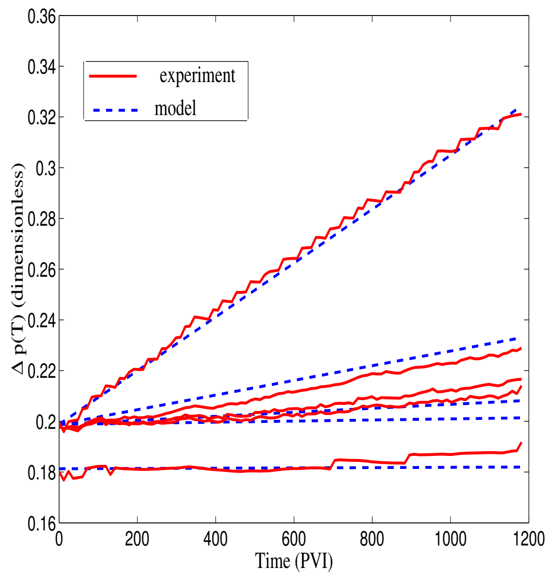

a) Pressure drop.

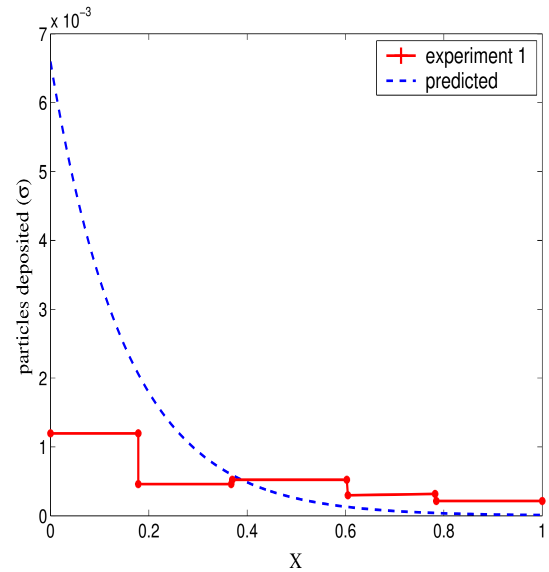

b) Particle deposition at end time.

Figure 8.2: Experiment 2.

determining a filtration regime that reproduces accurately both the pressure drop and effluent concentration histories. The final deposition distribution is never reproduced accurately. Seeking other causes for these differences, we used polynomials of higher order in the filtration function for all the recoveries, with no noticeable improvement. This indicates that increasing the number of parameter, only increases the correlation between them, see sensitivity analysis in Chapter 7.

Summarizing, the predicted deposition particle distribution at the end time is never accurate, while the predicted effluent concentration and pressure drop histories can be accurate by using appropriate weights. This disagreement would indicate that the pressure and effluent concentration experimental data set cannot be used for recovering the permeability reduction and filtration functions with this model, but this disagreement is not conclusive because one could pose the following questions: are there weights w_p and w_c allowing appropriate recovery of both the deposition particle distribution and effluent concentration history? Could appropriate recovery be attained using parametrizations different from those in Eqs. (8.1)-(8.2)? We were unsuccessful in our attempts to find better weights and parametrizations. However, this failure is not due to any limitations in the procedures for solving the inverse problem, as we explain now.

Remark 8.1 *A relationship between inlet and outlet concentration can be obtained as follows: Eq.* (2.37) *suggests the definition of the parameter* $\mathcal{R}(T)$ *as*

$$\mathcal{R}(T) \equiv \frac{\sigma(1,T)}{c(1,T)} \frac{c(0,T-1)}{\sigma(0,T-1)}, \tag{8.3}$$

relating suspended and deposited concentration at the endpoints. Equation (8.3) *shows that for the model described by Eq.* (2.1)-(2.2), $\mathcal{R}(T) \equiv 1$ *for* $T > 1$ *PVI.*

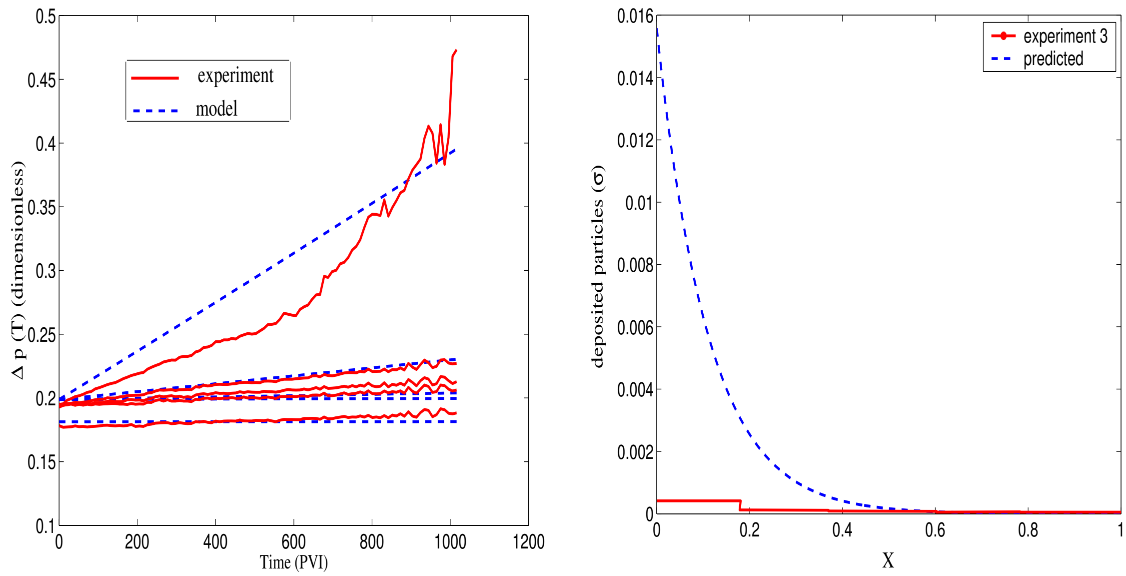

a) Pressure drop. b) Particle deposition at end time.

Figure 8.3: Experiment 3.

For the experimental data measured in [1] $\mathcal{R}(A)$ can be evaluated at the end time A. In fact, $c(0, A)$ and $c(1, A)$ are the injected and effluent suspended concentration, and $\sigma(0, A-1)$ and $\sigma(1, A)$ are obtained from the post-mortem deposition measurements; $\sigma(0, A-1)$ is approximated by $\sigma(0, A)$. The error due to the delay of 1 PVI should be of the order of 0.2% or less for end time exceeding 500 PVI.

The ratio defined by Eq. (8.3) should be $\mathcal{R}(T) \equiv 1$. However, this condition is not satisfied in any experiments at the end time, where we have sufficient experimental data to evaluate $\mathcal{R}$, i.e., $\mathcal{R} = 0.18, 0.30, 0.15, 0.22, 0.21$ for experiments 1, 2, 3, 4 and 5 respectively. The particle deposition and the effluent concentration at the inlet and outlet of the core have experimental behavior that cannot be reproduced by the model.

The disagreement between the experiment and the model can perhaps be explained by the formation of external cake, as suggested by Peter Currie of TUDelft. In more detail, this means that the increase in the deposition of particles at the core wall produces a compact cake layer that blocks the rock. As a result, the particles cannot enter freely the porous medium, and the effective inlet particle concentration $c(0, T)$, which was assumed to be constant in the model, changes as well.

Notice that (see Fig.8.7b) the particle deposition at the inlet is higher than at the outlet, while the inlet and effluent concentrations maintain the same order of magnitude. Thus, the change in the inlet concentration, in principle, can balance the difference between the particle deposition at the inlet $\sigma(0, A)$ and at the outlet $\sigma(L, A)$ of the core, guaranteeing that Eq. (8.3) holds. The influence of the external cake layer is currently being studied. To do so, Al Abduwani et al. are measuring the particle deposition $\sigma(X, T)$ at some points (X_l, T_j), $l = 1, \ldots n$, $j = 1, \ldots, m$ using X-ray tomography.

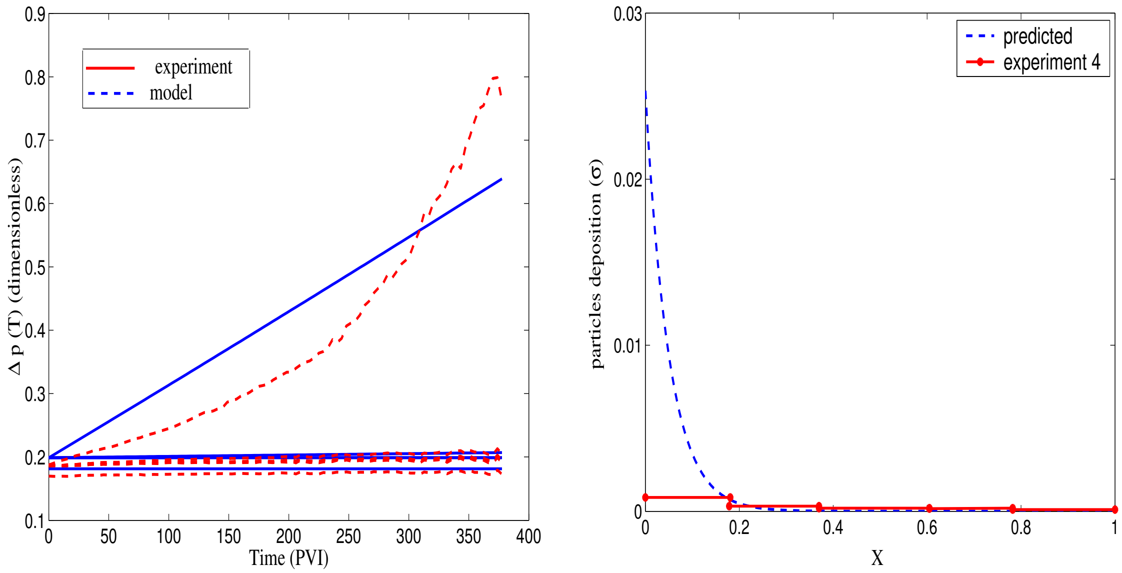

a) Pressure drops. b) Particle deposition at end time.

Figure 8.4: Experiment 4.

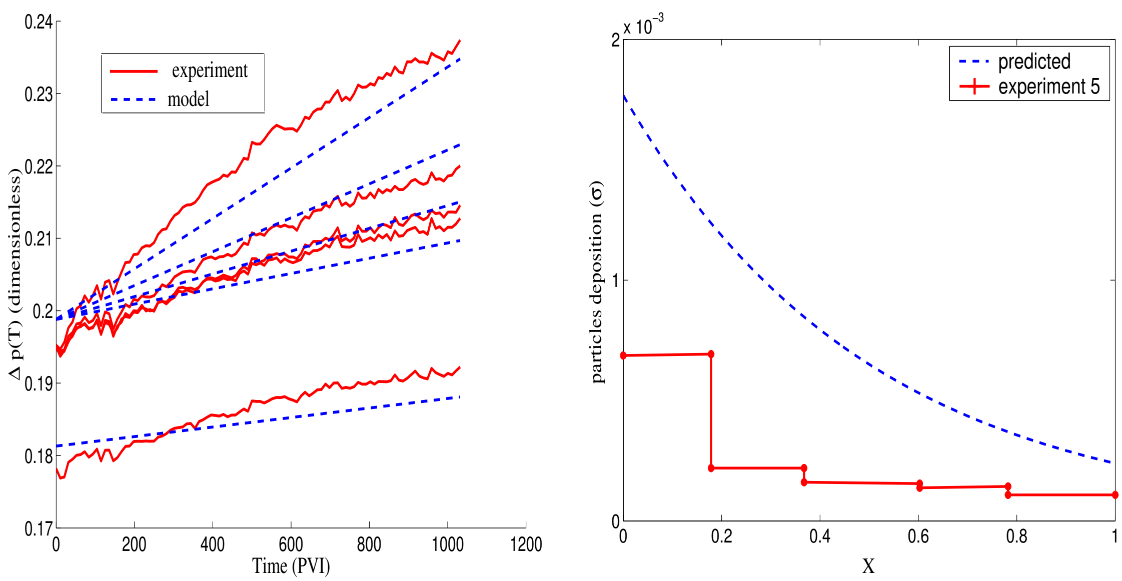

a) Pressure drops. b) Particle deposition at end time.

Figure 8.5: Experiment 5.

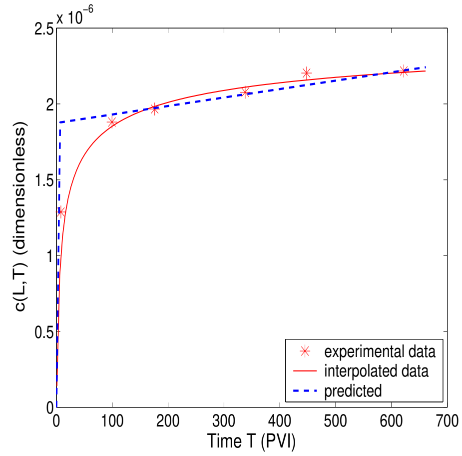

Figure 8.6: Predicted effluent concentration history in Experiment 1, with $w_p \approx w_c$.

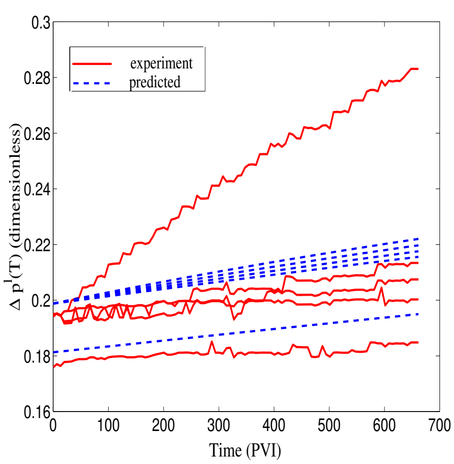

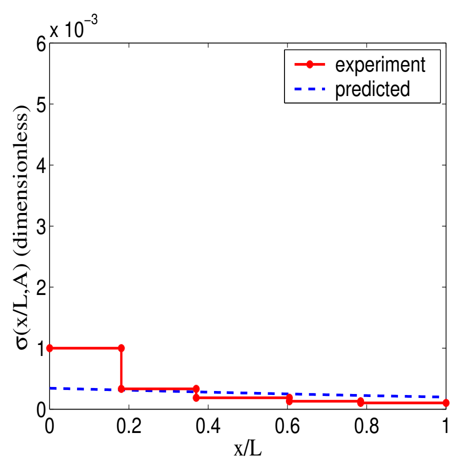

a) Pressure drop histories. b) Deposition distribution at end time.

Figure 8.7: Predicted data in Experiment 1, with $w_p \approx w_c$.

Chapter 9

Conclusion

In this work several inverse problems in the general deep bed filtration model were solved. We assume non-constant injected particle concentration. In this case, the inverse problem of recovering the filtration function from the effluent particle concentration reduces to solving a functional equation. This functional equation has a unique differentiable solution, which is determined by a stable iterative procedure. Taking continuous differentiable experimental data functions we obtain a well-posed inverse problem.

Under the assumption that the filtration function has already been determined, a method for recovering the permeability reduction function was studied. This recovery method reduces to solving a linear integral equation, which has stable solutions.

Using Tikhonov's regularization method, we obtained reliable methods for recovering the permeability damage function $k(\sigma)$ and the filtration function $\lambda(\sigma)$ from synthetic data for the classical filtration theory. The synthetic data represent the pressure drop history and the effluent concentration history. An appropriate subsets of the feasible solution for proving the well-posedness in Tikhonov's sense of several inverse problem was described. Convergence and stability of the regularized solution was proved. The optimization method is used to implement the recovery procedures.

However, when using any of these methods in the recovery of $k(\sigma)$ and $\lambda(\sigma)$ based on the experimental data from [1], [3] we found some incompatibility that prevents us from reproducing accurately all the data set. Thus, under usual assumption of constant particles concentration entering the body of the porous rock, we conclude that the classical model of Hertzig et al. ([60]) is not adequate to describe this experimental data set, so either other factors must be take into account in the model or more reliable experimental data must be obtained or both. Perhaps it would be important to take into account effective diffusion in the evolution equations ([9]), or more sophisticated reaction models are needed.

Refining the model is one of the continuations of our work. In this sense, the influence of the external layer cake blocking the entry of injected particles is currently being studied. Some introductory material for injected particle concentration that decreases in time was presented in the last section of Chapter 2, where the asymptotic behavior of the solution was described.

This work showed that the most important quantity to be measured in deep bed filtration is the deposition particle distribution history, which was described in Chapter 6. Experimental methods for measuring the particle deposition $\sigma(X,T)$ at many points (X_l,T_j), $l=1,\ldots,n$,

$j = 1, \ldots, m$ by means of X-rays are currently being developed at the Technical University of Delft. We hope that the methods sketched in Chapter 6 will be useful in the analysis of these data.

Bibliography

[1] Al-Abduwani F. A. H., Shirzadi A., Broek W. M. G. T. van den & Currie P. K., *Formation Damage vs. Solid Particles Deposition Profile during Laboratory Simulated PWRI*, SPE 82235. SPE European Formation Damage Conference. The Hague, The Netherlands,13-14, 2003.

[2] Al-Abduwani F. A. H., Farajzadeh, R., Broek W. M. G. T. van den & Currie P. K., *Utilizing Static filtration experiments to test existing filtration theories for conformance*, Second Produced Water Workshop. Aberdeen, UK, 2004.

[3] Al-Abduwani F. A. H., Farajzadeh, R., Broek W. M. G. T. van den & Currie P. K. & Zitha P.L.J., *Filtration of micron-sized particles in granular media revealed by X-ray computed Tomopraphy*, submitted to Review of Scientific Instruments in 2004.

[4] Anderssen, R. S., de Hoog F. R. & Lukas M. A., *The application and numerical solution of integral equations*, Sijthoff & Noordhoff, 1980.

[5] Ascher, U. & Haber, E., *Grid refinement and scaling for distributed parameter estimation problem.* Inverse Problem, 17, 571-590, 2001.

[6] Baumeister, J., *Stable Solution of Inverse Problems.* Friedr. Vieweg & Sohn Verlagsgesellschaft mbH, Braunschweig, 1987.

[7] Beck, J. V. & Arnold, K. V., *Parameter Estimation in Engineering and Science*, New York, Wiley, 1977.

[8] Bedrikovetsky, P., *Mathematical Theory of Oil and Gas Recovery.* Kluwer Academic Publishers, London/Boston, 1993.

[9] Bedrikovetsky, P., Private Communication, 2004.

[10] Bedrikovetsky P., Marchesin D., Souza A.G., Shecaira F. S., & Resende E., *Well impairment during Sea/Produced water flooding: Treatment of Laboratory Data.* SPE 69546 presented at the 2001. SPE Latin American and Caribbean Petroleum Engineering Conference, Buenos Aires. 2001

[11] Bedrikovetsky, P. et al., *Damage characterization of Deep Bed Filtration from Pressure Measurements.* SPE 73788, SPE International Symposium and Exhibition on Formation Damage Control, Lafayette, 20-21, 2002.

[12] Bedrikovetsky, P. G. and Marchesin, D. and Hime, G. and Siqueira, A. G. and Serra, A. L. and Rodriguez, J. R. P. and Marchesin A. O. and Vinicius, M., *Inverse problem for treatment of laboratory data on injectivity impairment.*, Society of Petroleum Engineers. SPE 86523., 2004.

[13] Bedrikovetsky, P. G. and Marchesin, D. and Shecaira, F. and Serra, A. L. and Resende, E., *Characterization of Deep Bed Filtration System from Laboratory Pressure Drop Measurements.* Journal of Petroleum Science and Engineering, 64, 3, 167-177, 2001

[14] Bennett, A. F., *Inverse Methods in Physical Oceanography.* New York, Cambridge University Press, 345p, 1992.

[15] Berryman J. G., *Nonlinear Inversion and Tomography*, Earth Resources Laboratory. Massachusetts Institute of Technology, 1-100, 1990.

[16] Binder, A., Heinz, W. H., Groetsch, C. W., Neubauer, A. & Scherzer, O.,*Weakly closed nonlinear operators ans parameter identification in Parabolic equations by Tikhonov regularization*, Applicable Analysis, Vol. 55, 215-234, 1994.

[17] Birgin, E. G., Martinez, J. M. & Raydan, M., *Nonmonotone spectral projected gradients methods on convex sets*, SIAM J. Optim, Vol. 10, No. 4, 1196-1211, 2000.

[18] Birgin, E. G., Chambouleyron, I. E. & Martinez, J. M., *Optimization problems in the estimation of parameters of thin films and the elimination fo the influence of the substrate*, Journal of Computational and Applied Mathematics, Vol. 152, 35-50, Amsterdam, Holanda, 2003.

[19] Birgin, E. G., Martinez, J. M. & Raydan, M., *Algorithm 813: SPG- Software for convex-constrained optimization. ACM* Transactions on Mathematical Software, 27, 340-349, 2001.

[20] Bui, D. D. & Nelson, P., *Existence and uniqueness of an inverse problem for a hyperbolic system of lidar probing*, Inverse Problem, 8, 821-829, 1992.

[21] Burger, M., Capasso, V. & Engl, H. W., *Inverse Problems related to Cristallization of Polymers.* Johannes Kepler Universitat Linz. Industrial Mathematics.Institute, Technical report 11, 1998.

[22] Chanvent G. Jaffré J. & Jégou S. J., *Estimation of relative permeability in three-phase flow in porous media*, Inverse Problems, 15, 33-39, 1999.

[23] Coleman, T. F. & Li, Y., *An interior trust region approach for nonlinear minimization subject to bounds*, SIAM, J. Optimization, Vol. 6, No. 2, 418-445, 1996.

[24] Coleman, T. F. & Li, Y., *On the convergence of interior-reflective Newton methods for nonlinear minimization subject to bounds*, Mathematical Programming, 67, 189-224, 1994.

[25] Colonius, A. & Kunisch K., *Output least square stability in Elliptic System*, Appl. Math. Optim, 19, 33-63, 1989.

[26] Courant R. & Hilbert D., *Methods of Mathematical Physics*, Vol. II, John Wiley, 1962.

[27] Cullum, J., *Numerical differentiation and regularization*, SIAM, J. Numer. Anal, Vol. 8, No. 2, 337-344, 1971.

[28] DuChateau, P., *An inverse problem for the hydraulic properties of porous media*, SIAM, J. Math. Anal. Vol. 28, No. 3, 611-632, 1997.

[29] de Hoog, F., *Review of Fredholm equations of the first kind, application and numerical solution of integral equations*, (R.S.Anderssen, F.de Hoog and M.A.Lucas, eds.), Sijthoff & Noordhoff, Alphen aan den Rijn, Germantown, 119-134, 1980.

[30] Engl, H. W., *Regularization methods for the stable solution on inverse problems*, Surv. Math. Ind., Springer-Verlag, 3, 7-143, 1993.

[31] Engl, H. W. & Kugler, P., *The influence of the equation type on the iterative parameter identification problems which are elliptic or hyperbolic in the parameter*, Euro Jn. of Applied Mathematics, 14, 2, 129-164, 2003.

[32] Engl, H. W. & Groetsch, C.W., *Inverse and Ill–Posed Problems*, Academic Press, London, 1987.

[33] Engl, H. W., Hanke, M. & Neubauer, A., *Regularization of Inverse Problems*. Kluwer Academic Publishers, 2000.

[34] Engl, H. W. & Neubauer, A., *Optimal discrepancy principles for the Tikhonov regularization of integral equations of the first kind*, Constructive Methods for the Practical Treatment of Integral Equations, (G.Hämmerlin and K.-H.Hoffmann, eds.), Birkhäuser, Basel, Boston, Stuttgart, 120-141, 1985.

[35] Espedal, M. S., Fasano, A. & Mikelic, A., *Filtration in Porous Media and Industrial Application*, Lecture Notes in Mathematics, **1734**, Springer-Verlag, Berlin, 2000.

[36] Friedlander, A., Martinez, J. M. & Santos, S. A., *A new trust region algorithm for bound constrained minimization*, Applied Mathematics and Optimization, 30, 235-266, 1994 .

[37] Friedlander, A., & Martinez, J. M., *On the maximization of a concave quadratic function with box constraints*, SIAM Journal on Optimization, 4, 177-192, 1994.

[38] Friedlander, A., Martinez, J. M., & Santos, S. A., *On the resolution of large scale linearly constrained convex minimization problems*, SIAM Journal on Optimization, 4, 331-339, 1994.

[39] Forestier, R., Chastel, Y. & Massoni, E., *Development of an Inverse Analysis Method Coupled with a 3D Finite Element Model*, AIP Conf. Proc. 712(1) 2149, 2004.

[40] , John, F., *Partial Differential Equations*, Springer,1982.

[41] George, S., & Nair, M. T., *Parameter choice by discrepancy principles for ill–posed problems leading to optimal convergence rates*, J. Optim. Theory Appl., 83, 217-222, 1994.

[42] George S., & Nair, M. T., *On a generalized Arcangeli's method for Tikhonov regularization with inexact data*, Research Report, CMA–MR 43–93; SMS–88–93, Australian National University, 1993.

[43] Goncarskii A. V., & Jagola, A. G., *Uniform approximation of monotonic solutions of noncorrect problems*, Dokl. Akad. Nauk SSSR, 184, 4, 1-2, 1969.

[44] Gorenflo, V. & Vassella, R.,*Abel Integral Equatons. Analysis and Applications*, Lecture Notes in Mathematics, 1461, Springer-Verlag, 1991.

[45] Groetsch, C. W., *The Theory of Tikhonov regularization for Fredholm Equations of the First Kind*, Pitman, Boston, 1984.

[46] Groetsch, C. W., *Inverse Problems in the Mathematical Sciences*, Vieweg Publishing, Wiesbaden, 1993.

[47] Groetsch, C. W. & King, J. T., *The saturation phenomena for Tikhonov regularization*, J. Austral. Math. Soc. Series A, 35, 254-262, 1983.

[48] Golub, G., *Matrix Computations*, Baltimore, Johns Hopkins University Press, 1983.

[49] Haber, E., Ascher, U. & Oldenburg, D., *On optimization techniques for solving nonlinear inverse problems*, Inverse Problems, 16, 1263-1280, 2000.

[50] Hanke, M., *A regularizing Levenberg-Marquardt scheme, with applications to inverse groundwater filtration problems*, Inverse Problems, 13, 79-95, 1997.

[51] Hanke, M. & Scherzer, O., *Inverse problems light: Numerical Differentiation*, Amer. Math. Monthly, 108, 512-521, 2001.

[52] Hanke, M. & Scherzer, O., *Error analysis of an equation method for the identification of the diffusion coefficient in a quasi-linear parabolic differential equation*, SIAM J. Appl. Math., Vol. 59, No. 3, 1012-1027, 1999.

[53] Hansen, P. C., *Numerical tools for analysis and solution of Fredholm integral equations of the first kind*, Inverse Problems, 8, 849-872, 1992.

[54] Hansen, P. C., *The L-curve and its use in the numerical treatment of inverse problems*; invited paper for P. Johnston (Ed.), Computational Inverse Problems in Electrocardiology, WIT Press, Southampton, 119-142, 2001.

[55] Hansen, P. C., *Regularization Tools: A Matlab package for analysis and solution of discrete ill-posed problems*, Numerical Algorithms, 6, 236-240, 1994.

[56] Hansen, P. C., *Perturbation bounds for discrete Tikhonov regularization*, Inverse Problems, 5, L41-L44, 1989.

[57] Hansen, P. C., *Regularization Tools. A matlab package for analysis and solution of discrete Ill-posed problems*, version 3.1 for Matlab 6.0, http://www.imm.dtu.dk/ pch, 1992.

[58] Hegland, M., *An optimal order regularization method which does not use additional smoothness assumptions*, SIAM J. Numer. Anal., 29, 1446-1461, 1992.

[59] Hegland, M., *Variable Hilbert Scales and their Interpolation Inequalities with Applications to Tikhonov regularization*, Applicable Anal. 59 , 207-223, 1995.

[60] Herzig, J. P., Leclerc, D. M. & Le Goff, P., *Flow of suspensions through porous media-application to deep filtration*, Industrial and Engineering Chemistry, 65, 5, 8-35, 1970.

[61] Hildebrandt, T. H., *Introduction to the Theory of Integration*. Academic Press New York and London, pp.45-47, 1963.

[62] Hille, E., *Lectures Notes on Ordinary Differential Equation*. Addison-Wesley Pub. Co, 1969.

[63] John, F., *Partial Differential Equations*, Springer, 1982.

[64] Kantorovich, L. V. & Akilov, G. P., Functional analysis. Oxford; New York, Pergamon Press, 1982.

[65] Kato, T., *Perturbation Theory for Linear Operators*, 2nd Edition, Springer–Verlag, Berlin, Heidelberg, New York, 1976.

[66] Kirsch, A., *An introduction to the mathematical theory of inverse problems*. Springer-Verlag, New York, 1996.

[67] Kravaris, C. & Seinfeld, J. H., *Identification of parameters in distributed parameter system by regularization*, SIAM J. control and Optimization. Vol. 23, No. 2, 1985.

[68] Krein, S. G. & Petunin, J. I., *Scales of Banach spaces*, Russian Math. Surveys, 21, 85-160, 1966.

[69] Krejic, N., Martinez, J. M., Mello, M. P. & Pilotta, E. A., *Validation of an augmented Lagrangian algorithm with a Gauss-Newton Hessian approximation using a set of hard-spheres problems*, Computational Optimization and Applications, 16, 247-263, 2000.

[70] Kress, R., *Linear Equations*, Springer Verlag. Berlin Heidelberg. 1989.

[71] Kuczma, M., *Functional Equations in a Single Variable*, Polish Scientific Publishers. Warszawa, 1968.

[72] Kuczma, M, Choczewski, B & Roman, G. *Iterative Functional Equations*. Cambridge University Press, 1990.

[73] Kudriavtsev, L. D., *Curso de Analisis Matematico*. Moscou, MIR, Vol. 2, 1983-84.

[74] Kuhnen, F., Barmettler, K., Bhattacharjee, S., Elimelech, M., & Kretzschmar, *R. Transport of iron oxide colloids in packed quartz sand media: monolayer and multilayer deposition*, Journal of Colloid and Interface Science, No. 231, 23-41, 2000.

[75] Lamm, P. K., *A survey of regularization methods for first-kind Volterra equations*, Surveys on Solution Methods for Inverse Problems D. Colton, H. W. Engl, A. Louis, J. R. McLaughlin, W. Rundell, Editors Springer (Vienna, New York), 53-82, 2000.

[76] Lavrent'ev, M. M. & Savel'ev, L. Ya., *Linear Operators and ill-posed problems*, Spring Sheet, NY, 1991.

[77] Lax, P., *Linear Algebra and Applications*, John Wiley Sons, 1997.

[78] Locker, J. & Prenter, P. M., *Regularization with differential operators. I: General theory*, J. Math. Anal. and Appl., 74, 504-529, 1980.

[79] Locker, J. & Prenter, P. M., *Regularization with differential operators. II: Weak least squares finite element solutions to first kind integral equations*, SIAM J. Numer. Anal., 17, 247-267, 1980.

[80] Logan, D. J., *Transport Modeling in Hydrogeochemical Systems*, Springer-Verlag, New York, 113-133, 2001.

[81] Marti, J. T., *Numerical solution of Fujita's equation*, Improperly Posed Problems and Their Numerical Treatment, Intern. Ser. Numer. Math.63 (G.Hämmerlin and K.-H. Hoffmann, eds.), Birkhäuser, Basel, 179-187, 1983.

[82] Martinez, J. M., *Augmented Lagrangians and sphere packing problems*, International Journal of Computer Mathematics, 70, 75-86, 1998.

[83] Martínez, et al., *Software "EASY"*, http://www.ime.unicamp.br/ martinez/software.htm, 2001.

[84] McDowell-Boyer, L., Hunt, J., & Sitar, N., *Particle transport through porous media.* Water Resources Research, Vol. 22, No. 13, 1901-1921, 1986.

[85] Micchelli, C. A. & Rivlin, T. J., *A survey of optimal recovery*, Optimal Estimation in Approximation Theory, (C.A. Micchelli and T.J. Rivlin, eds.), Plenum Press, New York, London, 1-53, 1977.

[86] Morozov, V. A., *Methods of Solving Incorrectly Posed Problems*, Springer–Verlag, New York, Berlin Heidelberg, 1984.

[87] Nabokov, R., *An inverse problem for the porous medium equation. Identification of the permeability*, Ruprecht-Karls-Universitt Heidelberg, Thesis, 1996.

[88] Nair, M. T., *On Morozov's method for Tikhonov regularization as an optimal order yielding algorithm*, Journal for Analysis and its Applications, Vol. 18, No. 1, 37-46, 1999.

[89] Nair, M. T, *The trade-off between regularity and stability in Tikhonov regularization*, Mathematics of Computation, Vol. 66, No. 217, 193-206, 1997.

[90] Nair, M. T., *A generalization of Arcangeli's method for ill–posed problems leading to optimal rates*, Integral Equations Operator Theory 15, 1042-1046, 1992.

[91] Natterer, F., *Error bounds for Tikhonov regularization in Hilbert scales*, Applicable Anal., 18, 29-37, 1984.

[92] Neubauer, A., *An a posteriori parameter choice for Tikhonov regularization in Hilbert scales leading to optimal convergence rates*, SIAM J. Numer. Anal., 25, 1313-1326, 1988.

[93] Pang, S. and Sharma, M. M., *A model for predicting injectivity decline in water injection wells*, 69th Annual Technical Conference and Exhibition. New Orleans., Society of Petroleum Engineers. SPE 28489, 1994

[94] Phillips, D. L., *A technique for the numerical solution of certain integral equations of the first kind*, J. Assoc. Comput. Mach., 9, 84-97, 1962.

[95] Plato, R., *Optimal algorithms for linear ill–posed problems yield regularization methods*, Numer. Funct. Anal. and Optim., 11, 111-118, 1990.

[96] Ramm, A. G., *On stable numerical differentiation*, Math. Comp., 70, 1131-1153, 2001.

[97] Reinsch, C. H., *Smoothing by spline Functions*, Numerische Mathematik, 10, 177-183, 1967.

[98] Richter, G. R., *Numerical Solution of integral equations of the first kind nonsmooth kernels*, SIAM J. Numer. Anal., Vol. 15, No. 3, 511-522, 1978.

[99] Schock, E., *Parameter choice by discrepancy principles for the approximate solution of ill–posed problems*, Integral Equations Operator Theory, 7, 895-898, 1984.

[100] Stone, M. H., *Linear transformation in Hilbert space and their application to analysis*, New York, AMS. 165-166, 1932. First Ed.

[101] Schock, E., *On the asymptotic order of accuracy of Tikhonov regularizations*, J. Optim. Theory Appl., 44, 95-104, 1984.

[102] Schroter, T. & Tautenhahn, U., *Error Estimates for Tikhonov regularization in Hilbert scales*, Numer. Funct. Anal. and Optimiz., 15, 155-168, 1994.

[103] Sun, N., Sun, N. Z., Elimelech, M. & Ryan, N., *Sensitivity analysis and parameter identifiability for colloid transport in geochemically hererogeneous porous media*, Water Resources Research, Vol. 37, No. 2, 209-22, 2001.

[104] Tarantola, A., *Generalized nonlinear inverse problems solved using the least square criterion*, Reviews of Geophysics ans space physics, Vol. 20, No. 2, 219-233, 1982.

[105] Tikhonov, A. N. & Arsenin, V. Y., *Solutions of Ill–Posed Problems*, Wiley, New York, 1977.

[106] Trénoguine,V., Pissarevski, B. & Soboleva, T., *Problèmes et Exercices d'Analyse Fonctionnelle*, Moscou, Ed. Mir, 1987.

[107] Trummer, M. R., *A method for solving ill-posed linear operator equations*, SIAM J. Numer. Anal., 21, 729-737, 1984.

[108] Van Loan, C. F., *Generalized the singular value decomposition*, SIAM J. Numer. Anal., Vol. 13, No. 1, 1976.

[109] Varah, J. M., *Pitfalls in the numerical solution of linear ill–posed problems*, SIAM J. Sci. Stat. Comput., 4, 164-176, 1983.

[110] Vogel, C. R., *Non-convergence of the L-curve regularization parameter selection method*, Inverse Problems, 12, 535-547, 1996.

[111] Vogel, C. R., *Computational methods for inverse problems*, Philadelphia: Society for Industrial and Applied Mathematics, 2002.

[112] Wennberg, K. I. and Sharma, M. M., *Determination od the filtration coefficient and the transition time for water injection wells*, Society of Petroleum Engineers. SPE 38181, 1997.

[113] Yoshida, K., *Functional Analysis*, Berlin; New York, Springer-Verlag. 1966.

[114] Zeidler, E., *Nonlinear Functional Analysis and its applications. I. Fixed point theorems*, Springer-Verlag. New York Inc, 1985.

Appendix A

Basic results

A.1 Functional analysis

In this section we review some well known results in Functional Analysis that are needed later.

Let X, Y be Banach spaces, let D be a dense vector subspace of X, and let $T : D \to Y$ be a linear operator. The product $X \times Y$ with the norm

$$||(x, y)|| = max(||x||, ||y||), \tag{A.1}$$

is a Banach space. The set

$$G(T) = \{(x, Tx); \quad \text{such that} \quad x \in D\} \subset X \times Y \tag{A.2}$$

is defined to be the *graph* of T. The graph $G(T)$ is a vector subspace in $X \times Y$.

With the definition above we can state the Closed Graph theorem ([113]) as follows.

Theorem A.1 *Let $T : D(T) \subset X \to Y$ be a linear operator defined on the Banach space X, then the graph $G(T)$ is closed if and only if T is a continuous operator.*

Definition A.2 *The linear operator $T : D(T) \subset X \to Y$ on Banach spaces X and Y is called compact if the image of every bounded set M is relatively compact, i.e., the closure of $T(M)$ is a compact set.*

Let us denote by $C[a, b]$ the Banach space of real continuous functions on interval $[a, b]$ with norm

$$||f||_\infty = \sup_{x \in [a,b]} |f(x)|. \tag{A.3}$$

We are interested in obtaining compact subsets in $C[a, b]$. To do so, the following theorem of Arzelà-Ascoli ([76], pag. 140) is useful.

Theorem A.3 *A closed subset $\mathcal{M} \subset C[a, b]$ is compact if $\mathcal{M}$ is uniformly bounded and equicontinuous.*

Because integral operators are very useful in our work, we summarize some important theorems about such operators ([66], pag. 225, and pag. 230).

Theorem A.4 *(a) Let $k \in L^2([c,d] \times [a,b])$ be a real valued function on $[c,d] \times [a,b]$; let $x \in L^2[a,b]$. Then the integral operator Tx given by*

$$Tx(t) = \int_a^b k(t,s)x(s)ds, \quad t \in [c,d], \quad s \in [a,b], \tag{A.4}$$

is well-defined, linear, and bounded from $L^2[a,b]$ into $L^2[c,d]$; furthermore,

$$||T|| \leq \left(\int_c^d \int_a^b |k(t,s)|^2 dsdt \right)^{1/2}. \tag{A.5}$$

(b) Let k be a continuous real valued function on $[c,d] \times [a,b]$. Then T is also well-defined, linear, and bounded from $C[a,b]$ into $C[c,d]$; furthermore

$$||T||_\infty = \max_{t\in[c,d]} \int_a^b |k(t,s)|ds. \tag{A.6}$$

Another property of the integral operator (A.4) is its compactness:

Theorem A.5 *Let $k \in L^2([c,d] \times [a,b])$. The integral operator* (A.4) *from $L^2[a,b]$ into $L^2[c,d]$ is compact.*

Moreover the following theorem is valid ([64], pag. 245).

Theorem A.6 *Let $k \in C([c,d] \times [a,b])$. The integral operator* (A.4) *from $C[a,b]$ into $C[c,d]$ is compact.*

A.2 Hilbert scales

In this section we introduce the concept of Hilbert scales, which will be used to prove results on the convergence of regularized solution of ill-posed integral equations. Moreover, they will be used to characterize the degree of ill-posedness of linear equations. Classical examples of Hilbert scales can be obtained from the singular value decomposition of compact self-adjoint operators. More details and results can be found in [6].

Definition A.7 *A family $(H_s)_{s\in\mathbb{R}}$ of separable Hilbert spaces (with inner products $(\cdot,\cdot)_s$) is called a Hilbert scale if the following properties hold:*
i) $H_s \subset H_0 \subset H_t$ are dense and continuous embeddings for any $s \geq 0 \geq t$.
ii) $H_s^* = H_{-s}$; $|(u,v)_0| \leq (u,u)_s^{1/2}(v,v)_{-s}^{1/2}$ for all $u \in H_s, v \in H_{-s}$; $s \in \mathbb{R}$,
iii) $(u,u)_r \leq (u,u)_s^{2(1-\psi)}(u,u)_t^{2\psi}$ for all $u \in H_s$; $s \geq r \geq t, s \neq t, \psi := (s-r)(s-t)^{-1}$.

Here we mention two important examples of Hilbert scales. The first example is the following. Let H be a separable Hilbert space with inner product $(\cdot,\cdot)_H$ and orthonormal basis $(e_j)_{j\in\mathbb{N}}$ and let $(\alpha_j)_{j\in\mathbb{N}}$ be a sequence of real numbers between 0 and 1 with

$$0 < \alpha_{j+1} \leq \alpha_j \leq 1, \quad j \in \mathbb{N}, \quad \lim_{j\to\infty} \alpha_j = 0. \tag{A.7}$$

Let N be the set of elements in H represented by finite linear combinations of the elements $(e_j)_{j\in\mathbb{N}}$. Then for each $s \in \mathbb{R}$ we define on N an inner product $(\cdot,\cdot)_s$ as

$$(x, y)_s := \sum_{j=1}^{\infty} \alpha_j^{-2s}(x, e_j)_H(y, e_j)_H. \tag{A.8}$$

Due to the definition of N the series above is actually a finite sum. The closure H_s of N in the norm $||\cdot||_s = (\cdot,\cdot)_s^{1/2}$ is a Hilbert space.

It is possible to prove that the above family of Hilbert spaces constitutes a Hilbert scale ([6], pag 73). Now, let T be a compact injective operator from a Hilbert space H_0 into another Hilbert space. Let (σ_j, e_j, f_j) be the singular value decomposition of T . Then from the pair (σ_j, e_j) the Hilbert scale can be built as above.

The second example is the following. Let $T : D(T) \to H$ be a densely defined, strictly positive definite and self-adjoint operator on H. The Hilbert scale $(H_s)_{s\in\mathbb{R}}$ is the family of Hilbert spaces $\{H_s\}_{s\in\mathbb{R}}$, where H_s is the closure of $\cap_{k=1}^{\infty} D(T^k)$ with respect to the norm $x \to ||x||_s = ||T^s x||$; here T^s(the s-power of T) is defined using the spectral representation of T ([68]).

A.3 Inverse problem

Consider a mathematical model for a physical process given by a system of related quantities such as input variables, function parameters and output variables. In several situations the description of such a system is given in terms of a set of equations (ordinary and/or partial differential equations, integral equations), containing certain function that must be determined.

Thus, the analysis of the given physical process via the mathematical model has three distinct stages: direct problem, reconstruction problem and identification problem.

In general, an inverse problem can be stated in the framework of operator equations. As a model we consider the following equation:

$$Gu = y, \tag{A.9}$$

where $G : U \to W$ is a map between the Banach spaces U and W.

Definition A.8 *The problem of solving Eq.* (A.9) *is well-posed (in the sense of Hadamard) if the inverse map $G^{-1} : W \to U$ exists and is continuous. Otherwise the problem is called* ill-posed.

According to the definition above we distinguish between three types of ill-posedness. If w is not in the range of the map G, then (A.9) has no solution (nonsolvability). If G is not one-to-one, G^{-1} does not exist and Eq. (A.9) may have several solutions if $y \in G(U)$ (ambiguity). Finally, if G^{-1} exists but is not continuous on W, a solution of (A.9) cannot depend continuously on the right hand side y (instability).

If the problem in (A.9) is ill-posed one could try to restore well-posedness taking the spaces U and W with appropriate topologies determined by practical needs. In the case of restoration of continuity (stability) the use of a priori information on the solution is needed. We will see that compact sets are very useful as classes of admissible solutions.

Now, we summarize without proof some results related with stability restoration.

Theorem A.9 *Let X and Y be Hilbert spaces and assume that $K \in B(X,Y)$ is injective. Then the following conditions are equivalent:*
a) $R(K)$ is closed;
b) $K^{-1} : R(K) \to X$ is continuous.

The theorem above shows that the problem of solving the operator equation $Kx = y$ is ill-posed if, and only if, $R(K)$ is not closed. This suggests that stability properties of ill-posed problems can be obtained by a restriction of the operator such that the range becomes closed. The strategy above is particularly useful for compact operators; it is subsumed in the following Lemma of Tikhonov ([105]):

Lemma A.10 *Let $K : X \to Y$ be a continuous one-to-one operator and let the compact subset $\mathcal{M}$ be contained in X; then the inverse map of the restriction of K to $\mathcal{M}$ is continuous.*

For practical purposes, mere continuous dependence of the solution on the data is not sufficient since the continuity may be arbitrarily weak. A measure of the continuity of $K^{-1} : R(K) \to X$ is given by the modulus of continuity

$$\omega_{\mathcal{M}}(\rho) := sup\{||u - v||_X : ||K(u - v)||_Y \leq \rho; u, v \in \mathcal{M}\}, \quad \rho > 0. \tag{A.10}$$

One distinguishes two types of continuity:

$$\omega_{\mathcal{M}}(\rho) = O(\rho^{\alpha}), \alpha \in (0, 1] \tag{A.11}$$

and

$$\omega_{\mathcal{M}}(\rho) = O(|log(\rho)|^{-\alpha}), \quad \alpha > 0. \tag{A.12}$$

Several issues about estimating $\omega_{\mathcal{M}}(\rho)$ are discussed in [6]. In order to estimate the modulus of continuity $\omega_{\mathcal{M}}(\rho)$ we have to specify the restriction set $\mathcal{M}$. In practical situations, conditions are given by the physical restrictions of the problem, such as monotonicity, positivity and bounds on the feasible solutions. Such conditions are as important as the operator equations for the recovery of the solution.

In mathematical framework, we need to find an appropriate Hilbert or Banach space and $\mathcal{M}$ is usually taken as a compact subset of this space. In this way, convergence results are obtained. In addition, stable numerical algorithms with solutions in this subset are built and used.

The choice of $\mathcal{M}$ can be done in the following way. Let V, X and Z be Hilbert spaces and let B be a continuous linear operator. Assume that the following conditions hold:
i) V is a dense subspace of X and the imbedding of V into X is continuous
ii) B is surjective.
We set $\mathcal{M} := \mathcal{M}_e = \{v \in V : ||Bv||_Z \leq e\}$, where $e > 0$.

This method to specify a restriction set $\mathcal{M}$ is called restoration of continuity by a priori bounds. In our case, the bounds e in $\mathcal{M}_e$ represent upper and lower bounds on the permeability reduction function or on the filtration function. Moreover, B represents some differentiation operator.

So, it is convenient to modify slightly the definition of $\omega_{\mathcal{M}}(\rho)$ as follows:

$$\omega(\rho, e) = \sup\{||v||_X : ||Kv||_Y \leq \rho, ||Bv||_Z \leq e, v \in V\}, \text{ where } \rho > 0, e > 0. \tag{A.13}$$

For the time being, we present another basic result in inverse theory that will be useful for obtaining a conditionally well-posed problem. To do so, it is necessary to introduce the following concept of well-posedness in Tikhonov's sense. Let us define the linear equation

$$Ku = y, \tag{A.14}$$

where K is a continuous operator.

Definition A.11 *Let $K : \mathcal{M} \subset X \to Y$ be the continuous linear operator defined in Eq.* (A.14)*, and $\mathcal{M}$ a compact subset of X. The problem in Eq.* (A.14) *is said to be well-posed in Tikhonov's sense if the following conditions are fulfilled:*
(i) it is known a priori that a solution of Eq. (A.14) *exists and belongs to $\mathcal{M}$;*
(ii) the solution of Eq. (A.14) *is unique in $\mathcal{M}$;*
(iii) the solution f depends continuously on the RHS y, and y belongs to the interior of $K_\sigma(\mathcal{M})$, i.e., a sufficiently small perturbation of y does not lead to a solution outside the set $\mathcal{M}$.

Once the existence and uniqueness issues are solved, the stability condition must be studied. To do so, we must restrict the operator K to some compact subset $\mathcal{M}$ where the condition (iii) in Definition (A.11) holds. Then, stability is guaranteed by the Lemma of Tikhonov. However, in practical situations it is not obvious how to find such a compact set. Thus, a priori information on the solution is required.

As it is not always true that y in (A.14) belongs to $R(K)$, we need to extend the concept of solution of Eq. (A.14). In this sense, the least squares solution can be an useful alternative for approximating a wide variety of physical models.

A.3.1 Generalized inverse

In this part we introduce a somewhat more general notion of the inverse of a bounded linear operator K from a Hilbert space X into a Hilbert space Y. Details and proofs can be found in [45].

First, we take as solution of Eq. (A.14) a vector $u \in X$ such that

$$||Ku - y|| = \inf_{x \in X} ||Kx - y||. \tag{A.15}$$

Such a vector u is called a least squares solution of Eq. (A.14). The following theorem provides equivalent characterizations of solutions obtained through the least square method.

Theorem A.12 *Assume that $K : X \to Y$ is a bounded linear operator between the Hilbert spaces X and Y. The following conditions are equivalent:*
i) $||Ku - y|| = \inf\limits_{x \in X} ||Kx - y||$

ii) $K^*Ku = K^*y$
iii) $Ku = Py$,
where P *is the orthogonal projection operator of* Y *onto* $\overline{R(K)}$.

From (iii) we see that Eq. (A.14) has a least square solution if and only if $Py \in R(K)$, that is, if and only if y is a member of the dense subspace $R(K) + R(K)^\perp$ of Y. Assuming this to be the case, each of the conditions shows that the set of least squares solutions is a closed convex set. So, this set of least square solutions has a unique element of smallest norm which is denoted by $K^\dagger y$.

The operator $K^\dagger$ defined on the dense subspace $\mathcal{D}(K^\dagger) = R(K) + R(K)^\perp$ is called the Moore-Penrose generalized inverse of K. It is not difficult to show that $K^\dagger$ is a closed linear operator with $N(K^\dagger) = R(K)^\perp$ and $R(K^\dagger) = N(K)^\perp$. Moreover, notice that $K^\dagger y$ is the unique least squares solution of (A.15) lying in the subspace $N(K)^\perp$.

With this more general concept of solution, the existence and uniqueness questions are solved for the triple $(K, N(K)^\perp, \mathcal{D}(K^\dagger))$. However, the stability problem requires more properties for the operator K, as shown in the following theorem:

Theorem A.13 *$K^\dagger$ is bounded if and only if $R(K)$ is closed.*

In this work we study compact operators, and for such operators $R(K)$ is not closed, in general. Indeed, if K is compact and $R(K)$ is closed then $K^\dagger$ is bounded and hence $KK^\dagger$ is compact. Thus, as $KK^\dagger$ is the identity operator on $R(K)$, it follows that it is finite dimensional. Hence we have:

Corollary A.14 *If $K : X \to Y$ is a compact linear operator, then $K^\dagger$ is bounded if and only if $R(K)$ is finite dimensional.*

So, it is possible to shows that the triple $(K, N(K)^\perp, D(K^\dagger))$ is well-posed only in the relatively trivial case when K has finite rank.

The above result has an immediate consequence for the problem of finding a solution of Fredholm integral equations of the first kind. In general, $R(K)$ is not finite dimensional, so we must devise means of imposing stability when solving some kind of operator equation. To do so, we introduce Tikhonov regularization in Section A.4, which stabilizes several ill-posed problems.

A.3.2 Singular value decomposition

The singular value decomposition (SVD) is a useful tool in the study of Fredholm equations of the first kind. A brief introduction to this concept in terms of spectral theory is given in Appendix B ([100], [65] [77] and [108]). It constitutes the basis for explaining regularization theory in continuous and discrete frameworks.

Now, we give an explicit representation of the Moore-Penrose generalized inverse of a compact operator.

Let X and Y be Hilbert spaces and let $K : X \to Y$ be a compact linear operator with singular value decomposition $\{u_n, v_n; \mu_n\}$ and $y \in D(K^\dagger)$

$$K^{\dagger}y = \sum_{n=1}^{\infty} \mu_n (Py, u_n) v_n = \sum_{n=1}^{\infty} \mu_n (y, u_n) v_n, \tag{A.16}$$

where P is the orthogonal projection operation of Y onto $\overline{R(K)}$.

Picard Condition

The Picard condition has great utility in validating the discretization of continuous problems and in guaranteeing the existence of solutions of integral equations of the first kind.

This condition arises from the Picard Theorem.

Theorem A.15 *Let $K : X \to Y$ be a compact linear operator with (SVD) $\{v_n, v_n, \mu_n\}$. The equation $Kx = y$ has a solution if and only if $y \in N(K^*)^{\perp}$ and the following inequality holds*

$$\sum_{n=1}^{\infty} \mu_n^2 |(y, v_n)|^2 < \infty. \tag{A.17}$$

The condition $y \in R(K)$ may viewed as an abstract smoothness or regularity condition in the sense that y inherits part of the smoothness of the kernel (with respect to the first variable). The Picard Theorem reinterprets this regularity by requiring that the components $|(y, v_n)|$ decay quickly relative to the growth of the singular values.

A.4 Tikhonov regularization

In the solution of ill-posed operator equations, Tikhonov regularization with a suitable regularizing operator has played a seminal role ([105], [30], [66] and [70]). There exist two main reasons. On one hand, it has had a considerable success in generating stable approximations to the solutions of practical inverse problems ([53], [5]). On the other hand, it has useful equivalent mathematical representations, such as the Euler-Lagrange equations and the minimum-norm least square interpretation, which permit a rigorous study of its mathematical and numerical properties.

In this section we summarize the main concepts and results of Tikhonov regularization used for solving several inverse problems that arise throughout this work.

We always let $K : X \to Y$ denote a bounded linear or nonlinear operator between Hilbert spaces X and Y with range $R(K)$, not necessarily closed in Y. As the canonical ill-posed problem to which Tikhonov regularization will be applied, we consider the operator equation

$$Kx = y, \quad y \in Y. \tag{A.18}$$

Furthermore, we denote by L a densely defined closed linear operator with domain $D(L) \subset X$ and range $R(L) \subset Z$, where Z is a Hilbert space too. Now, *Tikhonov regularization*, with regularizing operator L applied to (A.18), is defined variationally as the problem of minimizing,for $\alpha > 0$, the Tikhonov functional G_α defined by

$$G_\alpha(x) = ||Kx - \tilde{y}||^2 + \alpha ||Lx||^2, \quad x \in D(L). \tag{A.19}$$

The Euler-Lagrange or regularized equation formulation of Tikhonov regularization is

$$(K^*K + \alpha L^*L)x_\alpha = K^*y, \tag{A.20}$$

where x_α denotes the regularized solution of (A.18), for a fixed value of regularization parameter α and regularizing operator L.

Any minimizer of G_α solves also the Euler-Lagrange equation, and it is an element of $D(L^*L)$; conversely, any solution of the Euler-Lagrange equation minimizes G_α.

For $L = I$, Eq. (A.20) is uniquely solvable, and, if $y \in D(K^\dagger)$ is the domain of the Moore-Penrose inverse $K^\dagger$, then $x_\alpha \to \hat{x}$ as $\alpha \to 0$, where $\hat{x} := K^\dagger y$ is the minimum–norm least squares solution of (A.18).

However, from a practical point of view, it is more appropriate to seek the least squares solution x_0 which minimizes the seminorm $\|Lx\|$ for $L \neq I$ ([109]); i.e., one looks for x_0 such that

$$x_0 \in S_y := \{x \in D(L) : \quad \|Kx - y\| \leq \|Ku - y\|; \quad \forall u \in D(L)\}$$

and

$$\|Lx_0\| \leq \|Lx\|, \quad \text{for all } x \in S_y.$$

In applications, K is often a compact integral operator with a nondegenerate kernel, and L is a differential operator ([79]).

Choices for the regularizing operator L, different from I, were suggested in the earliest papers discussing regularization ([94]). Practical computations show that this approach leads to smaller errors in some cases ([107]). For special choices of L, theoretical improvements in convergence were established in [91]. A parameter choice strategy for such situations was proposed in [92].

If the data y is only given approximately by y^δ, with $\|y - y^\delta\| \leq \delta$, $\delta > 0$, then one must solve

$$(K^*K + \alpha L^*L)x_\alpha^\delta = K^*y^\delta \tag{A.21}$$

instead of (A.20). Here, the choice of the regularization parameter α (depending on δ and possibly y_δ) is important, because in general, the family $\{x_\alpha^\delta\}_{\alpha>0}$ does not need to be bounded. As an example, consider K such that $R(K)$ is not closed and $L = I$. In this case, the family $\{(K^*K + \alpha I)^{-1}K^*\}_{\alpha>0}$ is not uniformly bounded. It can then be seen from the Uniform Boundedness Principle that, for each $\delta > 0$, there exists $y^\delta \in Y$ with $\|y - y^\delta\| \leq \delta$ such that $\{x_\alpha^\delta\}_{\alpha>0}$ is not bounded in X.

Practical considerations suggest that it is desirable to choose the regularization parameter α during the computation of x_α^δ, using a so-called a posteriori method rather than an a priori method based on δ only ([29]). Another choice consists in using a modified form of a method suggested by Schock ([99]) for the case $L = I$, where α is computed to satisfy

$$\|Kx_\alpha^\delta - y^\delta\| = \frac{\delta^p}{\alpha^q}, \quad p > 0, \ q > 0. \tag{A.22}$$

Convergence for this method has been further investigated in [90], [41] and [42]. Below, this analysis is extended to a more general class of L.

In this work, the error in a Tikhonov regularization approximation is compared with $\omega(\rho, \delta)$ in (A.13).

A method for obtaining approximations $x^\delta := R(\delta, y^\delta)$ to x_0 corresponding to a reconstruction algorithm R, is said to be an optimal–order regularization method with respect to an operator B, if one has

$$\|x_0 - x^\delta\| = O(\omega(\rho, \delta)) \tag{A.23}$$

for all $x_0 \in D(B)$, with $\|Bx_0\| \leq \rho$.

The quantity $\omega(\rho, \delta)$ will be determined for some operators that arise in this work in order to demonstrate the validity of our numerical results.

A.4.1 Solvability of the regularized equation

In order to guarantee the unique solvability of the regularized equations (A.19) and (A.21), we assume that the following (*completion condition*) (see [86], pag. 3) holds for some $\gamma > 0$

$$\|Kx\|^2 + \|Lx\|^2 \geq \gamma \|x\|^2, \quad x \in D(L). \tag{A.24}$$

Thus, for a given K the operator L must be chosen so that condition (A.24) holds. It is known that if K and L satisfy condition (A.24), then the map in (A.19) attains its minimum at a unique element $x_\alpha(y)$ in $D(L)$, see, e.g., [78], [79] and [89]. It is also known that if $y \in R(A) + R(A)^\perp$, $A = K_{|D(L)}$, then

1. the set $S_y := \{x \in D(L) : ||Kx - y|| \leq ||Ku - y|| \quad \forall u \in D(L)\}$ is non-empty,
2. there exist a unique $\hat{x}(y) \in S_y$ such that $||L\hat{x}(y)|| \leq ||Lx||$ for all $x \in S_y$,
3. $x_\alpha(y) \to \hat{x}(y)$ as $\alpha \to 0$.

So, we would like $x_\alpha(\tilde{y})$ to converge to some $\tilde{x}$ as $\alpha \to 0$, where $\tilde{x}$ is close to $\hat{x}(y)$ whenever δ is close to 0. Thus a strategy has to be adopted for choosing the regularization parameter $\alpha = \alpha(\delta, y)$ such that (A.24) holds. For this purpose we consider the simple procedure suggested in [86], namely, to choose $\alpha = \alpha(\delta, y)$ such that

$$||K\tilde{x}_\alpha - \tilde{y}|| = \delta, \tag{A.25}$$

where $\tilde{x}_\alpha = x_\alpha(\tilde{y})$. It is known that if

$$||(I - P_L)y|| > 0 \quad \text{and} \quad ||(I - P_L)\tilde{y}|| > \delta, \tag{A.26}$$

where $P_L : Y \to Y$ is the orthogonal projection onto the closure of the set

$$\{Kx : x \in D(L) \quad \text{with} \quad Lx = 0\}, \tag{A.27}$$

then there exists a unique α depending on δ and $\tilde{y}$ satisfying (A.25). Notice that if L is injective, then $P_L = 0$, and in that case (A.26) can be replaced by the assumption $||y|| > 2\delta$.

In our work, Tikhonov regularization is used together with appropriate parameter choice strategies. This enables us to obtain realistic convergence estimates, i.e., this method yields an optimal-order algorithm with respect to the stabilizing set

$$M_\rho = \{x \in D(L) : ||Lx|| \leq \rho\}. \tag{A.28}$$

In this section, we revisit some results on optimal-order methods. We will use Theorem 2.2 in [88] for obtaining convergence results. This theorem is sufficient for studying the compact operator appearing in Section 4.1.

The choice of the regularizing operator imposes restrictions on the convergence rate. It is shown in [45] and [101] that, for $L = I$, the best possible convergence rate is $\|x_\alpha^\delta - x_0\| = O(\delta^{2/3})$, and that this happens if $x_0 \in R(K^*K)$ and $\alpha = c\delta^{2/3}$ for some constant $c > 0$. If $x_0 \in R((K^*K)^\nu)$ with $\nu > 1$, the same rate holds, while, for $\nu < 1$, it is smaller.

For compact, nondegenerate K, Tikhonov regularization with $L = I$ and $x_0 \in R(K^*K)$ is optimal with respect to $B = (K^*K)^\dagger$, since

$$\omega(\rho, \delta) = O(\delta^{2/3}).$$

However, when $x_0 \in R((K^*K)^\nu)$, $B = [(K^*K)^\dagger]^\nu$, and $\nu \geq 1$, one obtains

$$\omega(\rho, \delta) = O(\delta^{2\nu/(2\nu+1)}),$$

while, for other B, one can achieve even higher rates ([58]). In such situations, Tikhonov regularization with $L = I$ does not have optimal convergence rates. Nevertheless, optimality can be achieved through an appropriate choice of the regularizing operators.

An example of Tikhonov regularization having optimal convergence rates was given in [91]. That work considered the case where $Z = X$ and $L = T^k$, $k > 0$, where $T : D(T) \to X$ is a densely defined strictly positive definite and self-adjoint operator. Furthermore, it assumed that there exist positive real numbers γ_1 and γ_2 such that

$$\gamma_1 \|x\|_{-a} \leq \|Kx\| \leq \gamma_2 \|x\|_{-a}, \quad x \in X, \tag{A.29}$$

for some positive real a. Here, $\|x\|_r := \|T^r x\|$, $x \in D(T^r)$, for real r. Taking H_r to be the Hilbert space obtained through the completion of $\bigcap_{i=1}^\infty D(T^i)$ with respect to the norm $x \mapsto \|x\|_r$, the following result was proved in [91]

Theorem A.16 *If $x_0 \in H_s$ with $\|x_0\|_s \leq \rho$, $s \leq 2k + a$ and $\alpha = c\left(\frac{\delta}{\rho}\right)^{\frac{2(a+k)}{a+s}}$, then*

$$\|x_0 - x_\alpha^\delta\| = O(\delta^{\frac{s}{a+s}}).$$

The above estimate is optimal with respect to the choice $M = T^s$, as it is known, for this case, that $\omega(\rho, \delta) = O(\delta^{\frac{s}{a+s}})$. Notice that, in the above result, an a priori parameter choice was used. In [92] an a posteriori method which leads to the above result of [91] was suggested. A similar result using an a posteriori choice can be found in [58]. Thus, for $x \in R((K^*K)^\nu)$ (e.g., $T = [(K^*K)^{\frac{1}{2}}]^\dagger$), $s = 2\nu$ and $a = 1$, the order is $O(\delta^{2\nu/(2\nu+1)})$ if $k \geq \nu - 0.5$. This is achieved by imposing minimal *smoothness* on the regularizing operator L. However, by choosing a smoother operator, the convergence rate governed by the smoothness of the data is maintained. This idea was further pursued in [58] and has led to a method which gives optimal convergence rates for all $\nu > 0$.

A.4.2 Discrete ill-posed problem and its regularization

In general, the ill-posed problem given by Eq. (A.18) is defined on an infinite dimensional domain $D(K)$. Regularization methods are alternative tools for solving such a problem. A natural regularization method is the discretization of the problem through a projection of the domain $D(K)$ on several finite dimensional subspaces V_n and choose the regularized solution by fixing some appropriate n.

An example of discretization can be seen in the classical Fredholm integral equation of first kind with square integral kernel.

$$\int_a^b K(s,t)f(t)dt = g(s), \quad c \leq s \leq d, \tag{A.30}$$

where the right-hand side g and the kernel K are given, and where f is the unknown solution. Now applying a collocation method such as a Galerkin-type method, we arrive to a linear system of equations

$$Ax = b, \quad A \in \mathbb{R}^{m\times n}, \quad \text{with} \quad m \geq n, \tag{A.31}$$

where the elements a_{qj} and b_q of the matrix A and the right-hand side b are given by

$$a_{qj} = \int_a^b \int_c^d K(s,t)\phi_q(s)\psi_j(t)dsdt, \quad b_q = \int_c^d \phi_q(s)g(s)ds. \tag{A.32}$$

The solution of (A.31) can be computed by a linear least squares problem

$$\min_x ||Ax - b||_2. \tag{A.33}$$

This discretization has properties very similar to those of the original continuous ill-posed problem, i.e., the matrix is ill-conditioned. This implies that small perturbations in b produce high oscillations in the solution. This is because Eq. (A.30) with square integrable kernels are extremely sensitive to high-frequency perturbations ([45] and [56]). So, it is natural to associate the term *discrete ill-posed problem* to (A.32).

More precisely, we say that a linear system of type (A.31) is a discrete ill-posed problem if the following criteria are satisfied:

1. the singular values of A decay to zero,
2. the ratio between the largest and the smallest nonzero singular values is large.

The second statement implies that the matrix A is ill-conditioned, i.e., that the solution is potentially very sensitive to perturbations. In this case the standard methods in numerical linear algebra for solving (A.31), such as LU, Cholesky, or QR factorization, ([48]), cannot be used in a straightforward manner to compute its solution. Instead, a regularization method must be applied in order to find a meaningful solution.

The main difficulty in a discrete ill-posed problem (A.33) is that it is essentially underdetermined due to a cluster of small singular values of A. Hence, it is necessary to incorporate further information about the desired solution in order to stabilize the problem.

Details about the numerical implementation and theory can be found in [55] and [30]. Here, we summarize the fundamental issues in the regularization method for the discrete ill-posed problems used in this work.

Although many additional types of information about the solution x in (A.33) are possible, e.g., positivity and monotonocity, the predominant approach to regularization of discrete ill-posed problems is to require smallness of the solution in the 2-*norm*, or in an appropriate seminorm. An initial estimate x^* of the solution may also be included in the side constraints. Hence, the side constraint involves minimization of the quantity

$$\Omega(x) = ||L(x - x^*)||_2. \tag{A.34}$$

Here, the matrix L is typically either the identity matrix I_n or a $p \times n$ discrete approximation of the $(n-p)-th$ derivative operator, in which case L is a banded matrix with full row rank.

Thus, the idea of Tikhonov-Phillips regularization ([105] and [94]) is to define the regularized solution x_α as the minimizer of the following weighted combination of the residual norm and the side constraint

$$x_\alpha = argmin\{||Ax - b||_2^2 + \alpha^2||L(x - x^*)||_2^2\}, \tag{A.35}$$

where the regularization parameter α controls the weight given to the side constraint in the minimization of the residual norm. It is known that α controls the sensitivity of the regularized solution x_α to perturbations in A and b, and the perturbations bound is proportional to α^{-1}. Thus, the regularization parameter α is an important quantity that controls the properties of the regularization solution. In Section 4.2.3, we return to the numerical method for actually choosing α.

A.4.3 Numerical implementation of Tikhonov regularization

In either linear or nonlinear cases, practical implementation of Tikhonov regularization usually takes one of two approaches (see [75]), which we summarize below

- Solve the infinite-dimensional Tikhonov problem directly, via either an infinite dimensional minimization procedure or a direct solution of the necessary conditions (operator equation) associated with the minimization; afterwards, the solution is obtained by computer with an appropriate discretization.
- Discretize the operator K and the data y^δ first, then apply Tikhonov regularization method directly to the discretized inverse problem.

An alternative that stays within the framework of the first approach is to avoid the necessary conditions (normal equation) entirely, and instead find solutions by applying an iterative optimization method directly to Tikhonov's functional in Eq. (A.19).

The Discrete Picard Condition and filters factors

It is known that the integration of Eq. (A.30) with a square integrable kernel K has a smoothing effect on f. Therefore, the opposite operation, namely, solving Eq. (A.30) for f, tends to amplify oscillations in the right-hand side g. Hence, if we require that the solution f be a square integrable solution with finite L^2-norm , then not all functions are allowable right-hand sides g. Indeed, g must be sufficiently smooth to permit the inversion back to f. The mathematical formulation of this smoothness criterion on g, once the kernel K is given, is called the Picard condition.

Strictly speaking, for discrete ill-posed problems there is no Picard condition because the norm of the solution is always bounded. Nevertheless, it makes sense to introduce a discrete Picard condition as follows. In a real-world application, the right-hand side b is always contaminated by various types or errors, such as measurement errors, approximation errors, and rounding errors. Hence, b can be written as

$$b = \bar{b} + e \tag{A.36}$$

where e are the errors, and $\bar{b}$ is the unperturbed right-hand side. Both $\bar{b}$ and the corresponding unperturbed solution $\bar{x}$ represent the underlying unperturbed and unknown problem. Now, if we want to be able to compute a regularized solution x_{reg} from the given right-hand side b that approximates the exact solution $\bar{x}$, then it is shown in [56] that the corresponding exact right-hand side $\bar{b}$ must satisfy a criterion very similar to the Picard condition.

For the numerical implementation of Tikhonov regularization in (A.35), one uses the singular value decomposition (SVD) of A and the generalized singular value decomposition(GSVD) of a pair (A, L). A summary of these concepts we put in Appendix B ([48], [55] and [108]).

Let the singular value decomposition (SVD) of A be denoted by $(A, \mathbf{u}_i, \mathbf{v}_i, \sigma_i)$ and the generalized singular value decomposition (GSVD) of a pair (A, L) by $(A, L, \mathbf{u}_i, \mathbf{v}_i, \mathbf{x}_i, \sigma_i, \mu_i, \gamma_i)$.

Using the SVD, it is easy to show that the solution of system (A.33) is given by

$$x_{lsq} = \sum_{i=1}^{n} (\mathbf{u}_i^T b/\sigma_i)\mathbf{v}_i. \tag{A.37}$$

Thus, the least squares solution method (A.37) has the following difficulty: since the Fourier coefficient corresponding to the smallest singular values σ_i does not decay as fast as the singular values, but rather tends to level off, the solution x_{lsq} is dominated by the terms in the sum corresponding to the smallest σ_i. As a consequence, the solution x_{lsq} has many sign changes and thus appears to be completely random.

The first test to be applied in Tikhonov regularization is to verify if the discrete ill-posed problem in (A.31) satisfies a discrete Picard condition (see Section A.3.2, Theorem A.15), i.e., the amplitudes of the Fourier coefficients $|\mathbf{u}_i^T \mathbf{b}|$ on the average decay to zero faster than the generalized singular values γ_i. If the discrete Picard condition holds, we apply a damper to filter out the contribution to the solution corresponding to the small generalized singular values.

Finally, the regularized solution in (A.35) with $x^* = 0$ can be written as follows

$$x_{reg} = \sum_{i=1}^{n} f_i(\mathbf{u}_i^T b/\sigma_i)\mathbf{v}_i \quad \text{if} \quad L = I_n, \tag{A.38}$$

and

$$x_{reg} = \sum_{i=1}^{p} f_i(\mathbf{u}_i^T b/\sigma_i)\mathbf{x}_i + \sum_{i=p+1}^{n} (\mathbf{u}_i^T b)\mathbf{x}_i \quad \text{if} \quad L \neq I_n. \tag{A.39}$$

Here, the numbers f_i are *filter factors* for the particular regularization method. For Tikhonov regularization, the filter factors are either $f_i = \sigma_i^2/(\sigma_i^2 + \alpha^2)$ for $\sigma_i < \alpha$ and $f_i = 1$ for $\sigma_i \geq \alpha$, in the case $L = I_n$, or $f_i = \gamma_i^2/(\gamma_i^2 + \alpha^2)$ for $\gamma_i < \alpha$ and $f_i = 1$ for $\gamma_i \geq \alpha$ in the case $L \neq I_n$.

We discuss in Appendix D a promising optimization method used in parameter estimation theory for solving the nonlinear ill-posed problem.

A.4.4 Regularization for nonlinear operators

As opposed to linear ill-posed inverse problems, a reasonably unified theory for nonlinear ill-posed inverse problems does not exist. However, for a certain special case of nonlinear operators of our interest, there exist some results of convergence and stability. A summary is presented here. In general, we want to solve

$$K(x) = y, \tag{A.40}$$

where K is a nonlinear operator. Under ill-posedness of the nonlinear problem, we will always mean that the solution does not depend continuously on the data.

Basic results

A more general definition of compact operator is available ([114]).

Definition A.17 *Let X and Y be Hilbert spaces, and let*

$$K : X \to Y, \tag{A.41}$$

a nonlinear operator. K is called compact if and only if
i) K is continuous
ii) K maps bounded sets into relatively compact sets.

The operator K in (A.41) is called weakly closed if the graph $G(K)$ is weakly closed in the product space $X \times Y$, i.e., for any sequence of $\{x_n\} \subset D(K)$, weak convergence of x_n to x in X and weak convergence of $F(x_n)$ to y in Y imply that $x \in D(K)$ and $K(x) = y$. From now on, " $\rightharpoonup$ " denotes weak convergence and " $\to$ " strong convergence in Hilbert spaces.

More generally than in the linear case, where the minimum-norm is chosen to obtain a least squares solution, for the nonlinear problem (A.40), we define the concept of an x^*-minimum norm solution $x^\dagger$ ([33], pag. 241), i.e.

$$K(x^\dagger) = y, \tag{A.42}$$

and

$$||x^\dagger - x^*|| = \min_x \{||x - x^*|| \quad | \quad K(x) = y\}. \tag{A.43}$$

In the nonlinear $x^* = 0$ plays no special role.

The following theorem is valid

Theorem A.18 *Let K be a (nonlinear) compact and weakly closed operator, and $D(K)$ be weakly closed. Moreover, assume that $K(x^\dagger) = y$ and that there exists an ϵ such that $K(x) = \bar{y}$ has a unique solution for all $\bar{y} \in R(K) \cap B_\epsilon(y)$. If there exists a sequence $\{x_n\} \subset D(K)$ satisfying*

$$x_n \rightharpoonup x \quad but \quad x_n \nrightarrow x, \tag{A.44}$$

then K^{-1} (defined on $R(K) \cap B_\epsilon(y)$) is not continuous in y.

Assumption A.19 *Throughout this section all nonlinear operators considered are continuous and weakly closed.*

Convergence analysis

As in the linear case, we replace problem (A.40) by the minimization problem

$$\min_{x\in D(K)}\{||K(x)-y^\delta||+\alpha||x-x^*||\}, \tag{A.45}$$

where $\alpha > 0$, $y^\delta \in Y$ is an approximation of the exact right-hand side y of problem (A.40) and $x^* \in X$. From Assumption (A.19) on K, problem (A.40) admits a solution. Since K is nonlinear, the solution will be non unique, in general. We denote the solution of (A.45) as x^δ_α. The following theorem shows the continuous dependence of the solutions on the data y^δ.

Theorem A.20 *Let $\alpha > 0$ and let $\{y_k\}$ and $\{x_k\}$ be sequences where $y_k \to y^\delta$ and x_k is a minimizer of* (A.45) *with y^δ replaced by y_k. Then there exist a convergent subsequence of $\{x_k\}$ and the limit of every convergent subsequence is a minimizer of* (A.45).

Another theorem we will use in the issue of convergence of the regularization solution is the following

Theorem A.21 *Let $y^\delta \in Y$ with $||y-y^\delta|| \leq \delta$ and let $\alpha(\delta)$ be such that $\alpha(\delta) \to 0$ and $\delta^2/\alpha(\delta) \to 0$ as $\delta \to 0$. Let $\delta_k \to 0$, $\alpha_k := \alpha(\delta_k)$ and $\{x^\delta_\alpha\}$ be a solution of* (A.45)*. Then every sequence $\{x^\delta_\alpha\}$ has a convergent subsequence. The limit of every convergent subsequence is an x^*-minimum norm solution. If in addition, the x^*-minimun norm solution $x^\dagger$ is unique, then*

$$\lim_{\alpha\to 0}\{x^\delta_\alpha\} = x^\dagger. \tag{A.46}$$

Now, we survey briefly some aspects of a widely-studied and important class of nonlinear ill-posed problems, appearing in parameter identification problems.

A.4.5 Parameter identification problem

A class of nonlinear inverse problems that is widely studied and very important in many fields (physics, engineering, biology, ecology, etc.) is the parameter identification problem ([85], [104]). When building a mathematical model for a real-world problem, one often knows in principle the governing equations, but not the precise values of physical parameters (which are often dependent also on space, time, and/or the solution itself) contained in the equation. These have to be computed (identified) from measurements of the solution of the equations or of quantities derived from it (such as boundary values; identification from boundary measurements).

Such problems are usually ill-posed and nonlinear, even if the governing equations are linear. Examples will be studied in Sections 5.4 and 5.5.

Issues to be addressed are the uniqueness question for the parameter to be determined (identifiability), the stability and regularization aspect, and to find an appropriate numerical algorithm. Two approaches on which these are based are the equation error approach, where the parameter is to be determined so the residual error in the equation is minimized ([14], [5]), and the output least-squares approach, where the error criterion involves the solution of the direct problem.

We will use the second approach. In such a method it is well known that several parameters can produce the same results. So, a posteriori analysis is necessary. These are the tasks related to sensitivity and uncertainty analysis. We warn that as a result of the error introduced by numerical computations and experimental measurements the values of the parameter are not precise, but may vary within a range of uncertainty.

A.5 Convergence analysis

Once we develop a regularization method, the problem of convergence of the regularized solution $\tilde{x}_\alpha$ to the "true" solution $\hat{x}$ (the least squares solution) arises.

More precisely, if we have the operator equation

$$Ku = y, \tag{A.47}$$

then if K is a compact linear operation from a Hilbert space X into a Hilbert space Y, the regularization consists of constructing some operator $R_\alpha : Y \to X$ which is continuous and approximates $K^\dagger$ in the sense that

$$R_\alpha y \to K^\dagger y \tag{A.48}$$

as $\alpha \to 0$ for each $y \in D(K^\dagger)$.

The convergence depends strongly on whether y is known exactly or not. From the experimental point of view, y represents some quantities that are measured with some error δ. We assume that we know the data y^δ with error such as $\| y^\delta - y\| < \delta$. In our work we concentrate in the theoretical and practical issues of Tikhonov regularization .

Let $\{H_s : s \in \mathbb{R}\}$ a Hilbert scales. The condition (iii) of Definition A.7, called *interpolation inequality*, can be rewritten as

$$||u|| \leq C||u||_r^{\frac{a}{r+a}}||u||_{-a}^{\frac{a}{r+a}}, \quad x \in H_r, \tag{A.49}$$

for some constant $C > 0$, where $||\cdot||_s$ denotes the norm in H_s. This inequality can be used to study the dependence of δ on some approximation u_δ of the solution u of Eq. (A.47) ([59]).

Regularization methods attempt to make the residual $||Ku_\delta - y||$ small as well as imposing some stability condition. For the error $e_\delta = ||u_\delta - u|| \in D(K)$, the residual is often bounded as

$$||Ke_\delta|| \leq O(\delta^t), \quad \text{for some} \quad t > 0. \tag{A.50}$$

Stability for $e_\delta \in H_r$ is imposed in terms of a Hilbert scale norm such as

$$||e_\delta||_r \leq O(\delta^\eta), \quad \text{for some} \quad \eta > 0. \tag{A.51}$$

If there exists an $a > 0$ independent of δ such that

$$||e_\delta||_{-a} \leq ||Ke_\delta||, \tag{A.52}$$

then the interpolation inequality (A.49) gives the required convergence rate

$$||e_\delta|| \leq O\left(\delta^{\frac{tr+\eta a}{r+a}}\right). \tag{A.53}$$

Estimates using Hilbert scales

Notice that the convergence results obtained in [91] (see Theorem A.16) assume as valid the inequalities in (A.29) and the regularization parameter α is chosen a priori.

In [88] a more realistic estimate is obtained for the error $||\hat{x}-\tilde{x}_\alpha||$ relating the operators K and L to a Hilbert scale $(X_s)_{s\in\mathbb{R}}$, with $X_0 = X$. This estimate is obtained with assumptions weaker than the ones derived in [91] because only part of the inequalities in (A.29) is assumed, and the regularization parameter is chosen by the discrepancy principle of Morosov. Moreover, the convergence of the regularization solution to some point close to minimum–norm least squares solution is obtained. This result is more realistic from the numerical point of the view, because actually the numerical method enables us to obtain an approximate solution. We use this result to obtain convergence in the case of a compact operator defined by a first kind Volterra integral equation (see Section 4.1). Here we summarize the results above. Details can be found in [88] and [89].

The assumptions are the following:
(i) there exist $a > 0$ and $c > 0$ such that

$$||Kx|| \geq c||x||_{-a}, \quad \text{for all} \quad x \in X; \tag{A.54}$$

(ii) there exist $b \geq 0$ and $d > 0$ such that $D(L) \subseteq X_b$ and

$$||Lx|| \geq d||x||_b \quad \text{for all} \quad x \in D(L). \tag{A.55}$$

Taking M_ρ as in Eq. (A.28) we have the following

Theorem A.22 *If $\hat{x} \in M_\rho$ for some ρ, then*

$$||\hat{x} - \tilde{x}_\alpha|| \leq 2\left(\frac{\rho}{d}\right)^{\frac{a}{a+b}} \left(\frac{\delta}{c}\right)^{\frac{b}{a+b}}. \tag{A.56}$$

Appendix B

The Singular Value Decomposition (SVD)

Assume that $K{:}X \to Y$ is a compact linear operator and let K^* be its adjoint. Then $K^*K : X \to Y$ is a compact self-adjoint linear operator and any eigenvalue ρ of $K^\dagger K$ satisfies

$$\rho = (\rho x, x) = (K^\dagger K x, x) = ||Kx||^2 \geq 0, \tag{B.1}$$

where x is the associated eigenvector with norm one. Therefore, the nonzero eigenvalues of $K^\dagger K$ can be ordered as

$$\lambda_1^2 \geq \lambda_2^2 \geq \ldots. \tag{B.2}$$

If we designate by $v_1, v_2, \ldots$ the associated sequence of orthonormal eigenvectors and set $\mu_n = \lambda_n^{-1}$ and $u_n = \mu_n K v_n$, then u_n is an orthonormal sequence in Y and

$$\mu_n K^* u_n = v_n. \tag{B.3}$$

In addition, from the spectral theorem we have that $\{u_n\}$ is a complete orthonormal set for $\overline{R(K)} = N(K^*)^\perp$ and $\{v_n\}$ is a complete orthonormal set of $\overline{R(K^*)} = N(K)^\perp$.

The sequence $\{u_n, v_n, \mu_n\}$ is called the singular value decomposition of K.

B.1 SVD on matrices

A matrix factorization with great importance in numerical linear algebra is the singular value decomposition:

Theorem B.1 *(The singular value decomposition (SVD)). If A is a real $m \times n$ matrix, then there exist orthogonal matrices $U(m \times m)$ and $V(n \times n)$ such that*

$$U^T A V = diag(\sigma_1, \ldots, \sigma_q), \quad q = \min(m, n), \tag{B.4}$$

where $\sigma_1 \geq \sigma_2 \geq \ldots, \geq \sigma_r > \sigma_{r+1} = \ldots = \sigma_q = 0$ and $r = rank(A)$.

The proof of the SVD can be found in [77].

Using the theorem B.1 we see that the singular value decomposition of A is a decomposition of the form

$$A = U\Sigma V^T = \sum_{i=1}^{n} \mathbf{u}_i \sigma_i \mathbf{v}_i^T, \tag{B.5}$$

where $U = (\mathbf{u}_1, \ldots, \mathbf{u}_m)$ and $V = (\mathbf{v}_1, \ldots, \mathbf{v}_n)$ are matrices with orthogonal columns, $U^T U = I_m$, $V^T V = I_n$, and where $\Sigma = diag(\sigma_1, \ldots, \sigma_n)$ has non-negative diagonal elements in non-increasing order

$$\sigma_1 \geq \ldots \geq \sigma_n \geq 0. \tag{B.6}$$

The number σ_i are called *singular values* of A, while the vectors $\mathbf{u}_i$ and $\mathbf{v}_i$ are the left and right singular vectors of A, respectively. The condition number of A is equal to the ratio σ_1/σ_r.

B.2 Generalized Singular Value Decomposition (GSVD)

The following decomposition is a generalization of the SVD.

Theorem B.2 *(The L-singular value decomposition (GSVD)). Consider $A \in \mathbb{R}^{m\times n}, L \in \mathbb{R}^{p\times n}$ and $m \geq n \geq p$. There exist orthogonal matrices $U(m \times m)$ and $V(p \times p)$ and a nonsingular matrix $X(n \times n)$ such that*

$$U^T A X = \Sigma = diag(\sigma_1, \ldots, \sigma_p), \quad \sigma_i \geq 0, \tag{B.7}$$

$$V^T L X = M = diag(\mu_1, \ldots, \mu_p), \quad \mu_i \geq 0, \tag{B.8}$$

where $r = rank(L)$ and $\mu_1 \geq \mu_2 \geq \ldots, \geq \mu_r > \mu_{r+1} = \ldots = \mu_p = 0$.

The proof of the GSVD can be found in [108]. On the other hand the generalized singular value decomposition is an extension of the SVD of A in the sense that the generalized singular value of (A, L) are the square roots of the generalized eigenvalues of the matrix pair $(A^T A, L^T L)$. Then the GSVD is a decomposition of A of the form

$$A = U \begin{pmatrix} \Sigma & 0 \\ 0 & I_{n-p} \end{pmatrix} X^{-1}, \quad L = V(M, 0)X^{-1}. \tag{B.9}$$

Moreover, the diagonal entries of Σ and M are non-negative and ordered as follows

$$0 \leq \sigma_1 \ldots \leq \sigma_p \leq 1, \quad 1 \geq \mu_1 \geq \ldots \geq \mu_p > 0, \tag{B.10}$$

and they are normalized so that

$$\sigma_i^2 + \mu_i^2 = 1, \quad i = 1, \ldots, p. \tag{B.11}$$

Then the *generalized singular values* γ_i are defined as the ratios

$$\gamma_i = \sigma_i/\mu_i, \quad i = 1, \ldots, p. \tag{B.12}$$

We describe the Tikhonov regularization method in terms of SVD and GSVD in section A.4.3

Appendix C

Experimental data

Here we summarize the experimental data used in Chapter 8. The characteristics of the core and the flow, the injected particle concentration and the end time in units of porous volume injected (PVI) are presented in table C.1. More details about the experiments are found in [1].

Table C.1: Characteristics of the core and the flow.

	c_{io} (ppm)	$CoreLength$ (m)	$Corediam.$ (m^2)	$Ave.flow(l/hr)$	$FinalPV$
$Exp1$	3.89	0.13	0.03	5.48	662.5
$Exp2$	3.93	0.13	0.03	5.4	1179.53
$Exp3$	7.7	0.13	0.03	5.45	1017.16
$Exp4$	15.3	0.13	0.03	4.95	401.62
$Exp5$	4.11	0.13	0.03	10.25	1032.82

A preprocessing was performed on the data because the flow $U(t)$ is not exactly constant. This complication is resolved by a time dependent scaling so that the nondimensional time unit is the number of pore volume injected (P.V.I.)

Table C.2: Absolute permeability k_0^l in square meters (m^2).

	$segment.1$	$segment.2$	$segment.3$	$segment.$ 4	$segment.5$
$Exp1$	2.6e-12	3.0e-12	2.5e-12	3.1e-12	2.2e-12
$Exp2$	1.4e-12	1.5e-12	1.5e-12	1.5e-12	1.1e-12
$Exp3$	1.4e-12	1.3e-12	1.5e-12	1.8e-12	1.6e-12
$Exp4$	1.1e-12	1.5e-12	1.5e-12	1.4e-12	1.5e-12
$Exp5$	1.6e-12	1.6e-12	1.6e-12	1.7e-12	1.2e-12

Table C.3: Length of each segment in meters and deposition at end time in parts per million (ppm).

	segment 1	segment 2	segment 3	segment 4	segment 5
length	0.025	0.025	0.0254	0.025	0.023
σ (ppm)	1000.5	333.6	187.4	129.7	103
σ (ppm)	1168.6	440	519.7	279.1	210.1
σ (ppm)	419.8	110.2	79.7	55.3	43.5
σ (ppm)	991.6	330	221	146.6	129.6
σ (ppm)	821	256	189.2	163.1	119.3

Appendix D

Optimization

In this section we present a summary of some optimization techniques that are frequently used for solving ill-posed inverse problems. In our work, we test three optimization methods in order to identify the utility of each one.

D.1 Gauss-Newton-Levenberg-Marquardt method

Inverse problem are often solved by minimizing approximately the least squares functional

$$||u^{\delta} - F(a)||^2, \tag{D.1}$$

where $F : D(F) \subset X \to Y$ is a nonlinear differentiable operator between the Hilbert spaces X and Y, and u^{δ} are the given data. In many applications, it follows from physical considerations that u^{δ} is a reasonably close approximation of some ideal $u = F(a^{\dagger})$ in the range on F, hence the minimization of (D.1).

In the Gauss-Newton-Levenberg-Marquardt method, we have a current approximation a_n for $a^{\dagger}$; the nonlinear mapping $F(a)$ in (D.1) is replaced by its linearization around a_n prior to the minimization process. If the inverse problem is ill-posed, however, neither the original minimization problem (D.1) nor its linearized counterpart need to have a solution; even worse, if a minimizer does exist, it can be arbitrarily far off from the true solution $a^{\dagger}$. This is important for the inverse problems studied in this work, because we are interested in the properties of $a^{\dagger}$ that arise from certain physical restrictions on the solution.

To overcome these difficulties one can proceed along several lines, leading to different motivations for essentially the same algorithm ([5], [111], [105] and [46]). In the Gauss-Newton-Levenberg-Marquardt method, a trust region is chosen around a_n, i.e., a ball of radius η_n, and the linearizing functional is minimized within this ball. This is easily seen to be equivalent to minimizing

$$||u^{\delta} - F(a_n) - F^{'}(a_n)y||^2 + \alpha_n||y||^2, \tag{D.2}$$

where $F^{'}$ is the Frechet derivative of F. Here $y = y_n$ and α_n is the corresponding Lagrange multiplier. Then this procedure is repeated with $a_{n+1} = a_n + y_n$ instead of a_n in some updated trust region η_{n+1} until convergence is reached. The difficulty in this approach is finding an appropriate strategy for choosing $\{\eta_m\}$, which must rely on heuristic considerations.

Notice that in (D.2) we have a regularization induced by adding the penalty term $\alpha_n||h||^2$ to the linearized functional. This is equivalent to Tikhonov regularization ([46]) applied to the linearized problem

$$F^{'}(a_n)y = u^\delta - F(a_n). \tag{D.3}$$

It is known that other penalization terms can be used for regularizing (D.3). Convergence and stability conditions of the Gauss-Newton-Levenberg-Marquardt method and its variants can be found in [50]. Applications of this method for solving ill-posed problems are extensive ([103], [31] and [21]).

The optimization of the Tikhonov functional in (A.19) may not always be an attractive alternative for nonlinear inverse problems. One of the difficulties in the nonlinear case is that the functional in Eq. (A.19) is no longer strictly convex (in contrast to the linear case), leading to the possibility of multiple local minima.

A useful alternative for obtaining the solution of nonlinear inverse problems consists in optimizing a continuous nonlinear function (A.19) restricted to some bounded convex subset. To do so, we parametrize the functions and define the functional as the difference between model and experimental data. Based on the available information about the feasible solution subset we can impose certain bounds on the parameters.

This way of solving inverse problem can be regarded as a refined regularization, since the restriction of the parameters is equivalent to a restriction of the feasible solution class in the least square optimization problem. Since we cannot guarantee that the problem has a unique solution, sensitivity analysis is a good choice for determining the most probable solution.

D.2 Spectral projected gradient method

The nonmonotone spectral gradient projection algorithms (SPG) summarized in this section apply to problems of the form

$$\text{minimize} \quad f(x) \quad \text{subject to} \quad x \in \Omega, \tag{D.4}$$

where Ω is a closed convex set in $\mathbb{R}^n$. Each iteration of the SPG method consists basically of two stages: starting from the k-th iterate $x^k \in \mathbb{R}^n$, first a step is taken in the direction $-\nabla f(x^k)$, and then the resulting point projected onto Ω, possibly with additional one-dimensional searches in either one of the stages.

The algorithms SPG1 and SPG2 introduced in this section compute at least one projection on the feasible set Ω per iteration. Therefore, these algorithms are especially interesting in cases where this projection is easy to compute. An important situation in which the projection is trivial is when Ω is an n-dimensional box, possibly with some infinite bounds. In fact, good algorithms for box constrained minimization are the essential tool for the development of efficient augmented Lagrangian methods for general nonlinear programming ([37] and [82]).

In this work we use the spectral projected gradient algorithm for the case in which Ω is described by bounds on the variables. This algorithm is simple to code. To do so, it is useful to compare with the software "EASY" ([83]), which is an implementation of SPG with an augmented Lagrangian method.

Nonmonotone gradient projection algorithms

Now we describe formally the SPG method. We assume that f is defined and that it has continuous partial derivatives on an open set that contains Ω. In this section $||\cdot||$ denotes the 2-norm of vectors and matrices.

Given $z \in \mathbb{R}^n$ we define $P(z)$ as the orthogonal projection on Ω. We denote $g(x) = \nabla f(x)$. The algorithms starts with $x_0 \in \Omega$ and uses an integer $M \geq 1$, a small parameter $\alpha_{min} > 0$, a large parameter $\alpha_{max} > \alpha_{min}$, a damping parameter $\gamma \in (0,1)$, and safeguarding parameters $0 < \sigma_1 < \sigma_2 < 1$. Initially, $\alpha_0 \in [\alpha_{min}, \alpha_{max}]$ is arbitrary. Given $x_k \in \Omega$ and $\alpha_k \in [\alpha_{min}, \alpha_{max}]$, Algorithms 2.1 and 2.2 describe how to obtain x_{k+1} and α_{k+1} and when to terminate the process.

Algorithm 2.1.
Step 1. Detect whether the current point is stationary.
If $||P(x_k - g(x_k)) - x_k|| = 0$, stop, declaring that x_k is stationary.
Step 2. Backtracking.
Step 2.1. Set $\lambda \leftarrow \alpha_k$.
Step 2.2. Set $x_+ = P(x_k - \lambda g(x_k))$.
Step 2.3. If

$$f(x+) \leq \max_{0 \leq j \leq \min\{k, M-1\}} f(x_{k-j}) + \gamma < x_+ - x_k, g(x_k) >, \tag{D.5}$$

here $< \cdot, \cdot >$ denotes the inner product. Then define $\lambda_k = \lambda$, $x_{k+1} = x_+$, $s_k = x_{k+1} - x_k$, $y_k = g(x_{k+1}) - g(x_k)$, and go to Step 3.
If (D.5) does not hold, define

$$\lambda_{new} \in [\sigma_1 \lambda, \sigma_2 \lambda], \tag{D.6}$$

set $\lambda \leftarrow \lambda_{new}$, and go to Step 2.2.
Step 3. Compute $b_k =< s_k, y_k >$.
If $b_k \leq 0$, set $\alpha_{k+1} = \alpha_{max}$; else, compute $\alpha_k =< s_k, s_k >$, and

$$\alpha_{k+1} = \min(\alpha_{max}, \max(\alpha_{min}, a_k/b_k)). \tag{D.7}$$

Another refined algorithm presented in [17] is called SPG2. This algorithm coincides with SPG1 except at the backtracking step, as described below.

Algorithm 2.2.
Step 2. Backtracking
Step 2.1. Set $d_k = P(x_k - \alpha_k g(x_k)) - x_k$. Set $\lambda \leftarrow 1$.
Step 2.2. Set $x_+ = x_k + \lambda d_k$.
Step 2.3. If

$$f(x+) \leq \max_{0 \leq j \leq \min(k, M-1)} f(x_{k-j}) + \gamma\lambda < d_k, g(x_k) >, \tag{D.8}$$

then define $\lambda_k = \lambda$, $x_{k+1} = x_+$, $s_k = x_{k+1} - x_k$, $y_k = g(x_{k+1}) - g(x_k)$, and go to Step 3.
Step 3.
If (D.8) does not hold, define λ_{new} as in (D.6), set $\lambda \leftarrow \lambda_{new}$, and go to Step 2.2.

In both algorithms, the computation of λ_{new} uses one-dimensional quadratic interpolation and it is safeguarded taking $\lambda \leftarrow \lambda/2$ when the minimum of the one-dimensional quadratic lies outside $[0.1\lambda, 0.9\lambda]$. Notice also that the line search conditions (D.5) and (D.8) guarantee that the sequence x_k remains in $\Omega_0 = \{x \in \Omega : f(x) < f(x_0)\}$.

D.3 Interior trust region method

The Matlab subroutine for nonlinear optimization is based on the interior trust region approach and the interior reflective Newton method.

The interior trust region approach is presented in [23]. This method minimizes a nonlinear function subject to simple bounds. In the quadratic programming subproblem, the interior reflective Newton method is described in [24].

D.4 Implementation

As we have seen in previous sections, many procedures led us to solve optimization problem of nonlinear functionals. In this section we show how to use one available package program for such end the "EASY" program.

The problem consists in the minimization the smooth function $F : \mathcal{R}^n \rightarrow \mathcal{R}$ with box constraints in the variables. The minimization is achieved by the augmented Lagrangian algorithm with a Gauss-Newton Hessian approximation. The algorithm combines an unconstrained method, including a line-search which aims to add many constraints to the working set in a single iteration, with spectral projected gradient techniques for dropping constraints from the working set.

In the computer implementation we use the EASY! program. To use this code the following steps are needed.

We must provide a file *easy.dat* with the following structure: the first line must contain two integers, n and m; n must be the number de variables, m must be the number of nonlinear constraints; in our case $m = 0$. The second line of the file *easy.dat* must contain the vector of the lower bounds l, which in this case can be taken as a vector with arbitrary components. The third line must contain the vector of upper bounds u, which in our case has arbitrary positive components with high values. The fourth line must contain an initial estimate of the solution. In the next lines we provide the effluent concentration $c(1, T)$, the pressure data in five segments and the alternative matrix for penalizing the cost function F.

In the subroutine "feasy" we must provide the procedure to calculate the value of the function $F(x)$. To do so we must take from the *easy.dat* file the values of the experimental data and then the algorithm for solving the direct problem (2.9) and (2.10) is implemented.

To increase the efficiency of the method we must change the value of the parameters: $accuracy$, $acumenor$, $delta0$, $deltamin$, $mitqu$ and $ftol$ in the code. In our case the number of variables is small so the values $accuracy$ and $acumenor$ can be taken very small. On the other hand, the values of the parameter $delta0$ and $deltamin$ determine the scales of the problem, i.e., the size of the trust region. In this case we tested various examples to choose the most appropriate values.

D.5 Regularization method and simple iterative procedure

In this section we show a procedure that combines optimization techniques and Tikhonov's iterative procedure ([15]). This procedure allows to increase the rate of convergence and to choose the possible penalization term in the regularization method to obtain an approximation of the ill-posed problem.

D.5.1 Scaling method

Since the solution of the nonlinear problem reduces to its linearization, we study certain issues on the algorithm implemented in the optimization method for solving the ill-posed linear system of equation.

It may be difficult or impossible to solve the linear system by regularization methods unless an appropriate preconditioning is used, since the matrix in an ill-posed problem may be poorly conditioned or non-invertible. We will see that the iterative procedure converges if the eigenvalues of the matrix $\mathbf{M}$ falls in some interval of convergence. To guarantee this condition we choose the following preconditioning.

Let $F_{ii} = \sum_{j=1}^{n} l_{ij}$, with $i = 1, \ldots, m$ and $F_{ij} = 0$ for $i \neq j$ and let $G_{jj} = \sum_{i=1}^{m} l_{ij}$, with $j = 1, \ldots, n$ and $G_{ij} = 0$ for $i \neq j$. Setting $\mathbf{M}^{'} = F^{-\frac{1}{2}}\mathbf{M}G^{-\frac{1}{2}}$, $f^{'} = G^{\frac{1}{2}}f$, and $a^{'} = F^{\frac{1}{2}}a$, we obtain the scaling problem

$$\mathbf{M}^{'} f^{'} = a', \tag{D.9}$$

where the eingenvalues on the matrix $\mathbf{M}^{'}$ falls in the interval $[-1, 1]$.

D.5.2 Optimization method

We show that the solution of the damped least-squares minimization problem regularizes the linear system in Eq. (D.9).

Let us perform the following minimization

$$\min_{f^{'} > f_0^{'}} \| \mathbf{M}^{'} f^{'} - a^{'} \| \tag{D.10}$$

which consists of minimizing with respect of $f^{'}$ the functional

$$\Psi(s^{'}) = (a' - \mathbf{M}^{'} f^{'})^T (a' - \mathbf{M}^{'} f^{'}) + \mu (f^{'} - f_0^{'})^T (f^{'} - f_0^{'}), \tag{D.11}$$

where μ is a Lagrange's multiplier. The normal equation resulting after the process of minimization is:

$$(\mathbf{M}^{'\mathbf{T}} \mathbf{M}^{'} + \mu I)(f^{'} - f_0^{'}) = \mathbf{M}^{'\mathbf{T}} (f^{'} - \mathbf{M}^{'} f_0^{'}). \tag{D.12}$$

The result of the optimization for the untransformed f is the same as in the previous case, provided the following functional is used:

$$\Psi(s) = (a - \mathbf{M}f)^T F^{-1} (a - \mathbf{M}f) + \mu (f - f_0)^T (f - f_0). \tag{D.13}$$

In either case the result is:

$$f = f_0 + (\mathbf{M^T} F^{-1} \mathbf{M} + \mu G)^{-1} \mathbf{M^T} F^{-1} (a - \mathbf{M} f_0). \tag{D.14}$$

Then the first approximation of the solution in Eq. (D.9) is obtained by Eq. (D.14).

D.5.3 Iterative procedure

We continue by using an iterative procedure in order to obtain a more accurate solution. The beginning of the procedure consists of setting the value of ϵ and initial value f_0; then the solution in step $k+1$ is obtained by

$$f^{k+1} = f^k + \mathbf{M^T} F^{-1} (a - \mathbf{M} f_0) + (\mathbf{M}^T F^{-1} \mathbf{M} + \mu G)(f^k - f_0) \tag{D.15}$$

and we stop when $\| f^{k+1} - f^k \| / \| f^k \| \leq \epsilon$. Here the value of μ is changed until an acceptable approximation is obtained. Denoting by f_j^k, a_j, the j-th component of the vectors f^k and a, respectively, it is possible to obtain from Eq. (D.15)

$$f_j^{k+1} = \left[\frac{1 - (1 - \lambda_j^2 - \mu G_{jj})^{k+1}}{\lambda_j^2 + \mu} \right] (\lambda_j \tau_j + \mu f_j^0) + (1 - \lambda_j^2 - \mu G_{jj})^{k+1} f_j^0, \tag{D.16}$$

where the eigenvalues λ_j and τ_j are obtained from the spectral decomposition of the matrix $\mathbf{MM^T}$, and G_{ii} are the element of the diagonal of the matrix G. The convergence of the iterative method is guaranteed if the following inequality

$$-2 < \lambda_j^2 + \mu G_{jj} < 2 \quad \text{for all} \quad j = 1, \ldots, n \tag{D.17}$$

holds. This inequality is useful to choose a parameter value μ that provides convergence of the iterative method.

Appendix E

Topics on differentiation

The mathematical analysis of filtration process requires the calculation of derivatives measured experimentally function; hence, there is only a finite number of available function values and these values contain errors. The effluent concentration history is an example. It is known that the differentiation process is numerically unstable. Stabilization of this process must be studied.

Now, we summarize topics related to the existence, uniqueness and stability of the differentiation process ([105], [27], [97], [52], [96] and [51]). In several works, it is shown that the differentiation operation is equivalent to solving a particular Fredholm integral equation of the first kind. This integral equation can be solved using the regularization tools, i.e., a family of well-posed optimization problems is obtained and the corresponding family of solutions converges to the least square solution. Let us define the integral equation

$$K(u)(x) := \int_0^x u(s)ds = f(x), \quad K : D(K) \subset X \to Y, \quad f(0) = 0, \tag{E.1}$$

where X is some Hilbert space, $Y = L^2[a,b]$ and f is given. We say that the derivative $f^{'}$ exists if Eq. (E.1) is solvable and the solution $f^{'} \in X$.

In general this problem is ill-posed in the sense of Hadamard, but it is well-posed in the Tikhonov's sense. To obtain Tikhonov solution, it is necessary to restrict the operator to an appropriate class of functions to guarantee existence, uniqueness and stability.

For example, in [27] is shown that taking $X = H^1[a,b]$, $Y = L^2$ and S as some bounded subset in $H^1[a,b]$ the differentiation operation is continuous in $K(S)$. Existence and uniqueness are also proved. The proof consists of a straightforward application of the following lemmas:

Lemma E.1 *Any bounded subset of $H^1[a,b]$ is sequentially compact in the Banach spaces $C[a,b]$, (i.e., continuous functions with the uniform norm).*

Lemma E.2 *The limit in $C[a,b]$ of any sequence of functions that are uniformly bounded in $H^1[a,b]$ is in $H^1[a,b]$.*

Lemma E.3 *For any bounded set $S \subset H^1[a,b]$, the operation of differentiation is continuous in $L^2[a,b]$ on the set $K(S)$.*

Now, let us assume that $f \in H^1[a,b]$ satisfies Eq. (E.1) and the approximation $\bar{y}_i$ of the values $f(x_i)$ are known at the points of a uniform grid $\Delta = \{a = x_0, \ldots, x_n = b\}$. So, the problem of numerical differentiation can be written as an optimization problem, i.e., the minimization of the functional

$$\Phi_\alpha(f) = \sum_{i=1}^{n-1} \omega_i(\bar{y}_i - f(x_i))^2 + \alpha\Omega(f), \tag{E.2}$$

among all smooth functions satisfying $f(a) = \bar{y}_0$, $f(b) = \bar{y}_n$, where $\Omega(f)$ is called stabilizing functional and the regularization parameter α is such that the minimizing element f_α of (E.2) satisfies

$$\sum_{i=1}^{n-1} \omega_i(\bar{y}_i - f_\alpha(x_i))^2 = \delta^2. \tag{E.3}$$

The effects of setting different weights ω_i and using various stabilizing functionals without constraints on the boundary of the interval the problem in (E.2) has been investigated in [97], where it is also shown that the solution of such optimization problem results in natural cubic splines over the grid Δ.

The instability due to error propagation using a priori information on the solution of equations such as (E.1) is described in [27]. Useful estimates of error in the differentiation were obtained in [51], fixing the values of the interval boundary that lead to annoying boundary artifacts for practical data sets. In [96], the author studied conditions to obtain a stable approximation of the derivative. In [44], optimal order estimates for the differentiation for certain class of continuous function were also obtained.

Several techniques have been developed for numerical differentiation such as difference methods, interpolation methods and regularization methods. Since we want to study the stability of a certain operator, we focus our attention to the latter method, i.e., we choose stable approximation methods, which suitable for computer implementation.

We conclude that it is possible to find an appropriate subset where the differentiation is well-posed. Moreover, smoothing splines is a method recommended in the literature to obtain the derivative of the experimental data.